XX JUBILEE INTERNATIONAL SCIENTIFIC CONGRESS

WINTER SESSION

08 - 11.03.2023, BOROVETS, BULGARIA

MACHINES. TECHNOLOGIES. MATERIALS 2023

PROCEEDINGS

VOLUME II
TECHNOLOGIES

ISSN 2535-0021 (PRINT)
ISSN 2535-003X (ONLINE)

SCIENTIFIC-TECHNICAL UNION OF MECHANICAL ENGINEERING - INDUSTRY 4.0
BULGARIA

XX JUBILEE INTERNATIONAL CONGRESS
WINTER SESSION
"MACHINES.TECHNOLOGIES.MATERIALS"
08–11.03.2023 BOROVETS, BULGARIA

PROCEEDINGS

YEAR VI, ISSUE 2 (26), BOROVETS, BULGARIA 2023

VOLUME II
TECHNOLOGIES.

ISSN 2535-0021 (PRINT)
ISSN 2535-003X (ONLINE)

PUBLISHER:

SCIENTIFIC TECHNICAL UNION OF MECHANICAL ENGINEERING INDUSTRY-4.0

108, Rakovski Str., 1000 Sofia, Bulgaria
tel. (+359 2) 987 72 90,
tel./fax (+359 2) 986 22 40,
office@mtmcongress.com
www.mtmcongress.com

INTERNATIONAL EDITORIAL BOARD

C O N T E N T S

TECHNOLOGIES

ПРЕДПОСЫЛКИ ДЛЯ РАЗРАБОТКИ НОВОЙ ИННОВАЦИОННОЙ ТЕХНОЛОГИИ ФОРМИРОВАНИЯ И УПРОЧНЕНИЯ ВИНТОВОГО АРМАТУРНОГО СТЕРЖНЯ С ГРАДИЕНТНОЙ УЛЬТРАМЕЛКОЗЕРНИСТОЙ СТРУКТУРОЙ

PREREQUISITES FOR THE DEVELOPMENT OF A NEW INNOVATIVE TECHNOLOGY FOR THE FORMATION AND STRENGTHENING OF A SCREW REINFORCEMENT ROD WITH A GRADIENT ULTRAFINE-GRAINED STRUCTURE

Sergey Lezhnev[1], Evgeniy Panin[2], Dmitry Kuis[3], Andrey Tolkushkin[4], Alexandr Arbuz[5]

[1]Rudny Industrial Institute, Rudny, Kazakhstan
[2]Karaganda Industrial University, Temirtau, Kazakhstan
[3]Belarusian State Technological University, Minsk, Belarus
[4]Ural Federal University, Yekaterinburg, Russia
[5]Nazarbayev University, Astana, Kazakhstan
sergey_legnev@mail.ru

Abstract: *The work is devoted to the review of the issue of obtaining screw fittings and methods of its hardening. Based on the review conducted in this paper, a new innovative technology for the formation and hardening of a screw reinforcement rod was proposed, which consists in deforming a round cross-section workpiece on a radial shear rolling mill and subsequent twisting of the workpiece in a special design molding matrix, which allows to obtain screw reinforcement with a gradient ultrafine-grained structure.*
Keywords: *SCREW REINFORCEMENT, ROD, ULTRAFINE-GRAINED STRUCTURE, GRADIENT STRUCTURE.*

1. Введение

Сегодня возведение панельных зданий и других конструкций невозможно без использования арматуры, которая значительно повышает прочность бетона. Распространение технологии монолитного бетонирования привело к тому, что сегодня этот вид металлопроката применяется во всех крупных сооружениях, таких как здания различного назначения, плотины и дамбы. Также он необходим и при возведении не таких крупных объектов - постаментов, памятников, плит перекрытия и других. Соединение его прочности и сжатия с растянутостью арматуры позволило создать железобетон, в настоящее время являющийся одним из самых используемых в строительстве материалов. Входя в состав железобетона, арматура не подвергается коррозии, что гарантирует отсутствие постепенного разрушения зданий и других конструкций. Строительная арматура представляет собой прутья, которые могут быть как абсолютно гладкими, так и иметь рифленую поверхность с расположенными на ней выступами, параллельными или перекрестными друг к другу.

Винтовой арматурный прокат отличается от обычного тем, что ребра его периодического профиля служат не только для усиления сцепления с бетоном, но и благодаря особому расположению образуют модифицированную крупную винтовую резьбу на всей длине стержней, делающую возможным навинчивание разного рода резьбовых крепежных элементов - гаек, соединительных муфт, анкерных гаек с аналогичной внутренней резьбой. Таким образом, арматурный стержень по сути превращается в резьбовую шпильку большой длины (до 12 м из условий транспортирования), что открывает разнообразные возможности для применения такой арматуры в строительстве. Так, например, прутки винтовой арматуры в комплекте с гайками могут в построечных условиях использоваться для крепления щитов опалубки при бетонировании монолитных бетонных и железобетонных конструкций, при этом арматурные прутки выполняют роль винтовых стяжек (эти стяжки могут быть многократного использования (извлекаются после распалубки) или остающимися в бетоне). Особо актуальным является использование винтовой арматуры в монолитных конструкциях, в которых сварка не разрешается по соображениям пожарной безопасности, например, это монолитные железобетонные дымовые трубы и градирни тепловых и атомных электростанций, где арматура соединяется по длине с использованием стыков внахлестку без сварки анкерными гайками, соединительными муфтами и т.п.

Хочется отметить, что в строительстве применяется и большое число типов фундаментных болтов, которые служат в основном для крепления к железобетонным фундаментам технологического оборудования и разного рода металлических конструкций: стальных опор ЛЭП, стальных стропильных и подстропильных ферм, балок и т.п. Как известно, чаще всего болты изготавливают, в основном, из стали группы марок Ст.3, исходя из температурных условий их эксплуатации, также желательна повышенная стойкость болтов к действию динамических нагрузок. В связи с этим возможно применение в качестве болтов арматуры винтового профиля класса А500С, изготовляемой из стали марок Ст.3пс или Ст.3сп с использованием термомеханического упрочнения. Кроме того, винтовая арматура в качестве болтов имеет следующие преимущества: имеет крупную трапециевидную резьбу, менее подверженную повреждениям в процессе монтажа по сравнению с метрической резьбой, и обладает хорошим сцеплением с бетоном фундаментов. В связи с тем, что винтовая арматура по существу является винтовой шпилькой большой длины, она может применяться в строительстве для разных целей также в качестве тяжей и стяжек, в частности для ремонтных и восстановительных работ, крепления сантехнического оборудования, трубопроводов и временных лесов для проведения монтажных и отделочных строительных работ. Отдельной сферой целесообразного применения винтовой арматуры является ее использование в качестве анкерных элементов крепления стен в грунте, широко применяемых в подземном монолитном строительстве.

2. Постановка проблемы

Винтовую арматуру впервые начали изготовлять и применять в Германии в конце 60-х годов по инициативе строительной фирмы ДИВИДАГ (DIWIDAG), производство арматуры было освоено на металлургическом заводе Peine-Salzqitter. Арматура выпускается двух основных видов: для ненапряженного железобетона класса BSt420RU (в настоящее время BSt500S) диаметром 16-50 мм и высокопрочная (классов 835/1030, 900/1100 и 1080/1230) диаметром 15,0-36,0 мм. В Японии фирмой Сумитомо (SUMITOMO) производится и применяется винтовая арматура классов 5030,5035 и 5040

диаметром от 19 до 57 мм. В Венгрии в начале 80-х годов на Оэдском металлургическом заводе освоено производство винтовой арматуры классов В81420/500 и В81835/1030. На металлургических предприятиях бывшего СССР с конца 70-х годов предпринималось несколько попыток освоения производства винтовой арматуры, но в настоящее время только несколько предприятий стран СНГ выпускают винтовой арматурный профиль, это, например, ОАО «Западно-сибирский металлургический комбинат» (Россия), ОАО «Череповецкий металлургический комбинат», ПАО «АрселорМиттал Кривой Рог» (Украина). В Казахстане винтовой арматурный профиль на данный момент не производиться. Поэтому развитие производства винтового арматурного проката в Казахстане позволит избавиться от зависимости от его поставки из-за рубежа, что может обеспечить серьёзный экономический эффект, особенно в строительстве транспортных и подземных сооружений.

Процесс производства любой арматуры, в том числе винтового профиля, отличается трудоемкостью. Он проходит под строгим контролем, а при изготовлении соблюдаются требования, указанные в государственных стандартах качества. Благодаря этому изделие отличается высоким качеством и имеет высокие прочностные и эксплуатационные характеристики.

Традиционно стальную арматуру получают из круглого подката горячей прокаткой для образования арматурного профиля и последующей закалкой низколегированной стали для обеспечения требуемых механических и пластических свойств [1]. Недостатком таких способов является использование энергоемких процессов горячей деформации и термической обработки.

Современные же способы совмещают процессы формирования подката, его горячую пластическую деформацию для образования арматурного профиля и термического упрочнения (закалки).

Известен, например, способ термомеханической обработки проката [2], относящийся к черной металлургии, в частности к изготовлению термоупрочненной стержневой арматурной стали в крупных профилях с использованием тепла прокатного нагрева из непрерывно-литой низколегированной стали при термическом упрочнении проката в потоке среднесортных станов. Однако способ требует создания специализированной поточной линии с наукоемкой системой согласования скоростей обработки и предусматривает энергоемкую операцию пластического формирования арматурного профиля. К тому же обеспечить тепловые условия обработки непрерывно-литой заготовки удается только для крупных профилей.

Известен способ прокатки арматуры периодического винтового профиля из легированной стали 25Г2С, 30ХГ2С, 35ГС для железобетонных конструкций [3], включающий горячую прокатку арматуры из трубчатой заготовки и накатку гребней на ее поверхности в виде рифов, при этом гребни накатывают в горячем состоянии поперечной накаткой по правой или левой однозаходной или многозаходной винтовой спирали. Способ включает горячую прокатку и накатку винтовой спирали, которые являются весьма энергоемкими операциями и заметно повышают себестоимость продукции.

Также известен способ упрочнения арматурного стержня из материала, обладающего площадкой текучести [4], включающий скручивание арматурного стержня вокруг своей продольной оси с превышением предела текучести на растяжение материала наружных волокон арматурного стержня до достижения уровня предела прочности, при этом при скручивании один конец арматурного стержня закреплен, а скручивание арматурного стержня производят с другого конца до образования нераскручивающейся винтовой формы по всей длине стержня. Недостатком данного способа является то, что процесс получения арматуры разделен на отдельные операции, такие как: резка заготовки арматурного стержня; закрепление одного конца заготовки арматурного стержня; скручивание заготовки арматурного стержня; раскрепление конца арматурного стержня. Такая последовательность операций процесса получения арматурных стержней требует больших затрат времени и, соответственно, представляется малопроизводительным процессом. Кроме того, данный способ не обеспечивает необходимых эксплуатационных и прочностных характеристик.

3. Новая схема ИПД

Альтернативным вариантом решения проблемы упрочнения арматурного профиля является использования интенсивной пластической деформации (ИПД) [5] при его производстве. В настоящее время уже разработано целый ряд совмещенных процессов [6-14], которые позволяют обрабатывать длинномерные заготовки с достаточной степенью проработки литой структуры металла для получения в нем ультрамелкозернистой структуры. При этом многие из данных совмещенных способов деформирования позволяют получать в процессе их реализации не только полуфабрикаты, но и готовые изделия. Одной из последних таких разработок является процесс, предложенный в работе [15], который совмещает редукционную прокатку стержня круглого или квадратного поперечного сечения в квадратном калибре со скручиванием в формовочной матрице (скручивающем механизме). Данный совмещенный способ позволяет получать упрочненный арматурный профиль с градиентной ультрамелкозернистой структурой [16]. Несмотря на достаточно простую конструкцию и эффективную проработку исходной заготовки (за один цикл деформирования происходит развитие деформации от 0,8 в центральных слоях заготовки до 1,4 в поверхностных слоях), данный способ имеет существенный недостаток, связанный с его технологичностью. При переводе производства на сортамент другого размера понадобится не только новая матрица, но и новая пара валков с калибром заданных размеров.

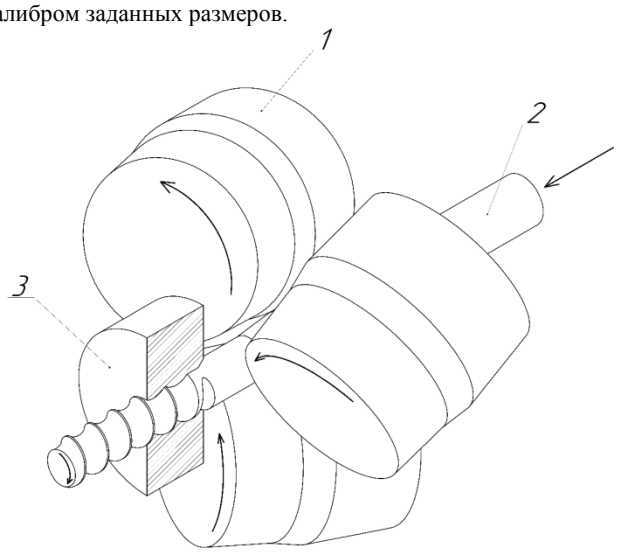

Рис. 1. *Совмещенный способ получения арматурного профиля: 1 – прокатные валки, 2 – заготовка, 3 – матрица*

С целью повышения технологичности процесса получения упрочненного арматурного профиля, нами была предложена новая схема его формирования, включающая деформирование заготовки круглого поперечного сечения на стане радиально-сдвиговой прокатки (РСП) и последующее скручивание заготовки в формовочной матрице специальной конструкции (рис. 1) (аналогичной представленной в работе [15]). При реализации предложенной технологии на практике не потребуется замена пары валков с калибром заданных размеров на новую пару при переналадке производства на новый типоразмер арматурного профиля, а потребуется только замена матрицы на новую матрицу с нужными геометрическими размерами. Это связано с тем, что при деформировании

заготовок различного диаметра на стане радиально-сдвиговой прокатки регулируется простым сведением или разведение валков. Помимо всего прочего использование вместо продольной прокатки именно радиально-сдвиговой прокатки обеспечит более интенсивную проработку исходной структуры металла и обеспечит формирование градиентной ультрамелкозернистой структуры, за счет того что, в очаге деформации при радиально-сдвиговой прокатке реализуется схема напряженного состояния близкая к всестороннему сжатию с большими деформациями сдвига [16-20]. Именно такая схема деформирования является оптимальной для формирования в различных материалах градиентной ультрамелкозернистой структуры при минимальном количестве проходов.

Данное исследование финансировалось Комитетом науки Министерства науки и высшего образования Республики Казахстан (Грант № AP14869135).

Литература

1. Железобетонные конструкции. Общий курс / В.Н. Байков, Э.Е. Сигалов. - М.: Стройиздат, 1991. - 767 с.

2. Белов Е.Г., Галиуллин Т.Р., Дикань О.В., Ефимов О.Ю., Зезиков М.В., Клепиков А.Г., Никиташев М.В., Чернов И.М., Чинокалов В.Я. Способ термомеханической обработки проката. Патент RU 2340684, 2008г.

3. Артюшин Д.В., Нежданов А.К., Нежданов К.К. Способ проката горячекатаной арматуры периодического профиля. Патент RU 2467075, 2009 г.

4. Федоров А.Д., Федорова А.Д. Способ упрочнения арматурного стержня из материала, обладающего площадкой текучести. Патент RU 2457259, 2012г.

5. Qi Y., Kosinova A., Kilmametov A.R., Straumal B.B., Rabkin E. Stabilization of ultrafine-grained microstructure in high-purity copper by gas-filled pores produced by severe plastic deformation. Scripta Materialia. 2020, Vol. 178, pp. 29-33.

6. Cheng Xu, Steven Schroeder, Patrick B. Berbon, Terence G. Langdon, Principles of ECAP-Conform as a continuous process for achieving grain refinement: application to an aluminum alloy, Acta Mater. 58 (4) (2010) 1379-1386.

7. I.P. Semenova, A.V. Polyakov, G.I. Raab, R.Z. Valiev, T.C. Lowe, Enhanced fatigue properties of ultrafine-grained ti rods processed by ECAP-Conform, Journal of materials science 47 (22) (2012) 7777-7781.

8. В.Н. Баранов, Д.С. Ворошилов, Р.И. Галиев, И.Н. Довженко, Н.Н. Довженко, Е.С. Лопатина, С.Б. Сидельников, С.В. Солдатов, Устройство для непрерывного литья, прокатки и прессования цветных металлов и сплавов, Патент РФ 2457914.

9. A. Naizabekov, S. Lezhnev, E. Panin, I. Volokitina, A. Arbuz, T. Koinov, I. Mazur, Effect of combined rolling - ECAP on ultrafine-grained structure and properties in 6063 Al alloy, Journal of Materials Engineering and Performance 28 (2019) 200-210.

10. A. Naizabekov, I. Volokitina, S. Lezhnev, A. Arbuz, E. Panin, A. Volokitin, Structure and Mechanical Properties of AISI1045 in the Helical Rolling–Pressing Process, Journal of Materials Engineering and Performance 29 (2020) 315 – 329.

11. М.В. Чукин, Д.Г. Емалеева, М.П. Барышников, М.А. Полякова, Способ получения длинномерных заготовок круглого поперечного сечения с ультрамелкозернистой структурой, Патент РФ 2446027, 2012 г.

12. М.А. Полякова, М.В. Чукин, Э.М. Голубчик, А.Е. Гулин, Устройство для изготовления проволоки с ультрамелкозернистой структурой, Патент РФ 130525.

13. K. Muszka, M. Wielgus, J. Majta, K. Doniec, M Stefanska-Kaclziela, Influence of strain path changes on microstructure inhomogeneity and mechanical behavior of wire drawing products, Mater. Sci. Forum 654-656 (2010) 314-317.

14. I.E. Volokitina, A.V. Volokitin, A.B. Naizabekov, S.N. Lezhnev, Change in structure and mechanical properties of grade A0 aluminum during implementation of a combined method ECAP-drawing technology, Metallurgist 63 (2020) 978-983.

15. Г.И. Рааб, А.Г. Рааб, Способ упрочнения и формирования винтового арматурного стержня. Патент РФ 2640705, 2018г.

16. G.I. Raab, A.G. Raab, A new combined method of intensive plastic deformation with the formation of the screw profile of the rod, Machines. Technologies. Materials (2018) 320-322.

17. С.П. Галкин, И.В. Доронин, А.Е. Антощенков, Ю.А. Лукина, Е.Н. Романова, Использование радиально-сдвиговой прокатки для получения в сталях ледебуритного класса структуры естественных дисперсно-упрочненных композиционных материалов, Технология металлов 4 (2007) 6-8.

18. И.Ш. Валеев, А.Х. Валеева, Изменение микротвердости и микроструктуры меди М1 при радиально-сдвиговой прокатке, Письма о материалах 3 (1) (2013) 38-40.

19. Галкин С.П. Траекторно-скоростные особенности радиально-сдвиговой и винтовой прокатки. «Современные проблемы металлургии». – Днепропетровск: "Системні технології", 2008. Т. 11. – С. 26-33.

20. Формирование наноструктурированных состояний и связанных с ними улучшенных свойств материалов медицинского и технического назначения/ Колобов Ю.Р., Иванов М.Б., Голосов Е.В.// Наносистеми, наноматеріали, нанотехнології (Nanosystems, Nanomateri-als, Nanotechnologies). 2011. Т. 9, № 2. – С. 489-498.

ИЗУЧЕНИЕ ЗАКРЫТИЯ ВНУТРЕННИХ ДЕФЕКТОВ ПРИ ДЕФОРМИРОВАНИИ В СТУПЕНЧАТО-КЛИНОВИДНЫХ БОЙКАХ

STUDY OF THE INTERNAL DEFECTS CLOSURE DURING DEFORMATION IN STEP-WEDGE STRIKERS

Evgeniy Panin[1], Abdrakhman Naizabekov[2], Andrey Volokitin[1], Irina Volokitina[2], Andrey Tolkushkin[3], Oxana Salko[2]

[1]Karaganda Industrial University, Temirtau, Kazakhstan
[2]Rudny Industrial Institute, Rudny, Kazakhstan
[3]Ural Federal University, Yekaterinburg, Russia
cooper802@mail.ru

Abstract: *In this paper, the influence of the technological process of forging workpieces in step-wedge strikers on the closure of internal defects is studied. The studies were carried out using model ingots with natural cast metal defects corresponding to a real object. A non-destructive testing method was used as a method of investigating the closure and healing of internal defects. The analysis of the data obtained during the experiments showed that the use of the proposed technology for forging blanks in step-wedge-shaped strikers has an advantage over forging according to the current technology in flat strikers, since according to the proposed technology, not only the closure of internal defects occurs when forging 1,2, but also the brewing of part of the defects, which is not observed when forging according to the current technology.*

Keywords: *FORGING, STEP-WEDGE STRIKERS, MODEL INGOT, INTERNAL DEFECTS, CLOSING AND HEALING OF DEFECTS, NON-DESTRUCTIVE TESTING METHOD.*

1. Введение

При производстве слитков различными методами литья (непрерывное, сифонное, в изложницу) в них неизбежно образуются дефекты литья, снижающие качество металла и соответственно его механические и эксплуатационные характеристики. Для устранения дефектов литья слитки подвергаются обработке давлением, и в том числе ковке.

Существующие в настоящее время технологии ковки основаны на использовании традиционного кузнечного инструмента и режимов деформирования, характеризующихся невысоким уровнем механических свойств и неравномерным распределением их по сечению металла поковок. Использование же нового кузнечного инструмента, реализующего сдвиговые или знакопеременные деформации, позволяет повысить качество металла поковок за счет измельчения исходной микроструктуры до мелкозернистого состояния [1].

В настоящее время разработано множество кузнечных инструментов, позволяющих реализовывать в процессе деформирования сдвиговые или же знакопеременные деформации. Результаты анализа влияния различных конструкций кузнечных инструментов на повышение качества получаемых поковок и заготовок представлено в многочисленных работах [2-9].

Одним из инструментов для ковки (протяжки), обеспечивающим знакопеременную схему деформирования, являются ступенчато-клиновидные бойки [10] (рис. 1). Данные бойки имеют следующую конфигурацию: наклонный участок и меньшая ступень верхнего бойка в поперечном сечении выполнены в виде клина, а нижнего бойка в виде аналогичной клиновидной впадины, причем длина меньшей ступени с клиновидной впадиной нижнего бойка сделана длиннее верхнего во избежание образования зажимов на заготовке.

Целью данной работы является исследование влияния процесса ковки заготовок в ступенчато-клиновидных бойках на закрытие внутренних дефектов.

Как известно, для анализа эффективности работы того или иного кузнечного инструмента в том числе применяют и методы оценки закрытия искусственных дефектов. Но недостатками этих методов является то, что при моделировании дефекта нарушается естественность исходного строения металла, а этап подготовки образцов для экспериментальных исследований получается достаточно трудоемким. Поэтому авторами работы [11] при исследовании влияния процесса ковки заготовок в различных кузнечных инструментах на закрытие внутренних дефектов было предложено использовать модели с естественными дефектами литого металла, соответствующими действительному реальному объекту, а также применять при этом методику исследования залечивания внутренних дефектов неразрушающими методами контроля [12]. И именно данная методика была применена для достижения поставленной цели.

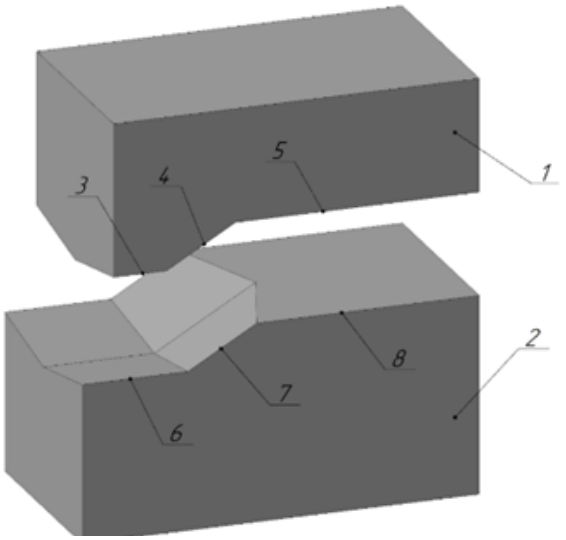

Рис. 1. Ступенчато-клиновидные бойки: 1 – верхний боек; 2 – нижний боек; 3 – меньшая ступень с клином верхнего бойка, 4 – наклонный участок с клином верхнего бойка; 5 – большая плоская ступень верхнего бойка; 6 – меньшая ступень с клиновидной впадиной нижнего бойка; 7 – наклонный участок с клиновидной впадиной нижнего бойка; 8 – большая плоская ступень нижнего бойка

2. Методика эксперимента

Для проведения запланированных лабораторных исследований в условиях кислородно-конвертерного цеха АО «АрселорМиттал Темиртау» были получены модельные слитки из стали 08 кп. Модельные слитки отливали в специально подготовленные конусные изложницы прямоугольного поперечного сечения, имеющие внутренние размеры тела изложницы у нижнего основания (35×65) мм, высота тела изложницы 220 мм, толщина стенки 10 мм, угол наклона стенок тела изложницы 7°. Для предотвращения приваривания жидкого металла к стенкам изложницы перед каждой заливкой внутренняя поверхность изложницы известковалась раствором

гашеной извести с последующей просушкой до температуры 150°С. Для уменьшения обезуглероживания поверхностных слоев заливаемого в изложницу металла, на известковый слой наносилась смесь графитового порошка с жидкой консистентной смазкой типа негрол. После нанесения графита изложницы также прокаливались при температуре 280 ÷ 300°С. Метал перед заливкой в изложницу раскисляли порошком алюминия. Кристаллизация и остывание полученных моделей слитков до температуры 900°С осуществлялась в естественных условиях. Для улучшения условий ультразвукового контроля модельные изложницы с моделями слитка после кристаллизации залитого металла и остывания до 900°С резко охлаждали под проточной струей воды, добиваясь закалки и фиксирования мелкозернистой ферритно-перлитной структуры. Это обеспечивает малое рассеяние ультразвука [13].

Раздетые модели слитков профрезеровали с верхнего и нижнего торцов, а затем вдоль боковых сторон до параметра шероховатости порядка R_Z (20÷60). На рисунке 2 представлена боковая поверхность отфрезерованного слитка и вышедшие на нее дефекты в виде газовых пузырей.

Рис. 2. Фрагменты поверхности модели слитка с газовыми пузырями

Далее на фрезерованную боковую поверхность модели каждого слитка нанесли ортогональную разметочную сетку с шагом 10 мм и провели ультразвуковой контроль в каждой ячейке на предмет выявления дефектов, их размеров и глубины залегания. Контроль полученных результатов осуществлялся эхометодом с помощью дефектоскопа УД-13УР В1П1 по ГОСТ 24507 – 80. Тарировка дефектоскопа осуществлялось с помощью контрольных образцов №1 КЫ5. 170. 004 и ЗР Щ08. 899. 248. Прозвучивание образцов осуществлялось раздельно–совмещенными прямым и наклонным преобразователями. Причем луч наклонного преобразователя при контроле сначала направляли слева направо, а затем справа налево для повышения вероятностей обнаружения различно ориентированных дефектов. Угол ввода луча наклонного преобразователя выбран равным 45°. Это сделано для упрощения процедуры определения координат местонахождения дефекта и фиксирования дефектов, находящихся на вертикали под пересечениями ортогональной координатной сетки, нанесенной на боковую поверхность модельного слитка.

Анализ результатов данных исследований показал, что имеющиеся в модельных слитках дефекты имеют сферическую форму и произвольную ориентацию в пространстве. При этом размер дефектов от 1,2 мм до 5 мм, т.е. были получены дефекты газовый пузырь различных размеров. Это позволит при дальнейших исследованиях, выбирать газовый пузырь необходимого размера и местоположения и обеспечивает соблюдение условия масштабного и физического моделирования.

Сам лабораторный эксперимент по деформированию модельных слитков в ступенчато-клиновидных бойках проводили на гидравлическом прессе в условиях Карагандинского индустриального университета. Для проведения эксперимента были подготовлены в ступенчато-клиновидные бойки с углом наклона 30° и с углом клина верхнего бойка и клиновидной впадины нижнего бойка равным 160°.

Для равномерного распределения деформации кузнечный инструмент был нагрет до температуры 250ºС, а стальные модельные образцы - до ковочной температуры 1050ºС. Деформирование заготовок осуществляли следующим образом: нагретые заготовки подавали в ступенчато-клиновидные бойки на первую ступень с клином на верхнем бойке и клиновидной впадиной на нижнем бойке. После обжатия заготовки на первой ступени осуществляли подачу заготовки на наклонный участок и так же производили обжатие. После чего заготовку уже подавали на вторую плоскую ступень, на которой производили выпрямление данной заготовки (рис. 3). Таким образом заготовку подвергали обжатию по всей длине. Уков при этом составил 1,1. Вторую партию модельных заготовок подвергли двум проходам деформирования без кантовки по схеме деформирования представленной выше. Уков после 2-х проходов составил - 1,2.

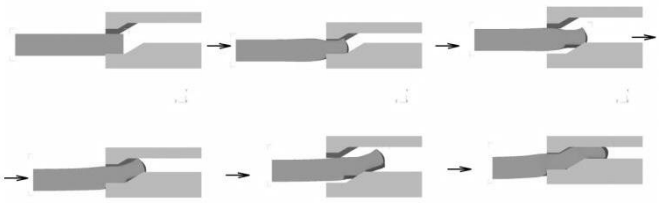

Рис. 3. Схема деформирования заготовок в ступенчато-клиновидных бойках

Третья и четвертая партия модельных заготовок были продеформирована по действующей технологии в плоских бойках, также с уковами 1,1 и 1,2.

3. Результаты и обсуждение

Степень закрытия дефектов после деформирования модельных заготовок фиксировали по выше представленной методике. При этом проводили ультразвуковой контроль в каждой ячейке на предмет выявления дефектов, их размеров и глубины залегания.

По результатам проведенного исследования выявили, что при ковке заготовок в плоских бойках с уковом 1,1 дефекты в осевой зоне приняли сплющенную форму, но закрытие дефектов не наблюдалось, в периферийной и промежуточной частях заготовки дефекты приняли просто овальную форму. Поведение дефектов в заготовках, откованных в ступенчато-клиновидных бойках с аналогичным уковом, носит другой характер: дефекты с малыми размерами по всему поперечному сечению начали закрываться, а дефекты размерами 4-5 мм сильно сплющились не только в поперечном, но и в продольном направлении. Такое поведение дефектов обосновывается тем, что из-за реализации дополнительных знакопеременных деформаций при ковке заготовок по предлагаемой технологии в ступенчато-клиновидных бойках происходит благоприятное течение металла, влияющее на закрытие и заваривание внутренних несплошностей.

Как известно, при закрытии дефектов, и в частности газовых пузырей, поверхность закрытого дефекта еще фиксируется неразрушающим контролем, так как является границей раздела сред металл – окисная пленка. После заваривания поверхность дефекта исчезает, так как окисная пленка разрушается, и она не отражает контрольной волны, то есть становится невидимой [14].

При ковке 1,2 в заготовках, продеформированных в плоских бойках дефекты малых размеров в зоне ковочного креста закрылись, а дефекты больших размеров (4÷5 мм) в зоне ковочного креста и практически все дефекты (малые и большие) в остальных зонах заготовки из-за растягивающих напряжении приняли просто сплющенную форму.

Анализ результатов прозвучивания дефектов в модельных заготовках, откованных с уковом 1,2 в ступенчато-клиновидных бойках, показал, что волны в большинстве случаев перестали отражаться в местах, где находились

дефекты размерами 1,5÷2 мм, что свидетельствует о заваривании этих дефектов практически по всему объему деформируемых заготовок. Также произошло и закрытие всех дефектов размерами больше 2 мм практически по всему объему деформируемой заготовки, но ультразвуковая волна продолжала отражаться. Именно закрытие этих дефектов, а не заваривание, может быть объяснено тем, что при разливке в объеме слитка могли находиться неметаллические включения, которые в ходе деформирования мешают полному исчезновению дефектов.

Выводы

В ходе проведенных исследований было установлено, что при использовании предлагаемой технологии ковки заготовок в ступенчато-клиновидных бойках уже при малых степенях обжатий (при укове 1,2) происходит не просто закрытие внутренних дефектов, но и их заваривание, что не наблюдается при ковке заготовок по действующей технологии в плоских бойках. Эти исследования еще раз доказали преимущество использования на практике кузнечных инструментов, при ковке в которых в процессе деформирования реализуются дополнительные сдвиговые или знакопеременные деформации, так как ковка в таких кузнечных инструментах позволяет получать более качественные поковки и заготовки (без дефектов) при меньшем укове.

Данное исследование финансировалось Комитетом науки Министерства науки и высшего образования Республики Казахстан (Грант № AP09057965).

Литература

1. Найзабеков А.Б. Научные и технологические основы повышения эффективности процессов ковки при знакопеременных деформациях. - Алматы: Гылым, 2000. - 336 с.

2. Андреященко В.А., Ичева Ю.Б., Особенности деформационного поведения конструкционной стали при ковке, Вестник Пермского национального исследовательского политехнического университета. Механика, 2018, № 4, С. 7-19.

3. Markov O.E., Perig A.V., Zlygoriev V.N., Markova M.A., Grin A.G. (2017) A new process for forging shafts with convex dies. Research into the stressed state. Int J Adv Manuf Technol 90(1):801–818. The International Journal of Advanced Manufacturing Technology volume 90, pages801–818 (2017) doi:10.1007/s00170-016-9378-6

4. Banaszek G., Berski S., Dyja H. Numerical analysis of the torsion stretch forging operation in asymmetrical anvils. Metall. Min. Ind. 2011;3:98–101.

5. Каргин С.Б. Компьютерное моделирование напряженно-деформированного состояния в круглой заготовке, обжатой вырезными профилированными бойками // Обработка материалов давлением: сб. науч. тр. – Краматорск: ДГМА, 2012 №1 (30). – С. 16-23.

6. Lezhnev S., Naizabekov A., Panin E., Stepankin I., Kuis D. Simulation of the forging process with an additional macro-shift in “DEFORM” software package// Journal of Chemical Technology and Metallurgy, 57, 1, 2022, 195-204.

7. Naizabekov A.B., Lezhnev S.N., Panin E.A. Research of the deformation process of blanks in the dies with elastic elements.// Journal of Chemical Technology and Metallurgy, 52, 2, 2017. – pp. 205-212.

8. Development and investigation of the forging method of long-length blanks with mutual displacement of anvils. Vladimir P. Volkov, Denis R. Salikhyanov, Ivan S. Kamantsev. Journal of Chemical Technology and Metallurgy, 55, 3, 2020. pp. 571-579.

9. Алиев И.С., Жбанков Я.Г., Грачев И.А. Исследование процесса ковки плит плоскими бойками со скосами // Обработка материалов давлением: сб. науч. тр. – Краматорск: ДГМА, 2014 - №2 (39). – С. 69-74.

10. Инновационный патент РК №30420. Инструмент для изготовления поковок. Найзабеков А.Б., Лежнев С.Н., Панин Е.А., Толкушкин А.О. 2015, Бюл. 10.

11. Моделирование дефекта типа «газовый пузырь» для последующего исследования в процессах обработки металлов давлением/ Найзабеков А.Б., Исаенко В.В., Кулжабаева А.А., Шевцов А.Н.// Труды международной научно-технической конференции «Научно-технический прогресс в металлургии», 2003. - С. 384 – 388.

12. Сегал В.М., Павлик Д.А. Анализ условий залечивания микродефектов при горячей деформации литого металла/ Кузнечно-штамповочное производство. 1982, №9. – С. 6-9.

13. Ультразвуковой и рентгеновский контроль отливок/ Гусев Е.А., Карпильсон А.Е., Потапов В.П. и др. – М.: Машиностроение. 1990. – 208 с.

14. Неразрушающий контроль. Акустические методы контроля: Практическое пособие/ Под редакцией Сухорукова В.В. – М.: Высшая школа, 1991. -283 с.

Study of the radial shear rolling effect on the gradient microstructure formation in technical titanium and mechanical properties changes

Abdrakhman Naizabekov[1], Irina Volokitina[1], Alexandr Arbuz[2], Andrey Tolkushkin[3], Darkhan Nurakhmetov[1]
[1]Rudny Industrial Institute, Rudny, Kazakhstan
[2]Nazarbayev University, Astana, Kazakhstan
[3]Ural Federal University, Yekaterinburg, Russia
naizabekov57@mail.ru

Abstract: *The work is devoted to experimental studies of the influence of radial shear rolling on the microstructure evolution of the VT-1 titanium alloy and its gradient distribution over the cross section, as well as changes in mechanical properties. In the course of the conducted studies, two different types of microstructure were obtained. At the periphery of the bar near the surface, a relatively equiaxed ultrafine-grained structure with a grain size of 300-600 nm was obtained, while in the axial zone of the bar, an oriented striped texture was obtained. The resulting structure difference of the peripheral and central zones indicates the gradient nature of the structure distribution. This type of distribution is confirmed by the results of the microhardness study over the cross section of a bar rolled to a diameter of 15 mm. The ultimate strength after deformation increased by 58%, while the elongation decreased by 15%.*
Keywords: *RADIAL SHEAR ROLLING, GRADIENT MICROSTRUCTURE, TECHNICAL TITANIUM, MECHANICAL PROPERTIES.*

1. Introduction

The achievements of modern medicine in the field of implantation are impossible without the productive joint work of scientists, doctors themselves and technical specialists of various specialties, including materials scientists. It was their joint work that made it possible to achieve a long stay in the human body of various implantation materials and structures made of them: rods and plates for connecting damaged bone structures; dentures; endoprostheses and others. But, despite the existing achievements in this direction, there are still problems and questions in the field of development and application of modern materials for implantation. Therefore, the development of both new biocompatible implantation materials and technology for the formation of enhanced, and sometimes unique, properties already in known biocompatible materials is still an urgent direction. At the same time, special attention should be paid to the development of technology for producing long-length products from biocompatible materials with an increased level of mechanical properties.

One of the main and most commonly used methods for increasing the mechanical properties of both ferrous and non-ferrous metals and alloys for more than a decade is the grinding of the structure of these materials to an ultra-fine-grained, and preferably to a nanostructured state [1]. However, for most materials, the growth of strength properties in ultrafine-grained materials is accompanied by an inevitable decrease in its plastic properties, and as a result, such a material becomes brittle and is subject to destruction during stretching. The solution of this problem prompted scientists to develop a new direction in the field of obtaining new materials – the creation of (functional) gradient materials [2]. One of the main features of such materials is the anisotropy of their properties in a given direction, and this is achieved most often by the formation of appropriate structures. The authors of [3-6] have proved that the production of metallic materials with a gradient structure (the coarse-grained state of the metal in the central part of the workpiece, smoothly growing to an ultra-fine-grained state on the surface) is an effective way to increase the plasticity, not of the metal itself, but of metal products as a whole.

It has long been proved that one of the promising and less expensive methods of obtaining ultrafine-grained materials is severe plastic deformation (SPD) [7-8], which can be implemented in metal in various ways [9-13], including the so-called radial shear rolling [14], which just has prospects for obtaining precisely gradient ultrafine-grained materials. This is due to the fact that in the deformation focus during radial shear rolling, a stress-strain state scheme is implemented, which is very close to the all-round compression scheme with large shear deformations. Radial shear rolling also has its own features:

- nonmonotonicity and turbulence of deformation;
- different plastic flow of metal due to the trajectory-velocity features of the process and, as a consequence, different elaboration of the structure of different zones of the workpiece.

2. Experimental part

Due to the peculiarities of the metal flow during radial shear rolling, intense shear deformations are localized in the annular cross-sectional area characteristic of the three-roll scheme. At the same time, in the outer layer of the deformable workpiece, each small trajectory-oriented element undergoes compression deformation along its radius and in the direction of outflow (along the helical trajectory), and stretching deformation across the helical trajectory [15]. It should also be noted that during radial-shear rolling, a constant gradient of velocities and directions of flow along the radius is observed, which also adds additional shear elements to the overall complex picture of the stress-strain state. During such processing, the elements of the structural structure of the metal subjected to an expanding flow with a two-sided sediment (along the trajectory and along the radius) take the form of isotropic isolated particles of high dispersion [15].

As it is known, titanium has biocompatible properties, therefore, the purpose of this work is to study the effect of radial shear rolling on the possibility of forming a gradient structure in it and an increased level of mechanical properties.

The experiment was carried out on the SVP-08 radial shear rolling mill, which is designed for hot deformation of bars of solid circular cross-section made of various metal (ferrous and non-ferrous metals and alloys) and composite materials. VT-1 titanium rods (0.08% C; up to 0.25% Fe; up to 0.07% C; up to 0.1% Si; up to 0.04% N; up to 0.2% O, 99.24-99.7% Ti) with an initial diameter of 30 mm were used as initial blanks. The choice of this grade of titanium is due to the fact that it has mechanical properties commensurate with the mechanical properties of non-rusting steels, and titanium alloying and heat treatment of alloys based on it can achieve the strength level of high-strength steels. Based on the recommendations of works [16-17], titanium rods were rolled on a radial shear rolling mill at a temperature equal to 500 ° C. At the same time, rolling was carried out to the final diameter of 15 mm in stages, i.e. in 5 passes, with compression of 3 mm in each pass. After the 5th pass, the bars were subjected to intensive cooling with water. The bars were also subjected to intensive cooling with water after each pass, which were intended not for further deformation, but for studying the evolution of the microstructure and changes in mechanical properties.

3. Results and discussion

After rolling and cooling, cylinders with a length of 30 mm were cut out of rods of various diameters (from 27 to 15 mm), as well as the original rod. After that, samples for mechanical tests, microhardness measurements and microstructure studies on a

transmission electron microscope were cut into strips of 0.3×3×30 mm in size along these cylinders on a high-precision AccuTom-5 cutting machine. Subsequently, samples for microstructure research on a transmission electron microscope JEM-2100 (JEOL, Japan) at an accelerating voltage of 200 kV were subjected to electrolytic thinning on a TenuPol-5 installation to obtain a thin foil from the peripheral and axial zones of the rod along the rolling direction. The most characteristic view of the microstructure of both parts of the rod is shown in Figure 1.

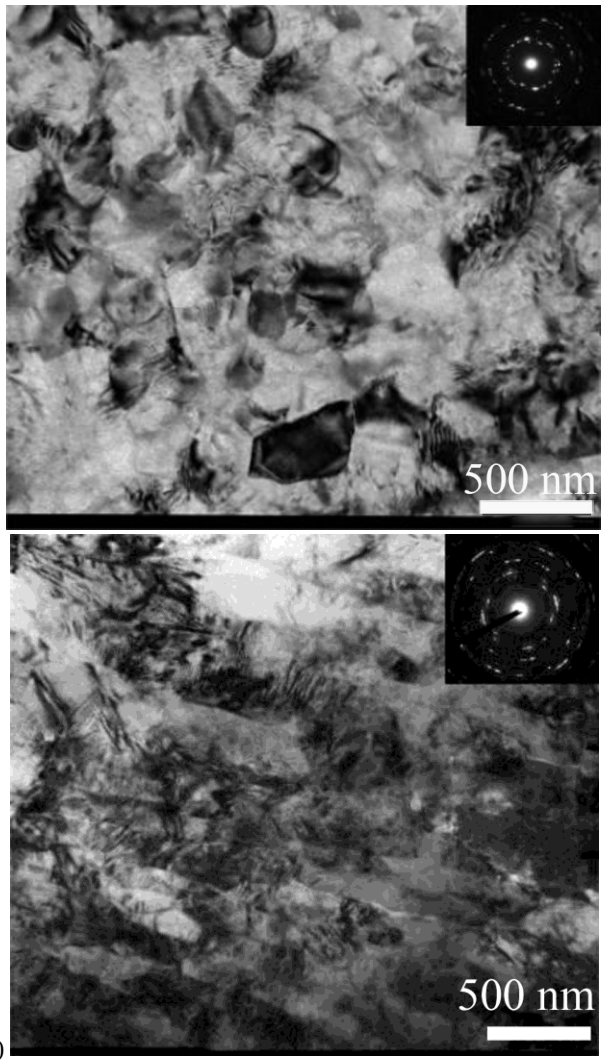

Fig. 1. *Titanium structure after radial shear rolling up to a diameter of 15 mm and cooling in water: a - peripheral part of the bar; central part of the bar*

Metallographic analysis showed that technical titanium of the VT-1 brand in its initial state has a coarse-grained structure with an average grain size of 70-80 microns. As expected, the microstructure of the peripheral and axial zones after radial shear rolling up to a diameter of 15 mm was not the same. Thus, in the peripheral region of the rod, the microstructure is represented to a greater extent by equiaxed ultrafine grains of 300-600 nm in size, which have high misorientation angles, which is established by the diffraction pattern. The microstructure of the axial zone of the rods after deformation on the radial shear rolling mill is represented by long and narrow grains elongated in the direction of rolling, that is, it is a fibrous texture. The diffraction pattern also confirms the small angles of grain misorientation. That is, as a result, in the peripheral part of the rod, where shear deformation with high turbulence of the metal flow prevailed, we have an equiaxial ultrafine-grained structure, and in the axial zone, where the metal flow had a laminar character along the rolling axis, we have an elongated, oriented structure, resembling the texture of rolling.

Tensile tests carried out on the Instron-1195 testing machine (ITW Inc., USA) showed that the tensile strength after radial shear rolling increased from 704 MPa to 1215 MPa, which is 58%, and the elongation after the fifth pass decreased from the initial 26% to 11%. The values of the tensile strength and relative elongation averaged after each pass (according to the results of 3 experiments with each degree of compression) are shown in Figure 2.

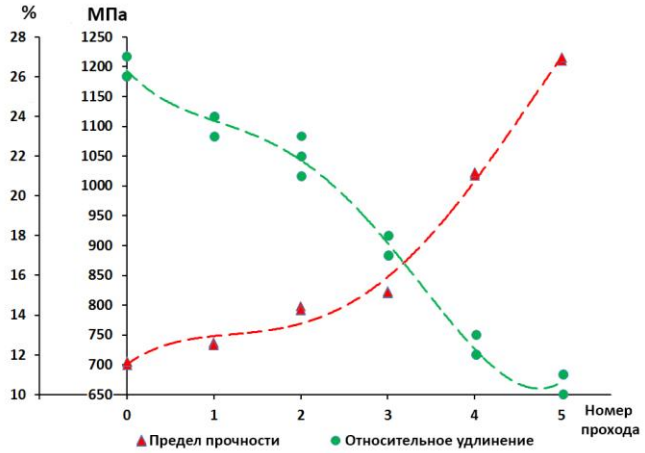

Fig. 2. *Change in the tensile strength and elongation of titanium grade VT-1 after radial shear rolling by passes*

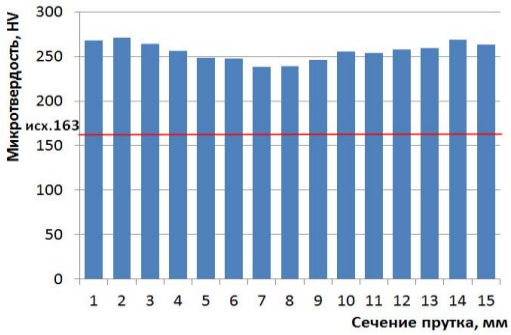

Fig. 3. *Change in microhardness of titanium grade VT-1 along the cross section of the bar after radial shear rolling up to a diameter of 15 mm*

Taking into account the heterogeneity of the resulting microstructure, microhardness was measured by the cross section of a titanium rod rolled to a diameter of 15 mm on the HVS-1000B microhardness meter (Winex Instrument, UK), which allowed us to construct the microhardness profile shown in Figure 3. Microhardness measurement was carried out by Vickers with a force of 9.87 N at a shutter speed of 15 seconds. The microhardness profile was constructed based on the results of measurements at 15 consecutive points located 1 mm apart.

After radial-shear rolling of a titanium bar to a diameter of 15 mm, the initial microhardness level rose from a value of 163 RM to 238-271 RM, i.e. on average by 60%. At the same time, due to the structural heterogeneity in the cross-section of the bar after rolling, the expected gradual decrease in the microhardness level in the central part by 12.4% relative to the periphery of the part of the bar is observed.

Conclusion

In the course of the conducted research on the deformation of rods made of technical titanium of the VT-1 brand on a radial shear rolling mill, a microstructure of two different types was obtained in them. Thus, a relatively equiaxed ultrafine-grained structure with a grain size of 300-600 nm was obtained at the periphery of the rod, while an oriented, striped texture was obtained in the central zone of the rod. The discrepancy in the structure of the peripheral and central zones of titanium alloy rods formed on the SVP-08 radial shear rolling mill indicates the gradient nature of the structure formed in the resulting rods. This was also confirmed by the results of measur-

ing and constructing a micro-hardness profile along the cross section of a bar rolled up to a diameter of 15 mm. A significant change in the initial microstructure of the titanium rod led to a significant increase in the tensile strength of this rod (by 58% after drawing equal to 4) and a decrease in the plastic characteristic (elongation) with this drawing from 26% to 11%. At the same time, there was a systematic increase in strength characteristics and a decrease in plastic characteristics after each deformation cycle.

This research was funded by the Science Committee of the Ministry of Science and Higher Education of the Republic of Kazakhstan (Grant no. AP14869128).

References

1. Structural nanocrystalline materials: Fundamentals and applications.// C.C. Koch, I.A. Ovid'ko, S. Seal, S. Veprek// Cambridge, Cambridge University Press, 2007.

2. Лисовский А.Ф. Формирование градиентной структуры в спеченных твердых сплавах (Обзор)// Сверхтвердые материалы, 2010, № 4, pp. 36-53.

3. Raab G.I., Simonova L.A., Aleshin G.N. Tailoring the gradient ultrafine-grained structure in low-carbon steel during drawing with shear // Metalurgija 55 (2016) 2, 177–180.

4. Raab A.G., Zhilyaev A.P., Kodirov I.S., Aleshin G.N. Features of structure formation and mechanical behavior of metallic materials under conditions of application of gradient deformations.// International Journal «Machines, Technologies, Materials», 2019, p.105-106.

5. Raab G.I., Raab A.G., Zhilyaev A.P. Gradient structure and methods for their preparation.// International Journal «Machines, Technologies, Materials», 2019, p.132-133.

6. Raab G.I., Kodirov I.S., Aleshin G.N., Raab A.G., Tsenev N.K. Influence of special features of the gradient structure formation during severe plastic deformation of alloys with different types of a crystalline lattice. Vestnik Magnitogorskogo Gosudarstvennogo Tekhnicheskogo Universiteta im. G.I. Nosova [Vestnik of Nosov Magnitogorsk State Technical University]. 2019, vol. 17, no. 1, pp. 64–75. https://doi.org/10.18503/1995-2732- 2019-17-1-64-75

7. Wojtas D., Wierzbanowski K., Chulist R., Pachla W., Bieda-Niemiec M., Jarzebska A., Maj L., Kawalko J., Marciszko-Wiackowska M., Wronski M. Microstructure-strength relationship of ultrafine-grained titanium manufactured by unconventional severe plastic deformation process. Journal of Alloys and Compounds. 2020. Vol. 837, № 155576.

8. Torabi H., Faraji G., Masoumi A. Processing characterization of binary Mg-Zn alloys fabricated by a new powder consolidation combined severe plastic deformation method. Journal of Alloys and Compounds. 2020. Vol. 832. № 154922.

9. Khelfa T., Munoz-Bolanos J.A., Li F., Cabrera-Marrero J.M, Khitouni M. Microstructure and Mechanical Properties of AA6082-T6 by ECAP Under Warm Processing. Metals and Materials International. 2020. Vol. 26, Iss. 8, pp. 1247-1261.

10. Shchetinin I.V., Bordyuzhin I.G., Sundeev R.V., Menushenkov V.P., Kamynin A.V., Verbetsky V.N., Savchenko A.G. Structure and magnetic properties of Sm 2 Fe 17 N x alloys after severe plastic deformation by high pressure torsion. Materials Letters. 2020. Vol. 274. № 127993.

11. Lin G.Y., Xiao M.Q., Feng D., Liu X.Y., Wang H.Y., Zhang R. Microstructural and mechanical properties of ZA10 alloy tubes and their weld seams prepared by Conform continuous extrusion. Rare Metals. 2020. Vol. 39, Iss. 6, pp. 707-715.

12. De Rango P., Fruchart D., Aptukov V., Skryabina N. Fast Forging: A new SPD method to synthesize Mg-based alloys for hydrogen storage. International Journal of Hydrogen Energy. 2020. Vol. 45, Iss. 14, pp. 7912-7916.

13. Konstantinov D.V., Korchunov A.G., Zaitseva M.V., Shiryaev O.P., Emaleeva D.G. Macro- and Micromechanics of Pearlitic-Steel Deformation in Multistage Wire Production. Steel in Translation. 2018. Vol. 48, Iss. 7, pp. 458-462.

14. Патент РФ № 2293619. Способ винтовой прокатки / С.П. Галкин. 20.02.2007. Бюл. 5.

15. Galkin S.P. Radial shear rolling as an optimal technology for lean production //Steel in Translation. – 2014. №44 (1). – P. 61-64.

16. C.S. Meredith, A.S. Khan. Texture evolution and anisotropy in the thermo-mechanical response of UFG Ti processed via equal channel angular pressing. International Journal of Plasticity 30–31 (2012) 202–217.

17. G.I. Raab , R.Z. Valiev , D. V. Gunderov , T. C. Lowe, A. Misra, Y.T. Zhu. Long-length Ultrafine-grained Titanium Rods produced by ECAP-Conform. Materials Science Forum Vols. 584-586 (2008) pp 80-85.

Cordon counting in the territory of the city of bitola

Atanasova Vaska[1], Stojanoska Marija[1], Krstanoski Nikola[1]
[1]Faculty of Technical Sciences – University of St. Kliment Ohridski, Bitola, Macedonia
E-mail: vaska.atanasova@uklo.edu.mk, marijastojanoska3112@gmail.com, nikola.krstanoski@uklo.edu.mk

Abstract: *The collection and analysis of transport data is of great importance for traffic engineers, who use that data to perceive existing problems and offer solutions. Depending on the type of data and the meaning available, there are different methods and equipment. Data collection can be done on sections, intersections, entire cities, hourly, daily, weekly, monthly and annually. For the city of Bitola, data collection was carried out for cars, buses and heavy goods vehicles in the peak hour according to the directions of movement, i.e. cordon counting, by setting up checkpoints with personnel on those roads that intersect with the cordon line. In this case, the vehicles in transit are important to us and we grouped them into two groups, cargo transit and individual traffic.*
Keywords: *PRIVATE TRANSPORT, PUBLIC TRANSPORT, CORDON, COUNTING, TRANSITIVE*

1. Introduction

In order to obtain information about the basic parameters of the traffic flow, the behavior of the participants in the traffic, etc. data collection is required. In the first, preparatory phase, the recording forms are prepared, the students are prepared for the data collection process for the defined area of coverage.

Traffic counting is performed manually, according to the type of vehicle (passengers, trucks, buses), counting is performed according to approaches/directions of movement. Each student was placed on a suitable approach and enters the data into a previously prepared form of a counting sheet.

The time period of data collection is 1 hour (peak hour).In this paper will be published the cordon counting of the city of Bitola, carried out at 3 counting points in the peak hour, from 14:00-15:00.

2. Collection and analysis of transport data

Every day we encounter a large amount of data. That data reaches the end users in a final and processed form. That data can be related to transportation, education, work, industry, etc. When it comes to transportation, the following data are presented to users: number of traffic accidents, number of transported passengers, cargo, harmful emissions, etc.

The collection and analysis of relevant data on the traffic system or its parts is of great importance for the performance of scientific research, studies, projects, expertise. These data allowes a clear understanding of the existing conditions and problems and represent a basis for solving the problems. The data collection phase implies going out into the field and serious preparations, with clearly defined objectives, methods, trained personnel and equipment for data collection.[4]

Depending on what kind of data we need, we choose the collection method, define the place and time of the collection, determine the necessary personnel and equipment, control the counters, arrive at the place on time, wear a fluorescent vest for greater security etc. Collecting can be manual, i.e. manual with a counting sheet and automatic with video cameras,control, cordon counting, etc.[2]

2.1. Cordon counting of vehicles

- **A cordon** is an imaginary boundary line around the space that is the subject of research. Usually it is a central city area or other center of activity, where it is important to determine the accumulation of vehicles in the given space. Vehicle counts in this case are carried out on all roads that cross the cordon line, classifying vehicles by direction and by time period from 15 minutes to one hour. This enables the estimation of the number of vehicles in the given area at a certain time. Sometimes cordon counts are done together with counts of a smaller intersection of roads, with this it is also possible to estimate the number of parking spaces.[2]

- **The cordon line** is placed so that it intersects all roads that enter the pre-defined area of interest. This intersection in the middle of blocks, between intersections, is done in order to avoid the problem of vehicles turning due to which it becomes unclear whether they enter the defined areaspace or not.It is convenient to choose the cordon line in such a way as to minimize the number of thoroughfares to be counted.[2]

- **The accumulation of vehicles** inside the cordon line is determined by summing up the total number of vehicles that enter and leave the given space in a certain period of time. The cordon counts should start when the street network inside the space that is the subject of the study is practically empty.If this is not possible, then counts are made of parked vehicles and vehicles on the streets to estimate the initial number of vehicles in the given space, when the cordon counting began. The accumulation of vehicles is calculated according to the formula:[2]

  $A_i = A_{i-1} + V_i - I_i$, where,

  A_i - number of vehicles in the period ‘’i’’ ,

  A_{i-1} - number of vehicles in the previous period ‘’i-1’’,

  V_i - number of vehicles entering period "i",

  I_i- number of vehicles leaving in period "i",

3. Cordon counting for the city of Bitola

On May 20, 2022 (Friday) from 14:00-15:00, a cordon counting of vehicles was carried out together with a group of students from the traffic department at the Technical Faculty-Bitola.[1]

The subject of research is to give an estimate of the accumulation of vehicles.

The aim of the research is to give an estimate of the number and structure of vehicles that transit through the territory of the city of Bitola.

The cordon supports an imaginary border line around the city of Bitola, and the counting of vehicles was carried out on all roads that cross the cordon line, namely: [3]

1. Road with approach to - from Prilep.

2. Road with access to - from Ohrid.

3. Road with approach to – from Greece.

These checkpoints are placed in such a way that they cross all the roads entering the city of Bitola, in order to avoid the problem of vehicles turning, which makes it unclear whether they enter the defined space or not. That is,

Zone 100-Prilep

Zone 101 Ohrid

Zone 102 Greece

Figure 1 shows the cordon line of the city of Bitola and the counting points.[1]

Fig.1**:** *Shows the cordon line and the counting points (Source: Google maps and the Paint tool)*

Figure 2 shows the cordon count form by vehicle structure where the location, date, count period, mobile phone, student, cars, buses, heavy goods vehicles are entered.[5]

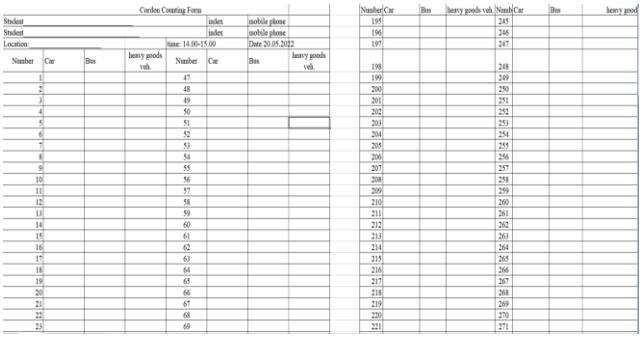

Fig.1: *Shows the form for cordon counting by vehicle structure(Source: Created in an Excel document)*

3.1 Results of counts by direction of movement

The results of the counts between 14:00 and 15:00 are shown in the following table by structure of vehicles and by direction of movement.

Table 1: *Results of counts by directions of movement*

	Greece -Bitola	**Bitola-Greece**	**Ohrid-Bitola**	**Bitola-Ohrid**	**Prilep-Bitola**	**Bitola-Prilep**
Car	534	491	141	143	613	586
Bus	47	13	1	1	16	27
HGV	31	23	49	22	36	69

From the obtained results we can conclude that the most intensive flows are on the direction from and to Prilep - Bitola, where about 660 vehicles are registered and in the opposite direction about 680 vehicles, while the second place in terms of intensity is the road direction from and to Greece - Bitola. There is a greater deviation on the road from and to Ohrid - Bitola, where we have registered about 190 vehicles. The largest flow of heavy goods vehicles appears on the road direction Bitola-Prilep, while the lowest flow of heavy goods vehicles occurs on the road direction Bitola-Ohrid, together with the direction Bitola-Greece.

3.2 Results of cordon counting

The accumulation of vehicles inside the cordon line is determined by summing up the total number of vehicles entering and leaving the given area in a certain period of time, with the results given in the following table.

Table 2: *Results of cordon counting*

	Greece -Prilep	**Greece -Ohrid**	**Ohrid-Prilep**	**Ohrid-Greece**	**Prilep-Ohrid**	**Prilep-Greece**
Car	41	9	4	14	6	38
Bus	12	0	0	0	0	2
HGV	6	2	4	2	0	3

3.3 Results for transit freight and individual traffic

Table 3: *Shows the results for transit freight traffic*

Transit freighttraffic			
External zone	**100**	**101**	**102**
100	0	0	3
101	4	0	2
102	6	2	0

Table 4: *Shows the results for transit individual traffic*

Transitindividual traffic			
External zone	100	101	102
100	0	6	40
101	4	0	14
102	53	9	0

3.4 Graphical display of output results

Graphic display of the number of cars by direction of movement

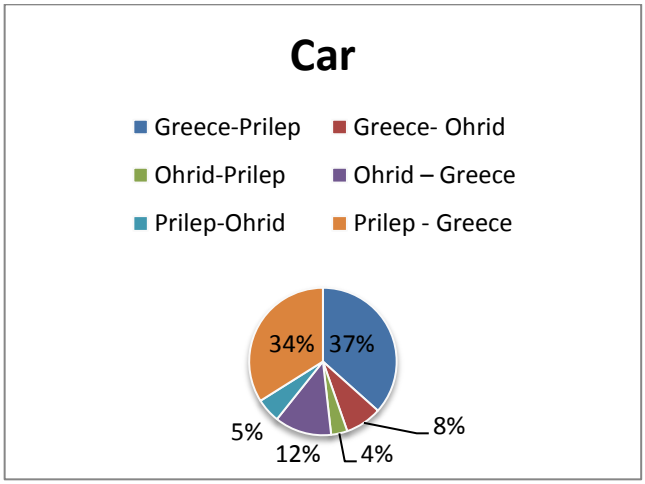

Chart 1: *The number of cars by direction of movement*

Graphic display of the number of buses by route

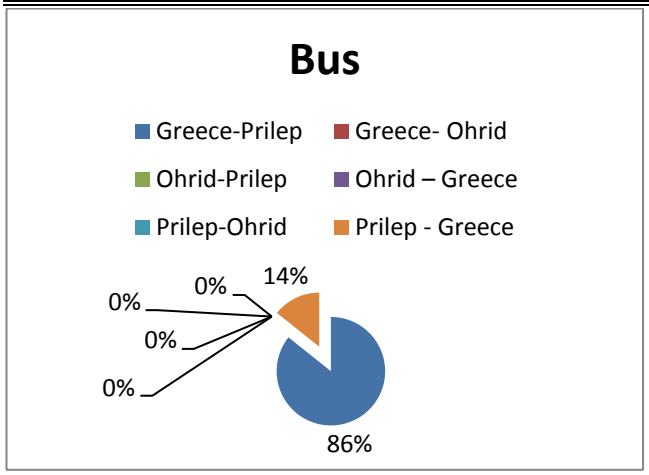

Chart 2: *The number of buses by route*

Graphic display of the number of heavy goods vehicles by direction of movement.

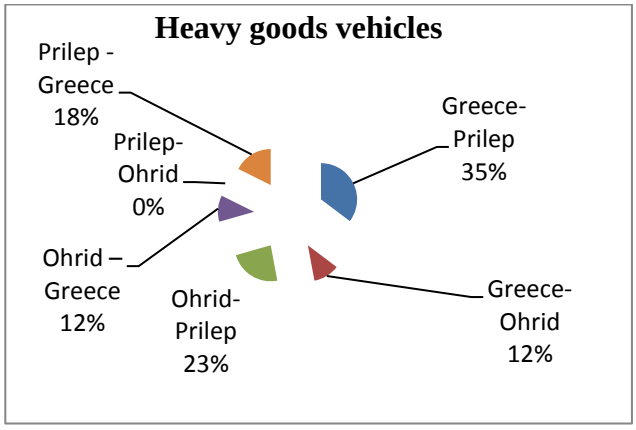

Chart 3: *The number of heavy goods vehicles by direction of movement*

Graphic display of the number of vehicles and the structure of vehicles by direction of movement.

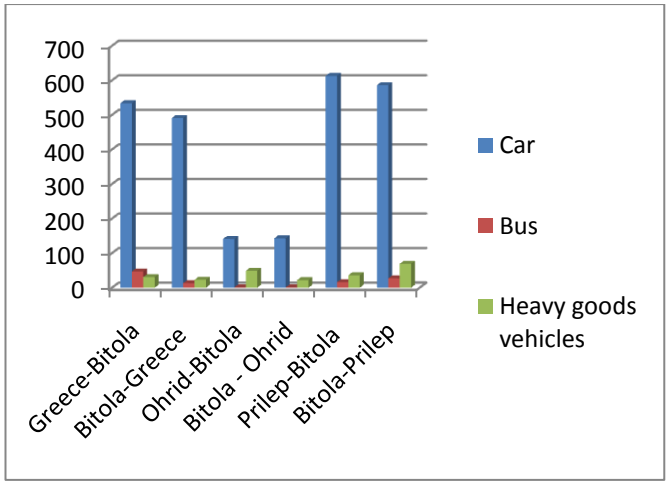

Chart 4: *The number of vehicles and the structure of vehicles by direction of movement*

4. Conclusion

The direction of movement, the composition of the traffic flow, the speed, the travel time, the following distance, the number of vehicles, the number of traffic accidents are only part of the data that are collected for various purposes, research. The cordon line is placed so that it intersects all roads that enter the pre-defined area of interest. The accumulation of vehicles inside the cordon line is determined by summing up the total number of vehicles that enter and leave the given space in a certain period of time. On the territory of the city of Bitola, 3 points were defined, that is, places where we have entry-exit flows to other cities, the collected data were analyzed and those vehicles that appear at the other point are taken as transit flows. From the obtained results we can conclude that the most intensive flows are on the direction from and to Prilep - Bitola, where about 660 vehicles are registered and in the opposite direction about 680 vehicles, while the second place in terms of intensity is the road direction from and to Greece - Bitola. There is a major deviation on the road from and to Ohrid - Bitola, where we have registered about 190 vehicles. The largest flow of heavy goods vehicles appears on the road direction Bitola-Prilep, while the lowest flow of heavy goods vehicles occurs on the road direction Bitola-Ohrid, together with the direction Bitola-Greece. In addition to tabular, a graphic presentation of the collected and processed data was also presented.

References

[1] https://www.google.com/maps

[2] "Collection and Analysis of Transport Data"Associate Professor Vaska Atanasova

[3] https://mk.wikipedia.org/wiki/Bitola

[4] https://data.ontario.ca/en/dataset/cordon-data-directional-traffic-counts

[5] https://www.oracle.com/database/what-is-database/

Влияние на вида тапицерска основа върху деформационното поведение на седалката на тапицираните мебели.

Influence type of upholstery base on the deformation behavior of the seat of upholstered furniture.

Rostislav Bozhkov
University of Forestry, Bulgaria
10 bulevard Sv. Kliment Ohridski, Sofia, Bulgaria
rostislav.bojkov@gmail.com

Abstract: *The upholstery base is one of the main structural elements used in the construction of the seats of upholstered furniture. According to their type, upholstery foundations are hard, semi-elastic and elastic. The type and materials used in their construction have an impact on the deformation behavior and softness of upholstered furniture.*

The study looked at the deformation behaviour of upholstery seat structure built of two types of polyurethane foam placed on three upholstery based variants - hard, semi-elastic and elastic. The criteria used to assess the material are a softness coefficient and parameters for general deformation of the upholstery, in the specifics of the elements of the seat.

Based on the results obtained, conclusions and recommendations have been made for their application in the upholstery structure of upholstered furniture.

Keywords*: Upholstery base, Polyurethane foam, upholstery, hard, semi-elastic, elastic, structure, deformation.*

1. Въведение

Делът на производство на тапицирани мебели възлиза на 35% от общия дял на произведените мебели в европейски и световен мащаб. С всяка изминала година, той бележи ръст поради непрекъснатото откриване на нови материали за изграждането на тапицерската структура, както и внедряването на модели с нови форми и конструкции.

При изграждане структурата на тапицираната мебел ясно се очертават няколко основни елемента, които задават основните характеристики на конструкцията, формата и функционалността и. Основните конструктивни елементи в структурата на тапицерията са носеща основа (скелет), основа на тапицерията (тапицерска основа), пружинираща част и облицовъчна част.(фиг.1), показани на фигура 1. Всеки един от тези основни елементи (корпус, тапицерска основа, пружинираща част и облицовъчна част) е изграден от различни по произход и по физико-механични показатели конструктивни елемента. Основен принцип при изграждане на тапицерската структура е, че материалите се разполагат като в основата да бъдат тези с по-висока плътност и малка еластичност, като към повърхността плътността на материалите намалява и еластичността им се увеличава.

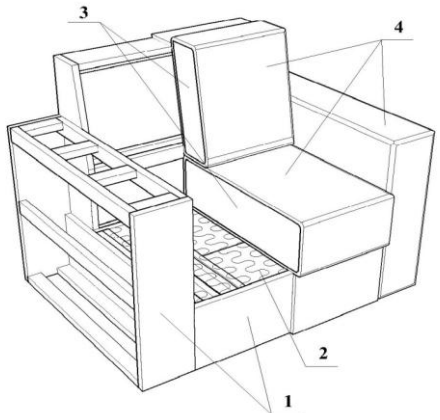

Фиг.1. *Структура на тапицирана мебел: 1-носеща основа (скелет); 2-основа на тапицерията (тапицерска основа); 3-пружинираща част; 4-облицовъчна част.*

Съгласно БДС 7669-89. „ Мебел. Тапицерия. Технически изисквания.”, тапицерската основа се класифицират като:

- Твърда основа.
- Полуеластична основа.
- Еластична основа.

, като материалите използвани при изграждането на тапицерската основа трябва да са:

- **<u>За твърда основа</u>**- масивна или слоеста дървесина, плочи от дървесни частици, плочи от твърди дървесни влакна или шперплат.
- **<u>За полуеластична основа</u>**- нетъкан текстил, стоманена лента, стоманена тел, тапицерски ленти: ленени,конопени и смесени, синтетични и др.
- **<u>За еластична основа</u>**- каучукови ленти, пружини зиг-заг, спирални-цилиндрични пружини, плоско-спирални пружини, ластична тапицерска лента и др.

Полиуретановите пеноматериали са синтетични, леки, с равномерна клетъчна структура. Разделят се на следните основни групи: меки, полутвърди, твърди и интегрални.

В последните години на пазара се налагат все повече трудногоримите меки пенополиуретани, които отговарят на европейските и американски стандарти за опазване здравето на хората и са задължителни при производството на тапицирани мебели за обществени сгради, градски транспорт и др.

Основните критерии за избора на пенополиуретаните са плътност, твърдост, еластичност и остатъчна деформация. Всички тези характеристики са тясно свързани с критериите за удобство и комфорт, дълготрайност и износоустойчивост.

Твърдостта е една от най-важните характеристики за поведението на полиуретановите пени, особено за малки натоварвания [4,5,10].

При проведени изследвания на три вида тапицерски структури изградени от пенополиуретанова пружинираща част върху твърда шперплатова основа, пенополиуретанова пружинираща част върху еластични ленти за тапицерия и пенополиуретанова пружинираща част върху основа на пружинен панел бе определено степента на влияние на вида тапицерска основа върху мекостта и степента на удобство и комфорт при изграждането на тапицерията на седалката на тапицираните мебели.

Резултатите от направените изследвания показват, че по отношение мекостта и степента удобство и комфорт полуеластичните и еластичните основи на тапицерията имат по-високи показатели, отколкото твърдата основа, която се препоръчва за използване (експлоатация) за период не по-дълъг от 4 часа. [12].

В България са направени задълбочени, подробни и аналитични проучвания на материали, използвани в различни видове тапицерия [3].Изследвани са влиянието на широк кръг от основи върху мекостта на тапицерията. На изследване са подложени - твърда основа от перфорирана ПДВ,текстилни ленти, еластични ленти, двойнокръстосани еластични ленти, плоскоспирални пружини, цилиндрични пружини на опън, пружини"зиг-заг" и комбинация от цилиндрични пружини за опън и пружини „зиг-заг". За пружинираща част на пробните тела са използвани комбинация от пенополиуретани и вати.

Макар и приети от науката и практиката тези изследвания трябва да се вземе под внимание факта, че те са правени през периода 1980г. – 1989 г. Тоест те са били актуални в посоченият период с използваните в този момент материали с техните специфични физико-механични характеристики, както и приложените методи за изследване в тези години. С развитието и осъвършенстването на технологиите и технологичният парк от 1988 г. до ден днешен в производството на тапицирани мебели са внедрени много нови материали, суровини и технологии, както и в научните среди са въведени много по-актуални, бързи и точни методи и методологии за изпитване. Към днешна дата не са изследвани стандартните трудногорими (СМЕ) меки пенополиуретанови пени, които навлизат все по-масово в изграждането на структурата на тапицерията и не е правен сравнителен анализ на деформационното им поведение спрямо конвенционалните полиуретанови пени (N).

Целта на това изследване е определянето на деформационното поведение при натоварване на тапицерии с пружинираща част, изградена от конвенционални и СМЕ пенополиуретани поставени върху три варианта на тапицерска основа - твърда, полуеластична и еластична.

2. Материали и метод

На изследване са подложени три основни типа тапицерии (фиг.2 и фиг.3): **А, В** и **С**- с пружинираща част, изградена от конвенционална полиуретанова пяна – KOVAFOAM N 3030 и трудногорима полиуретанова пяна KOVAFOAM СМЕ 3530, произведени по непрекъснат метод от Паралел Севлиево ООД. Пружиниращите части на тапициите поставени са поставени върху три вида тапицерски основи показани на фигура 2.:

- *Твърда основа* – произведена като рамкова конструкция от фризове от иглолистна дървесина със сечение 40х60 mm. (произведен съгласно EN 14080-2013, DIN 4074.), едностранно облицована с листообразен дървесен материал- шперплат Бреза с дебелина 12 мм. (произведен съгласно EN 13986:2004; EN 636-3S).
- *Полуеластична основа* – произведена като рамкова конструкция от фризове от иглолистна дървесина със сечение 40х60 mm. (произведен съгласно EN 14080-2013, DIN 4074.), към фризовете на рамковата конструкция посредством държачи и кламери са закрепени кръстосано текстилни колани в напречна и надлъжна посока.
- *Еластична основа* – произведена като рамкова конструкция от фризове от иглолистна дървесина със сечение 40х60 mm. (произведен съгласно EN 14080-2013, DIN 4074.), към фризовете на рамковата конструкция посредством държачи и кламери са закрепени зиг-заг пружини (произведен съгласно EN 1957-2000; EN 10270-1).

Пружините „зиг-заг" са произведени от стоманена пружинна тел с диаметър 3,8 mm. с клас на якост на опън 1550-1800 MPa, стъпка между отделните елементи 47 mm., и широчина на лентата - 47 mm.

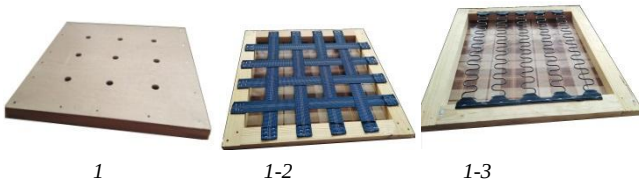

1 *1-2* *1-3*

Фиг.2. *Тапицерски основи: 1 –твърда основа: 1-2 –полуеластична основа: 1-3 –еластична основа.*

Всички останали материали, използвани при изграждането на тапицерската структура са идентични по вид и дебелина и с еднакви физико-механични характеристики. Това е необходимо, за да бъде достоверно направеното сравнение на деформационното поведение на изследваните материали.

Тестът се извършва по стандартен метод съгласно БДС 8962:1990 [1]. Тествани са образци с размери 600х600 mm., което от своя страна води до сравнимост на резултатите от теста с тези на тапицерия с подобни размери. Дебелината на изследваните конвенционалната полиуретанова пяна N 3030 и на трудногоримата полиуретанова пяна KOVAFOAM СМЕ 3530 е 140 mm. Общата дебелина на всички изследвани тапицерски структури е 250 mm. (фиг.2).

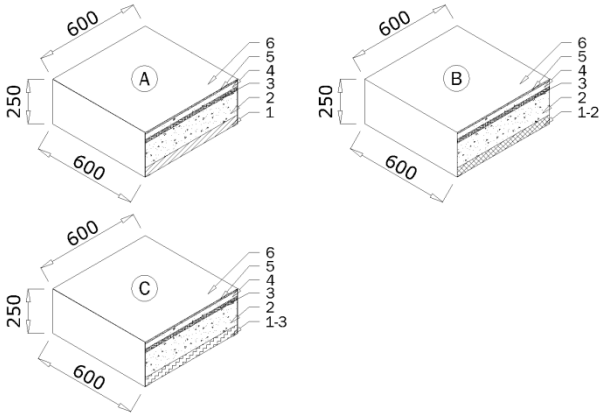

Фиг.3. *Схеми на изграждане на структурата на тапицерията: 1 – твърда основа на тапицерията: 1-2 –полуеластична основа на тапицерията: 1-3 –еластична основа на тапицерията: 2- трудногорима полиуретанова пяна - KOVAFOAM СМЕ 3530; 3 - Тапицерска вложка; 4- конвенционална полиуретанова пяна KOVAFOAM N 3030 5- Полиестерна вата; 6 - Мебелен плат.*

Преди изпитването, образците се кондиционират в продължение на 24 часа в среда от 23±2 ° С и относителна влажност 50±5 % .

Изпитваните образци са закрепени за хоризонтална, твърда, гладка основа с отвори ϕ 35 mm., позволявайки изтичането на въздух отдолу на образеца. Пробите предварително се зареждат с последващо разтоварване, след което са оставени 30 min за кондициониране. Първоначалната дебелина (височина) на образците е записана при товар от 3 daN. След постепенно увеличаване на силата, следващите дебелини на образците са отчетени на интервали от 5 daN (до 20 daN) и на интервали от 10 daN (от 20 daN до 100 daN).

Използваният натоварващ диск за изследването е плосък с кръгла форма, с диаметър 250 mm.

Изследваните показатели са:

- Коефициент на начална мекост ($M_н$), който се изчислява по формулата:

(1) $M_H = \frac{H_5 - H_{15}}{10}$, mm/daN. ,където:

H_5 е височината на образеца при натоварване със сила от 5 daN,mm.

H_{15} - височината на образеца при натоварване със сила от 15 daN,mm.

- Обща деформация на седалката (До.с.), изчислявайки се по формулата:

(2) $Д_{о.с.} = H_0 - H_{75}$, mm.

където:
H_0 е началната височината на образеца.
H_{75} - височината на образеца при натоварване със сила от 75 daN,mm.

- Коефициент на мекост на седалката ($К_{м.с.}$) и се изчисляват по формулите:

(3) $K_{M.C.} = \frac{H_{75} - H_{85}}{10}$, mm/daN.

където:
H_{75} - височината на образеца при натоварване със сила от 75 daN,mm.
H_{85} - височината на образеца при натоварване със сила от 85 daN,mm.

Съгласно БДС 7669-89. „ Мебел. Тапицерия. Технически изисквания.” [2], меката мебел се класифицира в зависимост от степента на мекост, определяща се от стойностите на деформацията и коефициент на мекост на:

- Полутвърда - такава тапицерия отговаряща на:
  $Д_{о.} \leq 35$ mm.
  $К_{м}$ – не е нормиран.

- Полумека - такава тапицерия отговаряща на:
  $Д_{о.}$ - от 35 mm. до 75 mm.
  $К_{м}$ - от 1,4 mm/daN. до 2,4 mm/daN.

- Мека - такава тапицерия отговаряща на:
  $Д_{о.} >$75 mm.
  $К_{м} \geq$ 2,4 mm/daN.

3. Резултати и анализ

Резултатите на показателите за мекостта на изследваните различни схеми на тапицерски структури са представени в таблица 1. Те се характеризират със стойности, покриващи изискванията на БДС 7669-89. „Мебел. Тапицерия. Технически изисквания“ за полумека и мека тапицерия [2].

От таблица 1 и фигура 4 е видно, че тапицерската структура тип А продължават своята деформация до натоварване с 80 daN, тапицерската структура тип В до 90 daN, докато тапицерската структура тип С до 60 daN . Това се дължи на различните типове тапицерски основи използвани при изследването на трите тапицерски структури.

***Табл. 1**. Показатели за мекост на изследваните тапицерски структури.*

Тип:	Мн (mm/daN)	До.с. (mm)	К м.с. (mm/daN)
А	0,9	120	2,4
В	1,5	131	2,7
С	1,8	148	2,9

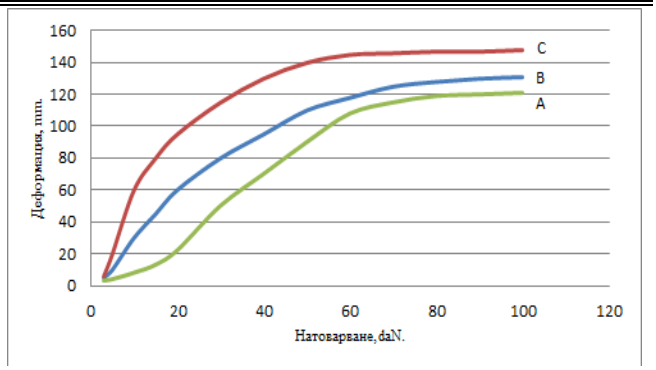

***Фиг. 4**. Деформация при натоварване на тапицерска структура с пружинираща част изградена от конвенционална полиуретанова пяна – KOVAFOAM N 3030 и трудногорима полиуретанова пяна KOVAFOAM CME 3530 поставени върху тапицерски основи тип: **А**-твърда , **В**-полуеластична и **С**-еластична.*

От таблица 1 и фигура 4 и направен анализ е видно, че изследваните тапицерски структури тип А,В и С покриват изискванията на БДС 7669-89. „Мебел. Тапицерия. Технически изисквания“ [2] и критериите за изграждане на тапицерската структура (седалката - мека тапицерия, облегалката - мека или полумека тапицерия и подлакътниците - твърда тапицерия), както и в голяма степен критериите за Удобство и Комфорт на тапицираните мебели.

Показателите на обща деформация на седалката ($Д_{о.с.}$) при тапицерия тип А, В и С покриват критериите за мека тапицерия.

Изчислените коефициенти на мекост на седалката ($К_{м.с.}$) при тапицерия тип А са на границата между критериите за полумека и мека тапицерия, докато при тапицерия тип В и С напълно покриват критериите за мека тапицерия. Това показва пригодността за използване на тапицерските структури тип В и С главно за изработване на седалката, и в по-малка степен за изработване на облегалката на тапицираните мебели, осигурявайки постигането на критериите за Удобство и Комфорт на тапицираните мебели. Тези факти ги правят пригодни за постигане на форми на седалката, отличаващи се със съвременен дизайн и добра ергономичност.

Стойността на показателите показват, че тапицерските структури тип В (с полуеластична основа) и тип С (с еластична основа) имат добри показатели за изработване на седалката на тапицираните мебели, осигурявайки постигането критериите за Удобство и Комфорт на тапицираните мебели. Тапицерската структура тип А се характеризира със стойности на показателите си за мекост, покриващи изискванията за полумека тапицерия в горните им граници. Това обстоятелство я превръща в не особено подходяща при изработване на седалката на тапицираните мебели. Препоръчва се използването на допълнителни материали в структурата и за постигане на стойности, отговарящи на изискванията за мека тапицерия и за постигането в голяма степен на деформационно поведение, което да покрива критериите за Удобство и Комфорт на тапицираните мебели.

4. Заключение

Въз основа на направените изследвания на тапицерските структури тип А (с твърда тапицерска основа), тип В (с полуеластична тапицерска основа) и тип С (с еластична тапицерска основа) могат да се направят следните изводи:

1. Видът на използваната тапицерската основа в структурата на тапицерията оказва влияние върху деформационното поведение на тапицерията;

2. Тапицерските структури тип В (с полуеластична тапицерска основа) и С (с еластична тапицерска основа) се характеризират с поведение подложени на напрежение на натиск което до голяма степен покриват

критериите за Удобство и Комфорт на тапицираните мебели, докато тапицерската структура тип А (с твърда основа) се характеризират с поведение подложени на напрежение на натиск което в този вариант на тапицерска структура на са подходящи за изработването на седалките на тапицираните мебели, препоръчва се използването и при производството на облегалките на тапицираните мебели.

3. Изследваните тапицерски структури отговарят на изискванията на БДС 7669-89. „Мебел. Тапицерия. Технически изисквания“ за полумека и мека тапицерия.
4. Изследваните тапицерски структури могат да бъдат използвани успешно за производството на седалките и облегалките на съвременни тапицирани мебели.

4. Литература

1. БДС 8962-90. *Мебел. Мебел за седене и лежане. Метод за изпитване на мекост.* К29. С., Комитет по стандартизация,сертификация и метрология, 1991.
2. БДС БДС 7669-89. *Мебел. Тапицерия. Технически изисквания.* К25. С., Комитет по качество, 1990.
3. Генчев, Я. *Оптимизиране структурата на тапицерията на меката мебел*. Дисертация за получаване на образувателна и научна степен „Доктор”. София, 1998.
4. BDS EN ISO 3386-1:2010. *Polymeric materials, cellular flexible – Determination of stressstrain characteristic in compression* – Part 1: Low density materials.
5. BDS EN ISO 2439:2009. *Flexible cellular polymeric materials – Determination of hardness (indentation technique)* (ISO 2439:2008).
6. Genchev, J., Lulchev T., Hristodorova D. (2016): *Influence of the type of upholstery materials on the softness of upholstery with inner spring units.* INNOVATION IN WOODWORKING IDUSTRY AND ENGINEERING DESIGN,1/2016(9)
7. Genchev, J., Lulchev T. (2015): *Comparative Analysis of the deformation behavior of upholstery materials.* SECOND INTERNATIONAL SCIENTIFIC CONFERENCE „WOOD TECHNOLOGY & PRODUCT DESIGN ―,2015, OHRID, REPUBLIC OF MACEDONIA
8. Jancova, V. *Reciprocni perfomace souboru poliuretanovy pen v konstrukcie alounenovi nabutku*. 2008.
9. Polyurethane foam association, (1991): *Density.* InTouch Technical Bulletin Vol.1, No.2.
10. Polyurethane foam association, (1994): *Firmness.*InTouch Technical Bulletin Vol.4, No.3.
11. Zubauskiene, D. Strazdiene, E. Urbelis, V. Sacevivience, V. *The Investigation of Soft Furniture Upholstery Deformational Behaviour.* L., ISSN 1392–1320 MATERIALS SCIENCE (MEDŽIAGOTYRA). Vol. 18, No. 4. 2012.
12. Smardzewski, J. Furniture Design., Poznan University of Life Sciences, Poland., Springer International Publishing Switzerland, 2015

Surface treatment - effect on spring parts in the automotive industry

Milena Hristova
"Angel Kanchev" University of Ruse, Ruse, ul. "Studentska" 8, 7017 Studentski grad, Bulgaria
mhristova@uni-ruse.bg; gawrilowa@abv.bg

***Abstract**: In modern automotive engineering, a particular car is composed of various parts that are manufactured using a wide variety of materials and technologies and that meet the high demands of modern customers and environmental norms. In the production process of a specific article for assembling cars, a problem with springs of a certain type is found. During the planned production, assembled products began to show the same defect. The mounted springs fall spontaneously. An analysis of the possible causes was made. A visual examination was made which showed a lack of plasticity, a change in geometry and raised doubts about the thermal surface treatment. Based on the results of the performed measurements and analysis, the possible causes of the problems during production were recognized. Several conditions could have caused this:*

- *Two different tools were available at the manufacturer, respectively two different technologies for the production of the springs;*
- *The manufacturer used two different sub-suppliers for surface treatment;*
- *insufficient corrosion protection;*

The results of the measurements show that despite the geometric deviations of the dimensions, the springs lose their function due to lack or improper surface treatment.

***Keywords**: surface treatment, automotive industry, springs elements, different technologies*

1. Introduction

Surface treatment is an important aspect of spring part design and manufacturing in the automotive industry, as it can significantly affect the performance and longevity of these components. Heat treatment of the surface and the improvement of its quality are the leading and profitable technologies today to improve the efficient use of materials to achieve the required properties of materials used in the automotive industry. Continuous improvements and refinement of surface treatments are widely used in the daily production of parts for the automotive industry [1]. The modern automotive industry places increasingly high demands on specific loads (thermal, mechanical, etc.), weight reduction, friction between them, longer life of mounting elements and improved corrosion resistance [2]. In the production process of a specific article for assembling cars, a problem with springs of a certain type is found.

This report discusses the production process of assembling automotive parts in a company operating in the territory of Rousse. The company carries out production activities and supplies to all car manufacturers worldwide. The company is certified to all standards of the automotive industry, which obliges it to supply products with 0-defects.

In this study, microscopic and hardness examinations of springs with changes in internal diameter after the installation were made. The analyzes and measurements made, as well as the results obtained, are very important in predicting the behavior of the springs installed in the specific products. They served as the basis for improving the design of the springs. Further analysis will include methods/measurements to determine elasticity and stiffness in an undamaged and damaged spring.

2. Materials and methods

During the planned production, assembled products began to show the same defect. The mounted springs fall spontaneously. Investigation of the installation process, machines and equipment, the delivery chain of the springs supplier was immediately launched. Following the analysis, the springs were suspected of a compromised assembly process. The material used for manufacturing the springs is unalloyed 1.1231 (DIN EN 10132, SEA 1070, JIS S70CM) steel with the composition listed in Table 1.

***Table 1:** Chemical composition of the steel used for manufacturing the examined springs*

Element	C	Si	Mn	P	S	Cr	Al	Fe
%	0.67	0.22	0.75	<0.01	<0.01	0.23	0.03	Bal.

It became clear that the Provider used two different tools for the production of springs. The Provider also used two different sub-supply and surface processing. The springs manufacturer did not want to provide detailed information as it is technological know-how.

The analysis of the springs included Vickers hardness (DESKTOP DIGITAL COMBINED BRINELL, ROCKWELL AND VICKERS HARDNESS TESTER model ZBRV-D) measurements as shown in Figure 1, microscopic (Zeiss AxioCam MRc CCD Microscope Camera) observations and Caliper tests. Measuring with a go-not-go gauge was applied

Analysis was made on fallen spring by using two different approaches:

- Observations of the spring element by comparing the color with that of the OK springs. The fallen spring element fell on the containment plan from the whole product.
- Measurement method - direct attempt to use the imprint of the instrument - without resin embedding.

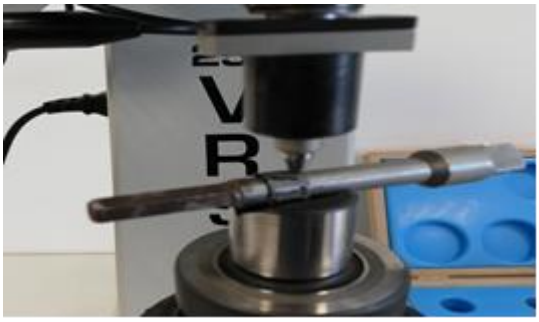

***Fig. 1**. Measurement of Vickers hardness of the springs*

3. Results and Discussions

The results of the hardness measurements are listed in Table 2.

***Table 2**: Values of the Vickers hardness tests of three springs*

Sample	Measurement №			Aver.	Evaluation
	1	2	3		
1	178.6	184.8	183.2	1828.2	NOK
2	181.5	189.8	188.1	186.5	NOK
3	337.6	347.7	328.5	337.9	NOK

Since the requirements of the hardness values are within the limits of 450 – 490 HV, the measured hardness is not sufficient because it is out of tolerance. It follows that the Provider used different production methods.

Comparison of Tool A and Tool B

Single parts which haven't been assembled are shown in Figure 2. A significant difference in behavior between both parts Tool A

and Tool B is observed. Tool A spring is stopping on the first pair of teeth, while tool B is stopping at its top teeth. Also, Tool B is bent in a bad position.

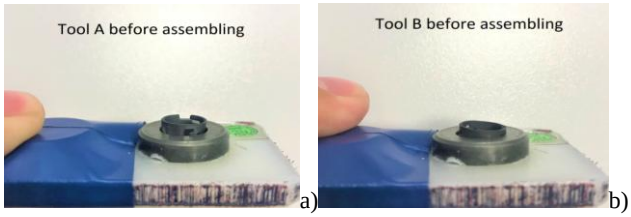

a) b)

Fig. 2*. Images of tool A (a) and tool B (b) before assembling.*

The microscopic analysis of mounted springs in an article is shown in Figure 3. The accumulated deformation of the spring from tool B is clearly visible from the photographs taken under the microscope.

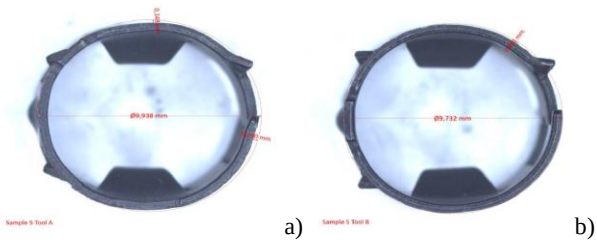

a) b)

Fig. 3. *Micrographs of tool A (a) and tool B (b)*

This spring has no elasticity and no longer fulfills its role as a spring. Springs with this type of deformation fall spontaneously after being installed in the product.

Random inspection of delivery show springs below the lower limit. Table 3 shows the measurement report of NOK springs. Such springs were never taken and mounted from the box.

Table 3: *Dimension limits and measurement results of a NOK spring*

Dimension limits	Measured results					Evaluation
	1	2	3	4	5	
Ø9.9 +0.4/-0.1	9.743	9.757	9.785	9.780	9.872	NOK

To be able to prove that springs arrive from the manufacturer in a condition that does not meet the specification, a 100% inspection is carried out on delivery. However, visual inspection of the parts is not a proper method for sorting due to the unavailability to catch the NOK dimensions by eye.

Investigation of springs from Tool B

After the spot check, there were found 4 out of 10 NOK springs from one problematic delivery batch. Then there were checked more than 500 springs from the same batch.

The following results were found:

1 spring - Ø9.50 to Ø9.60 mm
3 springs - Ø9.60 to Ø9.70 mm
18 springs - Ø9.70 to Ø9.80 mm
350 springs - Ø9.80 to Ø9.90 mm
118 springs - Ø 9.90 to Ø 10.00 mm

500 springs were selected from a random box. The measurement shows that there is a big deviation in the dimensions

Assay tests were performed with the springs that are below the lower limit (< 9.8). Overall 34 springs that were below the lower tolerance were tested on machine run test and were then checked on a containment plan. The test results indicated that 3 out of 34 tested NOK springs have fallen out after assembly. It follows that the slight deviation from geometric dimensions (which in 5-10% of cases go beyond the lower limits of the tolerance field), did not significantly affect the reason for the springs falling from the finished products.

Figure 4 illustrates OK and NOK spring tests with the go-not-go gauge. It is seen how NOK spring is attached inside the caliber. Tool B spring is out of specification (lower borderline) and the process of supplier is moved to lower tolerance of the spring

Fig. 4. *OK and NOK spring test with the go-not-go gauge*

Therefore, the design of the spring is secured, even if the springs are far below the lower tolerance, they still hold in the turning element. It follows that the essential role was played by the correct surface treatment. Some of the springs from the box were highly rusted on site as shown in Figure 5, while other parts had passed no surface treatment

Fig. 5*. Appearance of some tested springs.*

4. Conclusions

Were made on unmounted Tool B springs. Springs were separated by dimensional differences. It was found that the springs are manufactured on the border and below the lower limits. the drawing specifications. However, even if the springs are far below the lower tolerance, their design is secured and they still hold in the turning element. Without surface treatment, the springs do not have the necessary plasticity, do not fulfill their function as a spring, which causes a lack of functionality of the entire assembled product. The consequences for the serial production used by these springs are:

- 100% control of each product ongoing.
- Costs will exceed 300k Euro soon
- Spring elements are still falling from the assembled product
- The supplier is denying any costs, sorting and claims

5. References

1. J.Vetter, G.Barbezat, J.Crummenauer, Surf & Coat Techn **200,** 5-6 (2005) https://doi.org/10.1016/j.surfcoat.2005.08.011
2. Peter Hutmann, BMW Group Munich, *The Application of Mechanical Surface Treatment in the Passenger Car Industry*, Ed: Prof. Dr.-Ing Lothar Wagner (2003) https://doi.org/10.1002/3527606580.ch1

Welding technology of martensitic steel P91 and austenitic steel 304H – State of the art

Aleksandra Krstevska[1], Dobre Runchev[1], Filip Zdraveski[1]
University „Ss. Cyril and Methodius“, Faculty of Mechanical Engineering, Rugjer Boshkovikj 18, P.O. Box 464, MK-1000 Skopje, Republic of N. Macedonia[1]
aleksandra.krstevska@mf.edu.mk

Abstract: *Many industries nowadays with the development of technology require joints between different types of steel due to its various benefits such as production of lightweight machine parts, production of less expensive components with acceptable properties, high strength, acceptable corrosion resistance. One of the dissimilar welding challenges is the joint between martensitic steel P91 and austenitic steel 304H due to the dissimilarities in their chemical, physical and metallurgical properties. In this paper is going to be analysed the best way of joining the two different types of steel, the proper welding technique, the choice of filler material which according to carbon content can match only to one of the steels. At the end is discussed if the welding performance can meet the requirements of high-quality weld.*
Keywords*: P91, 304H, DISSIMILAR METAL WELD, WELDING TECHNOLOGY*

1. Introduction

The coal-fired power plant systems today are striving to work in supercritical steam parameters and assure higher efficiency. The need for higher efficiency is met with higher steam parameters, increase of steam pressure and steam temperature. Another parameter that coal-fired power plants need to incorporate is the method for clean energy, the use of coal needs to satisfy the environmental requirements and take care about the air pollutants [1]. When it is discussed about higher efficiency in power plants and satisfying the environmental requirements for clean energy in coal-fired power plants it means a saving in fuel and less emission of carbon dioxide which reduces the rate at which damage is done to the global environment.

The need for higher efficiency in power plants today relates to the development of new materials with great properties on high temperatures. The possibility for higher steam parameters and working of the plant on super-critical temperatures is met with the development of new enhanced materials.

The new materials resistant to high operating temperatures, also called heat resistant steels, are used for manufacture of ultra-super critical parts of boiler plants such as steam lines, tubes for super heaters, collectors. Regarding construction of power units based on steam with ultra-supercritical parameters the operation of pressure elements in the high range of thermal and mechanical loads require the use of creep resisting construction materials with increased creep strength and advanced welding technologies for joining these materials. All the demands for high efficiency in power plants lead to development of enhanced materials like martensite steels, austenitic steels, Ni-alloys, alloys that work in high temperature applications.

2. Heat resistant steels in power industry

Steels which are used at temperatures up to the recrystallisation temperature are called heat resistant steels. They are characterized with good creep strength at high temperature. The materials that meet the above criteria are the ferritic (martensitic, bainitic) steels and austenitic steels. In table 1 is given the classification of creep resistant steels. The ferritic and martensitic steels have body-centered cubic crystal structure and in the iron is added chromium as one of the methods for improvement in high-temperature creep resistance and creep strength of steels used in power industry. Also adding alloy elements such as molybdenum, vanadium, niobium and nitrogen to improve their heat resistance [2].

Martensitic steels with chromium addition up to 12% are used for elements in construction that can withstand higher pressure and higher service temperature for application up to 650°C. Over 650°C are used austenitic steels that have nickel added to the iron-chromium composition and the alloy changes his body-centered cubic crystal structure to face-centered cubic crystal structure. In comparison, austenitic steels have highly strength and ductility, greater creep-rupture strength than martensitic steels. However, the austenitic steels are much expensive than martensitic steels for their high contents of alloy element additions.

Chromium is added for oxidation resistance, high temperature strength and carburization resistance. Nickel is added to increase ductility, high temperature strength and resistance to carburization and nitriding. With adding element nickel the atomic structure becomes austenitic.

Table 1*: Classification of creep resistant steels*

Heat-resistant steels and special materials				
Bcc structure (body-centered cubic)				Fcc structure (face-centered cubic)
Up to 400°C	Up to 500°C	500 to 600°C	600 to 650°C	Above 700°C
Unalloyed	Alloyed		High-alloyed	
Ferritic-pearlitic steels, fine-grain structural steels	Mo- alloy steels	Bainitic (martensitic) ferritic steels	Martensitic 9 to 12% chromium steels	Austenitic steels, Ni and Co-materials
P235GH	16Mo3	13CrMo4-5	X10CrMoVNb9-1	X8CrNiNb16-13
P355NH	18MnMo4-5	10CrMo9-10	X22CrMoV12-1	X8NiCr32-20
No extra proven methods; higher purity; fine grain	Tr-increase through molybdenum alloying	Carbide/nitride formation + tempering	Precipitation hardening + spec. heat treatment	Fcc structure with high crystal recovery temperature

In this paper the emphasis is on martensitic steel type P91 and austenitic steel type 304H. For example, for boiler components materials, the austenitic steel 304H is used for boiler super heater tubes, elements that are experiencing 630°C and for steam headers and piping is used martensitic steel P91. The heater tubes need to be welded with the steam headers, that is why the need for dissimilar welds become necessary.

A dissimilar metal weld (DMW) is when grades with different chemical compositions are welded together. In fossil-fired power plants dissimilar metal welds are very common in the present. Austenitic stainless steel attachments welded onto ferritic steel tubes and pipes, stainless steel thermowells or steam sampling lines in ferritic steel pipes. On figure 1 is shown the possible combination of materials used and the fabrication techniques and welding processes involved in the fabrication of a steam boiler component [3].

***Fig. 1**: Combination of materials, fabrication techniques and welding processes in fabrication of steam boiler [3]*

3. Welding of heat resistant steels

Heat resistant steels with its strength at high temperatures needs to have sufficient resistance to creep processes. Creep usually occurs at high temperatures, where plastic deformation of materials takes place well below its yield strength under prolong stresses.

The dissimilar welded joints, used in piping systems, always represent a critical place in the system, in terms of possible occurrences of defects. The creep takes significant role in failure of these weld joints since it is the main cause of failure at elevated temperatures [4]. The dissimilar welded joints between martensitic and austenitic steel are often used in energy and process industry for new and refurbishment of existing plants. For creation of this type of joints and creation of weld with acceptable structural characteristics all recommendations and parameters of the welding process and heat treatment needs to be followed.

Matching filler metals for the new heat resistant steels and their great properties at elevated temperatures have been developed and qualified for all commonly used welding processes.

According to the different chemical composition of the materials for creation of dissimilar joint, one of the materials will encounter the carbon diffusion due to the difference in Cr content. Carbon moves from the material with low Cr content to material with high Cr content. The decarburization zone can be avoided with the use of nickel-base filler metal (fig.2), since carbon does not diffuse into the nickel-base material, using welding parameters such as preheating, and post weld heat treatment (PWHT) suitable to P91 [2].

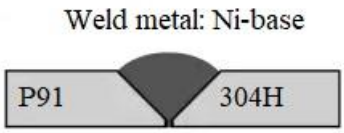

***Fig. 2** Dissimilar weld between martensitic and austenitic steels*

After 1970s, in research carried out by Electric Power Research Institute (EPRI) and other organizations, an increasing number of dissimilar metal welds in superheater and reheater tubes were fabricated as fusion welds using nickel-based filler metals, such as INCO 82, INCO 182 etc. The technical purpose for the switch to the nickel-based filler metals was the improved compatibility in thermal-physical properties with the lower alloyed materials [5].

Heat-resistant steels can be welded with use of various arc welding processes. In most cases, manual metal arc welding and tungsten inert gas welding are used. With tungsten inert gas welding of chromium-alloyed materials special attention must be dedicated to shielding the weld root, for this argon is suitable as a shielding gas.

To maintain and assure quality welds special attention should be dedicated to temperature time cycle of steel P91 as shown in figure 3 [6]. All heat treatment operations are a key factor when welding P91 steel for obtaining the required toughness and creep resistance. An extremely well controlled preheat, interpass temperature and PWHT are mandatory to ensure that the required creep rupture properties and toughness are obtained in the weldment.

The time at temperature for PWHT depends on the thickness of the part. The PWHT temperature should also be controlled so that the formation of austenite, which would result in the formation of untempered martensite, is avoided.

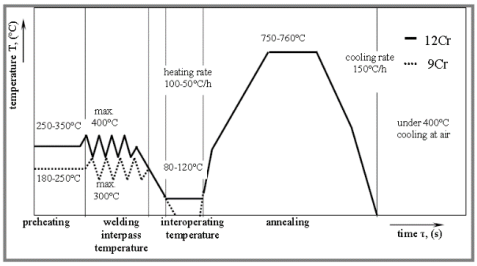

***Fig 3:** Temperature time cycle during welding of martensitic 9 or 12% chromium steels [6]*

On fig. 4 [7] is shown a reduction in dimensions of structural components used in power plant for work at elevated temperatures. The use of P91 results in lower costs by reducing the mass of the structure and the labor. The design parameters are: design pressure 280 bar and design temperature 550°C.

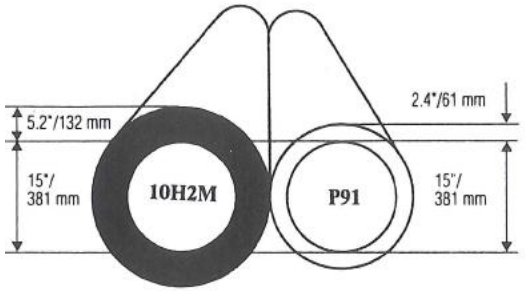

***Fig.4**: Wall-thickness of pipes used for same design parameters [7]*

When it comes about welding P91 certain welding procedures and specification needs to be managed. Creep strength martensitic steels are highly hardenable, and upon cooling after welding, they undergo phase transformation that results in a fully martensitic structure. To obtain the desired properties the welds must undergo PWHT and an interpass temperature must be maintained. All the welding procedures and recommendation needs to be fulfilled to obtain quality welds and avoiding failures in the fossil fired power plants [8].

P91 is used for heavy sections such as pipes and headers in the advanced fossil fired power plants and austenitic stainless steel 304H is candidate steel for superheaters and reheater pendants, where the temperature is high. The best way of joining and producing quality welds is TIG process [9]. Current dissimilar metal welds involve buttering one end of the base metal with a suitable filler metal, PWHT and joining to the other base metal. The buttering is used to deposit surfacing metal on the base metal surface to provide compatible weld metal for the subsequent completion of the weld (fig. 5) [10].

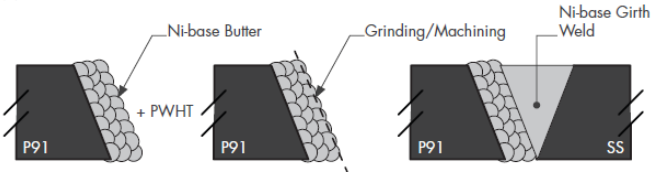

***Fig. 5**: Buttering of P91 steel [10]*

In the EPRI publication (11) several weld metal composition and choice of welding process is considered. The composition

ranges differ for several elements but significant are nickel and manganese which influence on critical temperatures such as Ac1, Ms and Mf. The base metal specification allows maximum of 1% (Ni + Mn) whereas it is possible to have much higher levels in filler metal. When Ni+Mn reaches 1.4% the Ac1 decreases to 780°C, The Ms decreases below 350°C and Ms decreases below the required preheat temperature of 200°C. Cooling the weldment to room temperature prior to the PWHT is one way to avoid the formation of fresh martensite after PWHT. For good toughness in the weld seam, it is desirable to aim towards high nickel contents.

The filler material is mainly nickel based alloys which provide transition in coefficients of thermal expansion as well as proven to be beneficial for stopping the carbon diffusion from ferritic to austenitic side compared with conventional austenitic base filler [12].

4. Defects in Dissimilar Metal Welds

The dissimilar welded joints between martensitic and austenitic stainless steel always represent a critical place in the system, in terms of possible occurrences of defects. The chemical composition gradients (tab. 2) present unique issues relative to their design, behavior and life management especially operating at elevated temperatures.

Tab.2: *Chemical composition of base metals and filler material (in wt.%)*

	BM P91	BM 304H	FM Thermanit Nicro 82
C	0,08 ÷ 0.12	0,04 ÷ 0.08	0.02
Mn	0.30 ÷ 0.60	max. 2.00	3.0
Si	0.20 ÷ 0.50	max. 1.00	0.1
P	max. 0.015	max. 0.035	
S	max. 0.010	max. 0.015	
Cr	8.00 ÷ 9.50	17.00 ÷ 19.00	20.0
Ni	max. 0.40	8.00 ÷ 11.00	>67.0
Mo	0.85 ÷ 1.05		
V	0.18 ÷ 0.25		
Al	Max. 0.04		
Nb	0.06 ÷ 0.10		2.5
N	0.03 ÷ 0.07	max. 0.11	
Fe	Bal.	Bal.	<2

Failure mechanisms were noticed in thicker section between dissimilar weld with austenitic steel. For joining these two different materials, nickel base alloy filler material is used applying all the recommended welding parameters, preheat, interpass and PWHT for P91 steel. In EPRI report [13] where documented service experience of thick section of grade 91 in dissimilar welds. The most common failure has been cracking along the weld fusion line between grade 91 and the nickel base weld metal presented on fig. 6 [13].

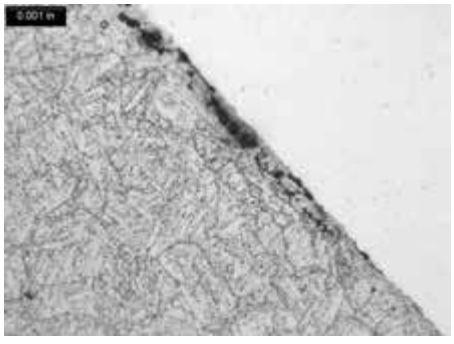

Fig. 6*: Failure in grade 91 in DMW with nickel base weld metal [13]*

The premature failures are creep related, occurring in short service life duration of the weld and typically along the grade 91 to nickel-base weld metal fusion line. There is a need for research work between dissimilar welds of P91 steel and 304H stainless steel because of increased demand for this type of joints in ultra-super critical power plants because of their better performance [14]. For accurate prediction of weld joints, its accuracy in service life is essential. Therefore, special attention needs to be paid to creep phenomenon which occurs at elevated temperatures, applying PWHT in acceptable range of annealing temperature which contribute to accelerate damage during service and results in type IV cracking. The degraded microstructure of the dissimilar welded joints is seen occurring within HAZ on the P91 steel side [15].

5. Conclusion

When joining metals with different chemical compositions and metallurgical properties of importance is the welding technology with particular attention paid to filler metal chemistry and PWHT. Tungsten inert gas (TIG) welding is the most preferred method for joining these two metals, it gives a strong weld with the required parameters.

As coal fired power plants will remain major source of energy it is necessary to research in improvement in plant efficiency and reduction of carbon footprint. New materials with better high temperature creep properties are developed and special attention should be paid on the selection of a suitable welding process and the performance of a suitable welding technology. Because of the good great properties at elevated temperatures and their applications in ultra-super critical power plants needs to predict creep failure controlling mechanism for better performance of the power plant fulfilling the requirement for higher efficiency and clean energy.

6. References

1. Viswanathan, R., Henry, J.F., Tanzosh, J. et al., U.S. program on materials technology for ultra-supercritical coal power plants. J. of Materi Eng and Perform 14, 281–292 (2005)
2. Tasak E., Ziewiec A.: Weldability of construction materials. Volume 1. Weldability of steels, Wydawnictwo JAK – Krakow 2009.
3. R. Viswanathan, R. Purgert, S. Goldstine, J. Tanzosh, G. Stanko, J. Shingledecker and B. Vitalis: Proc. 5th Int. Conf. on 'Advances in materials technology for fossil power plants', Marco Island, FL, USA, October 2007, 1–15
4. S. Chaudhuri, NML Jamshedpur 831007, India, 2008, pp. 85-114
5. EPRI report 2008, Report 1015699
6. J. Pecha, D. Stano, O. Peleš, Welding of 9% Cr creep resisting steels for power Engineering equipment, Zavarivanje i zavarene konstrukcije (4/2004), str. 159-168
7. The success of a new material P91/T91 steel enhances power station efficiency, Mannesmann Rohrwerke report, S28/29
8. W. F. Newell, Jr.: 'Welding and post weld heat treatment of P91 steel', Weld. J., 2010, 33–36.
9. Echezona, Nnamdi & Akinlabi, Stephen & Jen, Tien-Chien & Fatoba, Olawale & Hassan, Sunir & Akinlabi, E.. (2021). Tig Welding of Dissimilar Steel: A Review. 10.1007/978-981-16-3641-7_1.
10. T. Totemeier, Dissimilar Metal Welds in Grade 91 Steel, Structural integrity 2018, volume 44, pg15-18
11. Coleman K, Gandy D. Guideline for welding P(T) 91, document 1006590, EPRI, 1300 W.T. Harris Blvd., Charlotte, NC 28262, USA; 2002
12. J.M. Rase, Carbon Diffusion Across Dissimilar Steel Welds 1992
13. EPRI report 2014, Report 3002006759
14. Krstevska, Aleksandra & Poser, Maja & Zdraveski, Filip. (2022). WELDABILITY BETWEEN STEEL TYPE 304H AND STEEL TYPE P91 FOR HIGH TEMPERATURE APPLICATIONS.
15. A Zielinski, G Golanski, P Urbanczyk, J Slania, J Jasak, Microstructure and properties of dissimilar welded joint between p91 and tp347hfg steels after 105 000 h service, Prace IMZ 1 2015

Design for Sustainability: A Review

Jelena Djokikj, Elisaveta Doncheva
"Ss. Cyril and Methodius" University in Skopje, Faculty of Mechanical Engineering, 1000 Skopje, North Macedonia
jelena.djokikj@mf.edu.mk

Abstract: *Sustainability is topic of great concern since the last decade and still today does not lose of its popularity. Reason for that is that the contemporary way of living is causing great damages to the environment. Designers have been talking about changing the ways in which the products are designed in order to have sustainable product. But, for achieving sustainability many aspects need to be addressed, such as: cultural, social, economical and technological. Nowadays, we believe that these aspects are on higher level and we can talk about sustainable design.*

Every product development process starts with the design phase and this is why we believe that it is most important for making improvements of the products. In this paper we have the premise that good and appropriate design can have positive influence on the sustainability. In order to check the validity of the premise we are reviewing paper dealing with sustainability, eco design, and engineering materials.
Keywords*: DESIGN PROCESS, SUSTAINABILITY, CIRCULAR ECONOMY*

1. Introduction

Since the of the time homo sapience's humans depended on the nature, and therefore cared for it and nurture it. However, with the industrialization and globalization humans have been obsessed with satisfying their needs. Satisfying those needs meant cutting down forest, endangering lives of hundreds if not millions species (animals, birds, fish, and plants), causing climate change and what not. Human activity has even been connected to a global "sixth mass extinction" of animal species and "massive anthropogenic erosion of biodiversity and of the ecosystem services essential to civilization" [1].

Over the years many different terms have been in circulation. Earliest are green design and then eco design, referring to ecofriendly design of products, meaning that in the design phase the designer takes care of minimizing the negative effects on the nature throughout the whole lifecycle of the product.

In the later years terms such as sustainable design have emerge, taking into account the whole process including the sociological and economic factors. So it can be said that the sustainability stands for much broader aspects, having the UN'S sustainable goals as reference. The concept of sustainable development stands for harmonizing development processes with respect for the environment, in the interest of future generations. Going by an analogy between the processes of natural transformation and those of industry, sustainability concepts take inspiration from nature's teachings in an attempt to optimize the flows of resources that characterize the entire industrial system and the life cycle of products [2].

"Sustainable development is development that meets the needs of the present without compromising the ability of future generations to meet their own needs" [3]. With this definition of sustainable development, in 1987 the World Commission on Environment and Development (WCED) outlined what is now widely recognized as the guiding objective of the current process of economic and technological development - to ensure that the use of environmental resources to satisfy present demands are managed in such a way that they are not left so damaged or impoverished that they cannot be used by future generations. After more than 30 years since the publication, it now seems that a complete vision of the problem has finally matured, where sustainable development is considered a process that includes all three key factors: **economic, sociocultural and environmental** [4]. It is important to stress that the science and the technology are in direct connection to every one of the key factors and are expected to provide data and tools for achieving balance [5] which is the necessary for sustainable development.

In order produce eco products or products that are ecofriendly the industry has to adapt as well. This is the beginning of industrial ecology (IE) which has to provide better understanding and application of the system necessary for achieving sustainability [6]. According to scholars [7; 8; 9] working in this discipline in order to obtain sustainability the industrial ecosystem must be closed cycle same as the biological ecosystems. In the recent years the term circular design has been in use, the term which clearly stands for achieving a closed loop of the product's life cycle. Throughout the years the IE slowly transitioned into circular economy (CE). The field of IE provided the foundations for the idea of a CE [10; 11; 12]. Building on original IE thinking [13; 14; 15] the CE has recently been (re-)popularized as both a public policy and business concept [16; 17]. Developed countries [18; 19; 20] are trying to adopt CE principles as guidelines for the envisioned redesign of their economies [12], which requires changes on the macro-level (cities, provinces, regions, and nations), meso-level (networks, eco-industrial parks), and micro-level (individual companies, consumers) [11].

We believe that the design has crucial role in achieving sustainable development or CE. In this paper, we are reviewing different sources on eco design, sustainability and circular economy in order to comprehend the influence that the design process has in each of these disciplines.

2. State of the art

Eco design can be considered as a part of the sustainable product design. It is a well-known discipline that provides designers with design methodologies, eco design strategies, methods and principles helping them and guiding them into the design process of or creating products that do not have large negative implication on the environment throughout the whole life cycle [21; 22; 23; 24; 25]. But the countries and so the companies are slowly shifting towards the circular economy (CE), which requires different approach when designing. Designers are lacking methodologies and strategies to guide them through circular product design when designing for the circular economy [26]. den Hollander and colleagues [27] in their research focus on creating methodology for circular product design, focusing of product integrity, which they believe is the key to no waste policy of the CE. The authors' propose a typology of three stages for product integrity: long use, extended use and recovery. Design approaches for long use are method of resisting the obsolescence, which encompasses: design for physical durability and design for emotional durability [28]. Design approaches for extended use are in fact postponing obsolescence and those are design for maintenance and design for upgrading. Design approaches for recovery are: design for decontextualizing, design for repair, design for refurbishment, and design for remanufacture, aimed at reversing the obsolescence [27].

Emotional durability researched by Page [28] is something that is rarely being discussed and researched. But that is not because it is not important but because is complex area requiring large subject sample in order to make objective conclusion. She conducts a literature review from which can be concluded that emotional durability and product attachment are influenced by different

factors. These factors can be used by the designer in order to design products that are more desirable and harder to toss away.

CE is slowly becoming something that the societies are striving upon, and the main goal of the CE is zero waste. This is why many researchers work on proposing different strategies and methodology that provide no waste.

The CE may be defined as "a regenerative system in which resource input and waste, emission, and energy leakage are minimized by slowing, closing, and narrowing material and energy loops. This can be achieved through long-lasting design, maintenance, and repair, reuse, remanufacturing, refurbishing, and recycling" [29].

In this age of extensive consumeristic human behavior, massive amount of waste are produced every day. One area of high number of waste is the garment industry, since the production is high and at the same time the styles are changing very fast. Achieving zero waste in the industry requires major changes in the production processes which is long and expensive task. No waste would mean that there should be 100% resource use in the production. Along with the changes in the production process, also there should be changes in the aesthetic/fit of the contemporary designs [30]. As their contribution to the CE, Kääriäinen and Niinimäki [31] conduct material research in order to create sustainable textile materials. The empirical basis of this study consists of five material research and development projects. They investigate the projects to understand not only the approaches to producing sustainable textile materials, but also to map the differences in the scientific dialogues.

On the other hand numerous authors critique the waste hierarchy. Behrens and colleagues [32] critique it for having a positive impact on dematerialization and decoupling, given that it focuses only on waste and does not address material inputs directly, nor consider economic output. Van Ewijk and Stegemann [33], provides a critique relating to the hierarchy's priority orders. First, they argue, inclusion of an option in a priority order legitimizes its existence (i.e., disposal). Second, the common understanding is that one needs to move up the hierarchy rather than necessarily achieve the highest outcome. It is about the direction of change rather than the end goal, which illustrates the relative nature of the waste hierarchy. McDonough and Braungart [34] refer to the waste hierarchy as the logic of death and argued that solution should be made to design for abundance. Their argument is that growth isn't in and of itself wrong, only the way we do it and that the things society and industry tends to want to grow like product sales and dividends – unless also tethered to the finite environmental (and social) limits of our planet – are the very things that can make abundance for all impossible to achieve.

3. Discussion

Authors of the review paper have different proposals for achieving sustainability and CE. The difference is that in the sustainable development the goal is to prevent occurrence of waste or to minimize it, where as in the CE there should not be waste. This main difference is the reason for different approaches and proposed methodologies. In the prevention of waste we must think in the design process on how to design products that do not use abundance of natural resources that do not require long and complex production processes, localised manufacturing, optimised transport, fast assembly and possibility for reuse, remanufacture od recycle. In the CE there should not be waste this is why there are just two approaches:

- Design for extending the useful life of a product and
- Design for recycling.

In Design for extending the useful life of a product are approaches for long use (design for durability and design for emotional durability), approaches for extended use (design for maintenance, design for upgrading) and approaches for recovery (design for decontextualizing, design for repair, design for refurbishment, design for remanufacture) [27].

Extended life cycle – ref

The ultimate goal of *design for product integrity* is to minimize and ideally eliminate environmental costs by preserving or restoring the product's added economic value over time. Extended product lifetimes, however, do not always result in a net reduction of environmental load. Over time, newer versions of products may be developed that incorporate more efficient technologies. From that moment on, the environmental impacts that arise from the prolonged use of a product may become larger than the embedded impacts of a more efficient replacement product [35]. Because the Inertia Principle does not account for this, product designers need to understand the ecological consequences of their design interventions.

Design for recycling consists approaches and strategies for waste management and transform it into resources. In order to ensure that, in the design process the appropriate type and amount of material should be selected. The selected material need to be recyclable, but also there should be market demand for it and the recycling process needs to be efficient and economical.

4. Conclusion

Sustainability and CE are important topics for the contemporary society and it is a positive thing that they attract so many researchers.

In this paper we analyzed different research papers with different approaches in the sustainability and CE. But every one of the implied that design phase is the crucial for achieving the goal, whether it is extended life, recyclability or zero waste. This only affirms the premise from the beginning of the paper that the designer is the one that needs to design product that can have extended life or be recycled.

For further research the number of researched paper has to be extended and their categorization according to the specific area of interest should be made.

References

1. Ceballos, Gerardo, Paul R. Ehrlich, and Rodolfo Dirzo. (2017). Biological annihilation via the ongoing sixth mass extinction signaled by vertebrate population losses and declines. *Proceedings of the national academy of sciences* 114.30.
2. Giudice, F., La Rosa, G., & Risitano, A. (2006). *Product design for the environment: a life cycle approach*. CRC press.
3. Holden, E., Linnerud, K., & Banister, D. (2014). Sustainable development: Our common future revisited. *Global environmental change*, **26**, 130-139.
4. Robèrt, K. H., Schmidt-Bleek, B., De Larderel, J. A., Basile, G., Jansen, J. L., Kuehr, R., ... & Wackernagel, M. (2002). Strategic sustainable development—selection, design and synergies of applied tools. *J. Clean. Prod*, **10**(3), 197-214.
5. Munasinghe, M. (2001). Sustainable development and climate change: applying the sustainomics transdisciplinary meta-framework. *I. J. G. Env. I*, **1**(1), 13-55.
6. Korhonen, J. (2004). Industrial ecology in the strategic sustainable development model: strategic applications of industrial ecology. *J. Clean. Prod*, **12**(8-10), 809-823.
7. Ayres, R. U. (1989). Industrial metabolism. *Technology and environment*, 23-49.
8. Allenby, B. R. (1992). Achieving sustainable development through industrial ecology. *International Environmental Affairs*, **4**(1), 56-68.
9. Jelinski, L. W., Graedel, T. E., Laudise, R. A., McCall, D. W., & Patel, C. K. (1992). Industrial ecology: concepts and approaches. *Proceedings of the National Academy of Sciences*, **89**(3), 793-797.

10. Bocken, N. M., Olivetti, E. A., Cullen, J. M., Potting, J., & Lifset, R. (2017). Taking the circularity to the next level: a special issue on the circular economy. *J. Ind. Ecol*, **21**(3), 476-482.
11. Ghisellini, P., Cialani, C., & Ulgiati, S. (2016). A review on circular economy: the expected transition to a balanced interplay of environmental and economic systems. *J. Clean. Prod*, **114**, 11-32.
12. McDowall, W., Geng, Y., Huang, B., Barteková, E., Bleischwitz, R., Türkeli, S., ... & Doménech, T. (2017). Circular economy policies in China and Europe. *J. Ind. Ecol*, **21**(3), 651-661.
13. Ayres, R., & Ayres, L. (1996). Industrial ecology: towards closing the materials cycle. In *Industrial Ecology*. Edward Elgar Publishing.
14. Ehrenfeld, J. (2004). Industrial ecology: a new field or only a metaphor?. *J. Clean. Prod*, **12**(8-10), 825-831.
15. Lifset, R., & Graedel, T. E. (2002). Industrial ecology: goals and definitions. In *A handbook of industrial ecology*. Edward Elgar Publishing.
16. Ellen MacArthur Foundation. (2012). *Towards the circular economy*. Ellen MacArthur Foundation.
17. European Commission. 2014. *Moving towards a circular economy*. http://ec.europa.eu/environment/circular-economy/. Accessed October 2015.
18. Tong, X., Tao, D., & Lifset, R. (2018). Varieties of business models for post-consumer recycling in China. *J. Clean. Prod*, **170**, 665-673.
19. Yuan, Z., Bi, J., & Moriguichi, Y. Yuan, (2006). The circular economy: a new development strategy in China. *J. Ind. Ecol*, **10**.
20. Andersen, M. S. 2007. An introductory note on the environmental economics of the circular economy. *Sustain. Sci*, **2**(1): 133–140.
21. Pigosso, D. C. A., McAloone, T. C., & Rozenfeld, H. (2015). Characterization of the state-of-the-art and identification of main trends for Ecodesign Tools and Methods: Classifying three decades of research and implementation. *J Indian Inst Sci*, **95**(4), 405-428.
22. Bovea, M. D., & Pérez-Belis, V. (2012). A taxonomy of ecodesign tools for integrating environmental requirements into the product design process. *J. Clean. Prod*, **20**(1), 61-71.
23. EC (European Commission). 2009. Directive 2009/125/EC of the European Parliaments and the Council of 21 October 2009 Establishing a Framework for the Setting of Ecodesign Requirements for Energy-related Products (Recast). (2011). Brussels, Belgium: European Commission Energy.
24. Luttropp, C., & Lagerstedt, J. (2006). EcoDesign and The Ten Golden Rules: generic advice for merging environmental aspects into product development. *J. Clean. Prod*, **14**(15-16), 1396-1408.
25. Tischner, U., & Deutschland, U. (2000). *How to do EcoDesign?: a guide for environmentally and economically sound design*. Verlag form Praxis.
26. Den Hollander, M. (2018). *Managing Obsolescence: Extending Product Lifetimes in a Circular Economy* (Doctoral dissertation, TU Delft).
27. Den Hollander, M. C., Bakker, C. A., & Hultink, E. J. (2017). Product design in a circular economy: Development of a typology of key concepts and terms. *J. Ind. Ecol*, **21**(3), 517-525.
28. Page, T. (2014). Product attachment and replacement: implications for sustainable design. *IJSDes*, **2**(3), 265-282.
29. Geissdoerfer, M., Savaget, P., Bocken, N. M., & Hultink, E. J. (2017). The Circular Economy–A new sustainability paradigm?. *J. Clean. Prod*, **143**, 757-768.
30. McQuillan, H. (2019). Waste, so What? A reflection on waste and the role of designers in a circular economy. *Nordes*, (8).
31. Kääriäinen, P., & Niinimäki, K. (2019). Towards Sustainable Textile Materials: Potential pathways and dialogues between disciplines. *Nordes*, (8).
32. Behrens, A., Giljum, S., Kovanda, J., & Niza, S. (2007). The material basis of the global economy: Worldwide patterns of natural resource extraction and their implications for sustainable resource use policies. *Ecol. Econ*, **64**(2), 444-453.
33. Van Ewijk, S., & Stegemann, J. A. (2016). Limitations of the waste hierarchy for achieving absolute reductions in material throughput. *J. Clean. Prod*, **132**, 122-128.
34. McDonough, W., & Braungart, M. (2010). *Cradle to cradle: Remaking the way we make things*. North point press.
35. Bakker, C., Wang, F., Huisman, J., & Den Hollander, M. (2014). Products that go round: exploring product life extension through design. *J. Clean. Prod*, **69**, 10-16.

Sustainability and application of life cycle assessment in welded structures

Elisaveta Doncheva[1], Jelena Djokikj[1], Nikola Avramov[1], Aleksandra Krstevska[1], Martin Petreski[1]
Ss. Cyril and Methodius University, Faculty of Mechanical Engineering, Skopje, North Macedonia[1]
e-mail: elisaveta.doncheva@mf.edu.mk

Abstract: *As global environmental impacts have increased, modern societies have expressed a strong interest in implementing sustainable solutions to reduce emissions and use operational energy and natural resources. The construction industry is a leading promoter of significant environmental impacts because it consumes a significant amount of water, energy, and materials. Steel and welding are critical in all three major sectors of the industry: construction, infrastructure, and industry. This paper discusses the significance of meeting sustainable development goals in welded structures and identifies ways that this industry can help to reduce environmental impact and improve employment conditions while achieving economic growth, saving time, and maintaining structural quality. The paper discusses how to optimize various aspects ranging from raw material extraction to construction waste disposal using the life cycle assessment (LCA) methodology. It provides a starting point and demonstrates how these tools can contribute to more sustainable welded structures.*
Keywords*:* LIFE CYCLE, SUSTAINABILITY, STEEL STRUCTURES, MATERIALS, WELDING

1. Introduction

Over the last few years, national and global interests have shifted towards sustainable, efficient, and environmentally friendly production. It's understandable given that high levels of air pollution, greenhouse gas emissions, dangerous substances, and waste pose a serious threat to the environment and humanity, as well as widespread concern about energy consumption and limited resources. The construction industry has a significant environmental impact. According to recent data, buildings account for approximately 40% of CO_2 emissions [1-2]. Buildings account for up to 40% of total energy consumption and 30% of greenhouse gas emissions, according to data from the United Nations Environment Programme (UNEP), and in some countries, these percentages can reach nearly 70% [5]. To address the significant impact of the construction and building industries on planetary and human health, The World Green Building Council (WorldGBC) has established the ultimate goal of reducing emissions to zero by the end of 2050, and many countries, including Canada and the United States, have developed new standards to meet these targets [1-4]. According to the most recent data on the construction industry's environmental impact, construction is responsible for 23% of air pollution, 50% of climate change, 40% of drinking water pollution, 50% of landfill waste, and 40% of global energy usage [5].

A construction is considered environmentally acceptable if it meets the prescribed green standards throughout its lifetime. These so-called eco-friendly or green buildings combine techniques, materials, and technologies to improve environmental and social performance. Certain practices, materials, and processes are expected to significantly reduce environmental impacts and efficient resource consumption throughout the lifecycle of a building [6]. LEED (Leadership in Energy and Environmental Design) is the most commonly used rating system (standard) for eco-buildings when designing for sustainability. Despite progress in implementation, there are still some challenges that remain. LEED is a good starting point but there are other paths to sustainable design that go beyond LEED by implementing alternative sustainable design methods and standards. Beyond eco-standards, sustainability refers to the environmental, social, and economic impact. It considers the planet, people, and profit and it promises long-term growth and increased competitiveness.

In production, steel is considered an excellent sustainable building material because of its durability, adaptability, and recycling capabilities, all of which are important principles for sustainable development [7-8]. It is widely used for fabricating steel structures such as ships, bridges, buildings, and pipelines. However, according to Kleiwerks' most recent research, building materials such as concrete, aluminum, and steel are directly responsible for large amounts of carbon dioxide (CO_2) emissions [5]. When these materials were compared, the steel industry produced the most harmful emissions and pollution, which is significant because steel is widely used in construction and is expected to grow significantly in the future [5]. However, this is not the only factor to consider when evaluating the sustainability of welded structures; the joining process should also be considered. Welding is a common joining process that has a direct impact on the overall value of the structure. On-site welding techniques can be used in construction or manufacturing. Depending on the technology and process parameters, the time of joining and the use of energy and resources can vary; some require a large amount of energy and resources, which is critical from an environmental standpoint. Socially, welding entails working in a hazardous environment, which has a negative impact on workers' health.

It is clear that many factors contribute to the overall assessment of the sustainability of welded structures, and a suitable assessment tool should be used to obtain relevant results. The life cycle assessment (LCA) tool is a well-known methodology that can account for a variety of environmental impacts such as ozone layer depletion, global warming, eutrophication, and pollution, among others. LCA considers all or some of the following product or process phases: extraction, production, application, disposal, and recycling. If steel structures are made of raw material, LCA can be used to examine the environmental impact in terms of resources and energy that are required to extract the raw material from the ground. The impact of steel production will be followed by the impact of steel application (maintenance, etc.), and finally, the impact of steel rejection and recycling will be considered. If the steel is transported to a landfill, the amount of land used, the potential for environmental leakage, and other factors can be taken. Then there are the joining processes, which also have an impact on the environment and must be evaluated in terms of energy and water consumption, waste, emissions, ease, economy, and time of production. All of these factors should be considered, and a decision on the best joining technique should be made accordingly.

This paper aims to improve understanding of welded structure sustainability while also evaluating and proposing potential solutions to the remaining challenges. It introduces LCA methodology and examines the sustainability of welded structures, as well as provides a basic framework. Furthermore, critically reviewing the progress made in the sustainability of welded structures to date will help current and future engineers understand the problems that need to be solved.

2. Sustainability and sustainable welded structures

Sustainability and sustainable development focus on three major areas: the environment, the economy, and society. The Bruntland definition of sustainable development from 1987 does not explicitly mention the environment, suggesting that it can entail more than just reducing negative environmental effects [7]. The connection between sustainable development and construction is evident, given that the construction industry is Europe's largest industrial employer and thus has significant environmental and social impacts [9]. Sustainable structures, in general, seek to achieve optimal operating conditions with minimal environmental impact, reduce material consumption, improve people's lives, provide more efficient and cost-effective work, and protect natural resources for future generations while maintaining high productivity and quality to

satisfy customers without increasing costs. The term " green building" is referring to a structure that meets the environmental standards through its life cycle [8], but that doesn't make the structure sustainable because sustainability cannot be achieved by focusing solely on environmental issues, these must be balanced against economic and social concerns [9]. The life cycle of a structure includes its construction, use, and deconstruction, as well as the underlying activities and material and energy flows that have an unavoidable positive and negative impact on the environment [10]. In this paper, the term "sustainability of structures" refers to the major health and environmental aspects associated with the life cycles of welded steel structures. Social issues are not the primary focus and are not addressed in depth.

In welded structures, steel is the most commonly used material. It is an excellent choice for structural applications due to its high strength-to-weight ratio, low cost, and ease of design and construction [7, 11]. One of the most appealing characteristics is that it can be fully recycled multiple times without losing quality. There are two billion tons of steel waiting to be recycled, and the recovery rate of structural steel products is currently around 95% and rising, which may be the most compelling sustainability argument for using steel in construction[10]. The high rate of recyclability and prefabrications is directly linked to benefits like less waste generation, the off-site production of steel means small construction sites, the structures are light with high strength and the time for production is short making it flexible and applicable for possible extensions of existing buildings [7,10,11]. Steel structures have an increased lifecycle, long design life, and high-quality remains over time. Also, there are flexible solutions for low maintenance and effective anti-corrosion measures that can be undertaken. There are many other possibilities that steel offers like use for the construction of modular buildings on temporary locations, buildings with long spans that provide open spaces that can be adapted for all sorts of use, and large, prefabricated units from modular buildings that can be reused in other structures. The high rate of recyclability and prefabrication is directly related to benefits such as reduced waste generation, small construction sites, light structures with excellent strength, and a short production time, which makes it flexible and applicable for possible extensions of existing buildings [7,10,11]. Steel structures have a long design life and lifecycle while maintaining their high quality over time. There are also adaptable solutions available for low-maintenance and effective anti-corrosion measures. Steel can also be used to build modular buildings on temporary sites, buildings with long spans that provide open spaces that can be adapted for a variety of uses, and large prefabricated units from modular buildings that can be reused in other structures. Furthermore, steel is an excellent material for high-rise buildings. All these characteristics show that steel is a desirable construction material for reasons other than its low cost and ease of design and construction. There are, however, other aspects to consider that correspond to critical concerns in the field of sustainability. The production of steel generates more CO_2 than other materials and the energy required to produce makes us question if this material meets the overall sustainability goals. According to World Steel Association data, the steel industry in the United States consumes about 2% of all domestic energy each year [7]. Sustainable structural components have low energy costs, high durability, low maintenance requirements, and contain high proportions of recycled materials. The extraction, processing, transport, construction, operation, disposal, reuse, recycling, and off-gassing and volatile organic compounds associated with the material should all be considered. In Fig. 1, the sustainability and potential benefits of steel structure construction can be investigated in different phases [10].

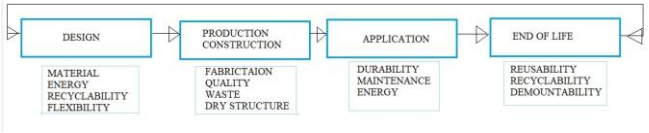

Fig. 1 *Considerations on the sustainability of a steel structure in different phases [10]*

In steel structures, welding is a very important joining technology in modern manufacturing, it accounts for a major part of the cost and directly affects the value of the structure and the product. Structures such as ships, bridges, buildings, and coastal foundations are made of structural steel. Depending on the material's dimensions welding can be performed in one or several passes and layers depending on the technology and process parameters. In order to reduce the time of the process, it is recommended to use high-energy processes, which require a large amount of energy and resources, which is critical from an environmental perspective. From a social point of view, welding involves working in a dangerous environment, and has a harmful effect on the health of workers, resulting from welding gases, radiation, sound, etc. This aspect has been neglected in the selection of the welding process, due to the predominant focus on economics combined with a lack of adequate methods to assess these hazards. The majority of welding research and studies are aimed at developing new processes and technologies. There are few research papers on sustainability that cover all three critical aspects of welded products or structure development.

In construction, submerged metal arc welding (SMAW) is used for welding large profiles and beams, flux cored arc welding (FCAW) is more convenient for the fabrication of steel structures as well as heavy machinery repair, gas tungsten welding (GTAW) is used for joining various metals such as stainless steel, aluminum, bronze, and copper, and gas metal arc welding (GMAW) is used for structural and non-structural purposes. Compared to a separate analysis, these technologies are all different and have different effects on the environment, with some being more hazardous or economical. Fusion welding techniques and their environmental impacts are becoming more important for larger components and thicknesses as production time, material, and energy needs increase. According to a recent study on the environmental impact of manual metal arc welding (MMAW), when compared to laser arc-hybrid welding (LAHW) and gas metal arc welding (GMAW), MMAW has the greatest environmental impact in terms of global warming, acidification, eutrophication, and photochemical ozone creation [12]. MMAW is widely used in construction and uses coated electrodes; however, its productivity is low, and reducing energy consumption in the process is one of the most important ways to improve the environmental performance of the process. [13]. Also, the use of titanium dioxide for electrode coating in MMAW plays an important role in contributing to the overall burden of acidification and eutrophication [13].

The manufacturing or construction phase is one chain in the overall assessment of the welded structure's sustainability. There are separate research papers on each phase's sustainability, but the results are limited to the defined framework conditions. The most significant constraints stem from the exclusive focus on each phase of construction. There are numerous factors to consider when selecting environmentally friendly processes. The very first step in assessing sustainability is to establish a clear goal and understand the steel structure that is under consideration. This is also important for the next step, which involves selecting and evaluating indicators and gathering primary data for the assessment. Fig.2 depicts the general steps for sustainability assessments that can be adapted to a particular case. It also, shows the criteria for selecting indicators for collecting primary data [13].

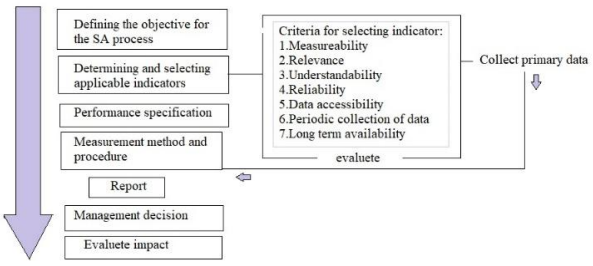

Fig. 2 *Sustainability assessment steps and evaluation of indicators [13]*

3. LCA methodology

An LCA methodology is a standardized approach for assessing the environmental impacts of a product, process, or even an entire industry. It examines the entire life cycle of a product or process, from raw material extraction and energy production to application, and takes into account numerous environmental impacts at each stage [12]. It is one of the tools developed by the European Commission to improve policy development strategy in 2015 [1]. It evaluates energy and raw material consumption, emissions, and other wastes associated with a product's or system's entire life cycle [1]. Among the effects that can be studied are climate change, resource depletion, and ecotoxicity. It can be used to assess the environmental impacts of building materials throughout their entire life cycle, from extraction to manufacturing, transportation, operation, maintenance, and disposal [1]. Allows stakeholders to compare different material options during the design phase. Many LCA software tools, such as GaBi, Athena, Building for Environmental and Economic Sustainability (BEES), and SimaPro, are used to calculate CO_2 emissions [1]. The obtainable programs contain environmental data on the most common materials used and can save a significant amount of time by presenting it in a simple and user-friendly format. Tools and databases have evolved in response to geographical location and application. In Fig. 3 a basic LCA framework is presented [14]. The objective and scope entail determining the system's purpose and limits, whereas the life cycle inventory (LCI) entails collecting data for each segment in relation to all its inputs and outputs [14]. LCA applications in construction are classified into four types: construction material selection, system evaluation and construction processes, construction industry tools and databases, and construction industry methodological developments [1]. An LCA can be useful because environmental impacts can be linked to specific decisions and can aid in making environmentally sound decisions about where to obtain steel, what joining technique to use, and maintenance coating, among other things, to minimize environmental impacts.

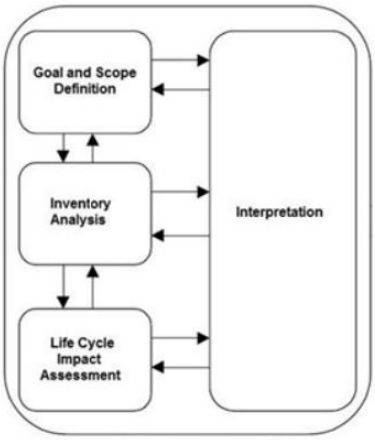

***Fig. 3** Basic LCA framework is presented [14]*

4. Conclusions

Sustainability decisions and making the right choices in the construction of economically and socially acceptable welded structures are difficult and complex. There are various stages that must be addressed, from design to end-of-life, and it has been demonstrated that the LCA methodology tool for sustainability assessment is applicable to each of them and offers acceptable solutions. When analyzing steel structures in the construction industry, the question of what kind of design, material, or manufacturing process can make a steel structure more sustainable arises. When compared to other building materials, steel has been identified as a sustainable building material. Furthermore, because there are various joining techniques that can be used for assembling structures with varying environmental impacts, choosing the right welding technology can play an important role in the overall structure's sustainability. Besides that, recent studies [13] show that the greatest environmental loads generated throughout the life of a specific structure occur during the operation and maintenance phase. This is primarily due to high energy consumption and significant atmospheric emissions. There are also social and economic indicators that should be considered throughout the entire process of implementing sustainability in steel structures. At the end of this study, it can be concluded that there is a strong need to push the boundaries of traditional structural analysis and provide new design and manufacturing knowledge to achieve sustainability of steel structures. The environmental and social impact of modern structural design should be considered, and each decision should be followed by a separate analysis at each stage of manufacturing and construction.

5. References

[1] Ahmed, Noha Ahmed Metwally, et al. "Impact of sustainable design in the construction sector on climate change." *Ain Shams Engineering Journal* (2020)

[2] WorldGBC report, "Sustainable Buildings for everyone, everywhere." (2020), available at www.worldgbc.org

[3] Canada Green Building Council office, "Zero Carbon Building Standard, Version 1 ", Ottawa, May 2017, available at www.cagbc.org

[4] Statements and releases, Fact sheet: President Biden Signs Executive Order Catalyzing America's Clean Energy Economy Through Federal Sustainability, The White House, 8 December 2021.

[5] P. Musmade1, S.Pathak, P.Patwari, "Comparative study of sustainable materials for replacement of steel reinforcement in construction", *International Research Journal of Engineering and Technology (IRJET)*, Vol. 09, 04 | 2022.

[6] Chan APC, Darko A, Ameyaw EE. Strategies for Promoting Green Building Technologies Adoption in the Construction Industry—An International Study. *Sustainability*. 2017; 9(6):969.

[7] Charles E., "Green Steel – Sustainable Steel Construction in the United States A Sustainability Learning Module for an Introductory Design of Steel Structures Course". Department of Civil and Environmental Engineering, Virginia Tech, Blacksburg. https://ecs.syr.edu/centers/SustainableEngineering/modules

[8] Taha, S., Ibrahim, M.G., & Ali, A.A. (2016). Steel as a sustainable choice towards the green building concept. *Sustainable development and planning, 210*, 123-134.

[9] Vilutiene, T.; Kumetaitis, G.; Kiaulakis, A.; Kalibatas, D. "Assessing the Sustainability of Alternative Structural Solutions of a Building: A Case Study". *Buildings* 2020, *10*, 36.

[10] Vassart O., Cajot L., Labory F., "Sustainability of buildings made of steel", *Meed Conference on Environment*, (2009).

[11] Coskun E., Seçkin E., "Sustainable design assessment of steel structures", *International civil engineering and architecture conference*, (2019).

[12] Kaliudis A., "Environmental impacts of welding methods." (2019). https://www.trumpf.com/en_INT/newsroom/stories

[13] Doncheva E., Djokikj J., Avramov N., Petreski M., Krstevska A., "Sustainability assessment of welding processes: a review", Proceedings IIW 2022 International Conference on Welding and Joining, (2022).

[14] Ferreira, Antonio Domingos Dias and Fernando Benedicto Mainier. "Application of Life Cycle Assessment (LCA) in Construction Industry." (2015).

ТЕХНОЛОГИЯ И ПРИСПОСОБЛЕНИЕ ЗА СГЛОБЯВАНЕ НА ЛЕВИ И ДЕСНИ ТРЪБИ ЗА ГРАЙФЕРНИ КОФИ

TECHNOLOGY AND FIXTURE FOR ASSEMBLING OF THE LEFT AND RIGHT TUBES FOR GRAPPLE BUCKETS

Asst. Prof. Nikolay Stankov, PhD
University of Ruse, Bulgaria
nstankov@uni-ruse.bg

Abstract: *The paper presents the developing of a technology and the designing of fixture for assembling of left and right tubes for grapple buckets. The presented clamshell grapple buckets are designed for bulk materials and they are part of the grapple construction. Grapples are installed on cranes, excavators and other specialized machines. The whole process related to the production of the two types of tubes is considered - from the 3D model to the real product. A technology and a fixture for assembling the tubes have been developed. The welding process is considered. Control cards to control the dimensions at each stage of the production of the tubes were made. Repair technology for the tubes has been developed. The 3D models are designed using the CAD system SolidWorks. Complete design documentation is created for the fixture and the process is automated by using SolidWorks template files*.

Keywords*: GRAPPLE BUCKETS, GRAPPLES, CRANES, EXCAVATORS, DEVELOPMENT, DESIGN, CONTROL, 3D MODELS, CAD SYSTEM, SOLIDWORKS TEMPLATE FILES, DESIGN DOCUMENTATION*

1. Въведение.

В доклада е представен съвместно разработен проект, свързан с конструирането и внедряването в производството на специализирана нестандартна технологична екипировка за изработването на леви и десни тръби за грайферни кофи. Разработката е на екип от Русенски университет „Ангел Кънчев“ и фирма „СЛ Индъстрис“ ЕООД, град Русе [19]. Фирмата е производител на различни заваръчни конструкции (шасита, стабилизатори, предни и задни мостове, колони и стрели за кранове), машинно обработени детайли и изделия, компоненти и специализирана екипировка за кранове, мотокари, товарачи, влекачи, багери и други машини. Фирмата произвежда екипировка за различни модели грайфери – грайферни кофи, централни тела, ротатори, носачи и други.

Грайферите се използват за товарно-разтоварни дейности на различни материали. Монтират се на кранове, автокранове, гондоли за скрап, лекотоварни автомобили, багери и други специализирани машини.

Грайферите представляват конструкция, състояща се от грайферни кофи (лява и дясна), централно тяло, ротатор и носач. Чрез кофите, грайфера загребва съответния материал. На централното тяло се установяват лявата и дясната кофа. Ротатора, осигурява завъртането на кофите по време на работа на 360°. Носача е тяло, което служи за установяване на грайфера към съответната машина.

На фиг. 1 е показан грайфер на фирма KINSHOFER с черупкови грайферни кофи [20]. Приложението на грайфера е основно за насипни материали.

Фиг. 1. Грайфер за товарно-разтоварни дейности с голям обем на кофите, фирма KINSHOFER.

В доклада е разгледан процеса на изработване на основните възли на грайферните кофи, това са левите и десните тръби. Те се монтират съответно на лявата и дясната грайферни кофи.

Основен проблем при изработване на грайферните кофи е сложната форма и конструкция, която имат. Необходимо е постигането на точното разположение на детайлите, за да се получат зададените в конструкторската документация форма и размери на кофите.

Съгласно изискванията в чертежите се прави механично обработване на функционалните повърхнини на някои от детайлите, след което те се сглобяват в определени възли от конструкцията на грайферната кофа.

Това налага за изработването на левите и десните тръби да се използва специализирано приспособление или т.н. нестандартна технологична екипировка.

2. Предпоставки и средства за решаване на проблема.

2.1. Общи сведения за грайферните кофи.

Различните модели грайферни кофи се различават по предназначението си, габаритните си размери, конструкцията и натоварването, което могат да понесат. На фиг. 2 е показан общият вид на грайферната кофа, която ще бъде разгледана. Изделието е част от производствената програма на фирмата.

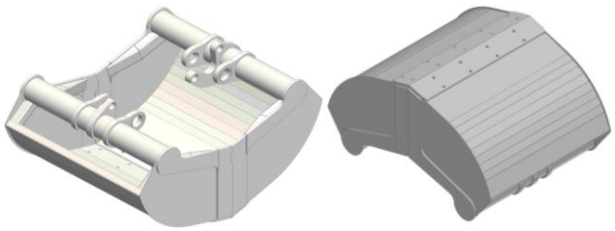

Фиг. 2. Общ вид на грайферна кофа 1000 mm.

Грайферните кофи от този модел са три вида, които се различават само по широчина – 640 mm, 800 mm и 1000 mm.

За всеки един комплект грайферна кофа (лява и дясна) трябва да се изработи комплект от лява и дясна тръба. Тоест тръбите, които трябва да се изработят за всички кофи от този модел са общо шест вида. Всяка една от тях се състои от тръба с определена дължина, две странични уши и едно централно ухо. Централното ухо е различно за лява и дясна тръба.

На фиг. 3 са показани тръбите на грайферна кофа 1000 mm.

а) б)

Фиг. 3. Тръби на грайферна кофа 1000 mm.
а) тръба лява, б) тръба дясна

Съгласно разработената технология за сглобяване на тръбите, със специализирано приспособление се изработват лявата и дясната тръба. След прихващане на детайлите, заваряване и контрол на размерите, тръбите с друго специализирано приспособление се сглобяват с всички останали детайли на грайферната кофа.

Тъй като трита модела кофи се различават конструктивно само по широчина, съответно тръбите им се различват само по дължина, като разстоянията между ушите са едни и същи, то за изработването на левите и десните тръби може да се използва едно и също приспособление. По-малкия брой приспособления значително ще намали времето за разработване и конструиране на необходимата технологична екипировка, както и разходите, свързани с производството ѝ.

2.2. Технологична подготовка на изделието.

Съгласно документацията на изделието, е необходимо предварително да се подготвят технологично детайлите и възлите му, за да бъдат изработени в условията на фирмата.

Етапите от технологичната подготовка на изделието са следните:

- създаване на тримерни модели на детайлите, възлите и изделието;
- разработване на технология за изработване на детайлите, възлите и изделието [18];
- създаване на нови възли в изделието;
- създаване на чертежи на детайлите, възлите и изделието;
- разработване на технология за сглобяване на изделието;
- разработване на технологична екипировка за сглобяване;
- разработване на технология за заваряване на изделието;
- разработване на технологична екипировка за заваряване;
- разработване на технология за механично обработване на изделието;
- разработване на технологична екипировка за механично обработване;
- разработване на методика за контрол на изделието;
- разработване на ремонтна технология на изделието.

Създаването на тримерни модели е важна стъпка от процеса на разработване на дадено изделие. Тримерните модели могат да се използват за създаване на нова конструкторска документация за нуждите на фирмата. В тримерните модели се задава необходимата информация чрез атрибути, която може да се използва за управление на документацията при налична PDM система, както и от другите отдели във фирмата при налична ERP система [4, 5, 13, 14].

На база моделите се разработва и технологията за изработване на детайлите – добавяне или премахване на отвори, прибавки за механично обработване, предварителна обработка на определени повърхнини и други. Това налага създаването на нова конструкторска документация, която да се използва в производството. След уточняване на всички особености, тримерните модели могат да се използват за създаване на файловете за разкрой на детайлите, които са от листов материал.

Много често се прилага метода на разделяне на изделието на възли, които предварително да се изработят, след което да се използва приспособление за сглобяването им в крайното изделие.

Последен етап е създаването на необходимата екипировка за сглобяване, за заваряване и за механично обработване на изделието.

В случая за грайферните кофи са разработени тримерните модели на детайлите, направени са технологични промени свързани с производството им и са създадени нови възли от изделието.

Тримерните модели са разработени с CAD системата SolidWorks [1, 2, 3, 6, 7, 21].

Детайлите на лява и дясна тръба се изработват съгласно работните чертежи.

Тръбите се отрязват на съответната дължина на лентоотрезна машина. Страничните и централните уши се изрязват от листов материал със съответната дебелина, след което на обработващ център с ЦПУ се обработват всичките им отвори. За установяването на ушите на машината също се използва специализирано бързосменно приспособление. Следва комплектацията на детайлите за лява и дясна тръба и сглобяването им чрез разработеното приспособление.

3. Решение на разглеждания проблем.

3.1. Приспособление за сглобяване на леви и десни тръби.

След като е уточнена технологията за изработването на детайлите, се разработва технологията за сглобяване на тръбите и необходимата екипировка за реализиране на тази технология.

Приспособлението е разработено чрез CAD системата SolidWorks и на фиг. 4 е показан общият му вид. Чрез приспособлението се извършва ориентиране и базиране на детайлите на тръбите в определено положение.

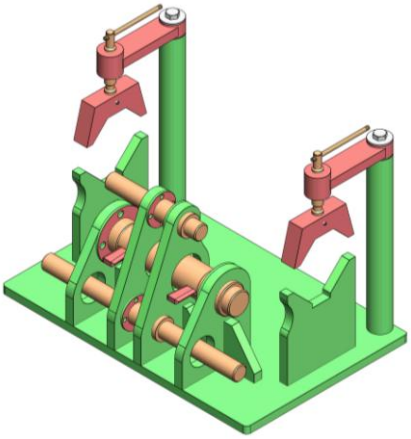

Фиг. 4. Общ вид на приспособлението за сглобяване на леви и десни тръби за грайферни кофи.

На приспособлението се извършва механично обработване на показаните с червен цвят повърхнини (фиг. 5). С механичното обработване се постига точност на размерите и на взаимното разположение на функционалните повърхнини на приспособлението.

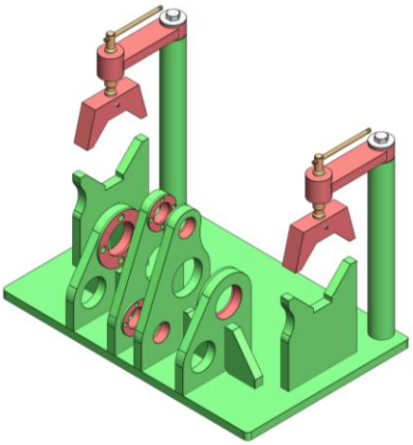

Фиг. 5. Приспособлението с механично обработените му функционални повърхнини.

Обработват се отвор Ø70 mm, през който минава Дорник 11 (фиг. 6) и два отвора Ø44 mm, през които минават Дорници 12 и 13 (фиг. 6), както и прилежащите им чела. Като база в осово направление се използва центъра на приспособлението.

На фиг. 6 е показано приспособлението с всичките му съставни елементи. То осигурява получаването на леви и десни тръби за грайферните кофи с ъглово ориентирани в определено положение уши и с точно определени разстояния между тях [8, 9, 10, 11, 12, 15, 16, 17].

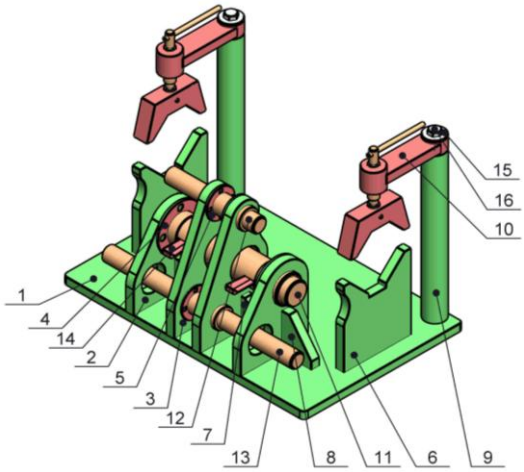

Фиг. 6. Съставни елементи на приспособлението.
1 – Основа, 2 – Планка базираща I, 3 – Планка базираща II,
4 – Шайба I, 5 – Шайба II, 6 – Призма, 7 – Ребро I, 8 – Ребро II,
9 – Опора, 10 – Фиксатор, 11 – Дорник I, 12 – Дорник II,
13 - Дорник III, 14 – Клин, 15 – Шайба с широка периферия M16,
16 – Болт M16x30

Приспособлението, заедно с всички установени детайли на лява и дясна тръба за грайферна кофа 1000 mm е показано на фиг. 7.

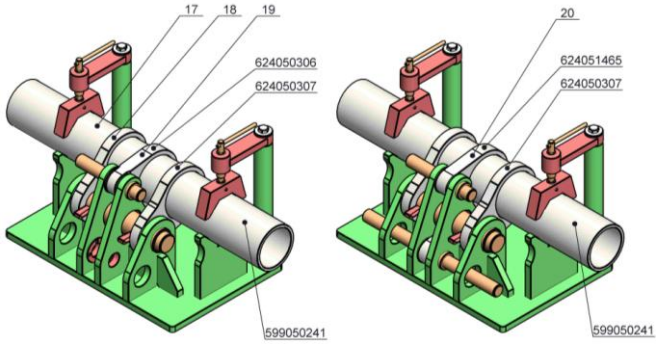

а) б)

Фиг. 7. Приспособлението с установени детайли на тръбите за грайферна кофа 1000 mm.
а) тръба лява, б) тръба дясна
17 – Тръба, 18 – Ухо странично,
19 – Ухо централно I, 20 – Ухо централно II

Технологията на сглобяване на тръбите е следната:

Технологията на сглобяване на лявата тръба включва предварителен монтаж на детайли Ухо странично 18 (2 броя) и Ухо централно 19 към Тръба 17. Тръбата заедно с ушите се базира в приспособлението на Призмите 6. Положението на Тръбата 17 в осово направление се определя чрез измерване, след което тя се фиксира с Фиксатори 10. Страничните уши 18 се центроват към страничните опори на приспособлението (2 и 4) с дорник 11 и се фиксират с Клинове 14. Следва центроване на Ухо централно 19 към централните опори на приспособлението (3 и 5) с дорник 12.

Технологията на сглобяване на дясната тръба включва предварителен монтаж на детайли Ухо странично 18 (2 броя) и Ухо централно 20 към Тръба 17. Тръбата заедно с ушите се базира в приспособлението на Призмите 6. Положението на Тръбата 17 в осово направление се определя чрез измерване, след което тя се фиксира с Фиксатори 10. Страничните уши 18 се центроват към страничните опори на приспособлението (2 и 4) с дорник 11 и се фиксират с Клинове 14. Следва центроване на Ухо централно 20 към централните опори на приспособлението (3 и 5) с дорници 12 и 13.

Чрез използване на приспособлението се гарантира успоредност на осите на отворите на ушите с оста на тръбата, ъгловото разположение на отворите на детайли Ухо странично и Ухо централно, както и перпендикулярност на контактните челни повърхнини на страничните уши с оста на отворите.

Приспособлението осигурява висока производителност, не е сложно за манипулация, с цел да се избегнат всякакви грешки от субективен характер.

На следващите фигури е показано изработеното приспособление и приспособлението с установени детайли на дясна тръба за грайферна кофа 1000 mm.

Фиг. 8. Приспособление за сглобяване на леви и десни тръби за грайферни кофи.

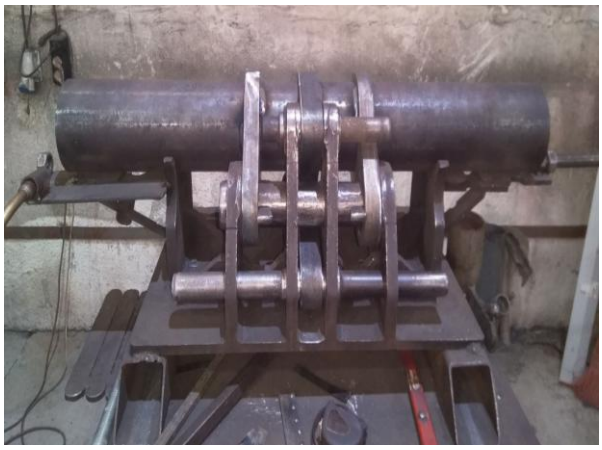

Фиг. 9. Приспособлението с установени детайли на дясна тръба за грайферна кофа 1000 mm.

Всички детайли на тръбите се закрепват в съответното им положение чрез прихващане.

На фиг. 10 са показани тръби за грайферна кофа 1000 mm, сглобени с приспособлението.

Фиг. 10. Леви и десни тръби за грайферна кофа 1000 mm, сглобени с приспособлението.

След изваждане на тръбите от приспособлението следва цялостното им заваряване съгласно изискванията на заваръчния чертеж.

3.2. Заваряване на леви и десни тръби.

След като е уточнена технологията за сглобяване, се разработва технологията за заваряване на тръбите.

Заваряването на тръбите е сложен процес и се изпълнява съгласно разработения за всяка една тръба заваръчен план. Заваряването може да бъде ръчно или роботизирано. Чрез роботизирано заваряване се постига висока производителност и много високо качество на заваръчните шевове.

Заваръчният апарат трябва да е за МИГ-МАГ заваряване. Зоните на заваряване трябва да бъдат предварително почистени.

На следващата фигура е показано уставяването на комплект лява и дясна тръба за грайферна кофа 1000 mm на заваръчен робот.

Фиг. 11. Комплект тръби за грайферна кофа 1000 mm, установени на заваръчен робот.

На фиг. 12 е показана дясна тръба за грайферна кофа 1000 mm след заваряване на робота.

Фиг. 12. Дясна тръба за грайферна кофа 1000 mm след заваряване.

След заваряване, всяка една тръба се почиства от пръски. Извършва се контрол на функционалните ѝ размери и контрол на разположението на детайлите ѝ. Ако има някакви отклонения в размерите и в разположението на детайлите, се извършват корекции за отстраняването им.

Извършва се контрол на качеството на изпълнение на заваръчните шевове, като се проверява за наличието на дефекти от типа на пукнатини и шупли. Ако има някакви отклонения и дефекти те се отстраняват.

След като комплект лява и дясна тръба са заварени, може да се пристъпи към следвашия етап от технологията за изработване на грайферните кофи, а именно сглобяването на грайферна кофа от съответния модел. За сглобяване на всеки модел грайферна кофа също се използва специализирано приспособление.

3.3. Контрол на леви и десни тръби.

След като е уточнена технологията за сглобяване и технологията за заваряване, се разработва методика за контрол на тръбите.

След заваряване на тръбите се извършва цялостен контрол съгласно документацията на изделието.

Контрола се извършва от контрольор по качеството (ОТКК), като за целта се попълва контролна карта за всяка една тръба.

Контролната карта е направена така, че размерите, които трябва да се изпълнят съгласно чертежа се контролират на всички етапи от производството на изделието. Това са – етап сглобяване, след прихващане на детайлите, след заваряване и окончателен контрол.

При констатиране на отклонения на контролираните размери извън допуска, се извършват коригиращи действия, съгласно разработената ремонтна технология.

Задължителен при производството на тръбите е контролът на качеството на изпълнение на заваръчните шевове. Проверява се за възникнали дефекти като пукнатини и шупли в зоните на заваряване. При констатиране на възникнали дефекти в заваръчния шев, се извършват коригиращи действия за отстраняването им, съгласно разработената ремонтна технология.

3.4. Особености при моделирането на тримерните модели в CAD системата SolidWorks.

За разработеното приспособление е направена пълна конструктивна документация. Процеса на създаването ѝ е автоматизиран, чрез използване на шаблонни файлове на документите, които използва CAD системата SolidWorks.

При създаването на тримерните модели на детайлите и на сглобените единици са използвани шаблонни файлове за Part и Assembly документите. За всеки един тримерен модел на детайл или сглобена единица, от меню File Properties, в прозореца Summary Information, в секцията Custom се избират необходимите атрибути. При разработването на конструктивната документация са използвани шаблонни файлове за Drawing документите, които представляват стандартните чертожни формати – A4, A3, A2, A1 и A0 [4, 5, 6, 7, 13, 14].

В шаблона на всеки един тримерен модел на детайл или сглобена единица се задава необходимата информация чрез атрибути – потребителски и служебни. Тази информация е нужна при разработването на конструктивната документация, тъй като излиза автоматично в таблиците на чертежите и спецификациите. Информацията от атрибутите може да се използва за управление на документацията при налична PDM система, както и от другите отдели във фирмата при налична ERP система [4, 5, 13, 14].

4. Заключение.

Въз основа на направеното по представената разработка, може да се направят следните изводи:

1. Разработена е технология и приспособление за сглобяване на леви и десни тръби за грайферни кофи. Приспособлението осигурява точно позициониране на детайлите на тръбите, не е сложно за манипулация, с цел да се избегнат всякакви грешки от субективен характер.
2. Приспособлението за сглобяване може да се използва за изработване на всички видове тръби за различните грайферни кофи от представения модел.
3. Направена е пълна конструктивна документация на разработеното приспособление. Процесът на създаване на конструктивната документация е автоматизиран чрез използването на шаблонни файлове за Part, Assembly и Drawing документите.
4. Така създадената база данни може да се използва при решаване на сходни проблеми при подобни изделия.

5. Литература

1. Ангелов П. CAD системи. Русе, Печатна база на Русенски университет „А. Кънчев”, 2015.
2. Ангелов П. CAD системи. Ръководство за упражнения. Русе, Печатна база на Русенски университет „А. Кънчев”, 2015.

3. Ангелов П., Н. Станков. http://e-learning.uni-ruse.bg – Web базирани материали за обучение по дисциплината „CAD системи“. Русенски университет „А. Кънчев”.

4. Станков Н. Лекции по дисциплината „Управление на жизнения цикъл на продуктите“. Русе, 2020.

5. Станков Н. http://e-learning.uni-ruse.bg – Web базирани материали за обучение по дисциплината „Управление на жизнения цикъл на продуктите“. Русенски университет „А. Кънчев”.

6. SolidWorks – моделиране и чертежи. ТехноЛогика ЕАД, София, 2019.

7. SolidWorks: Базово моделиране и чертежи. ТехноЛогика ЕАД, София, 2012.

8. Stankov N. Technology and fixtures for machining of parts for grapple buckets**.** XIX International Scientific Congress – Summer Session, “Machines. Technologies. Materials”, Section “Technologies”, vol. 4, p. 308-312, Varna, Bulgaria, 2022, ISSN 2535-0021 (Print), ISSN 2535-003X (Online).

9. Stankov N. Technology and fixtures for assembling and machining of a crane column. XIX International Scientific Congress – Winter Session, “Machines. Technologies. Materials”, Section “Technologies”, vol. 2, p. 161-165, Borovets, Bulgaria, 2022, ISSN 2535-0021 (Print), ISSN 2535-003X (Online).

10. Stankov N. Technology and fixtures for assembling of flanges for crane columns. XVIII International Scientific Congress – Summer Session, “Machines. Technologies. Materials”, Section “Machines” and “Materials”, vol. 2, p. 168-171, Varna, Bulgaria, 2021, ISSN 2535-0021 (Print), ISSN 2535-003X (Online).

11. Stankov N., Al. Ivanov, N. Denev, R. Milkov. Developing a technology and equipment for assembling of six sectional crane boom. XIII International Scientific Congress – Summer Session, “Machines. Technologies. Materials”, Section “Machines” and “Industrial Design Engineering & Ergonomics, vol. 3, p. 14-17, Varna, Bulgaria, 2016, ISSN 1310-3946.

12. Абрашева Д., Н. Станков, Ал. Иванов, Р. Милков. Разработване на технология и приспособления за сглобяване на леви и десни тръби на кофи за грайфери MG1500 и MG1800. Сборник доклади на студентска научна сесия – СНС‘16, стр. 90-101, Русе, 2016, ISSN 1311-3321.

13. Станков Н., Ал. Иванов. Управление на конструкторска документация чрез SolidWorks Enterprise PDM. Сборник научни трудове, том 54, серия 2, „Механика и машиностроителни технологии”, стр. 158-165, Русе, 2015, ISSN 1311-3321.

14. Трухчева Д., Н. Станков, Ал. Иванов. Управление и организация на конструкторска документация чрез SolidWorks и SolidWorks Enterprise PDM. Сборник доклади на студентска научна сесия – СНС‘15, стр. 20-30, Русе, 2015, ISSN 1311-3321.

15. Ахмед Е., Н. Станков, Ал. Иванов. Разработване на технология и приспособление за сглобяване на „Долна част” на грайфер MG300. Сборник доклади на студентска научна сесия – СНС‘15, стр. 31-37, Русе, 2015, ISSN 1311-3321.

16. Цонева Д., Н. Станков, Ал. Иванов. Разработване на технология и приспособление за сглобяване на грайфер SL500G на фирма ATLAS. Сборник доклади на студентска научна сесия – СНС‘13, стр. 77-87, Русе, 2013, ISSN 1311-3321.

17. Мичев Т., Д. Цонева, Н. Станков, Ал. Иванов. Разработване на технология и приспособления за сглобяване на хващач SL331H на фирма ATLAS. Сборник доклади на студентска научна сесия – СНС‘13, стр. 88-93, Русе, 2013, ISSN 1311-3321.

18. Koleva S. Some aspects of the informational support of technological processes. 8th International Scientific Conference "TechSys 2019" – Engineering, Technologies and Systems, IOP Conference Series: Materials Science and Engineering, Volume 618, p. 1-6, Plovdiv, Bulgaria, 2019, ISSN 1757-899X, DOI 10.1088/1757-899X/618/1/012052.

19. www.sl-industries.com. 2023.

20. www. kinshofer.com. 2023.

21. www.solidworks.com. SolidWorks, 3D Design Software. SolidWorks CAM, CAM Software. 2023.

Visualization and analysis of gear drives parameters with the help of computer-aided mathematics systems

Svetlin Stoyanov
University of Ruse "Angel Kanchev", 8 Studentska str., POB 7017, Ruse, Bulgaria
SStoyanov@Uni-Ruse.BG

Abstract: *The visualisation capabilities of the main software systems for computer-aided mathematics are reviewed. The advantages of the software system Matlab are described. The system is appropriate when visualization and analysis of engineering data are required. The author sets out to highlight the three-dimensional graphics and optimization synthesis of gear drives.*
Keywords*: THREE-DIMENSIONAL GRAPHICS, COMPUTER-AIDED MATHEMATICS, SOFTWARE SYSTEMS, MATLAB, GEAR DRIVES, LOAD CAPACITY, EFFICIENCY COEFFICIENT, MAXIMAL TORQUE*

1. Overview of the visualization capabilities of the leading systems for computer-aided mathematics

The contemporary growth of software systems provides powerful new opportunities in all areas of engineering and science. For example, in [14] is presented a study about applications of leading software systems for piezoelectric beams investigations. The development of extremely low power electronics and wireless systems has led to a strong interest in the fields of energy harvesting and development of miniature generators. Typically, these devices are used to power sensors and wireless communication systems, enabling standalone wireless sensors that are cheap to deploy. In the area of the mechanical structure vibrations investigations and the multiphysics simulations, four software systems have the lead positions. These are: ***ABAQUS***, ***COMSOL***, ***SolidWorks***, and ***MATLAB***. The software system ***MATLAB*** is a system for "*computer aided mathematics*" and "*matrix laboratory*", but in fact this software system is often used from scientist and engineers to solve mathematical models that describes problems in the area of the mechanical structure vibrations and the multiphysics simulations.

In [11, 12, 18] are presented selected investigations of structure vibrations conducted with the help of contemporary mechanical engineering software systems. Also, in [1, 11, 13, 14] are described investigations on gear transmissions performed with the finite element method in the integrated working environment of the system ***ABAQUS***.

In addition to studies described above, in this work the author set out to highlights the visualization capabilities of the leading systems for computer-aided mathematics: *MATLAB, Wolfram Mathematics,* and *Maple*.

1.1. Wolfram Mathematics

Wolfram Language provides powerful functions that automate the process of creating cognitively and aesthetically compelling representations of structured and unstructured data. This is valid not only for points, lines, and surfaces, but also for graphs and networks. This is available due to many original algorithms developed at ***Wolfram Research***.

On Fig. 1 and Fig. 2 are shown some examples for the visualization capabilities of ***Wolfram Mathematics*** [5, 6].

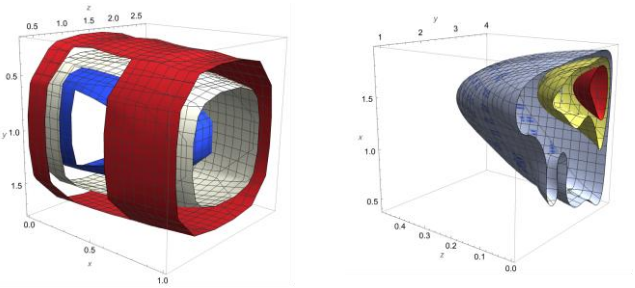

Fig. 1. *Boundaries and solutions of partial differential equations*

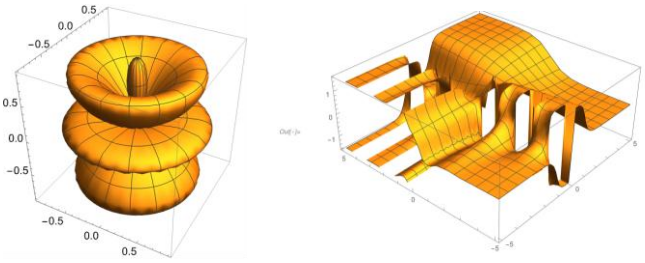

Fig. 2. *Spherical 3D graph and plot of a function with singularities*

1.2. MATLAB

The name "***MATLAB***" comers from ***MATrix LABoratory*** and has been chosen because of the powerful capabilities of this software system for working with matrices. Using this, the system ***MATLAB*** solves the problem of visualization of three-dimensional data in one. The data is plotted on a three-dimensional mesh with point size showing value of it. Edge color changes via *z* axis to distinguish coordinate of points easier. One can compare sets of data, track changes in data over time, or show data distribution. Also, the plots can be created programmatically using graphics functions or interactively using the *Plots tab* at the top of the ***MATLAB*** desktop.

Software system ***MATLAB*** incudes a tool with graphical user interface (GUI) for data interpolation – Fig. 3. This together with the discussed in the next paragraph optimization capabilities gives richest abilities to build automatized software for optimization and design of gear transmissions [2, 3, 19, 20].

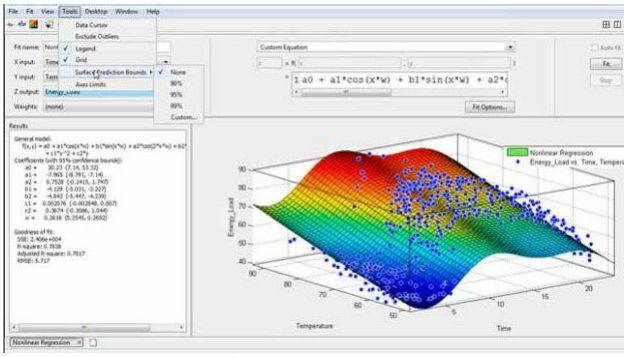

Fig. 3 *An example picture from* ***MATLAB*** *interpolation GUI*

MATLAB Optimization Toolbox provides functions for finding parameters that minimize or maximize objectives while satisfying constraints [4, 7]. The toolbox includes solvers for linear programming (LP), mixed-integer linear programming (MILP), quadratic programming (QP), second-order cone programming (SOCP), nonlinear programming (NLP), constrained linear least squares, nonlinear least squares, and nonlinear equations.

Optimization problems can be defined with functions and matrices or by specifying variable expressions that reflect the

underlying mathematics. One can use automatic differentiation of objective and constraint functions for faster and more accurate solutions.

The toolbox solvers can be used to find optimal solutions to continuous and discrete problems, perform tradeoff analyses, and incorporate optimization methods into algorithms and applications. Also, ***MATLAB Optimization Toolbox*** gives abilities to perform design optimization tasks, including parameter estimation, component selection, and parameter tuning.

1.3. Maple

Maple is a software tool that combines a powerful mathematics engine with an interface that makes it easy to manage calculations. It provides an environment that can maximize the value of calculation efforts. With Maple, one can easily validate, document, retain, reuse, and modify your calculations, reducing risk while saving time and effort in both current and future projects.

As ***MATLAB*** provides simulation environment named ***SimScape***, ***Maple*** has a tool named ***MapleSim***. It gives ability to simulate the dynamics of diverse physical systems, including mechanical systems. This is illustrated on Fig. 4 as an indicator for the visualization capacities of ***Maple***.

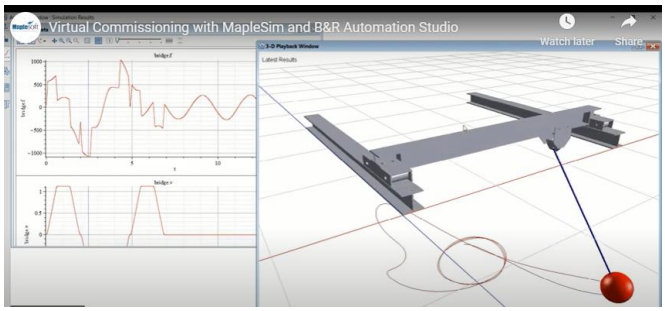

Fig. 4. *Virtual commissioning with MapleSim and B&R Automation Studio*

MapleSim has libraries with mechanical elements, for example bodies and joints. But these elements are idealized – the bodies are right and non-deformable, and the joints are without energy loses or with linear energy loses model. So, this is suitable for engineering tasks, but is insufficient for scientific investigations. In these cases, the systems ***ABAQUS*** or ***ANSYS*** are usually used [11, 15, 16, 18].

1.4. Conclusions

It can be concluded that, the software systems ***MATLAB***, ***Wolfram Mathematics***, and ***Maple*** have approximately equal three-dimensional plotting capabilities. The difference is that the system ***Wolfram Mathematics*** can be labeled as more mathematic scientists orientated, than the ***MATLAB***, which is more suitable for machine engineers and scientists. Also, while other programing languages usually work with numbers one at a time, ***MATLAB*** operates on whole matrices and arrays. Along with that ***MATLAB*** is one of the best choices when optimization needs to be done [1].

For the reasons described above, the *MATLAB* was chosen for the purposes of this investigation.

2. Description of the developed software

To interpolate and visualize the calculated in [8, 9] data, a software in the integrated working environment of the system ***MATLAB*** is developed. This gives two new abilities, as follows:

- ⇨ An ability to directly signify the relations between three parameters (or even between four parameters, if the color in set as independent indicator);
- ⇨ An ability to render relations in uninterrupted three-dimensional space (or even in four-dimensional space, if the color in set as independent indicator).

A generalized flow-chart of the developed software is presented on Fig. 5. It follows a description of each step of the flow-chart.

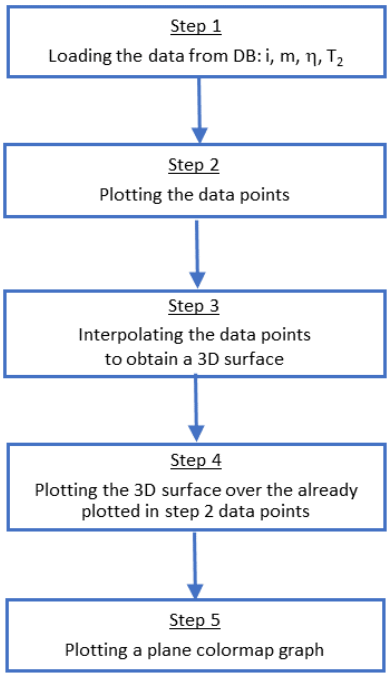

Fig. 5. *A flow-chart of the the developed software*

Step 1: Loading the input data. The input data is structured as a table with colons for: gears module *m*, transmission ratio *i*, coefficient of the efficiency η, and output torque T_2. The data can be loaded from plain text files, binary ***MATLAB*** files (*.mat) or from ***Excel*** datasheets.

Step 2: Plotting the data points. On this step, the software visualizes 3D coordinate system, label the axis with corresponding notations, set the axis limits and increment, and visualize appropriate grid. Then, the data points are plotted as solid red points – Fig. 6.

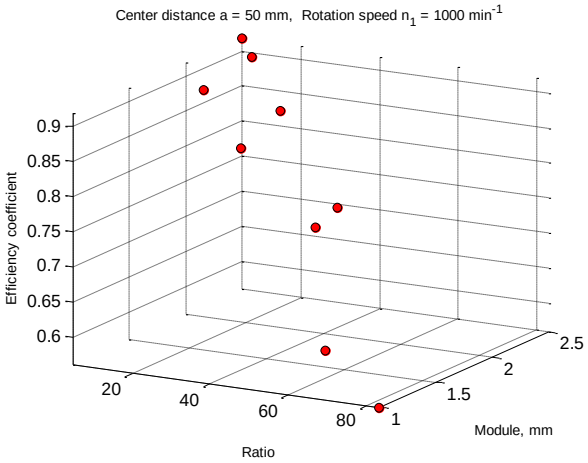

Fig. 6*. A 3D plot of the data loaded*

Step 3: Interpolate the data points. The function ***interp3*** of the system ***MATLAB*** is used. The function syntactic is:

Vq = interp3(X , Y , Z, V, Xq, Yq, Zq),

where: *Vq* contains the interpolated values of a function of three variables at specific query points using linear interpolation. The results always pass through the original sampling of the function;

X, *Y*, and *Z* contains the coordinates of the sample points;

V contains the corresponding function values at each sample point;

Xq, *Yq*, and *Zq* contains the coordinates of the query points.

Step 4: Plotting the 3D surface. On this step, the surface obtained is superimposed on the data points plotted in Step 2. Also, a legend is visualized – Fig. 7.

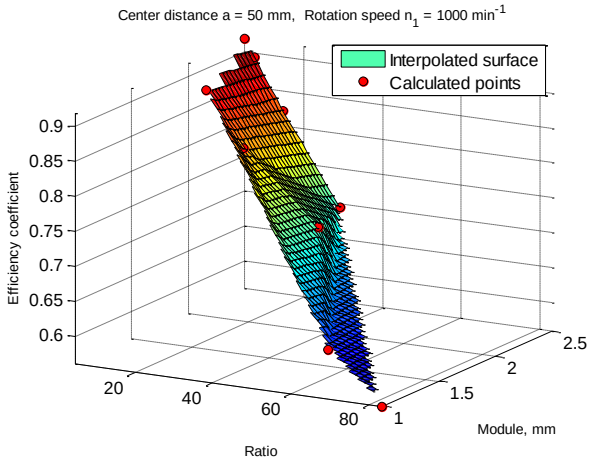

Fig. 7. *Efficiency coefficient in relation from ratio and module*

Step 5: Plotting a plane colormap graph. On this step, a new figure is plotted – Fig. 8. It is a plane graph – the efficiency coefficient values are indicated with a color map starting from dark blue and ending with dark red color.

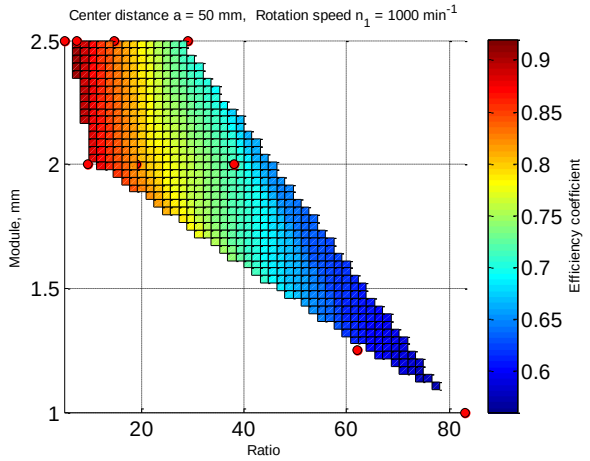

Fig. 8. *Color map representation*

In combination with computer-aided design software, the software developed gives an ability the investigation to be continued with development of an automatized optimization and design system. This can be done in the integrated working environment of the software systems ***MATLAB*** and ***SolidWorks***.

MATLAB also provides some frequently used minor capabilities, for example: saving the graphs created to image files, save the numerical results in plain text format or binary format files, export the results to MS Excel software, etc.

3. Results

The graphical visualizations obtained with the software created are presented and analyzed completely in [17]. In this paper, selected results are presented on the following figs. On Fig. 9 is shown a surface with a data point lower than other points in the plane interpolated surface. That is in the top left corner, i.e., in the area with higher values of the efficiency coefficient. From Fig. 9, it can be observed that the efficiency coefficient increases with the increase of the module and the decrease of the ratio.

The software system ***MATLAB*** gives the ability multiple three-dimensional surfaces to be superimposed. On Fig. 10b are presented two three-dimensional relations together for center distance a = 63 mm and rotation speed n_1 = 1500 min^{-1}. With this approach, one plot can represent the dependence of the efficiency coefficient from the ratio and module, and at the same time from the ratio and output torque. From Fig. 10, it can be observed that efficiency coefficient grows with decreasing the output torque and the ratio.

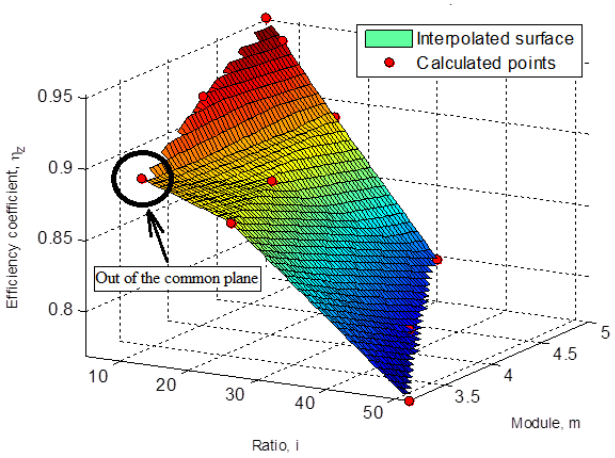

Fig. 9. *Efficiency coefficient in relation from ratio and module for center distance a = 100 mm and rotation speed n_1 = 1500 min^{-1}.*

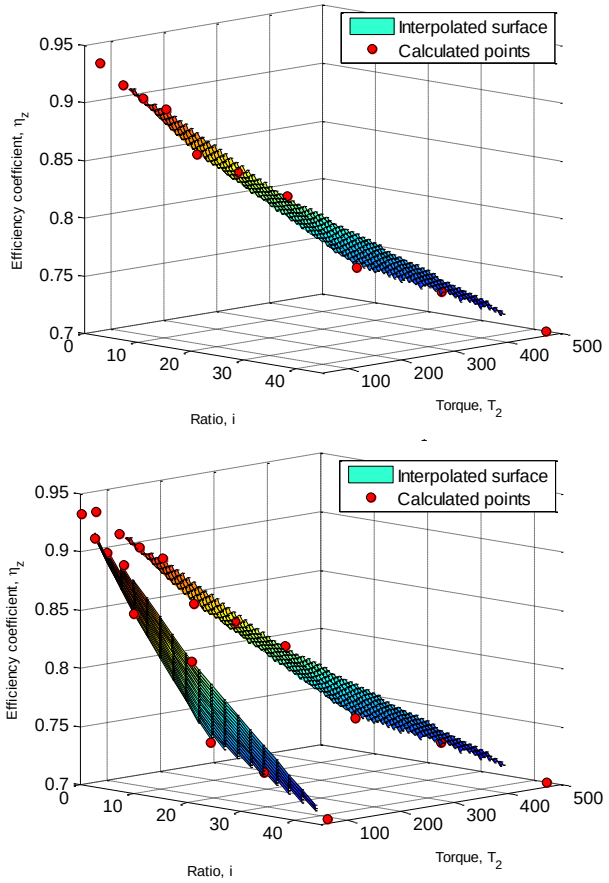

Fig. 10. *Efficiency coefficient for center distance a = 63 mm and rotation speed n_1 = 1500 min^{-1}: a – efficiency coefficient in function of ratio and torque; b – with superimposed surface of efficiency coefficient in function of ratio and module.*

4. Conclusions

The capabilities of the main software systems for computer-aided mathematics are reviewed. In this work the author set out to highlights the visualization capabilities of the leading systems for computer-aided mathematics: MATLAB, Wolfram Mathematics, and Maple.

It can be concluded that, the software systems ***MATLAB***, ***Wolfram Mathematics***, and ***Maple*** have approximately equal three-

dimensional plating capabilities. The difference is that the system ***Wolfram Mathematics*** can be labeled as more mathematic scientists orientated, than the ***MATLAB***, which is more suitable for machine engineers and scientists. ***MATLAB*** is a programming and numeric computing platform used by millions of engineers and scientists to analyze data, develop algorithms, and create models. It combines a desktop environment tuned for iterative analysis and design processes with a programming language that expresses matrix and array mathematics directly. Also, ***MATLAB*** includes the *Live Editor* for creating scripts that combine code, output, and formatted text in an executable notebook. In this work the author set out to highlights the visualization capabilities, so it is important that the ***MATLAB*** provides built-in libraries for visualizations. The built-in plots can be used to visualize engineering data, gain insights, and identify underlying patterns and trends. One can choose from the relevant plots presented, based on the selected data. This lets the optimal visualization to be done.

For the reasons described above, the ***MATLAB*** was chosen for the purposes of this study. Then, software for data interpolation and three-dimensional visualization are developed. The software is oriented to gear drives. Therefore, this investigation is continued in [17], were visualization and analysis of worm gear drives efficiency and load capacity are performed. This includes 3D graphical representation of the efficiency coefficient and maximal torque values for several combinations of modules, ratios, center distances, etc. Also, in [17] important conclusions are made, for example that the efficiency coefficient increases with the increase of the module and the decrease of the ratio.

3. References

1. A. Dobreva, S. Stoyanov. Optimization Research of Gear Trains with Internal Meshing. Ruse, University Publishing Centre, pp 144 (2012)

2. A. Pillai, A. Ray, S. Kaul. Design optimization of spur gear using genetic algorithm. International Conference on Design, Automation, and Control (2020)

3. A. Messac. Optimization in Practice with MATLAB®: For Engineering Students and Professionals 1st Edition. Cambridge University Press (2015)

4. C. Lopez. MATLAB Optimization Techniques. Springer, ISBN 978-1-4842-0292-0 (2014)

5. C. Hastings, K. Mischo, M. Morrison. Hands-on Start to Wolfram Mathematica and Programming with the Wolfram Language, 3rd ed. Edition, Wolfram Media Inc (2020)

6. D. Bahns, W. Bauer, I. Witt. Quantization, PDEs, and Geometry: The Interplay of Analysis and Mathematical Physics – Operator Theory: Advances and Applications, 1st ed., Birkhauser, (2016)

7. D. Valentine, B. Hahn. Essential MATLAB for Engineers and Scientists 7th Edition. Springer ISBN 978-1-4842-0292-0 (2018)

8. G. Mollova, A. Dobreva. Improving load capacity parameters of worm gears. MATEC Web of Conferences 366, 02002 (2022)

9. G. Mollova, V. Dobrev. Design methodology for investigating worm gear transmissions with significant dimensions. IN: Proceedings of University of Ruse, Vol 60, ISSN: 1311-3321, pp. 41-47, (2021)

10. J. Wu, L. Shu, X. Wang. Research on the Integrated Development System of NGW Planetary Gear Transmission. Applied Mechanics and Materials, Vol 109, pp. 355-359 (2011)

11. S. Stoyanov Vibration measurement and analysis of a friction stir welding process. Proceedings of University of Ruse, volume 61, pp. 47-52 (2022)

12. Stoyanov S. Software tools for mechanical structures resonant frequencies determination: Vibration signal processing for modal analysis. ACM International Conference Proceeding Series (2018)

13. S. Stoyanov, A. Dobreva. Systems Analysis and Design of Gear Drives through Innovative Software Approach. IEEE Xplore: 5th International Symposium on Multidisciplinary Studies and Innovative Technologies (2021)

14. S. Stoyanov. Applications of contemporary software systems for piezoelectric beams investigations. International Scientific Journal "Industry 4.0" (2020)

15. S. Stoyanov, V. Dobrev, A. Dobreva. Finite Element Contact Modelling of Planetary Gear Trains. Material Science and Engineeering, IOP Publishing (2017)

16. S. Stoyanov, V. Dobrev, A. Dobreva. Investigating Dynamic Behavior of Planetary Gear Trains through the Systematic Approach. VDI Verlag GmbH Duesseldorf VDI Berichte (2017)

17. S. Stoyanov, G. Mollova. Visualization and analysis of worm gear drives efficiency and load capacity. XX Jubilee International Congress – Machines, Technologies, Materials, winter session, Borovets, Bulgaria (2023) (to be published)

18. S. Stoyanov. An experimental setup for determination of the resonant frequencies of a mechanical frame structure. Fundamental Sciences and Applications, Journal of the Technical University – Sofia, Plovdiv branch, Bulgaria, ISBN: 1310-8271 (2018)

19. U. Amatya, B. Prajapati. Development of MATLAB Based Software for Simple Spur Gear Design and its Validation for Stress Simulations. Proceedings of 8th IOE Graduate Conference, Vol. 8, pp. 209-215 (2020)

20. V. Babu, M. Majumder, A. Ramprasad. Involute Tooth Spacing, Gear Profile and 3D Gear development with MATLAB® Graphical User Interface and Solidworks. International Journal of Industrial Engineering (2018)

Basic Analytical and Geometric Synthesis of Conic Convolute Helical Surfaces of Spatial Rack Drives. Software and Graphic Study

Emilia Abadjieva[1,2]
Institute of Mechanics- Bulgarian Academy of Sciences, Acad. G. Bonchev Str, block 4, Sofia, Bulgaria[1]
Center of Competence MIRACLe – Mechatronics Clean Technologies, Sofia, Bulgaria[2]
abadjieva@gmail.com

Abstract: *This study treats a study oriented to the basic synthesis of the conic convolute helicoid. On the base of the elaborated mathematical model, the written equations show a theoretical possibility, depending on the basic geometrical characteristics of the designed conic convolute worm, to generate the active flanks of the helical teeth as parts of these conical convolute helicoids. Analytical dependences of the cross-section and the axial section of the conic convolute surfaces are obtained. These relations, as well as the performed studies of the graphic images of these sections, precede the process of constructing the algorithms for computer synthesis and design of these conic helical surfaces. The realized studies of the graphic images of these sections are the basis of the algorithms for computer synthesis and design of these conical helical surfaces. The appearance of singular points on these surfaces is examined, which is of particular importance for their technological synthesis. Based on the developed algorithm, a computer program for the synthesis and visualization of conic helical surfaces is realized and illustrated.*

Keywords*: SPATIAL RACK DRIVES, CONIC LINEAR HELICOIDS, GEOMETRIC CHARACTERISTICS*

1. Introduction

In the group of gear mechanisms, a certain significance for the technique has spatial rack mechanisms, transforming motions of type ($R \leftrightarrow T$) [1]. The reason for this is that, as a mechanical system, this type of gear drives does not have an alternative for cases of motions' transformation with high power, as there are an alternative for small power and displacements, which are electrical drives with electronic control. Hydraulic transmissions represent a definite alternative, but high-tech and expensive servo systems are used to achieve high positioning accuracy.

The successful implementation of the spatial rack drives with new kinematic and strength characteristics into the techniques is retained by the insufficient studying of the general principles of this transformation, due to the lack of offered specific approaches to mathematical modeling, oriented to their synthesis.

The global structure of every mathematical model of the above-considered type is determined by [1-3]:

- The designation of the three-link mechanism under the preliminary defined law of motions transformation;
- the placement of the characteristic axes of the movable links and the nature of the conjugation of the elements of high kinematic joints (with a point or linear tangential contact);
- the technological devices, connected with the choice of the geometry of the generating (instrumental) surfaces and the chosen principle for generation by T. Olivier.

Further below, two ways of generation of the active tooth surfaces Σ_2 of the gear rack (link $i=2$) of the studied mechanism are marked [1 - 3]:

- Σ_2 is generated by enveloping in accordance with the second principle of T. Olivier; Σ_2 is cut with an instrument J, which generating (enveloping) surfaces Σ_J are geometrically identical with the tooth surfaces Σ_1 of the rotating link $i=1$, i.e. $\Sigma_J \equiv \Sigma_1$; the cutting instrument J occupies the same relative placement towards the blanks of the link $i=2$; the relative motion of the instrument J towards the blank of the link $i=2$ is the same as it is of Σ_1 towards Σ_2 when there are work mating. Hence, the generated surfaces Σ_2 have a line contact with Σ_1.
- Σ_2 is a cylindrical surface, for which it is easy to determine the analytical type of its normal section, which is the normal profile of the tooth of the gear rack. When the orientation of the longitudinal line of the tooth and the geometry of its normal profile are known, then Σ_2 can be generated by copying. In this case also Σ_1 and Σ_2 contact in a line.

In the current study, the first approach to the synthesis of these motions' transformers is applied. This determines the importance of the written here theory, which is referred to the synthesis of the surfaces $\Sigma_J \equiv \Sigma_1$ of the conic linear helicoids.

To realize a complete study of the conic convolute helical surfaces are written analytical descriptions of their cross-sections and axial sections. Other important characteristics of the technological synthesis of the spatial rack drives are the conditions for the appearance of singular points on the conic linear helical surfaces. In the study, this topic is briefly explained.

2. Synthesis of Conic Linear Helical Surfaces

Generation of Conic Convolute Mechanisms. The helicoids and especially the linear helicoids are widely applied as active tooth surfaces of spatial transmissions with crossed axes, both in work meshing and instrumental meshing conditions. Such choice of the active tooth surfaces for these gears is determined by technological manufacturing, especially when their synthesis is realized under the second Oliver's principle [1, 4 - 7]. In many cases (like the manufacture of the cylindrical worm gear and Spiroid[1] and Helicon gear-set), these surfaces are the only alternative.

On Fig. 1 is illustrated the generation of right-handed conic convolute helicoids $\Sigma_1^{(j)}$ $(j=1,\ 2)$ determined by different geometrical characteristics of the helical teeth (treads) of the particular gear mechanism [8 - 10]. The process of helical surfaces' generation is considered in a fixed coordinate system $S_p^{(j)}(O_p^{(j)}, x_p^{(j)}, y_p^{(j)}, z_p^{(j)})$ and it is as follows. The generatrix of $\Sigma^{(j)}$ doesn't cross the axis $O_p^{(j)} z_p^{(j)}$ which coincides with the geometric axis of the gear. $\Sigma^{(j)}$ and $O_p^{(j)} z_p^{(j)}$ conclude an angle $0{,}5\pi < \xi^{(j)} < \pi$. The line $L^{(j)}$ belongs to a plane $T^{(j)}$, which

[1] Spiroid and Helicon are trademarks registered by the Illinois Tool Works, Chicago, Ill.

is tangential to the directed circle cylinder $C^{(j)}$. The generation of the conic convolute helicoid $\Sigma_1^{(j)}$ by the line $L^{(j)}$ is realized by two generatrix motions [2, 8, 11]: axial helical motion along the longitudinal axis $O_p^{(j)}z_p^{(j)}$ with parameter $p_s^{(j)} = const.$; crossed helical motion in the plane $\Sigma^{(j)}$, perpendicular to the axis $O_p^{(j)}z_p^{(j)}$ with parameter $p_t^{(j)} = const.$ Here, it will be noted that $\Sigma_1^{(1)}$ is conic convolute helical surface, which is oriented to the positive direction of the axis $O_p^{(1)}z_p^{(1)}$, and $\Sigma_1^{(2)}$ is the helicoid, turned along the negative direction of the $O_p^{(2)}z_p^{(2)}$.

The vector equation of the conic convolute helical surface $\Sigma_1^{(1)}$, in accordance with Fig. 1, has the form [1, 2, 11]:

$$\bar{\rho}_1^{(j)} = \bar{r}_0^{(j)} + \bar{s}^{(j)} + \bar{t}^{(j)} + \bar{u}^{(j)}, \qquad (1)$$

where $\bar{\rho}_1^{(j)}$ is a radius-vector of a point $N^{(j)}$ that belongs to the conic convolute helicoid $\Sigma_1^{(j)}$; $\bar{r}_0^{(j)}$ - radius-vector of the directed cylinder $C^{(j)}$; $\vartheta^{(j)}$, $u^{(j)}$ - coordinates of the helical surface $\Sigma_1^{(j)}$; $s^{(j)} = p_s^{(j)}\vartheta^{(j)}$ - axial motion of the generatrix $L^{(j)}$; $t^{(j)} = p_t^{(j)}\vartheta^{(j)}$ - crossed displacement (tangential to the directed cylinder $C^{(j)}$) of the generatrix line $L^{(j)}$.

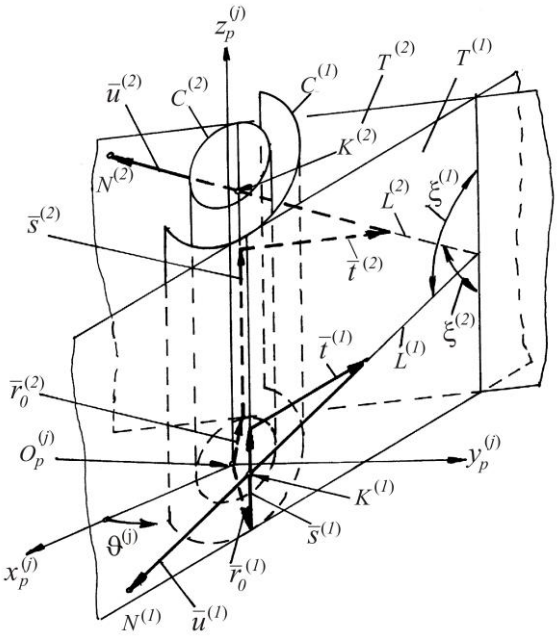

Fig. 1 *Conic convolute helicoids generation*

When (1) is written in a coordinate system $S_p^{(j)}$ it is obtained:

$$\begin{aligned} x_p^{(j)} &= r_0^{(j)}\cos\vartheta^{(j)} \pm A\sin\vartheta^{(j)}, \\ y_p^{(j)} &= r_0^{(j)}\sin\vartheta^{(j)} \mp A\cos\vartheta^{(j)}, \\ z_p^{(j)} &= p_s^{(j)}\vartheta^{(j)} \pm u^{(j)}\cos\xi^{(j)}, \\ A &= (u^{(j)}\sin\xi^{(j)} - p_t^{(j)}\vartheta^{(j)}), \end{aligned} \qquad (2)$$

For equation systems (2) the upper signs and $j = 1$ refer to the $\Sigma_1^{(1)}$, and the lower and $j = 2$ refer to the $\Sigma_1^{(2)}$.

Substituting in (2)

$$R_0^{(j)} = u^{(j)} - \frac{p_t^{(j)}\vartheta^{(j)}}{\sin\xi^{(j)}}$$

and (3)

$$p^{(j)} = p_s^{(j)} \pm p_t^{(j)}\cot\xi^{(j)}$$

it is obtained

$$\begin{aligned} x_p^{(j)} &= r_0^{(j)}\cos\vartheta^{(j)} \pm R_0^{(j)}\sin\xi^{(j)}\sin\vartheta^{(j)}, \\ y_p^{(j)} &= r_0^{(j)}\sin\vartheta^{(j)} \mp R_0^{(j)}\sin\xi^{(j)}\cos\vartheta^{(j)}, \\ z_p^{(j)} &= p^{(j)}\vartheta^{(j)} \pm R_0^{(j)}\cos\xi^{(j)}; \end{aligned} \qquad (4)$$

Equation (4) represents the conic convolute helical surface $\Sigma_1^{(j)}$ as a cylindrical one with helical parameter $p^{(j)} = const.$ and coordinates $\vartheta^{(j)}$ and $R_0^{(j)}$. (The point $K^{(j)}$ is the accounting origin of coordinate $R_0^{(j)}$. $C^{(j)}$ and plane $T^{(j)}$ are contacting in this generatrix $L^{(j)}$). The point $K^{(j)}$ is considered as a point from the directed helical line $\bar{\rho}_0^{(j)} = \bar{\rho}_0^{(j)}(\vartheta^{(j)})$ on the $C^{(j)}$.

For the synthesis of the conic linear helicoids (conic convolute, conic involute, and conic Archimedean) are written three computer programs [1] with analogical (typified) structure and organization of the calculated process. Here and further, it is illustrated the application of these programs, when is realized computer synthesis and visualization of the three types of conic linear helicoids (see Fig. 2, Fig. 3, Fig. 4).

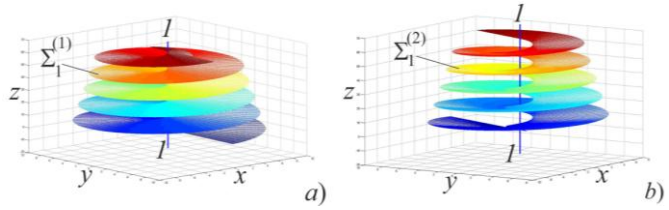

Fig. 2 *Spatial conic convolute gear: a) conic convolute right-handed worm* $\Sigma_1^{(1)} \Rightarrow \xi^{(1)} = 95^\circ$, $r_0^{(1)} = 0{,}90$ *mm;* $u^{(1)} \in [0{,}10]$, $\vartheta^{(1)} \in [0{,}5\pi]$; *b)* $\Sigma_1^{(2)} \Rightarrow \xi^{(2)} = 125^\circ$, $r_0^{(2)} = 1{,}19$ *mm;* $u^{(2)} \in [0{,}10]$, $\vartheta^{(2)} \in [0{,}5\pi]$

Conic involute helical surfaces generation. It is known [1, 2, 11] that each developable surface is a cylindrical one, conic one, or a locus of the tangent lines to an arbitrary curve and vice versa - each cylindrical, conic or a surface representing the locus of tangent lines to a curve is a developable surface.

The specific for each developable surface is, that the parameter of distribution is equal to zero, i.e.

$$h^{(j)} = p^{(j)} + r_0^{(j)}\cot\xi^{(j)} = 0,$$

or (5)

$$\cot\xi^{(j)} = -\frac{p^{(j)}}{r_0^{(j)}}$$

After observing condition (5), equation (4) describes the conic involute helicoid (Fig. 3), which is given in the form:

$$x_p^{(j)} = r_0^{(j)} cos\vartheta^{(j)} \pm R_0^{(j)} cos\lambda_0^{(j)} sin\vartheta^{(j)},$$
$$y_p^{(j)} = r_0^{(j)} sin\vartheta^{(j)} \mp R_0^{(j)} cos\lambda_0^{(j)} cos\vartheta^{(j)}, \quad (6)$$
$$z_p^{(j)} = p^{(j)}\vartheta^{(j)} \mp R_0^{(j)} sin\lambda_0^{(j)},$$

where $R_0^{(j)} = u^{(j)} - \frac{p_t^{(j)}\vartheta^{(j)}}{cos\lambda_0^{(j)}}$, $p^{(j)} = p_s^{(j)} \mp p_t^{(j)} tan\lambda_0^{(j)}$

and $\lambda_0^{(j)} = \xi^{(j)} - \pi/2$ is a spiral angle [1, 11] for the directed helical line on the cylinder $C^{(j)}$. In this case, the cylinder $C^{(j)}$ is called a basic cylinder.

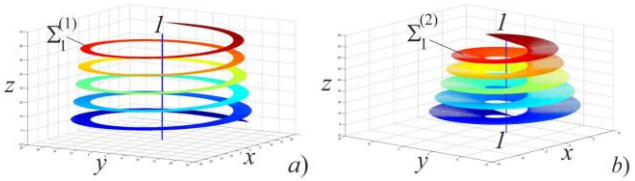

Fig. 3 *Spatial conic involute mechanism: a) conic involute right-handed worm* $\Sigma_1^{(1)} \Rightarrow \xi^{(1)} = 95^\circ$, $r_0^{(2)} = 18{,}40$ *mm;* $u^{(1)} \in [-5{,}15]$, $\vartheta^{(1)} \in [0{,}5\pi]$; *b)* $\Sigma_1^{(2)} \Rightarrow \xi^{(2)} = 125^\circ$, $r_0^{(2)} = 2{,}84$ *mm;* $u^{(2)} \in [-5{,}15]$, $\vartheta^{(2)} \in [0{,}5\pi]$

Conic Archimedean helical surfaces generation. The conic Archimedean helicoid is obtained when the generatrix $L^{(j)}$ (see Fig. 4) crosses the axis $O_p^{(j)} z_p^{(j)}$, i.e. when $r_0^{(j)} = 0$.

Then from (2), it is obtained:

$$x_p^{(j)} = \pm(u^{(j)} sin\xi^{(j)} - p_t^{(j)}\vartheta^{(j)}) sin\vartheta^{(j)},$$
$$y_p^{(j)} = \mp(u^{(j)} sin\xi^{(j)} - p_t^{(j)}\vartheta^{(j)}) cos\vartheta^{(j)}, \quad (7)$$
$$z_p^{(j)} = p_s^{(j)}\vartheta^{(j)} \pm u^{(j)} cos\xi^{(j)}.$$

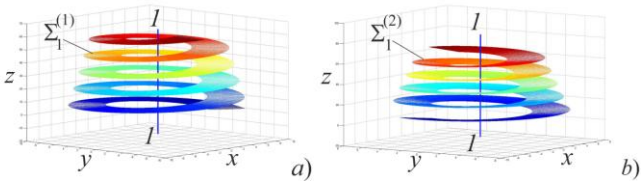

Fig. 4 *Spatial conic Archimedean mechanism: a) conic Archimedean right-handed worm* $\Sigma_1^{(1)} \Rightarrow \xi^{(1)} = 95^\circ$, $u^{(1)} \in [6{,}10]$, $\vartheta^{(1)} \in [0{,}5\pi]$; *b)* $\Sigma_1^{(2)} \Rightarrow \xi^{(2)} = 125^\circ$, $u^{(2)} \in [6{,}10]$, $\vartheta^{(2)} \in [0{,}5\pi]$

The curvilinear coordinate $\vartheta^{(j)}$ in (7) represents the angle on which rotates the normal vector $\bar{r}_0^{(j)}$ to the axial plane (determined by the $L^{(j)}$ and $O_p^{(j)} z_p^{(j)}$). If it is noted with $\vartheta_a^{(j)} = \vartheta^{(j)} + \pi/2$, the angle, that the plane ($L^{(j)}, O_p^{(j)} z_p^{(j)}$) concludes with the plane ($O_p^{(j)} x_p^{(j)} z_p^{(j)}$), then the equation systems (7) turn into:

$$x_p^{(j)} = \mp[B] cos\vartheta_a^{(j)},$$
$$y_p^{(j)} = \mp[B] sin\vartheta_a^{(j)},$$
$$z_p^{(j)} = p_s^{(j)}(\vartheta_a^{(j)} - \pi/2) \pm u^{(j)} cos\xi^{(j)}, \quad (8)$$
$$B = u^{(j)} sin\xi^{(j)} - p_t^{(j)}(\vartheta_a^{(j)} - \pi/2).$$

3. Basic Geometric Characteristics of the Conic Convolute Surface

Parameter of Distribution. It is known [6, 11, 12] that the main characteristic of surfaces with rectilinear generatrices is their parameter of the distribution. When surfaces of such type are generated, the rectilinear generatrix passes from its initial position to an infinitely closed vicinal position, rotating at an angle and displacing at some distance. These two quantities are infinitely small, but their ratio has its limits, which is titled a *parameter of the distribution.*

Following Fig. 5 the transition of the rectilinear generatrix $L^{(j)}$, (which is characterized by the parameter ϑ), in a position L', characterized by infinitely closed value $\vartheta + \Delta\vartheta$, then it rotates to an angle $\Delta\varphi$ and deviates from its initial position to a distance $\Delta\lambda = MM'$. As has been already mentioned, these values are infinitely small, and their ratio tends to a certain limit, which is called a parameter of distribution [12]:

$$h = \lim_{\Delta\vartheta \to 0} \frac{\Delta\lambda}{\Delta\varphi} \quad (9)$$

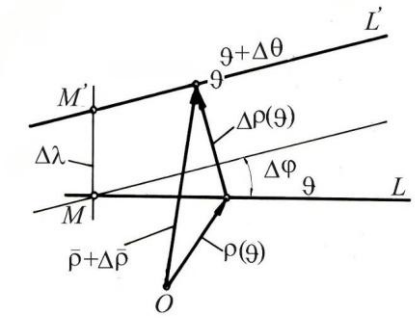

Fig. 5 *Transition of the generatrix* L *into an infinitely close position* L'

To determine the distribution parameter $\Sigma^{(j)}$ of the conic convolute helical surface $\Sigma_1^{(j)}$, the vector equation (1) is presented of the type [2]:

$$\bar{\rho}_1^{(j)} = \bar{\rho}_0^{(j)}(\vartheta^{(j)}) + R_0^{(j)} \bar{l}^{(j)}, \quad (10)$$

where $\bar{\rho}_0^{(j)} = \bar{\rho}_0^{(j)}(\vartheta^{(j)})\{\chi_1^{(j)}, \chi_2^{(j)}, \chi_3^{(j)}\}$ is an equation of a directed helical line on the directed cylinder $C^{(j)}$; $\chi_1^{(j)}, \chi_2^{(j)}, \chi_3^{(j)}$ - projection of the vector $\bar{\rho}_0^{(j)}$ in the coordinate system $S_p^{(j)}$; $\bar{l}^{(j)}\{l_1^{(j)}, l_2^{(j)}, l_3^{(j)}\}$ - directed unit vector of the generatrix line $\Sigma^{(j)}$; $l_1^{(j)}, l_2^{(j)}, l_3^{(j)}$ - projections of $\bar{l}^{(j)}$ in the coordinate system $S_p^{(j)}$.

For the case illustrated in Fig. 1, it is written:

$$\chi_1^{(j)} = r_0^{(j)} cos\vartheta^{(j)}, \quad \chi_2^{(j)} = r_0^{(j)} sin\vartheta^{(j)},$$
$$\chi_3^{(j)} = p^{(j)}.\vartheta^{(j)},$$
$$l_1^{(j)} = \pm sin\xi^{(j)} sin\vartheta^{(j)}, \quad l_2^{(j)} = \mp sin\xi^{(j)} cos\vartheta^{(j)}, \quad (11)$$
$$l_3^{(j)} = \pm cos\xi^{(j)},$$

Then, applying (9), as it is shown in [6, 12], for the studied conic convolute helical surface it can be written:

$$h^{(j)} = \frac{\begin{vmatrix} d\chi_1^{(j)} & l_1^{(j)} & dl_1^{(j)} \\ d\chi_2^{(j)} & l_2^{(j)} & dl_2^{(j)} \\ d\chi_3^{(j)} & l_3^{(j)} & dl_3^{(j)} \end{vmatrix}}{(dl_1^{(j)})^2 + (dl_2^{(j)})^2 + (dl_3^{(j)})^2}. \quad (12)$$

For $\Sigma^{(j)}$ from (12) it is obtained the following:

$$h^{(j)} = p^{(j)} + r_0^{(j)} cot\xi^{(j)}. \quad (13)$$

Cross section of the conic convolute helicoid

The equation of the illustrated in Fig. 1 conic convolute helical surfaces with the plane $O_p^{(j)} x_p^{(j)} y_p^{(j)}$, i.e. when $z_p^{(j)} = 0$, has the following parametric form:

$$\rho_p^{(j)} = \sqrt{(r_0^{(j)})^2 + \left(\frac{p^{(j)}\vartheta^{(j)}}{cot\xi^{(j)}}\right)^2}. \quad (14)$$

In Cartesian coordinates, the cross-section of the convolute helicoids $\Sigma_1^{(j)}$, when $z_p^{(j)} = C_{z_p}^{(j)} = const.$, is described with the following system of equations:

$$x_p^{(j)} = r_0^{(j)} cos\vartheta^{(j)} + C\vartheta^{(j)} sin\vartheta^{(j)},$$
$$y_p^{(j)} = r_0^{(j)} sin\vartheta^{(j)} - C\vartheta^{(j)} cos\vartheta^{(j)}, \quad (15)$$
$$C = [tan\xi^{(j)}\left(\frac{C_{z_p}^{(j)}}{\vartheta^{(j)}} - p_s^{(j)}\right) \mp p_t^{(j)}].$$

Equations (15) are written in the form:

$$x_p^{(j)} = r_0^{(j)} cos\vartheta^{(j)} + b^{(j)}\vartheta^{(j)} sin\vartheta^{(j)},$$
$$y_p^{(j)} = r_0^{(j)} sin\vartheta^{(j)} - b^{(j)}\vartheta^{(j)} cos\vartheta^{(j)}, \quad (16)$$

where $b^{(j)} = tan\xi^{(j)}\left(\frac{C_{z_p}^{(j)}}{\vartheta^{(j)}} - p_s^{(j)}\right) \mp p_t^{(j)}$.

The essence of the cross-section of the conic convolute helicoid can be clarified by introducing circular vector functions [4, 6] $\bar{l}^{(j)} = \bar{l}^{(j)}(\vartheta^{(j)})$ and $\bar{g}^{(j)} = \bar{g}^{(j)}(\vartheta^{(j)})$, for which the condition is fulfilled:

$$\bar{l}^{(j)} = \bar{i}_p^{(j)} cos\vartheta^{(j)} + \bar{j}_p^{(j)} sin\vartheta^{(j)},$$
$$\bar{g}^{(j)} = -\bar{i}_p^{(j)} sin\vartheta^{(j)} + \bar{j}_p^{(j)} cos\vartheta^{(j)}. \quad (17)$$

Since $d\bar{l}^{(j)}/d\vartheta^{(j)} = \bar{g}^{(j)}(\vartheta^{(j)})$ then the direction of the vector $\bar{g}^{(j)}(\vartheta^{(j)})$ is determined by the counterclockwise rotation viewed from the positive direction of the axis $O_p^{(j)} z_p^{(j)}$ and it is tangent to the directed circle (determined by the directed cylinder $C^{(j)}$). By using $\bar{r}_p^{(j)} = x_p^{(j)}\bar{i}_p^{(j)} + y_p^{(j)}\bar{j}_p^{(j)}$, for the cross-section of the conic convolute surface $\Sigma_1^{(j)}$ (following equations (16)) it can be written:

$$\bar{r}_p^{(j)} = r_0^{(j)}\bar{l}^{(j)}(\vartheta^{(j)}) - b^{(j)}\vartheta^{(j)}\bar{g}^{(j)}(\vartheta^{(j)}). \quad (18)$$

Let the cross-section of $\Sigma_1^{(j)}$ in the coordinate plane $O_p^{(j)} x_p^{(j)} y_p^{(j)}$ is illustrated, i.e. for the case $C_{z_p}^{(j)} = 0$, when $b^{(j)} = -\frac{p^{(j)}}{cot\xi^{(j)}} > 0$.

The above condition and the vector equality (18), determine the type of the cross-section of the studied conic convolute helicoids $\Sigma_1^{(j)}$, shown correspondingly in Fig. 6 [11].

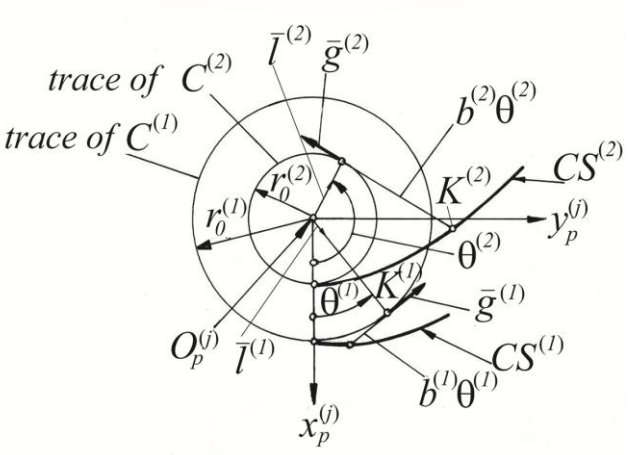

Fig. 6 *Cross-section of the conic convolute helicoids* $\Sigma_1^{(j)}$ *of I type:* $CS^{(j)}$ *- line of the cross-section of the* $\Sigma_1^{(j)}$

Axial section and axial angle of $\Sigma_1^{(j)}$**.** The equation of the axial section is obtained after the substitution of $y_p^{(j)} = 0$ in (2):

$$x_p^{(j)} = \frac{r_0^{(j)}}{cos\vartheta^{(j)}} = r_0^{(j)} \sec\vartheta^{(j)},$$
$$z_p^{(j)} = -p^{(j)} conv(\vartheta^{(j)}, k^{(j)}), \quad (19)$$

where $k^{(j)} = -\frac{r_0^{(j)}}{p^{(j)}}.cot\xi^{(j)} > 0,$

$$conv(\vartheta^{(j)}, k^{(j)}) = k^{(j)} tan\vartheta^{(j)} - \vartheta^{(j)}.$$

The analytical type (19) of the axial section of the helicoid described by system (2) corresponds to its special geometry of a conic convolute helical surface, which is generated according to Fig. 1.

$$\frac{dx_p^{(j)}}{d\vartheta^{(j)}} = r_0^{(j)} \frac{\sin\vartheta^{(j)}}{\cos^2\vartheta^{(j)}}, \quad \frac{dz_p^{(j)}}{d\vartheta^{(j)}} = -p^{(j)} \frac{k^{(j)} - \cos^2\vartheta^{(j)}}{\cos^2\vartheta^{(j)}}$$

$$\frac{dz_p^{(j)}}{dx_p^{(j)}} = -\frac{p^{(j)}}{r_0^{(j)}} \frac{k^{(j)} - \cos^2\vartheta^{(j)}}{\sin\vartheta^{(j)}}, \qquad (20)$$

$$\frac{d^2 z_p^{(j)}}{dx_p^{(j)2}} = -\frac{p^{(j)}}{(r_0^{(j)})^2} \frac{\cos^3\vartheta^{(j)}(1-k^{(j)}+\sin^2\vartheta^{(j)})}{\sin^3\vartheta^{(j)}}.$$

Since the axial section of $\Sigma_1^{(j)}$, in the most common case, is asymmetric, the study is carried out for $\vartheta^{(1)} \in [0, \pi/2)$ and $\vartheta^{(2)} \in (-\pi/2, 0]$.

When $\vartheta^{(j)} = 0$, $x_p^{(j)} = r_0^{(j)}$ and $z_p^{(j)} = 0$, this point corresponds to the peak of the "axial section" curve. When $\vartheta^{(j)}$ varies from 0 to $\pm\pi/2$, $x_p^{(j)}$ grows from $r_0^{(j)}$ to $+\infty$, and $z_p^{(j)}$ changes to $\pm\infty$. Therefore, the graphics of the curves of the axial section (19) have asymptotes of the form:

$$z_p^{(j)} = A^{(j)} x_p^{(j)} + B^{(j)},$$

$$A^{(j)} = \lim_{x_p^{(j)} \to \infty} \frac{z_p^{(j)}(x_p^{(j)})}{x_p^{(j)}} = \pm cot\xi^{(j)}, \qquad (21)$$

$$B^{(j)} = \lim_{x_p^{(j)} \to \infty} \left[z_p^{(j)} - A^{(j)} x_p^{(j)} \right] = \pm p^{(j)} \frac{\pi}{2}.$$

Then the equations of the asymptotes of the curves, constituting the axial section of $\Sigma_1^{(j)}$ are of the form

$$z_p^{(j)} = \pm cot\xi^{(j)} x_p^{(j)} \pm p^{(j)} \frac{\pi}{2}, \ (j = 1, \ 2), \qquad (22)$$

and for $j = 1$ the upper signs are valid, and for $j = 2$ - the lowers ones.

When the angle $\delta^{(j)} = \xi^{(j)} - \pi/2$ is introduced (see Fig. 7 and Fig. 8), then the equation (22) takes the form:

$$z_p^{(j)} = \mp tan\delta^{(j)} x_p^{(j)} \pm p^{(j)}.\pi/2. \qquad (23)$$

The points of intersection of the asymptotes with the coordinate axis $O_p^{(j)} z_p^{(j)}$ are determined from (23). Their applicate (z-axes) are:

$$z_p^{(j)} = \pm p^{(j)}.\pi/2, \qquad (24)$$

The points of intersection of the asymptotes with the axis $O_p^{(j)} x_p^{(j)}$ have abscissas defined by equality:

$$x_p^{(j)} = \frac{p^{(j)}}{tan\delta^{(j)}}.\frac{\pi}{2} = \frac{r_0^{(j)}\pi}{2k^{(j)}}. \qquad (25)$$

The inflection points of the curves of the axial section are obtained from the condition

$$\frac{d^2 z_p^{(j)}}{dx_p^{(j)2}} = 0. \qquad (26)$$

Considering (20), the condition (26) is satisfied, if $\cos^3\vartheta^{(j)}(1-k^{(j)}+\sin^2\vartheta^{(j)}) = 0$, i.e. when

$$\vartheta^{(j)} = \pm arcsin\sqrt{k^{(j)} - 1} \quad \left(\vartheta^{(j)} \neq \pm\frac{\pi}{2} \right) \qquad . (27)$$

If the condition $\vartheta^{(j)} = \pm\pi/2$ is fulfilled, the inflection points of the curves of the axial section go into $\pm\infty$. If condition (27) is satisfied, these points will exist for

$$1 < k^{(j)} < 2. \qquad (28)$$

The form of the curves of the axial section of the conic convolute helicoid $\Sigma_1^{(j)}$ is analyzed both for the case defined by condition (28).

Case $k^{(j)} = \pi/2$. According to (27) and (28), in this case, there will be inflection points on the curves of the axial section that corresponds to $\vartheta^{(j)} = \pm arcsin\sqrt{\pi/2 - 1}$ $(j = 1, \ 2)$. It follows from equality (25) that through the vertices of the curves delineating the axial section of $\Sigma_1^{(j)}$, their asymptotes go through. This case of an axial section is illustrated in Fig. 7 [11].

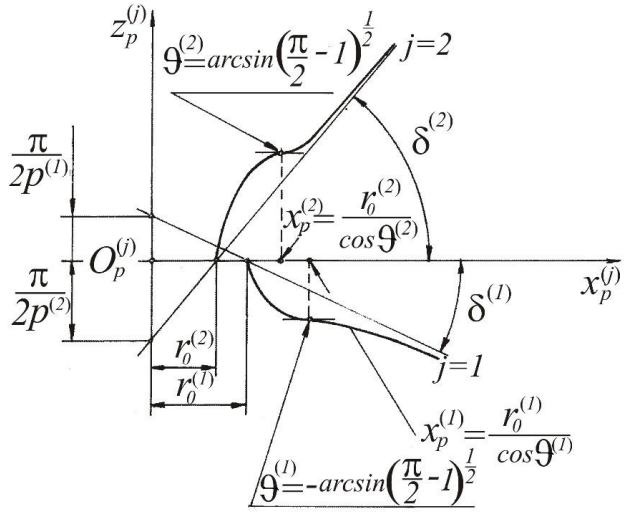

***Fig 7** Curves of the axial section of conic convolute helicoids* $\Sigma_1^{(j)}$ $(j = 1, \ 2)$ *when* $k^{(j)} = \pi/2$

Case $1 < k^{(j)} < \pi/2$. Applying the above reasoning, it can easily be seen that the curves of the axial section have the form illustrated in Fig. 8.

Each of the theoretical curves of the axial section of the conical convolute helicoid $\Sigma_1^{(j)}$, considered for the entire interval of $\vartheta^{(j)}$ (i.e. when $\vartheta^{(j)} \in [0, \pi/2)$ and $\vartheta^{(j)} \in (-\pi/2, 0]$, $(j = 1, \ 2)$) is symmetrical to the axis $O_p^{(j)} x_p^{(j)}$ and has a nodal point, at $\vartheta^{(j)} = \vartheta_1^{(j)}$, which has the following coordinates:

$$x_p^{(j)} = \frac{r_0^{(j)}}{k^{(j)}}.\frac{\vartheta_1^{(j)}}{\sin\vartheta_1^{(j)}}, \qquad (30)$$

$$z_p^{(j)} = 0.$$

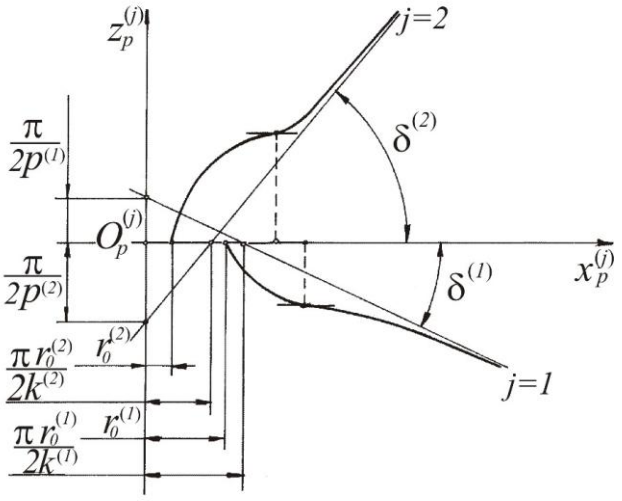

Fig 8. *Curves of the axial section of conic convolute helicoids* $\Sigma_1^{(j)}$ *when* $1<k^{(j)}<\pi/2$

In the considered case, the asymptotes of the axial section $\Sigma_1^{(j)}$, defined by equations (22) and (23), cross the axis $O_p^{(j)}x_p^{(j)}$ at points defined by the expression (25).

From the comparison of (25) and (30), it follows that the abscissas of the points of intersection of the curves of the axial section of the conic convolute helicoid $\Sigma_1^{(j)}$ ($j=1,\ 2$) with the axes $O_p^{(j)}x_p^{(j)}$ are smaller than those of the points of intersection with the asymptotes with the same axis, due to the fact known from mathematics that

$$1>\frac{\sin\vartheta^{(j)}}{\vartheta^{(j)}}\geq\frac{2}{\pi},\quad \text{for}\quad \vartheta^{(j)}\in\left[-\pi/2,0\right)\quad \text{and}\quad \vartheta^{(j)}\in\left(0,\pi/2\right].$$

The axial angle $\alpha_s^{(j)}$ in an arbitrary point of the axial section of the studied conic helicoid is obtained from the equations system (20):

$$tan\alpha_s^{(j)}=\left|\frac{dz_p^{(j)}}{dx_p^{(j)}}\right|=\left|-\frac{p^{(j)}}{r_0^{(j)}}.\frac{k^{(j)}-cos^2\vartheta^{(j)}}{\sqrt{1-cos^2\vartheta^{(j)}}}\right|,\quad (31)$$

where $k^{(j)}=-\frac{r_0^{(j)}}{p^{(j)}}cot\xi^{(j)},\quad cos\vartheta^{(j)}=\frac{r_0^{(j)}}{x_p^{(j)}},$

Then

$$\alpha_s^{(j)}=arctan\left|\frac{p^{(j)}\frac{r_0^{(j)}}{x_p^{(j)}}+x_p^{(j)}cot\xi^{(j)}}{\sqrt{x_p^{(j)2}-r_0^{(j)2}}}\right|,\quad (32)$$

After substitution of $x_p^{(j)}=r_p^{(j)}$ into (32), it is obtained the axial angle of $\Sigma_1^{(j)}$ in a point in an arbitrary conic surface, coaxial with the outer surface of the conic gear equipped with convolute helical teeth of the studied type.

4. Singular Contact Points on Conic Linear Helicoids

It is known [13, 14] that for the cases prevailing in technological practice when generating cylindrical worms and cylindrical worm cutters, whose tooth surfaces are linear helicoids, knives are used as cutting tools, the cutting edges of which are arranged in a certain way relative to the geometric axis (axis of rotation) of the generated product.

The cutting edges of the knives represent the generatrix lines $\Sigma^{(j)}$ ($j=1,\ 2$) (Fig. 1) that generate the linear surfaces. This technological approach is also applicable in the practical implementation of conical linear helicoids [2].

Conic convolute helicoid. To prevent the phenomenon of "undercutting" of the active tooth surfaces of gear transmissions and instruments, representing parts of conic linear helicoids, during their generation, it is necessary to define conditions for the appearance of the ordinary points (points of undercutting) on them. As already illustrated, the conic linear helicoids $\Sigma_1^{(j)}$ ($j=1,\ 2$) (and in particular the conic convolute helical surface) have the form: $\overline{\rho}_1^{(j)}=\overline{\rho}_1^{(j)}(u^{(j)},\vartheta^{(j)}).$

Then the normal vector $\overline{n}_1^{(j)}$ at $\Sigma_1^{(j)}$ ($j=1,\ 2$) in an arbitrary point $N^{(j)}$ is defined by

$$\overline{n}_1^{(j)}=\frac{\partial\overline{\rho}_1^{(j)}}{\partial u^{(j)}}\times\frac{\partial\overline{\rho}_1^{(j)}}{\partial\vartheta^{(j)}},\quad (33)$$

where $\frac{\partial\overline{\rho}_1^{(j)}}{\partial u^{(j)}}$ and $\frac{\partial\overline{\rho}_1^{(j)}}{\partial\vartheta^{(j)}}$ are vectors in point $N_1^{(j)}$ from the conic helical surface $\Sigma_1^{(j)}$, tangent to the coordinate lines $u^{(j)}=constant$ and $\vartheta^{(j)}=constant$.

It is known [12], that point $N^{(j)}$ from $\Sigma_1^{(j)}$ is singular (node), if in it a normal vector $\overline{n}_1^{(j)}$ cannot be defined, i.e. the following condition is fulfilled:

$$\overline{n}_1^{(j)}=\overline{0}.\quad (34)$$

Then from (2), for the projections of the normal vector $\overline{n}_1^{(j)}$ in the coordinate system $S_p^{(j)}$ can be written:

$$\begin{aligned}
n_{1,x_p}^{(j)}&=\mp h^{(j)}sin\xi^{(j)}cos\vartheta^{(j)}-Dcos\xi^{(j)}sin\vartheta^{(j)},\\
n_{1,y_p}^{(j)}&=\mp h^{(j)}sin\xi^{(j)}sin\vartheta^{(j)}+Dcos\xi^{(j)}cos\vartheta^{(j)},\\
n_{1,z_p}^{(j)}&=Dsin\xi^{(j)}.\\
D&=(u^{(j)}sin\xi^{(j)}-p_t^{(j)}\vartheta^{(j)})
\end{aligned}\quad (35)$$

From (35) it can be seen, that condition (34) is never satisfied for the conic convolute helicoid, since $h^{(j)}\neq 0$. This means that the conic convolute helicoid consists of only non-singular points.

5. Conclusion

Basic analytical and geometrical synthesis of conic convolute helicoids is realized. The obtained equations show a theoretical possibility, depending on the basic geometrical characteristics of the

designed conic convolute worm, to generate the active surfaces of its helical teeth as parts of the intended pairs of conic convolute helicoids. In this study are shown the analytical dependences of the cross-section and the axial section, which are important for the synthesis of the conic helical surfaces. On the base of the realized studies, is created a computer program, for illustrations of these helicoids. The illustrated, in this work, equations of conic helicoids, as well as the analytical descriptions of their cross-sections and axial sections, are important geometric characteristics of the active tooth surfaces of conic worms or conic hobs. They are related to the technological synthesis of gear mechanisms with the application of these new types of helical surfaces operating in the condition of working and/or instrumental meshing. The notes made about the appearance of undercutting cutting points on these surfaces, with the chosen generation approach, are also particularly essential for their technological synthesis.

6. Acknowledgment

This work has been accomplished with the financial support by the Grant No BG05M2OP001-1.002-0011-C02 financed by the Science and Education for Smart Growth Operational Program (2014-2020) and co-financed by the European Union through the European structural and Investment funds.

7. References

1. E. Abadjieva. Spatial Rack Drives. Mathematical Modelling for Synthesis. VDM Verlag Dr. Müller e.K., 2011, 72 pp., (ISBN: 978-3-639-24045-0)

2. V. Abadjiev. Gearing Theory and Technical Applications of Hyperboloid Drives, Sc. D. Thesis, Institute of Mechanics, Bulgarian Academy of Sciences, Sofia, 309, (2007),(in Bulgarian)

3. Abadjieva, E., V. Abadjiev. Regular Mechanical Transformation of Rotations into Translations: Part 2. Kinematic Synthesis of the Elements of High Kinematic Joints, Realizing the Process of Motions Transformations. J. of Theor. and Appl. Mech., Sofia, 47(3), 3-24 (2017)

4. Lashnev, S., Yulikov, M. Calculation and Design of Metal-Cutting Tools with an IBM Application. Mashinostroenie, Moscow, 391, (1975)

5. Litvin, F., Fuentes, A. Gear Geometry and Applied Theory. Second Edition, Cambridge University Press, 800, (2004)

6. Lyukshin, V. The Theory of Helical Surfaces in the Design of Cutting Tools. Mashinostroenie Publishing House, Moscow, 371, (1968)

7. Semchenko, I., Magyushin, M., G. Saharov. Design of Metal Cutting Tools. Mashgiz, Moscow, 952, (1962)

8. Abadjiev, V., Okhotsimsky, D., Platonov, A. Research on the Spatial Gears and Applications, Keldysh Institute of Applied Mathematics, Russian Academy of Sciences, Preprint No 89, Moscow, (1997).

9. BDS 8540-84, 1985. Gear sets. Common terms. Definitions and symbols. Institute of Standardization, Sofia, (1985).

10. Abadjiev, V. Mathematical Modelling for Synthesis of Spatial Gears, Journal of Process Mechanical Engineering., Proc Inst. Mech Engrs, Vol. 216, Part E, pp. 31-46, (2002).

11. Abadjiev V., E. Abadjieva. Conic Linear Helicoids: Part 1. Synthesis and Analysis of the Basic Geometric Characteristics. Gears in Design, Production, and Education. Mechanisms and Machine Science, 101. Springer, Cham, 339-360, (2021)

12. Rashevsky, P. Course of Differential Geometry. Ed. State Publishing House of Technical and Theoretical Literature, Moscow, 1956, 420, (1956).

13. Ginzburg, E., N. Golovanov, N. Firun, N. Halebsky. Gear Transmissions. Mashinostroenie, Leningrad, 416, (1980)

14. Golovanov, N., E. Gizburg, N. Firun Spatial Transmissions, and Worm Gear Mechanisms. Mashinostroenie, Leningrad, 515, (1967).

Application of the mathematical model of Johnson-Kendall-Roberts in the study of the Young's modulus of erythrocytes in patients with type 2 diabetes mellitus

Anika Alexandrova[1,2], Maria Kyulavska[3] , Nadia Antonova[1], Irena Velcheva[4], Elissaveta Zvetkova[5]
Institute of Mechanics, Bulgarian Academy of Sciences, Acad. G. Bontchev St., bl. 4, 1113 Sofia, Bulgaria[1]
e-mail: anikaalexandrova@abv.bg
Centre of competence at Mechatronics and Clean Technologies – MIRACle, Sofia, Bulgaria[2]
Institute of Polymers, Bulgarian Academy of Sciences, Sofia, Bulgaria[3]
Clinic of Nervous Diseases, Uni Hospital, Panagyurishte, Bulgaria[4]
Bulgarian Society of Biorheology, Sofia, Bulgaria[5]

Abstract: *The goal of the present study is to evaluate the elastic properties (Young's modulus) of erythrocytes from healthy donors and patients with type 2 diabetes mellitus (T2DM), by using an atomic force microscope (AFM). Morphological and mechanical characteristics of red blood cells are studied in parallel by PeakForce QNM (Quantitative NanoMechanical Mapping) mode of AFM Dimensional ICON Bruker NanoScope V9 Instrument. Young's modulus is calculated based on the mathematical model of Johnson-Kendall-Roberts by the application of the "two-point method". AFM images of the erythrocytes from the healthy donors show that erythrocytes with a normal biconcave shape predominate. In patients with T2DM, the so-called erythrocyte polymorphism is studied. The Young's modulus of erythrocytes, in patients with T2DM, significantly statistically increases by 27% ($p \leq 0,001$), compared to the data of healthy donors. The studied Young's modulus by AFM can be used in clinical practice as a precise biomarker for the state of the red blood cells in T2DM.*

Keywords: *YOUNG'S MODULUS, JOHNSON-KENDALL-ROBERTS MATHEMATICAL MODEL, ATOMIC FORCE MICROSCOPE, TYPE 2 DIABETES MELLITUS, ERYTHOCYTES (RED BLOOD CELLS, RBCs)*

1. Introduction

An elastic modulus (Young's modulus) is the stress divided by the corresponding strain, with greater values indicating the decreased deformability of a solid body [1, 2]. Young's modulus is a mechanical constant that characterizes the elastic properties of the material from which the solid body is made. It does not depend on the dimensions of the body and is associated with "hardness" – the rigidity of the solid body. The elastic properties of heterogeneous objects, such as cells, can be evaluated by Young's modulus [1, 2]. Larger values of Young's modulus mean an increase in rigidity, correspondingly a decrease in the elasticity (deformability) of the cells [3, 4].

Atomic force microscopy (AFM) can be used to evaluate and visualize the surface structure of cells [3, 4, 5]. One of its applications is to measure changes in the red blood cells (RBCs, erythrocytes), related to their deformability (Young's modulus), in type 2 diabetes mellitus (T2DM) [6, 7]. The incensement of glucose concentration in patients with T2DM results in a decrease of RBC deformability, which can be associated with changes in the shape of the erythrocytes [8]. The changes of morphological characteristics (shape, cell sizes, surface roughness, etc.) and mechanical parameters (Young's modulus, adhesion force, etc.) of erythrocytes can result in microvascular complications (diabetic retino-, nephro-, neuropathies, cardiovascular, neurovascular- and peripheral vascular diseases) in T2DM [6, 7, 8, 9].

The main approach to study the mechanical properties of objects by using AFM is a technique called (nano)indentation, i.e. deformation of the sample (the cell), as a result of the action of force with which the probe (top of the cantilever) of the atomic force microscope presses the cell [10, 11]. The main source of quantitative information about the mechanical characteristics of the sample (cell) is obtained from the so-called force curves, which show the dependence of the interaction force between the probe and the sample, and the distance between them [10, 11]. The analysis of these force curves allows the quantification of mechanical parameters such as deformation, stiffness, Young's modulus, etc. [10, 11, 12].

One of the main problems (tasks) in the accurate determination of Young's modulus of cells using AFM is the choice of a mathematical model for calculating the elastic modulus that will describe well the contact between the soft cell and the hard probe of AFM [10, 11, 12]. The most commonly used mathematical models for calculating the elastic modulus of various materials [14, 15] are the Hertz model, the Sneddon model, the Deryagin-Muller-Toporov model (DMT), and the Johnson-Kendall-Roberts model (JKR).

- In the Hertz and Sneddon models, the interactions between perfectly elastic homogeneous bodies, that are axisymmetric and smooth, are described. The adhesion forces between the probe tip (with the spherical shape in Hertz's model; or the shape of a cylinder, cone, or pyramid in Sneddon's model) and the sample (the cell) are not taken into consideration in these models. The mathematical models of Hertz and Sneddon are unsuitable for calculating Young's modulus of cells, which are soft and delicate objects – with a heterogeneous surface. Additionally, there are significant adhesion forces between the cell and the probe tip [16, 17].

- In the DMT model is accepted that adhesion forces act outside the contact area between the sample and the probe tip. This model is suitable for studies on the contact of solid materials with weak adhesion [10, 18].

- In the JKR model is accepted that adhesion forces act only in the contact area; it gives more accurate results when sticky and soft materials (such as blood cells), come into contact [19]. Therefore, we accepted that the most correct mathematical model for calculating Young's modulus of blood cells is the JKR model.

Determination of Young's modulus by the mathematical model of Johnson-Kendall-Roberts using the "two-points method"

Using the JKR model, it is assumed that the tip of the AFM probe and the sample (cell) are two elastic bodies. The AFM tip is represented as a sphere, and the spring represents the cantilever of the AFM (Fig. 1). When the AFM tip approaches a soft sample (cell), the adhesive interaction can draw the tip into the sample, and when the AFM tip retracts from a soft sample, the tip can pull and deform the sample by adhesive interaction [20].

The deformation of the sample Δ is obtained from the distance between the points where the external load $P = 0$ and where the external load $P = F_{adh}$ (Fig. 1).

- The deformation of the sample Δ defines the amount of deformation of the sample when it is pulled under the adhesive interaction between the tip and the sample.

- Z is the retraction distance of the AFM`s piezoelectric actuator, and D_{adh} is the deflection displacement of the AFM cantilever during this procedure.

- The total retraction distance Z_{adh} of the AFM piezoelectric actuator consists of the deflection displacement D_{adh} of the AFM cantilever and the deformation of the sample Δ [20].

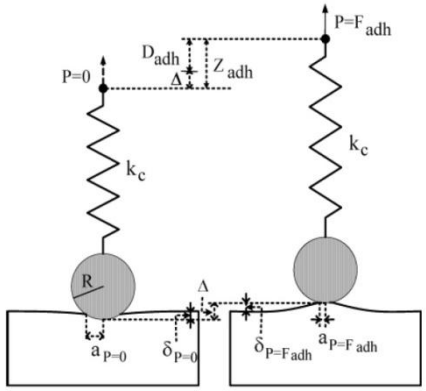

A) B)

Fig. 1. *The AFM tip and sample are considered two elastic bodies. The AFM tip is represented as a sphere, and the spring represents the AFM cantilever. A) The sample is deformed by adhesion when the external load P=0. (B) The sample is deformed by adhesion when the external load* $P=F_{adh}$ *[20].*

A typical force curve obtained by using AFM is presented in Fig. 2 A. In a "contact point" of the force curve, the interaction becomes attractive when the tip contacts the sample surface. Once the tip touches the surface, the tip is pulled into the sample by the adhesive interaction between the tip and the sample. This is shown as the sharp decrease of the force on the AFM cantilever in the extension part of the force curve in Fig. 2 A [19, 20].

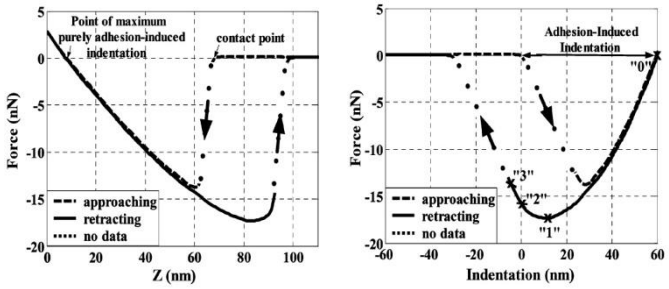

A) B)

Fig. 2. *AFM force plot: (A) A typical AFM force curve for the case of an AFM tip interacting with a soft sample under adhesive interaction; (B) The corresponding force vs. indentation plot. The forces on the AFM tip as it approaches the surface are indicated by the dashed lines while the forces upon retraction are shown by the solid lines. Point "0" is where the AFM tip has zero external force, "1" is where the tip has a maximum external force, "2" is where the tip has zero indentation in the sample, and "3" is where the tip ruptures from the sample [20].*

The force curve is converted to the corresponding force-indentation plot in Fig. 2 B. There are some distinct points on the force-indentation plot that correspond to the moments of interaction between the tip and the sample surface. At point "0" (Fig. 2 B), where the AFM tip is drawn in the sample surface due to adhesive interaction, the stored elastic and surface energy are balanced and zero external force acts on the AFM cantilever. The indentation between the point where the tip begins to contact the sample surface and point "0" is defined as adhesion-induced indentation. Point "1" is the place where a maximum external force acts on the tip; point "2" is the place where the tip has zero indentation in the sample; and point "3" is where the tip ruptures from the sample (Fig. 2 B). Points "0", "1" and "2" can be obtained directly from the force curves, and point "3" can be predicted by the JKR model [19, 20].

From the relationships between indentation (δ) - contact radius (a), and between external force (P) - contact radius (a), Young's modulus of samples can be determined by combining any two of the points in the retraction part of the force curve, and this method is called the "two-points method" [19, 20]. The indentation (δ) and the external force (P) are both functions of the contact radius (a), interfacial energy (γ_{12}), and the sample elasticity (E), i.e.: $\delta = \delta(a, \gamma_{12}, E)$, and $P = P(a, \gamma_{12}, E)$. For every two points on the force curve, there are four equations and four variables a_1, a_2, γ_{12} and E, where a_1 and a_2, are the contact radii at two points on the force curve. The indentation (δ) and the external force (P) at each point can be obtained directly from the force curve in Fig. 2 B [20].

According to the JKR model [16, 21], the contact radius (a) of the contact area is obtained from the following equations:

$$a^3 = \frac{R}{K}\left[P + 3\pi R\gamma_{12} + \sqrt{6\pi RP\gamma_{12} + (3\pi R\gamma_{12})^2}\right] \quad (1)$$

$$a_0^3 = \frac{6\gamma_{12}\pi R^2}{K} \quad (2)$$

$$\delta = \frac{a^2}{R}\left[1 - \frac{2}{3}\left(\frac{a_0}{a}\right)^{3/2}\right] \quad (3)$$

where (P) is the external force, is the interfacial energy, a_0 is the contact radius under zero external force, (δ) is the sample deformation, $R = R_1R_2/(R_1 + R_2)$ is the combined radius of the two spheres with radii of R_1 and R_2, $K = 4/3\pi(k_1 + k_2)$ is the combined elastic coefficient, k_1 and k_2 are the elastic constants of each sphere, as:

$$k_1 = \frac{1 - \nu_1^2}{\pi E_1} \quad (4)$$

$$k_2 = \frac{1 - \nu_2^2}{\pi E_2} \quad (5)$$

where ν_1 is the Poisson's ratio of the sample, ν_2 is the Poisson's ratio of the tip of the probe, E_1 is Young's modulus of the sample (cell), and E_2 is Young's modulus of the material from which the tip is made $(E_2 >> E_1)$ [20, 22].

For negative force, the spherical tip of the probe adheres to the sample. The contact radius a_3 at the rupture point is obtained by:

$$a_3 = \frac{a_0}{\sqrt[3]{4}} = 0{,}63a_0 \quad (6)$$

The point "3" in Fig. 2 B for the JKR model then can be located by using equation (6).

Combining points "0" and "3", it is obtained the following:

$$\delta_0 = \frac{1}{3}\sqrt[3]{\frac{16P_3^2}{K^2R}} \quad (7)$$

And

$$\delta_3 = \frac{1}{3}\sqrt[3]{\frac{P_3^2}{K^2R}} \quad (8)$$

By combining equations (7) and (8), it is written:

$$K = \left(\frac{1 + 16^{\frac{1}{3}}}{3}\right)^{\frac{3}{2}} \frac{P_3}{\sqrt{R(\delta_0 - \delta_3)^3}} \quad (9)$$

For the case when the modulus of elasticity of the tip significantly exceeds that of the sample ($E_2 >> E_1$), the modulus of elasticity E of the sample (cell) is obtained from the equation:

$$E = \frac{3(1-\nu^2)K}{4} \quad (10)$$

where ν is the Poisson's ratio of the sample and *K* is the combined elastic coefficient – equation (9) [20, 22].

By combining points "0" and "2", it can be obtained analogically:

$$E = \frac{3(1-\nu^2)P_2}{8}\left(\frac{3}{\delta_0^3 R}\right)^{\frac{1}{2}} \quad (11)$$

By combining points "0" and "1", *E* can be obtained by solving equations (1-3). First, a_0 and a_1 can be solved from (3), since because a_0 and a_1 are known from the force curves; second, one combines equations (1) and (2) and obtains:

$$a_1^3 = \frac{R}{K}\left[P_1 + \frac{a_0^3 K}{2R} + \left(\frac{P_1 a_0^3 K}{R} + \left(\frac{a_0^3 K}{2R}\right)^2\right)\right]^{\frac{1}{2}} \quad (12)$$

from which *K* can be written [20, 22].

The goal of the present study is to evaluate the elastic properties (Young's modulus) of erythrocytes from healthy donors and patients with type 2 diabetes mellitus, with the mathematical model of the Johnson-Kendall-Roberts by the "two-points method", using an atomic force microscope.

2. Materials and Methods

Preparation of blood samples from healthy controls and T2DM patients. Human blood samples are collected from volunteers following the ethical principles of medical research – Declaration of Helsinki, and all of them gave written informed consent. Healthy donors (control group) are selected if they did not have any chronic diseases, as non-smokers, females, who didn't take any hormone replacements or contraception, etc. Patients with T2DM are diagnosed, according to the guidelines of the American Diabetes Association (ADA) [23].

The *in vitro* experiments are realized with blood samples from 15 healthy individuals (*average age 53 ± 9,3 years*) and 15 T2DM patients (*average age 61,8 ± 7,7 years*). Venous blood samples are drawn by venipuncture and collected in 6 ml tubes with K_2EDTA as an anticoagulant.

Sample preparation for AFM. Erythrocytes are separated from each blood sample from the healthy subjects and the diabetic patients by a centrifugation method. The concentrated erythrocyte suspension is washed twice with saline, as the hematocrit is adjusted to 40%. From the obtained erythrocyte suspension, 3,5 µl are taken and fixed with 700 µl 0,5% glutaraldehyde (GA) for 30 min, at room temperature. Fixed erythrocytes are washed twice with saline and twice with distilled water, then plated on mica. The samples are dried for about 1 day, and after that, they are examined with AFM [24].

AFM imaging and measurements. The fixed erythrocytes are examined by using the AFM Dimensional ICON Bruker NanoScope V9 Instrument (AFM Bruker), which works in a PeakForce QNM (Quantitative Nano-Mechanical Mapping) imaging mode. This is one of the newest AFM modes of work, combining the advantages of static (contact) and dynamic (periodic) modes of operation [15, 25]. This method is similar to the standard tapping mode of scanning probe microscopy, where the probe and the sample are brought together intermittently. It operates by controlling the maximum force applied by the probe to the sample and allows a rapid force–distance curve to be generated at every pixel [26]. The force curves could be analyzed quantitatively to obtain a series of specific characteristics on the map of each sample. High-quality images of the relief (topography) and quantitative (nano)mechanical maps of the studied samples can be obtained in parallel, through high-speed scanning, using the PeakForce QNM mode [27].

The cantilever's deflection sensitivity, spring constant, and tip radius are calibrated in advance. Morphological and mechanical properties of red blood cells are studied simultaneously in PeakForce QNM mode using silicon cantilever RFESP (a tip radius of 8 nm, a resonance frequency of 75 kHz, and a spring constant of 3 N/m), at room temperature. The obtained images are analyzed with the program NanoScope Analysis 1.9 (Bruker).

From every blood sample, three arbitrarily selected erythrocytes are examined. The total number of erythrocytes studied in healthy individuals is *n'=45* cells, and the total number of studied erythrocytes in T2DM patients is *n'=45* cells. For every erythrocyte from healthy individuals and diabetic ones, the following AFM images are found: a 2D topography, a 3D topography, a cross-sectional profile of the cell, and a map of Young's modulus.

Evaluation of the topography of erythrocytes is made by determining the cell *diameter – d* (horizontal distance corresponding to the diameter of the cell is measured), and roughness of the cell (based on three arbitrarily selected cross-sectional profiles from the surface of each erythrocyte), by the specific parameters [24, 28]:

- *maximum height* – R_{max} (difference in height between the highest and lowest points on the cross-sectional profile relative to the center line (not the roughness curve), over the length of the profile);
- *average roughness in ten points* – R_z (average difference in height between the five highest peaks and five lowest valleys relative to the center line over the length of the profile; in cases where five pairs of peaks and valleys don't exist, this is based on fewer points.);
- *average roughness* – R_a (average value of the roughness curve relative to the center line).

The maps of the elastic modulus of red blood cells are compiled according to the values of *Young's modulus* determined in each nanoindentation point by calculation according to the Johnson-Kendall-Roberts mathematical model by the "two-point method". The Young's modulus of erythrocytes is presented as average values obtained from the force curves – up to 2000 for each cell, of all nanoindentation points entering an arbitrarily selected section of the peripheral parts of each cell.

Statistical analysis. Data analysis is performed based on the software packages Sigma Plot 11.0. All data are presented as average ± SD (standard deviation). The significance of differences is evaluated using the t-test and the Mann-Whitney Rank Sum Test. Differences are accepted as significant at $p<0,05$.

3. Results

AFM images of fixed erythrocytes from healthy donors show that the red blood cells with a biconcave shape, so-called *discocytes* or *normocytes*, are predominated in the samples (Fig. 3 A, B).

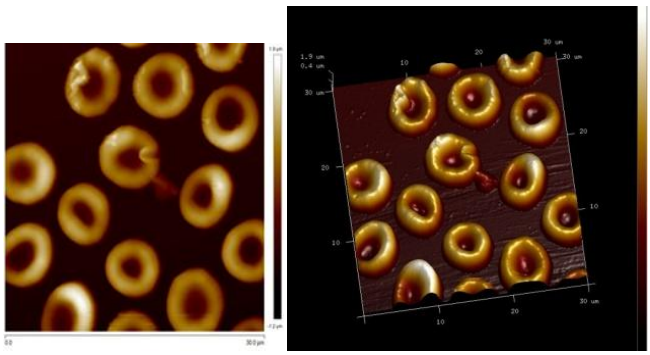

(A) (B)

Fig. 3. *AFM Bruker images of erythrocytes with normal biconcave shape (discocytes or normocytes), from a healthy donor: A) 2D topography; B) 3D topography.*

AFM images of fixed red blood cells from patients with T2DM illustrate a change in the size (*anisocytosis*) and shape (*poikilocytosis*): the so-called erythrocyte polymorphism. Erythrocytes with pathological changes in the shape, so-called *poikilocytes*, are observed as follows:

- *spherocyte* – erythrocyte, which has lost its double concave shape and turned into a spherical cell (Fig. 4 A, B);
- *echinocyte* – erythrocyte with many small, evenly spaced needle-like outgrowths throughout the membrane (Fig. 4 C, D);
- *knizocyte* – an erythrocyte that is a triple concave (Fig. 4 E, F);
- *elliptocyte (ovalocyte)* – erythrocyte, which has acquired an elliptical shape (with varying degrees of expression), etc.

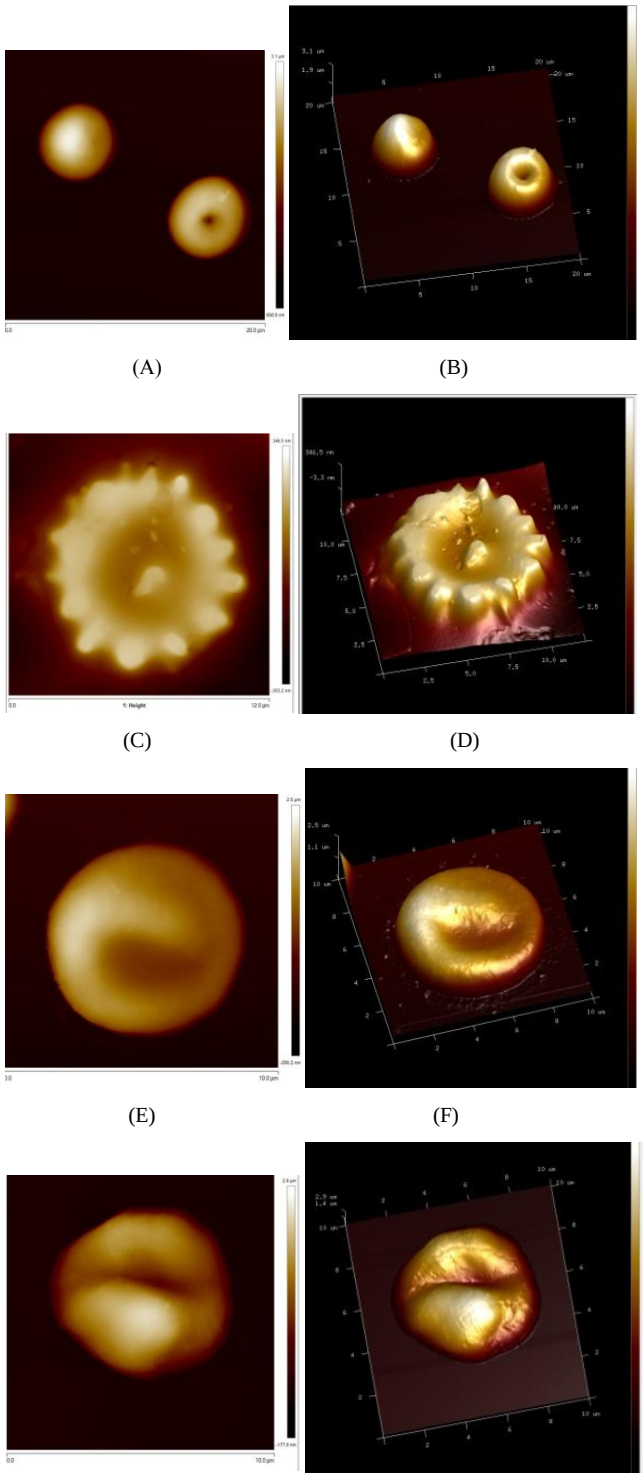

(A) (B)

(C) (D)

(E) (F)

(G) (H)

Fig. 4. *AFM Bruker images of erythrocytes from T2DM patients: A, C, E, G) 2D topography; B, D, F, H) 3D topography. A, B) spherocytes; C, D) echinocyte; E, F) knizocyte; G, H) atypical form of an erythrocyte.*

The diameter (*d, μm*) of fixed erythrocytes from healthy individuals is between *5,6 μm* and *6,7 μm*. In T2DM patients it is elevated and varies between *6,5 μm* and *7,5 μm* (Table 1; Fig. 5 A). In the diabetic patients, the diameter of erythrocytes increases statistically significantly by 14% (*p≤0,001*) in comparison to the data from healthy donors.

Table 1: *Averages values and standard deviations of morphological parameters and mechanical parameters of erythrocytes from control group healthy individuals (n=15) and patients with T2DM (n=15).* *Note: d – diameter; R_{max} – maximum height; R_z – average roughness in ten points; R_a – average roughness; E – Young's modulus; n – total number of examined persons from each group; n` – total number of examined cells from each group; t-test: *** p≤0,005.*

Parameter	Control group n=15, n`=45 cells	Patients with T2DM n=15, n`=45 cells
D, μm	6,16±0,56	7,03±0,51***
R_{max}, μm	1,42±0,21	1,74±0,24***
R_z, μm	1,1±0,19	1,19±0,31
R_a,μm	0,31±0,09	0,36±0,08
E, MPa	98,6±11,67	124,89±9,41***

The evaluation of the roughness (*R, μm*) of each erythrocyte (Fig. 6 A, C), is made by the profiles of three arbitrarily selected cross-sectional lines from the topography image of each RBC. From the cross-sectional profiles of the surface of erythrocytes in healthy individuals, it is found that they have a typical morphology – a double concave shape (Fig. 6 A, B), while in patients with diabetes, the RBC surface has an abnormal shape (Fig. 6 C, D).

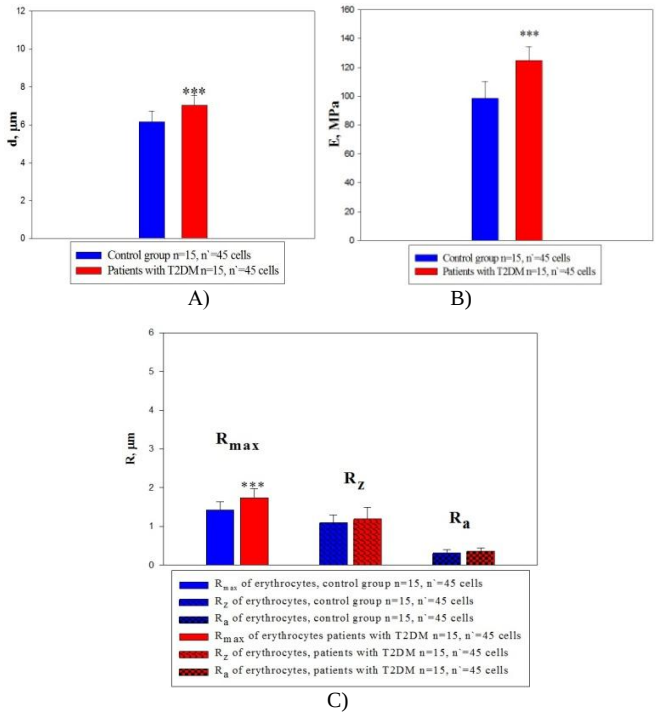

Fig. 5. *Average values and standard deviations of the morphological and mechanical parameters of erythrocytes from control group healthy individuals (n=15), and patients with T2DM (n=15): A) diameter – d; B) Young's modulus – E; C) roughness, evaluated by the parameters: maximum height – R_{max}; average roughness in ten points – R_z; average roughness – R_a.*

In patients with T2DM, the erythrocyte maximum height (R_{max}, *μm*) statistically significantly increases by 23% (*p≤0,001*), the average roughness at ten points (R_z, *μm*) increases by 8%, and the average roughness (R_a, *μm*) increases by 16%, compared to the control group of healthy individuals (Table 1; Fig. 5 C). Therefore, the erythrocytes from diabetic patients are higher and their relief of the surface, evaluated quantitatively by morphological parameters

for roughness (R_{max}, R_z, R_a) is changed, in comparison with the topography of erythrocytes in the control group of healthy objects.

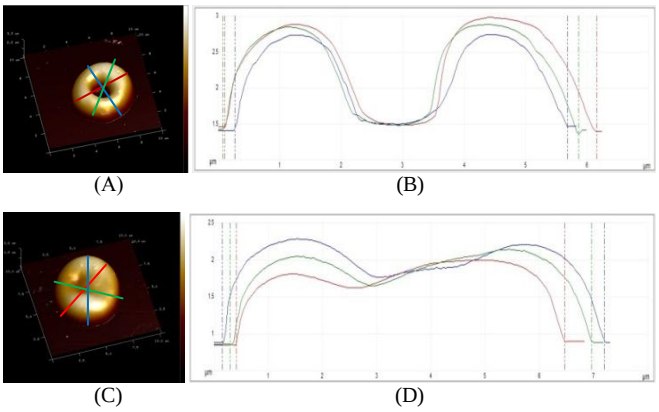

(A) (B)

(C) (D)

Fig. 6. *AFM Bruker images of: A) erythrocyte (discocyte) from a healthy donor; C) erythrocyte (elliptocyte) from a T2DM patient. A, C) 3D topography with three cross-sectional lines from the cell surface; B, D) profiles of three cross-sectional lines from the cell topography.*

For each of the RBCs studied (Fig. 7 A, D), corresponding Young's modulus distribution maps (Fig. 7 B, D), have been evaluated.

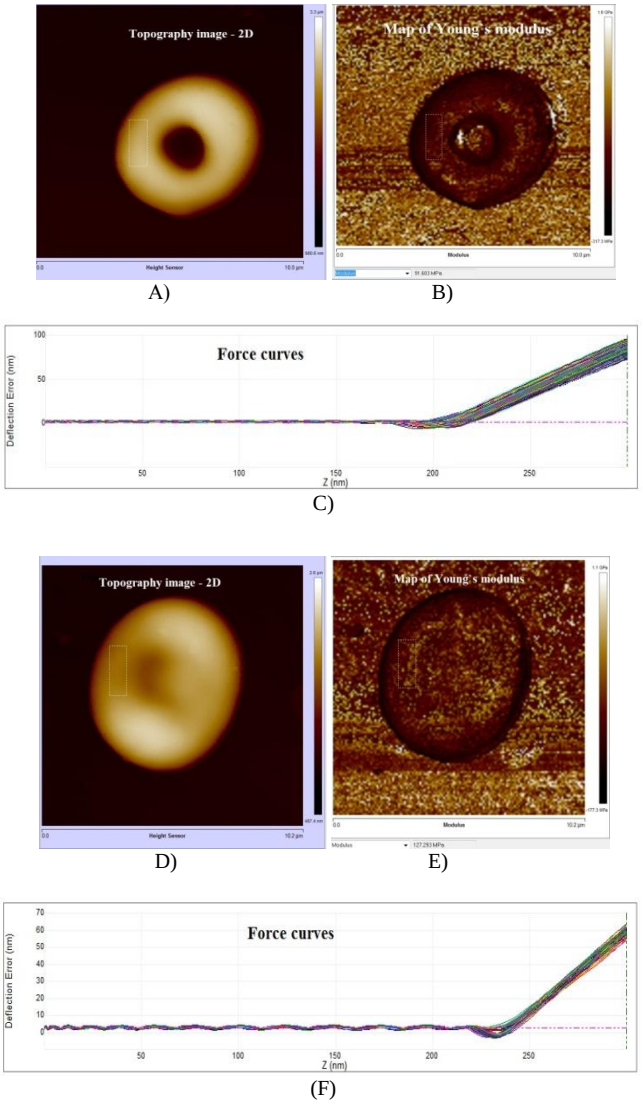

A) B)

C)

D) E)

(F)

Fig. 7. *AFM Bruker images of: A, B) erythrocyte (discocyte) from a healthy donor; D, E) erythrocyte (elliptocyte) from a T2DM patient. A, D) 2D topography; B, E) Young's modulus distribution map of erythrocyte; C, F) force curves of all nanoindentation points entering the arbitrarily peripheral section of the erythrocyte membrane, which are used for calculation of the average value of Young's modulus of erythrocyte.*

The values of the elastic modulus for every point of nanoindentation from Young's modulus distribution map are calculated according to the mathematical model of Johnson-Kendall-Roberts, by the "two-point method". The average value of Young's modulus of each RBC is determined for an arbitrary peripheral section (with a rectangular shape), from the membrane of the erythrocyte (Fig. 7 B, E). The force curves (Fig.7 C, F), of all nanoindentation points (up to 2000 for each cell) entering the arbitrary peripheral section of the erythrocyte membrane are used for the calculation of the average values of Young's modulus of the erythrocyte.

In patients with T2DM, the average value of Young's modulus (*E, MPa*) of erythrocytes increases statistically significantly by 27% ($p \leq 0,001$), in comparison with healthy individuals (Table 1, Fig. 5 B). These changes indicate the reduced deformability (increased rigidity) of erythrocytes in T2DM patients, compared to RBC deformability in healthy individuals.

The linear correlation analysis between the mechanical parameter – Young's modulus (*E, MPa*), and morphological parameter – maximum height (R_{max}, *μm*) of the erythrocytes in the control group, doesn't prove a correlation between them (Fig. 8 A).

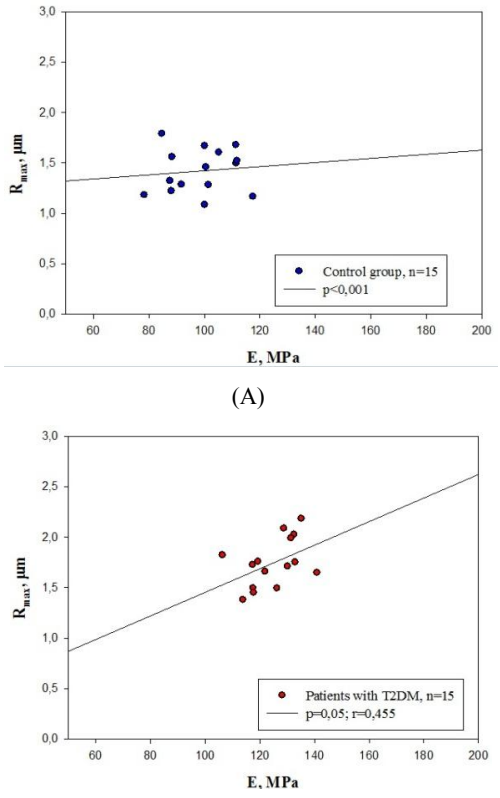

(A)

(B)

Fig. 8*. Linear correlation between Young's modulus (E, MPa), and maximum height (R_{max}, μm) of erythrocytes, from: A) control group of healthy individuals; B) patients with T2DM.*

A positive correlation between *E* and R_{max} of erythrocytes ($p=0,05$; $r=0,455$) is demonstrated in patients with T2DM (Fig. 8 B). Therefore, in diabetic patients, the modulus of elasticity is increased (the deformability of RBCs is decreased), in parallel with the changes in the relief of the cells (the R_{max} was increased).

4. Discussions

AFM can be considered as an informative technique that is used for structural studies of erythrocytes, and to measure Young's modulus indicating the elasticity (deformability) of cells. By application of the AFM, the morphological and mechanical characteristics of erythrocytes in healthy individuals and patients with T2DM can be studied simultaneously. Significant differences are found in the diameter, height, roughness, and Young's modulus

of erythrocytes in T2DM patients, compared with the results in healthy individuals.

In other studies [7, 24, 29, 30, 31, 32], conducted with atomic force microscopes and simultaneous application of experimental methods and mathematical models, different values of Young's modulus for erythrocytes in healthy donors and diabetic patients also were obtained.

The most commonly applied mathematical model for calculating Young's modulus using AFM is the Hertz model [29, 31, 32, 33, 34]. Through this model in a study [29], the elastic modulus of erythrocytes in diabetic patients (*E=0,0143±0,0014 MPa*) is found to be higher, than E of healthy donors (*E=0,0044±0,0006 MPa*). According to Hertz's mathematical model, Young's modulus of RBCs is calculated also in the study [30], in healthy donors E=74,47±4,97 MPa, and in patients with T2DM *E=102,75±4,78 MPa*, and in research [31] - in healthy donors *E=0,0083±0,0012 MPa*, and in patients with T2DM, E =0,0153±0,0039 MPa. In the publication [32], for the modulus of elasticity of erythrocytes calculated by the Hertz model is found that *E=85,8±11,9 MPa*, for the control group, and *E=122±5,7 MPa* – for diabetic patients. According to Sneddon's mathematical model, in a study [34], it was found that Young's modulus in healthy donors is *E=0,0018±0,0002 MPa*, and in diabetic patients, it is *E=0,0025±0,0006 MPa*.

From the maps of the elastic modulus of erythrocytes from healthy donors and patients with T2DM (Fig. 7 B, E), was established that the surface of the cells is heterogeneous – the peripheral parts of the RBCs have lower Young's modulus, than central parts. As a result of this, if Young's modulus is obtained from Hertz's or Sneddon's mathematical models (which can only be used for perfectly homogeneous bodies), then it will be incorrect.

In a study [7], it is established for the modulus of elasticity, calculated according to the mathematical model of DMT, that for the control group, it is *E=46710±39210 MPa*, and for the patients with T2DM *E=56483±64418 MPa*. Erythrocytes are soft, "delicate" objects, and the adhesion force between them and the tip of the cantilever could be significant and cannot be neglected. Therefore, Young's modulus values, which are obtained by the DMT model [7] can be assumed also that are inaccurate because in this model the adhesion forces act outside the contact area between the tip and solid sample.

Until now, in the scientific literature, cannot be found studies in which Young's modulus of erythrocytes is evaluated according to the mathematical model of JKR. In our study, the results obtained for the elastic modulus of the RBCs in healthy donors *E=98,6±11,67 MPa*, and patients with T2DM *E=124,89±9,41 MPa*, are calculated by the mathematical model of JKR by the "two-point method".

For erythrocytes in healthy individuals or patients with T2DM, the elastic modulus values were calculated by different mathematical models [7, 24, 29, 30, 31, 32, 34] and differ greatly from each other. To be able to compare Young's modulus values evaluated in different studies, this modulus must be calculated by one specific mathematical model, which could reflect most precisely the experimental cell model. The mathematical model of JKR describes more accurately the interaction between the cell and the tip of the cantilever. Thus, it is more appropriate to determine Young's modulus by this model. Therefore, we suppose that the values of the elastic modulus of erythrocytes in healthy donors and patients with T2DM obtained in our study are accurate.

The results obtained in our research (Table 1; Fig. 5 B), show that elastic modulus of RBCs in diabetic patients statistically significantly increases, when it is compared to the control group of healthy individuals. The deformability of erythrocytes plays an important role in their movement in blood vessels, oxygen transfer, etc. A decrease in erythrocyte deformability leads to a reduction in capillary blood flow and subsequent microvascular complications, which are often observed in T2DM patients [9, 35, 36]. Changes in erythrocyte deformability (decreased), increased diameter and their increased ability to aggregate - associated with increased blood viscosity, are closely connected with increased blood coagulation, causing the development of thrombosis in patients with T2DM [8, 24, 37].

Increased glycation of hemoglobin, altered cholesterol levels, and oxidative stress in T2DM patients can lead to changes in RBC morphology, and a formation of echinocytes and spherocytes with impaired deformability [38, 39]. Changes in erythrocyte shape can be used as an early biomarker of diabetic complications, allowing better monitoring and treatment of diabetic patients [24, 40].

The simultaneous study of changes in cell morphology and mechanical characteristics of RBCs is important to elucidate the pathogenesis of vascular complications and especially of thromboses in diabetic patients [24, 40]. The established positive correlation between the elastic modulus and the roughness of erythrocytes, found in this study (Fig. 8), can be used as biomarkers in the clinical management of T2DM [6, 9, 24].

5. Conclusion

The morphological (diameter, height, roughness) and elastic (Young's modulus) characteristics of erythrocytes have been studied in parallel by AFM. The mathematical model of Johnson-Kendall-Roberts was applied, as more suitable for calculating Young's modulus of the cells. The values of the elastic modulus of erythrocytes from healthy objects and patients with T2DM, obtained using a model of JKR by the "two-point method", are the most accurate. Significant differences are found in the diameter, height, roughness, and Young's modulus of erythrocytes in T2DM patients, compared with the results of healthy individuals. The studied AFM morphological and mechanical characteristics of erythrocytes can be considered as precise biomarkers for the state of patients with T2DM. This is important for the diagnosis, prevention and successful monitoring of treatment of the T2DM in the clinical practice.

6. Acknowledgment

This work has been accomplished with financial support by Grant № BG05M2OP001-1.002-0011-C02 financed by the Science and Education for Smart Growth Operational Program (2014-2020) and co-financed by the European Union through the European Structural and Investment funds. The study has been supported also by the Basic Research Project – 2018 (КП-06-Н27/13): "Development of experimental microfluidic system and methodology for assessing microrheological properties of blood. Analysis of the peripheral vasomotor reactivity and vascular endothelial function in patients with type 2 diabetes mellitus", funded by the Bulgarian National Science Fund.

7. References

1. Guz, N., Dokukin, M., Kalaparth, V., Sokolov, I. If cell mechanics can be described by elastic modulus: study of different models and probes used in indentation experiments. Biophysical J., **107**, 564-575 (2014).
2. Sokolov, I., Dokukin, M. E., Guz, N. V. Method for quantitative measurements of the elastic modulus of biological cells in AFM indentation experiments. Methods **1, 60(2)**, 202-213 (2013).
3. Yeow, N., Tabor, R. F., Garnier, G. Atomic force microscopy: From red blood cells to immunohaematology. Adv Colloid Interface Sci. **249**, 149-162 (2017).
4. Kim, J., Lee, H. Y., Shin S. Advances in the measurement of red blood cell deformability: A brief review. Journal of Cellular Biotechnology, **1**, **63-79** (2015).
5. Andreeva, T., Komsa-Penkova, R., Langari, A., et al. Morphometric and nanomechanical features of platelets from women with early pregnancy loss provide new evidence of the impact of inherited thrombophilia. Int J Mol Sci. **22(15):7778** (2021).
6. Girasole, M., Pompeo, G., Cricenti, A., et al. Roughness of the plasma membrane as an independent morphological parameter to

study RBCs: a quantitative atomic force microscopy investigation. Biochimica et Biophysica Acta, **1768(5)**, 1268-1276 (2007).
7. Pretorius, E., Bester, J., Vermeulen, N., et al. Poorly controlled type 2 diabetes is accompanied by significant morphological and ultrastructural changes in both erythrocytes and in thrombin-generated fibrin: implications for diagnostics. Cardiovasc Diabetol. **14:30** (2015).
8. Brun, J. F., Varlet-Marie, E., Myzia, J., de Mauverger, E. R., Pretorius, E. Metabolic influences modulating erythrocyte deformability and eryptosis. Metabolites, **12, 4** (2022).
9. Rask-Madsen, C., King, L. G. Vascular complications of diabetes: mechanisms of injury and protective factors. Cell Metab. **17(1)**, 20-33 (2013).
10. Cappella, B. Physical Principles of Force–Distance Curves by Atomic Force Microscopy. In: Cappella, B., Mechanical Properties of Polymers Measured through AFM Force-Distance Curves, Springer International Publishing Switzerland, 3-63 (2016).
11. Garcia, R. Nanomechanical mapping of soft materialswith the atomic force microscope: methods, theory and applications. Chem. Soc. Rev. **49**, 5850-5884 (2020).
12. Dulinska, I., Dokukin, M. E., Guz, N. V. Method for quantitative measurements of the elastic modulus of biological cells in AFM indentation experiments. Methods **60**, 202-213 (2013).
13. Roa, J. J., Oncins, G., Diaz, J., Sanz, F., Segarra, M. Calculation of Young's modulus value by means of AFM. Recent Pat Nanotechnol, **5(1)**, 27-36 (2011).
14. Zeng, G., Dirscherl, K., Garnæs, J. Accurate quantitative elasticity mapping of rigid nanomaterials by atomic force microscopy: effect of acquisition frequency, loading force, and tip geometry. Nanomaterials, **8**, 616-628 (2018).
15. Dokukin, M. E., Sokolov, I. Quantitative mapping of the elastic modulus of soft materials with HarmoniX and PeakForce QNM AFM modes. Langmuir **20;28(46)**:16060-71 (2012).
16. Ladjal, H., Hanus, J.-L., Pillarisetti, A., et al. Atomic force microscopy-based single-cell indentation: Experimentation and finite element simulation. IEEE/RSJ International Conference on Intelligent Robots and Systems, Oct 2009, St. Louis, MO, United States, 1326-1332 (2009).
17. Kuznetsova, T. G., Starodubtseva, M. N., Tegorenkov, et al. Atomic force microscopy probing of cell elasticity. Micron **38**, 824-833 (2007).
18. Barthel, E. Adhesive elastic contacts: JKR and more. J. Phys. D: Appl. Phys. **41** 163001 (2008).
19. Grierson, D. S., Flater, E. E., Carpick, R. W. Accounting for the JKR–DMT transition in adhesion and friction measurements with atomic force microscopy. J. Adhesion Sci. Technol., **19(3–5)**, 291-311 (2005).
20. Sun, Y., Akhremitchev, B., Walker G. C. Using the adhesive interaction between atomic force microscopy tips and polymer surfaces to measure the elastic modulus of compliant samples. Langmuir **20**, 5837-5845 (2004).
21. Chu, Y. S., Dufour, S., Thiery, J. P., Perez, E., Pincet, F. Johnson-Kendall-Roberts theory applied to living cells. Phys Rev Lett. **94(2):028102** (2005).
22. Nakajima, K., Ito, M., Wang, D., Liu, H., et al. Nano-palpation AFM and its quantitative mechanical property mapping. Microscopy, 193-207 (2014).
23. Meneghini L. Medical Management of Type 2 Diabetes. 8th ed. American Diabetes Association (2020).
24. Alexandrova-Watanabe, A. Study of rheological, mechanical and morphological properties of blood, its formal elements and parameters of hemocoagulation in type 2 diabetes mellitus. PhD thesis, Institute of Mechanics, Bulgarian Academy of Sciences, Sofia, Bulgaria (2021).
25. Zeng, G., Dirscherl, K., Garnæs, J. Toward accurate quantitative elasticity mapping of rigid nanomaterials by atomic force microscopy: effect of acquisition frequency, loading force, and tip geometry. Nanomaterials, **8**, 616-628 (2018).
26. Dufrêne, Y. F., Martínez-Martín, D., Medalsy, I., et al. Multiparametric imaging of biological systems by force-distance curve-based AFM. Nat Methods, **10:** 847–854 (2013).
27. Pittenger, B., Erina, N., Su, C. Quantitative Mechanical Properties Mapping at the Nanoscale with PeakForce QNM. Bruker Application Note **128** (2011).
28. Bruker. Dimension Icon User Guide. Bruker Corporation (2010).
29. Fornal, M., Lekka, M., Pyka-Fościak, G., et al. Erythrocyte stiffness in diabetes mellitus studied with atomic force microscope. Clin Hemorheol Microcirc. **35(1-2)**, 273-276 (2006).
30. Drozd, E. S., Chizhik, S. A., Konstantinova, E. E. Mechanical characteristics of erythrocyte membranes in patients with type 2 diabetes mellitus. Series on Biomechanics **25**, **3-4**, 53-60 (2010).
31. Krastev, R. Study of the morphological and mechanical characteristics of the erythrocyte membrane. Dependence on the rheological properties of blood. Master's thesis, Faculty of Physics, Sofia University "St. Kliment Ohridski", Sofia, Bulgaria (2011).
32. Antonova, N., Alexandrova, A., Melnikova, et al. Micromechanical properties of peripheral blood cells (erythrocytes, lymphocytes and neutrophils) in patients with diabetes mellitus type 2, examined with atomic force microscope (AFM). Series on Biomechanics **33 (4)**, 3-11 (2019).
33. Efremov, Y. M., Wang, W.-H., Hardy, S. D., Geahlen R. L., Raman, A. Measuring nanoscale viscoelastic parameters of cells directly from AFM force-displacement curves. Scientific Reports 7: 1541 (2017).
34. Ciasca, G., Papi, M., Claudio, D. S., Chiarpotto, M., et al. Mapping viscoelastic properties of healthy and pathological red blood cells at the nanoscale level. Nanoscale **7**, 17030-17037 (2015).
35. Keymel, S., Heiss, C., Kleinbongard, P., et al. Impaired red blood cell deformability in patients with coronary artery disease and diabetes mellitus. Horm. Metab. Res. **43**, 760-765 (2011).
36. Lee, H., Na, W., Lee, S. B., Ahn, C. W., et al. Potential diagnostic hemorheological indexes for chronic kidney disease in patients with type 2 diabetes. Frontiers in Physiology **10**:1062 (2019).
37. AlSalhi, M. S., Devanesan, S., AlZahrani, K. E., et al. Impact of diabetes mellitus on human erythrocytes: atomic force microscopy and spectral investigations. Int J Environ Res Public Health **15**:2368 (2018).
38. Gyawali, P., Richards, R. S., Nwose, E. U. Erythrocyte morphology in metabolic syndrome. Expert Rev. Hematol. **5(5)**, 523-531 (2012).
39. Shin, S., Ku, Y., Babu, N., Singh, M. Erythrocyte deformability and its variation in diabetes mellitus. Indian J Exp Biol. **45(1)**, 121-128 (2007).
40. Rajab, A. M., Rahman, S., Rajab, T. M., Haider, K. H. Morphology and chromic status of red blood cells are significantly influenced by gestational diabetes. Diab Met Syndr: Clin Res Rev **7**, **4**, 140-148 (2018).

Influence of the window profile on the final quality of the product

Elena Jevtoska[1]
Faculty for design and technology of furniture and interior-Skopje, Str. 16-ta Makedonska Brigada" N 3 Skopje
ejevtoska@gmail.com

Abstract *The current product on the market offers a wide range of diverse profiles for producing windows that are made of different materials, width and order of grills depending on the profile. Within the framework of this research the windows with same dimensions shall be elaborated, those which are made of the same production capacity and use the same fittings but different types of PVC profiles. The aim is to prove what kind of influence the used profile has over the final quality of the product. For this research, two groups and six subgroups will be tested. In each subgroup, one tests five windows made of the same profile. The groups are divided according to the used fittings. The testing of the quality shall be conducted in accordance with the European norms EN 1026:2016 (Windows and doors - Air permeability - Test method), EN 1027:2016 (Windows and doors - Water tightness - Test method), EN 12211:2016 (Windows and doors - Resistance to wind load - Test method).*
Keywords*: CONSTRUCTION CARPENTRY, WINDOW, AIR PERMEABILITY, WIND RESISTANCE, PVC PROFILES*

1. Introduction

The quality of one product is a characteristic worth being considered when it is proven that the same satisfies the needs for which it is produced. Having in mind that the purpose of one window is to provide light and desirable ventilation of a room, and, at the same time, to protect the object from external influences such as air permeability, water tightness and resistance to wind, we state that the window is of a higher quality as much as it can guarantee all these conditions. The window as a product is of complex content from diverse materials and parts. As different parts of the window we enlist the following below: Frame – the frame is a construction of the jamb and the construction of the side jamb.

Glass – the content of the construction that can be made of glass and glass packet.

Hinge – design, window handle, window lockers which offer the sliding of the window, meaning, the possibility for its opening and closing.

Throughout the production of window parts, different types of materials are used:

Frame – wood profiles from different types of wood, PVC profiles, aluminum profiles, as well as a combination of these materials.

Glass – one glass (4mm, 6mm), glass packet out of two, three or four glasses with different combinations of glasses layered with different protective paints.

Fittings – metal, plastic, rubber.

Un-plasticized Poly Vinyl Chloride is relatively new to the building industry as a material for windows and doors. UPVC is based on poly vinyl chloride(PVC), one of the most versatile polymers found. UPVC is prepared with a special formulation in which different stabilizers and modifiers are added to poly vinyl chloride to make rigid and suitable for use as window frames. UPVC contains poly vinyl chloride(PVC), calcium carbonate(CaCo3) and titanium dioxide (TiO2). PVC forms the major constituent of blend composition. Unlike other polymer PVC is heat sensitive and requires additives during processing. Hence the properties of PVC can be increased through additives like light and UV stabilizer, fillers, pigments and lubricants can be added during the blending process. Titanium dioxide is an expensive pigment used for imparting natural white color to the UPVC profile and provide necessary UV stability for the product. Calcium carbonate are fillers which are inorganic minerals as fine particles homogenized in PVC blend. Usage of filler has effect on mechanical property like tensile strength, elongation, impact strength, shrinkage and cost. Production of UPVC involves a complex extrusion process. Extrusion is a manufacturing process where material is drawn through a die of required cross section. The main advantage of extrusion process is that it can create very complex sections and also can be used for brittle objects. Additionally this process provide excellent surface finishes. UPVC extrusion process can be recycled. UPVC has excellent insulation properties resulting in high energy efficiency.(1)

The non-polyvinyl chloride as a material offers possibilities for creating different window profiles in terms of the dimensions and the order of the grills. This paper has the aim of researching how much the diversification of the profiles influences the final quality of the window. The quality will be elaborating on the water tightness, air permeability as well as resistance to deformity on wind load.

2. Materials and research metod

The samples which are subject of the research are divided into two groups. In each group there are six subgroups, each consisting of five windows. All the samples' dimensions are 800mm width and 1400 mm height. All the samples in the subgroup are made of the same production capacity and the same type of fittings and profile is used for their making (Table 1). For all the samples in the subgroups a different type of profile is used..

Table 1: *Groups of the test samples*

Subgroup	Picture of the sample	Profile of the sample
Group 1 Windows with dimensions 800/1400mm Fitting AGB		
Subgroup 1		REHAU GENEO [2] 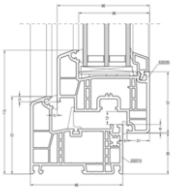
Subgroup 2		ALPHACAN 70R [3] 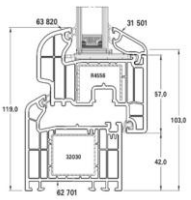
Subgroup 3		ALPHACAN PRESTIGIO [3] 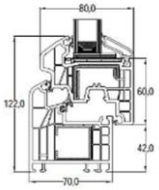

Subgroup 4		ALUPLAST IDEAL 4000 [4] 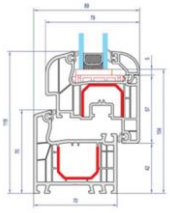
Subgroup 5		SCHUCO SYSTM CT 70 [5] 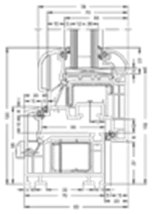
Subgroup 6		REHAU SYNEGO [2] 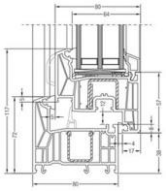
Group 2 Windows with dimensions 800/1400mm Fitting Sigenia		
Subgroup 7		KOMMERLINK [6] 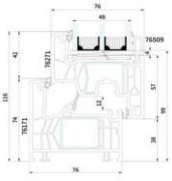
Subgroup 8		SCHUCO SI 82 [5] 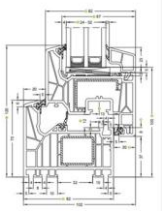
Subgroup 9		ALUPLAST IDEAL 8000 [4] 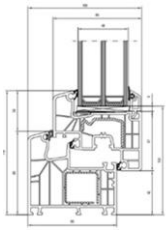
Subgroup 10		GEALAN S9000 [7] 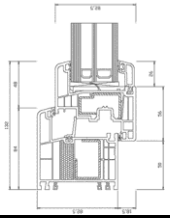

Subgroup 11		SALAMANDER STREAMLINE MD76 [8] 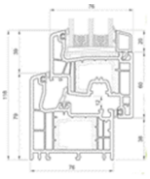
Subgroup 12		TROCAL 88mm [9] 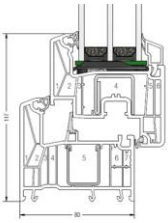

3. Results

3.1. Results of the air permeability

The testing of the air permeability is conducted with pressure and absorption of the different air pressure. The mean values for every subgroup will be presented individually in a diagram, just as the class according to the EN 1026:2016 “Windows and doors - Air permeability - Test method” standard. [10]

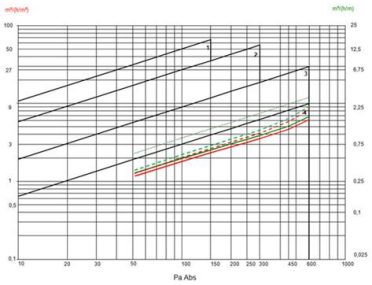

Fig.1 *Air permeability measures for subgroup 1*

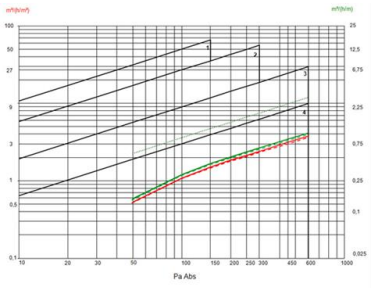

Fig.2 *Air permeability measures for subgroup 2*

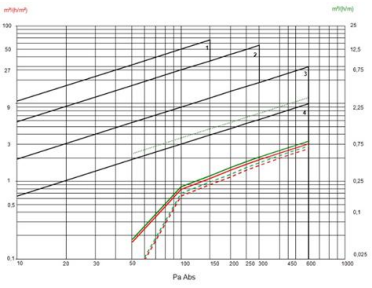

Fig.3 *Air permeability measures for subgroup 3*

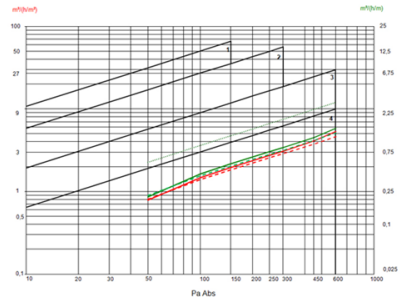

Fig.4 *Air permeability measures for subgroup 4*

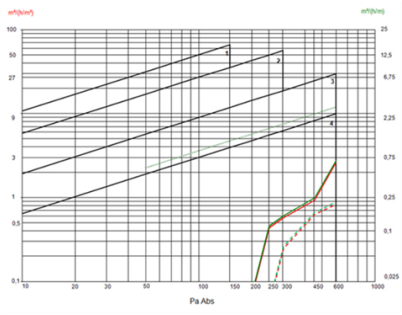

Fig.5 *Air permeability measures for subgroup 5*

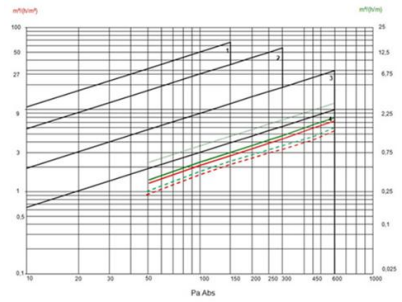

Fig.6 *Air permeability measures for subgroup 6*

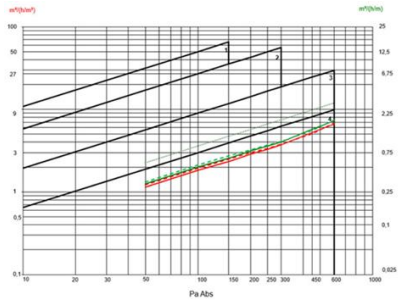

Fig.7 *Air permeability measures for subgroup 7*

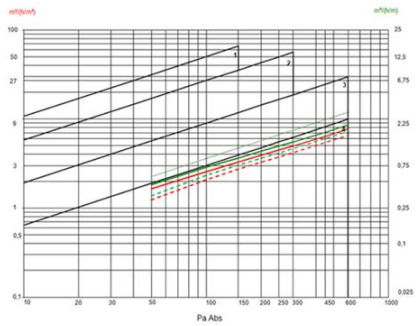

Fig.8 *Air permeability measures for subgroup 8*

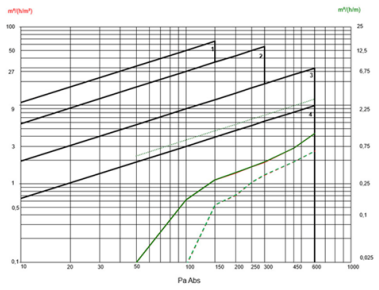

Fig.9 *Air permeability measures for subgroup 9*

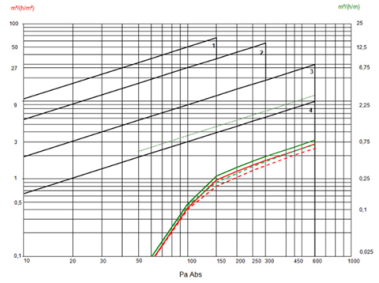

Fig.10 *Air permeability measures for subgroup 10*

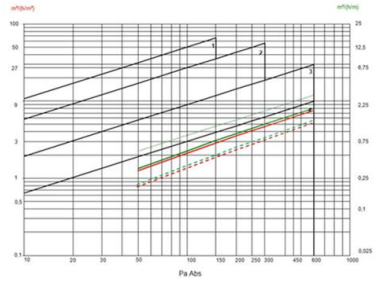

Fig.11 *Air permeability measures for subgroup 11*

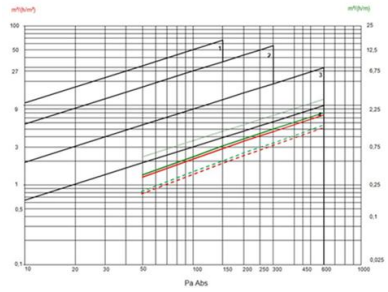

Fig.12 *Air permeability measures for subgroup 12*

3.2. Results – water tightness

Class according to the EN 1027:2016 "Windows and doors - *Water tightness - Test method*" standard. [11]

Table.2: *Subgroup 1 – water tightness*

class	Pressure in Pa		Time	Water strance		Observation
	Normal	Actual		Dripping	Flowing	
A1	0	0	15:00	**00:00**	**00:00**	**OK**
A2	50	50	05:00	**00:00**	**00:00**	**OK**
A3	100	100	05:00	**00:00**	**00:00**	**OK**
A4	150	150	05:00	**00:00**	**00:00**	**OK**
A5	200	201	05:00	**00:00**	**00:00**	**OK**
A6	250	250	05:00	**00:00**	**00:00**	**OK**
A7	300	301	05:00	**00:00**	**00:00**	**OK**
A8	450	449	05:00	**00:00**	**00:00**	**OK**
A9	600	601	05:00	**00:00**	**00:44**	**NOT OK**

Table.3: *Subgroup 2 – water tightness*

class	Pressure in Pa		Time	Water strance		Observation
	Normal	Actual		Dripping	Flowing	
A1	0	0	15:00	**00:00**	**00:00**	**OK**
A2	50	50	05:00	**00:00**	**00:00**	**OK**
A3	100	100	05:00	**00:00**	**00:00**	**OK**
A4	150	149	05:00	**00:00**	**00:00**	**OK**
A5	200	201	05:00	**00:00**	**00:00**	**OK**
A6	250	251	05:00	**00:00**	**00:00**	**OK**
A7	300	300	05:00	**00:00**	**01:25**	**NOT OK**

Table.4: *Subgroup 3 – water tightness*

class	Pressure in Pa		Time	Water strance		Observation
	Normal	Actual		Dripping	Flowing	
A1	0	0	15:00	**00:00**	**00:00**	**OK**
A2	50	50	05:00	**00:00**	**00:00**	**OK**
A3	100	100	05:00	**00:00**	**00:00**	**OK**
A4	150	148	05:00	**00:00**	**00:00**	**OK**
A5	200	201	05:00	**00:00**	**00:00**	**OK**
A6	250	251	05:00	**00:00**	**00:00**	**OK**
A7	300	300	05:00	**00:00**	**00:14**	**NOT OK**

Table.5: *Subgroup 4 – water tightness*

class	Pressure in Pa		Time	Water strance		Observation
	Normal	Actual		Dripping	Flowing	
A1	0	0	15:00	**00:00**	**00:00**	**OK**
A2	50	50	05:00	**00:00**	**00:00**	**OK**
A3	100	100	05:00	**00:00**	**00:00**	**OK**
A4	150	149	05:00	**00:00**	**00:00**	**OK**
A5	200	199	05:00	**00:00**	**00:00**	**OK**
A6	250	249	05:00	**00:00**	**00:00**	**OK**
A7	300	301	05:00	**00:00**	**03:13**	**NOT OK**

Table.6: *Subgroup 5 – water tightness*

class	Pressure in Pa		Time	Water strance		Observation
	Normal	Actual		Dripping	Flowing	
A1	0	-9	15:00	**00:00**	**00:00**	**OK**
A2	50	50	05:00	**00:00**	**00:00**	**OK**
A3	100	100	05:00	**00:00**	**00:00**	**OK**
A4	150	150	05:00	**00:00**	**00:00**	**OK**
A5	200	200	05:00	**00:00**	**00:00**	**OK**
A6	250	251	05:00	**00:00**	**00:11**	**NOT OK**

Table.7: *Subgroup 6 – water tightness*

class	Pressure in Pa		Time	Water strance		Observation
	Normal	Actual		Dripping	Flowing	
A1	0	0	15:00	**00:00**	**00:00**	**OK**
A2	50	50	05:00	**00:00**	**00:00**	**OK**
A3	100	100	05:00	**00:00**	**00:00**	**OK**
A4	150	150	05:00	**00:00**	**00:00**	**OK**
A5	200	200	05:00	**00:00**	**00:00**	**OK**
A6	250	251	05:00	**00:00**	**00:00**	**OK**
A7	300	300	05:00	**00:00**	**00:00**	**OK**
A8	450	451	05:00	**00:00**	**00:00**	**OK**
A9	600	600	05:00	**00:00**	**00:00**	**OK**

Table.8: *Subgroup 7 – water tightness*

class	Pressure in Pa		Time	Water strance		Observation
	Normal	Actual		Dripping	Flowing	
A1	0	0	15:00	**00:00**	**00:00**	**OK**
A2	50	50	05:00	**00:00**	**00:00**	**OK**
A3	100	100	05:00	**00:00**	**00:00**	**OK**
A4	150	150	05:00	**00:00**	**00:00**	**OK**
A5	200	201	05:00	**00:00**	**00:00**	**OK**
A6	250	250	05:00	**00:00**	**00:00**	**OK**
A7	300	300	05:00	**00:00**	**00:00**	**OK**
A8	450	451	05:00	**00:00**	**00:17**	**NOT OK**

Table.9: *Subgroup 8 – water tightness*

class	Pressure in Pa		Time	Water strance		Observation
	Normal	Actual		Dripping	Flowing	
A1	0	0	15:00	**00:00**	**00:00**	**OK**
A2	50	50	05:00	**00:00**	**00:00**	**OK**
A3	100	100	05:00	**00:00**	**00:00**	**OK**
A4	150	151	05:00	**00:00**	**00:00**	**OK**
A5	200	200	05:00	**00:00**	**00:00**	**OK**
A6	250	250	05:00	**00:00**	**00:00**	**OK**
A7	300	300	05:00	**00:00**	**00:00**	**OK**
A8	450	450	05:00	**00:00**	**00:00**	**OK**
A9	600	602	05:00	**00:00**	**00:00**	**OK**

Table.10: *Subgroup 9 – water tightness*

class	Pressure in Pa		Time	Water strance		Observation
	Normal	Actual		Dripping	Flowing	
A1	0	0	15:00	**00:00**	**00:00**	**OK**
A2	50	50	05:00	**00:00**	**00:00**	**OK**
A3	100	100	05:00	**00:00**	**00:00**	**OK**
A4	150	152	05:00	**00:00**	**00:00**	**OK**
A5	200	200	05:00	**00:00**	**00:00**	**OK**
A6	250	250	05:00	**00:00**	**00:00**	**OK**
A7	300	302	05:00	**00:00**	**00:00**	**OK**
A8	450	452	05:00	**00:00**	**04:28**	**NOT OK**

Table.11: *Subgroup 10 – water tightness*

class	Pressure in Pa		Time	Water strance		Observation
	Normal	Actual		Dripping	Flowing	
A1	0	0	15:00	**00:00**	**00:00**	**OK**
A2	50	50	05:00	**00:00**	**00:00**	**OK**
A3	100	100	05:00	**00:00**	**00:00**	**OK**
A4	150	150	05:00	**00:00**	**00:00**	**OK**
A5	200	200	05:00	**00:00**	**00:00**	**OK**
A6	250	250	05:00	**00:00**	**00:00**	**OK**
A7	300	299	05:00	**00:00**	**00:00**	**OK**
A8	450	450	05:00	**00:00**	**00:00**	**OK**
A9	600	603	05:00	**00:00**	**00:00**	**OK**

Table.12: *Subgroup 11 – water tightness*

class	Pressure in Pa		Time	Water strance		Observation
	Normal	Actual		Dripping	Flowing	
A1	0	0	15:00	**00:00**	**00:00**	**OK**
A2	50	50	05:00	**00:00**	**00:00**	**OK**
A3	100	100	05:00	**00:00**	**00:00**	**OK**
A4	150	150	05:00	**00:00**	**00:00**	**OK**
A5	200	200	05:00	**00:00**	**00:00**	**OK**
A6	250	250	05:00	**00:00**	**00:00**	**OK**
A7	300	302	05:00	**00:00**	**00:00**	**OK**
A8	450	453	05:00	**00:00**	**04:01**	**NOT OK**

Table.13: *Subgroup 12 – water tightness*

class	Pressure in Pa		Time	Water strance		Observation
	Normal	Actual		Dripping	Flowing	
A1	0	0	15:00	**00:00**	**00:00**	**OK**
A2	50	50	05:00	**00:00**	**00:00**	**OK**
A3	100	100	05:00	**00:00**	**00:00**	**OK**
A4	150	152	05:00	**00:00**	**00:00**	**OK**
A5	200	200	05:00	**00:00**	**00:00**	**OK**
A6	250	250	05:00	**00:00**	**00:00**	**OK**
A7	300	301	05:00	**00:00**	**00:00**	**OK**
A8	450	449	05:00	**00:00**	**00:00**	**OK**
A9	600	602	05:00	**00:00**	**00:00**	**OK**

3.3. Results – resistance to wind load

Class according to the *EN 12211:2016 "Windows and doors - Resistance to wind load - Test method"* standard. [12]

Table.14: *Maximum deflection to the classification at the base width*

Class		f (mm)
(a-c) 1250 mm		
A	(a-c)/150	8.33
B	(a-c)/200	6.25
C	(a-c)/300	4.67

Table.15: *Results of the frontal deflection in mm section/pressure – Subgroup 1*

Pa	1(a)	2(b)	3(c)	f (mm)
2000 Pa	0.64	3.11	0.37	2,60
0 Pa	0.00	0.00	0.00	0.0
-2001 Pa	0.79	2.09	0.50	1.45
0 Pa	0.03	0.02	0.00	0.01

Table.16: *Results of the frontal deflection in mm section/pressure – Subgroup 2*

Pa	1(a)	2(b)	3(c)	f (mm)
2001 Pa	0.46	5.41	0.95	4.71
0 Pa	0.01	0.04	0.01	0.03
-2003 Pa	0.29	5.31	0.76	4.79
0 Pa	0.00	0.01	0.00	0.01

Table.17: *Results of the frontal deflection in mm section/pressure – Subgroup 3*

Pa	1(a)	2(b)	3(c)	f (mm)
1999 Pa	0.50	5.44	0.85	4,77
0 Pa	0.01	0.04	0.01	0.03
-2001 Pa	0.27	5.38	0.72	4,89
0 Pa	0.00	0.01	0.00	0.01

Table.18: *Results of the frontal deflection in mm section/pressure – Subgroup 4*

Pa	1(a)	2(b)	3(c)	f (mm)
2003 Pa	0.59	6.02	0.36	5,54
0 Pa	0.05	0.04	0.04	0.01
-2001 Pa	0.41	6.82	0.49	6,37
0 Pa	0.02	0.00	0.00	0.01

Table.19: *Results of the frontal deflection in mm section/pressure – Subgroup 5*

Pa	1(a)	2(b)	3(c)	f (mm)
2003 Pa	0.54	0.85	0.36	0.40
0 Pa	0.10	0.07	0.05	0.01
-2000 Pa	0.53	0.85	0.50	0.34
0 Pa	0.00	0.00	0.00	0.00

Table.20: *Results of the frontal deflection in mm section/pressure – Subgroup 6*

Pa	1(a)	2(b)	3(c)	f (mm)
2007 Pa	0.58	5.17	0.68	4.54
0 Pa	0.00	0.00	0.00	0.00
-2003 Pa	0.83	5.23	0.93	4.35
0 Pa	0.00	0.00	0.00	0.00

Table.21: *Results of the frontal deflection in mm section/pressure – Subgroup 7*

Pa	1(a)	2(b)	3(c)	f (mm)
2005 Pa	0.51	6.06	0.42	5.60
0 Pa	0.00	0.00	0.00	0.00
-2006 Pa	0.22	4.56	0.21	4.35
0 Pa	0.00	0.00	0.00	0.00

Table.22: *Results of the frontal deflection in mm section/pressure – Subgroup 8*

Pa	1(a)	2(b)	3(c)	f (mm)
2001 Pa	2.54	2.89	0.60	1.29
0 Pa	0.00	0.00	0.00	0.00
-2004 Pa	1.21	1.45	0.37	0.66
0 Pa	0.00	0.00	0.00	0.00

Table.23: *Results of the frontal deflection in mm section/pressure – Subgroup 9*

Pa	1(a)	2(b)	3(c)	f (mm)
2008 Pa	0.34	1.08	0.85	0.49
0 Pa	0.00	0.00	0.00	0.00
-2005 Pa	0.16	0.72	0.45	0.42
0 Pa	0.00	0.00	0.00	0.00

Table.24: *Results of the frontal deflection in mm section/pressure – Subgroup 10*

Pa	1(a)	2(b)	3(c)	f (mm)
2010 Pa	0.68	1.60	0.58	0.97
0 Pa	0.00	0.00	0.00	0.00
-2012 Pa	0.38	0.79	0.41	0.40
0 Pa	0.00	0.00	0.00	0.00

Table.25: *Results of the frontal deflection in mm section/pressure – Subgroup 11*

Pa	1(a)	2(b)	3(c)	f (mm)
2010 Pa	0.56	5.90	0.66	5.29
0 Pa	0.05	0.06	0.04	0.02
-2012 Pa	1.00	4.57	0.96	3.59
0 Pa	0.01	0.00	0.00	0.01

Table.26: *Results of the frontal deflection in mm section/pressure – Subgroup 12*

Pa	1(a)	2(b)	3(c)	f (mm)
2007 Pa	0.23	1.44	0.38	1,14
0 Pa	0.00	0.00	0.00	0.00
-2008 Pa	0.14	0.85	0.35	0.61
0 Pa	0.00	0.00	0.00	0.00

4. Conclusion

From the analyzed results and their comparison of the individual samples, the following can be confirmed:

- The profile used for producing windows has a minimum influence on the air permeability. The examined samples which were made in the same production capacity, were divided into two groups and six subgroups. Each subgroup had six samples. All the samples of one group had the same fittings, but different type of PVC profile. The samples of the subgroups are of same profile, fittings and dimensions. The results given from the windows slightly differed and they circulated in one class of sustainability of the air permeability. The authors, in the form: initials of the first names followed by last name (only the first letter capitalized with full stops after the initials),

. - The profile used for producing windows has significant influence over the water tightness. The examined samples which were made in the same production capacity, were divided into two groups and six subgroups. Each subgroup had six samples. All the samples of one group had the same fittings, but different type of PVC profile. From the analysed samples a greater water tightness is shown at the windows made of the profile with greater dimensions and bigger sagging of the jamb and side jamb.

- The profile used for production of windows has significant influence over the deformities of the window itself. The examined samples which were made in the same production capacity, were divided into two groups and six subgroups. Each subgroup had six samples. All the samples of one group had the same fittings, but different type of PVC profile.The analysis of the results brought conclusion that the windows are made of profile which is strengthened with more steel making it more resistant to deformities when hit by wind load.

5. References

1. S. Vallabhy1, M. Arun Kumar2, V. Bharath2, E. Dhakshina Moorthy2, Hitesh Kumar Jain2 - DESIGN OF UPVC WINDOWS FOR LATERAL WIND LOADS SANDWICH WITH

HURRICANE BARS FOR MULTISTOREY STRUCTURES (2019)
2. www.rehau.com (28-10-2022)
3. www.alphacan.com (28-10-2022)
4. www.aluplast.net/de/index.php (28-10-2022)
5. www.schueco.com/com/ (12-11-2022)
6. www.koemmerling.com (12-11-2022
7. www.gealan.de/en/ (12-11-2022)
8. www.salamander-windows.com/en (14-11-2022)
9. www.trocal.com (14-11-202)
10. EN 1026:2016 “Windows and doors - Air permeability - Test method” standard
11. EN 1027:2016 “Windows and doors - Water tightness - Test method” standard
12. EN 12211:2016 "Windows and doors - Resistance to wind load - Test method" standard

Robust Control With Fuzzy Based Neural Network For Robot Manipulators

Aşkın Mutlu
Faculty of Engineering, Department of Mechanical Engineering, Istanbul University - Cerrahpaşa, Türkiye
askin@iuc.edu.tr

Abstract: *The utilization of robotic systems is prevalent in various industries, such as defence and automotive, and is commonly utilized in industrial settings. The movements of these systems can be controlled through software programming, allowing for the manipulation of objects and modification of trajectory as desired. However, it is important to exercise caution during these operations as improper manipulation may result in undesired outcomes. As a result, the control of robotic systems has become a crucial aspect in modern industry. The parameters of robotic systems are subject to change based on the loads they carry. Robust control is a method that adapts the control system to accommodate these changes in parameters, thereby maintaining stability and performance. This control method allows for the desired level of control to be maintained even in the presence of changing system parameters. In contrast to traditional robust control methods, robust control utilizes variable parameters with a constant upper limit for parameter uncertainty. Control parameters are updated over time using cosine and sine functions, however, determining appropriate values for these parameters can be challenging. To address this issue, a neural network model utilizing fuzzy logic compensator is employed to continuously calculate the appropriate control parameter values. The effectiveness of this proposed control method is demonstrated through graphical representation.*

Keywords: Robot manipulators, neural network control, robust control, fuzzy logic, adaptive control.

1. Introduction

Previous research on the adaptive control for robot manipulators has resulted in the development of parameter estimation laws by Slotine et al. [1] and Sciliano et al. [2]. Building on these works, Spong [3] proposed a robust control law. However, this robust control law [3] is susceptible to chattering and large tracking error when there is uncertainty in the system's parameters. To overcome this, it is essential to determine an appropriate upper uncertainty bound limit.

Burkan and Askin [4] aimed to improve upon the previously proposed robust control method by designing an uncertainty estimation algorithm for the robust controller [3] algorithm based on the Lyapunov theory, thereby ensuring the stability of the uncertain system. The control parameters were then estimated using trigonometric functions such as Cosine and Sine. However, determining the appropriate values for these fixed control parameters is challenging. To overcome this, a fuzzy logic control based compensator was designed and the effects on the robot's tracking errors were investigated.

Fuzzy logic control has been studied extensively by various researchers. Its advantages include the ability to handle uncertainty, time-varying and complex systems, and the ability to incorporate the expertise of system control experts. Furthermore, it can be applied to non-linear and unknown mathematical model systems. Following the work of Zadeh [5] and Mamdani [6], many research groups have undertaken studies in this area. Fuzzy sets have found application examples in a wide range of areas, from control systems to various estimation methods [7]. A fuzzy logic controller can be implemented directly on a system [8] as well as to control its various parameters, with the goal of enhancing the overall performance of the controller [9].

Neural networks have been widely studied and applied in various fields, including control systems. They are particularly useful in applications where the dynamics of the system are complex or unknown, and traditional control methods may not be effective. Neural network controllers (NNC) are designed to approximate the unknown dynamics of the system and provide accurate control actions [10]. In the present study, the coefficients of the robust control system were treated as variables and their optimal values were determined through the utilization of a neural network trained using a fuzzy logic-based algorithm.

2. Control Strategy

The dynamic model of an n-joint manipulator, in the absence of friction or other disturbance effects, can be represented mathematically as [3].

$$\begin{aligned} &\mathrm{M}(\theta)\ddot{\theta}+\mathrm{C}(\theta,\dot{\theta})\dot{\theta}+\mathrm{G}(\theta)=\tau \\ &\mathrm{Y}(\theta,\dot{\theta},\ddot{\theta})\pi=\tau \end{aligned} \tag{2.1}$$

The dynamic model of the n-joint manipulator in the absence of friction or other disturbance effects can be represented by a constant p-dimensional vector of robot parameters (π), generalized coordinates (θ), an n-dimensional vector of applied torques or forces (τ), an nxn symmetric positive definite inertia matrix (M), an n-dimensional vector of centripetal and coriolis terms $\mathrm{C}(\theta,\dot{\theta})\dot{\theta}$, and an n-dimensional vector of gravitational terms (G(θ)). The control parameters are defined as

$$\tilde{\theta}=\theta-\theta_d\,;\dot{\theta}_{\mathrm{r}}=\dot{\theta}_{\mathrm{d}}-\Lambda\tilde{\theta}\,;\sigma=\dot{\theta}-\dot{\theta}_{\mathrm{r}}=\dot{\tilde{\theta}}+\Lambda\tilde{\theta} \tag{2.2}$$

The control law, based on the control parameters defined in equation (2.2), is presented in reference [4].

$$\begin{aligned} \tau &= \tau_0+\mathrm{Y}(\theta,\dot{\theta},\dot{\theta}_{\mathrm{r}},\ddot{\theta}_{\mathrm{r}})(\mathrm{u}_1+\mathrm{u}_2) \\ &= \mathrm{Y}(\theta,\dot{\theta},\dot{\theta}_{\mathrm{r}},\ddot{\theta}_{\mathrm{r}})(\pi_0+\mathrm{u}_1+\mathrm{u}_2)-\mathrm{K}\sigma \end{aligned} \tag{2.3}$$

where u_2 and u_1 are supplementary control inputs that are implemented to enhance the robustness of the system against parametric uncertainty, allowing for improved stability and performance of the control system in the face of changes in the system's parameters.

$$\begin{aligned} &\mathrm{M}(\theta)\dot{\sigma}+\mathrm{C}(\theta,\dot{\theta})\sigma+\mathrm{K}\sigma \\ &=\mathrm{Y}(\theta,\dot{\theta},\dot{\theta}_{\mathrm{r}},\ddot{\theta}_{\mathrm{r}})(\pi_0-\pi)+\mathrm{u}_1+\mathrm{u}_2)+\mathrm{K}\sigma \\ &=\mathrm{Y}(\theta,\dot{\theta},\dot{\theta}_{\mathrm{r}},\ddot{\theta}_{\mathrm{r}})(\tilde{\pi}+\mathrm{u}_1+\mathrm{u}_2)+\mathrm{K}\sigma \end{aligned} \tag{2.4}$$

The function $(\beta^2/\alpha)\cos(\int\alpha Y^T\sigma dt)\sin(\int\alpha Y^T\sigma dt)$ is employed as a parameter estimation law. In order to derive the control law, a Lyapunov function candidate is defined as follows

$$V = \frac{1}{2}\sigma^T M(\theta)\sigma + \frac{1}{2}\tilde{\theta}^T B\tilde{\theta} + \frac{1}{2}\hat{\pi}^T \Phi^2 \hat{\pi}\ ;\ V \geq 0 \qquad (2.5)$$

where $B \in R^{nxn}$ is a positive diagonal matrix of size nxn, Φ is chosen as a pxp dimensional diagonal matrix that varies over time.

The time derivative of V along the system (2.5) is

$$\dot{V} = \sigma^T M(\theta)\dot{\sigma} + \sigma^T \frac{1}{2}\dot{M}(\theta)\sigma + \tilde{\theta}^T B\dot{\tilde{\theta}} \qquad (2.6)$$
$$+\hat{\pi}^T \Phi^2 \dot{\hat{\pi}} + \hat{\pi}^T \Phi\dot{\Phi}\hat{\pi}$$

As a result, the time derivative of the Lyapunov function is written as.

$$\dot{V} = -\dot{\tilde{\theta}}^T K\dot{\tilde{\theta}} - \tilde{\theta}^T \Lambda^T K\Lambda\tilde{\theta} + \sigma^T Y(u_1 + u_2) \qquad (2.7)$$
$$+\sigma^T Y\tilde{\pi} + \sigma^T Y\hat{\pi}$$

Control parameters are defined in Equation (2.6)

$$\dot{V} = -\dot{\tilde{\theta}}^T K\dot{\tilde{\theta}} - \tilde{\theta}^T \Lambda^T K\Lambda\tilde{\theta} + \sigma^T Yu(t)_2 + \sigma^T Y\tilde{\pi} \qquad (2.8)$$

The rest of the proof is given in [3].

The fuzzy logic controller implemented in this study has two inputs (e_1, e_2) and two outputs (α,β). The inputs to the controller are the orbital tracking error values for the first and second manipulator (e_1, e_2), whereas the outputs are the torque values to be applied to the joints. These torque values are used to calculate the values of the controller's parameters, α ([0.5;1.5]) and β ([1;15]) These parameters are then used to adjust the system's dynamics and achieve the desired control performance.

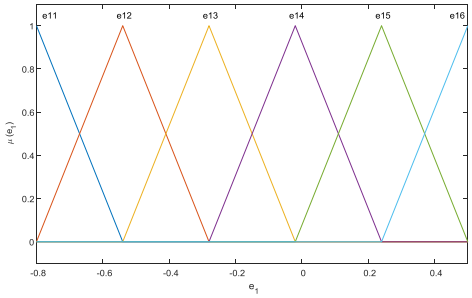

Figure 2.1 *Membership function for tracking error of first manipulator (Input value e_1 : [-0.8 ; 0.5])*

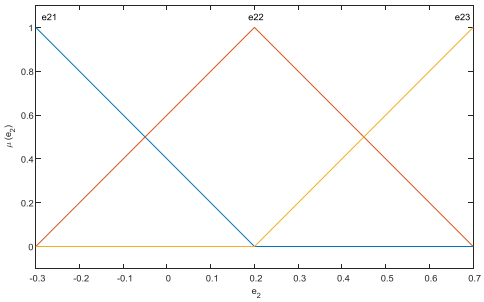

Figure 2.2 *Membership function for tracking error of second manipulator (Input values e_2 : [-0.3 ; 0.7])*

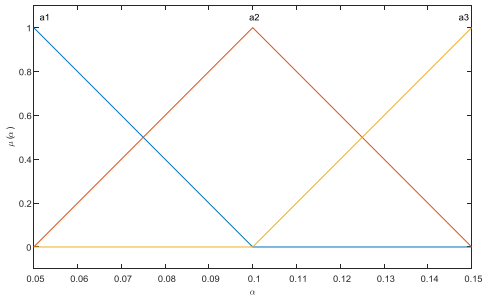

Figure 2.3 *Membership function of α:*

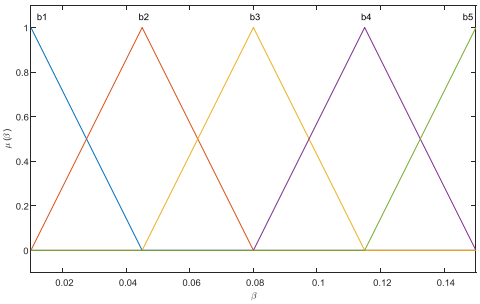

Figure 2.4 *Membership function of β*

Table 1*: Rule table for fuzzy logic*

e2 \ e1 (α / β)	e11	e11	e13	e14	e15	e16
e21	α1 / β5	α3 / β5	α2 / β2	α2 / β5	α2 / β5	α2 / β5
e22	α2 / β4	α2 / β4	α3 / β3	α3 / β5	α1 / β4	α3 / β4
e23	α3 / β3	α1 / β1	α1 / β4	α1 / β5	α3 / β3	α3 / β1

Using (If ... and ... Then ...) structure of the rule table is created.

In this study, a defuzzification method known as Centroid was employed to convert the fuzzy output of the fuzzy logic controller into a crisp value. The values of the controller's parameters, α and β, were then obtained and added to the system to improve its control performance and reduce the error found by the fuzzy logic controller.

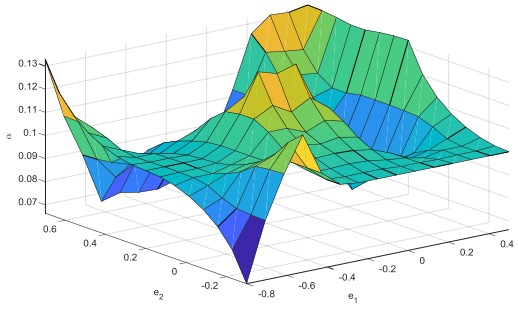

Figure 2.5 *Fuzzy Surface Model α(e_1,e_2)*

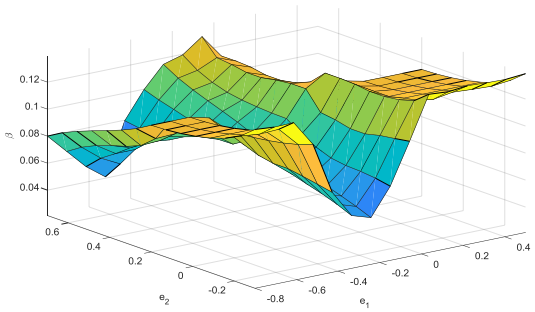

Figure 2.6 *Fuzzy Surface Model $\beta(e_1,e_2)$*

3. Neural Network Control

The efficacy of traditional control methodologies is dependent upon the veracity of the dynamic model of the system. However, the attainment of a precise mathematical model for complex systems with multiple variables, such as robotic manipulators, is often a challenging task. As a result, model-based control approaches may be inadequate in achieving the desired control performance and precision. To address this issue, a model-free intelligent controller based on fuzzy set theory, specifically fuzzy logic control, is proposed as a solution. The fuzzy logic controller employs appropriate linguistic fuzzy rules, derived from an operator's control experience and a database, for decision-making processes. These rules simulate human cognition through the application of fuzzy logic and fuzzy set operations.

Despite the advantages of fuzzy logic control, it presents inherent difficulties in implementation. Specifically, the definition of membership functions for linguistic variables exhibits a high degree of autonomy, and determining appropriate functions through trial and error can be laborious. Additionally, finding appropriate fuzzy logic control rules can also prove difficult. As an alternative, a neural network control strategy is proposed, as it possesses the ability to learn and adapt to the system's characteristics.

This study utilizes a multilayer feedforward neural network as the primary architecture due to its widespread use and versatility in various applications. The backpropagation learning algorithm is employed to adjust the weighting of the network, allowing it to learn and adapt in a manner similar to the neural networks of the human brain. The multilayer feedforward neural network consists of multiple processing elements connected through weighted data connections. The strength of these connections is determined by the weighting values. The activation value of each processing element is calculated by summing the input signals, each multiplied by their corresponding weighting values as described in reference [10].

$$net_j^k = \sum W_{ji}^k O_i^{k-1} \tag{3.1}$$

$$O_j^k = f\left(net_j^k\right) \tag{3.2}$$

where net_j^k is net input function, W_{ji}^k is the weighting, O_i^{k-1} is the output, and $f(*)$ activation function.

The training of the neural network utilizes the backpropagation algorithm, which adjusts the weight values in the network based on the discrepancy between the actual output and the desired output. The performance of the network is measured by an objective function, defined as the error between the actual output and the desired output. The objective of the training process is to minimize this error through adjustments of the weight values, thereby enabling the network to adapt to and learn the characteristics of the system. The object function defined as

$$E = \frac{1}{2}\sum_j \left(\theta_{dj} - O_j\right)^2 \tag{3.3}$$

The utilization of the steepest descent optimization method for the modification of the weighting values in the neural network, with the aim of minimizing the objective function, allows for the determination of the correction value for the weighting. It can be obtained

$$\Delta W_{ji}^k = \mu \delta_j^k O_i^{k-1} \tag{3.4}$$

$$\delta_j^k = -\frac{\partial E}{\partial net_j^k} \tag{3.5}$$

where μ is learning rate parameter, so

$$\delta_j^k = f\left(net_j^k\right)\sum_l \delta_l^{k+l} O_{lj}^{k+l}$$

The activation functions used for the neural network are a linear function, $f(x) = x$, for the output layer and a sigmoid function for the hidden layer. The linear function is chosen for the output layer as it allows for direct computation of the output, while the sigmoid function is used for the hidden layer as it allows for non-linearity and differentiability, which are important properties in neural networks.

$$f(x) = \frac{1}{(1+e^{-\mu x})} \tag{3.6}$$

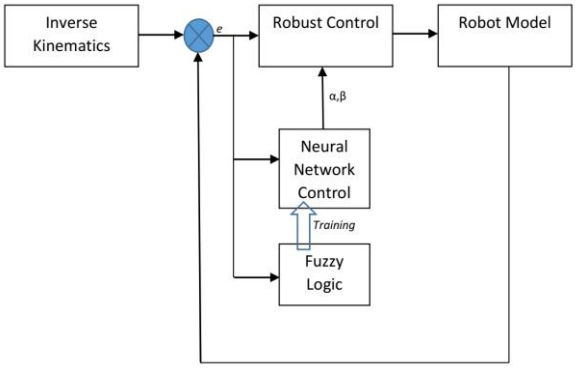

Figure 3.1 *Block diagram of the proposed neural network based on fuzzy-robust controller.*

In this study, as shown in Figure 3.1, alpha and beta parameters of the robust controller were determined by a neural network controller trained with fuzzy logic.

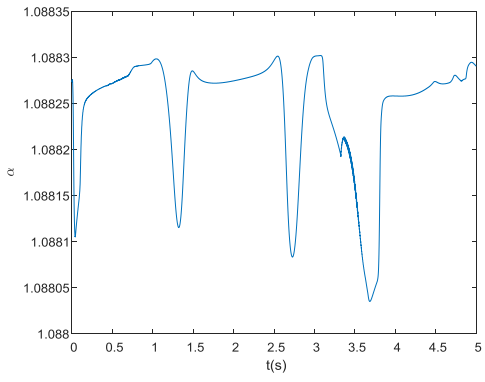

Figure 3.2 *Changing α parameter with time*

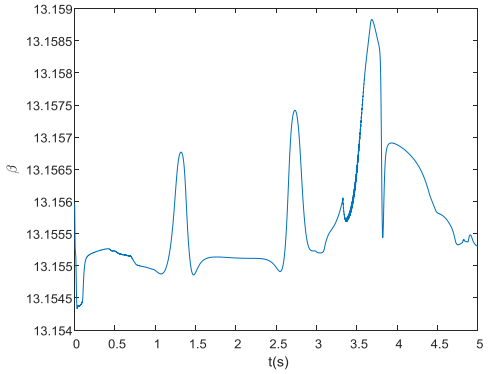

Figure 3.3 *Changing β parameter with time*

4. Simulation Results

To evaluate the effectiveness of the proposed control law, it was applied to a two-linked manipulator system. The performance of the controller was analyzed by monitoring the system's response to various inputs and evaluating the control performance metrics.

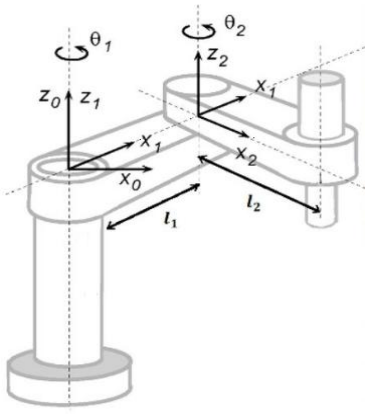

Figure 4.1 *Two-Link Robot Arm [3,4].*

Robot parameters are given as follows.

$$\begin{aligned}
\pi_1 &= m_1 l_{c1}^{\ 2} + m_2 l_1^{\ 2} + I_1 \\
\pi_2 &= m_2 l_{c2}^{\ 2} + I_2 \\
\pi_3 &= m_2 l_1 l_{c2} \\
\pi_4 &= m_1 l_{c1} \\
\pi_5 &= m_2 l_1 \\
\pi_6 &= m_2 l_{c2}
\end{aligned} \tag{4.1}$$

$$\mathrm{M}(\theta) = \begin{bmatrix} \pi_1 + \pi_2 + 2\pi_3 \cos(\theta_2) & \pi_2 + \pi_3 \cos(\theta_2) \\ \pi_2 + \pi_3 \cos(\theta_2) & \pi_2 \end{bmatrix} \tag{4.2}$$

$$\mathrm{C}(\theta, \dot{\theta}) = \begin{bmatrix} -\pi_3 \sin(\theta_2)\dot{\theta}_2 & -\pi_3 \sin(\theta_2)(\dot{\theta}_1 + \dot{\theta}_2) \\ \pi_3 \sin(\theta_2)\dot{\theta}_1 & 0 \end{bmatrix} \tag{4.3}$$

$$\mathrm{G} = \begin{bmatrix} \mathrm{g}(\pi_4 + \pi_5)\cos(\theta_1) + \mathrm{g}\pi_6 \cos(\theta_1 + \theta_2) \\ \mathrm{g}\pi_6 \cos(\theta_1 + \theta_2) \end{bmatrix} \tag{4.4}$$

To simulate the proposed control law, a specific trajectory was chosen for each joint of the two-linked manipulator system. The trajectory used in the simulation was 0.5cos (0.5πt)-0.5.

The simulation was performed under the same conditions and using the same trajectory for both the proposed control law and a comparison method. The results of the simulation are presented in Figures 4.2-4.3, which compare the performance of the proposed control law with the comparison method.

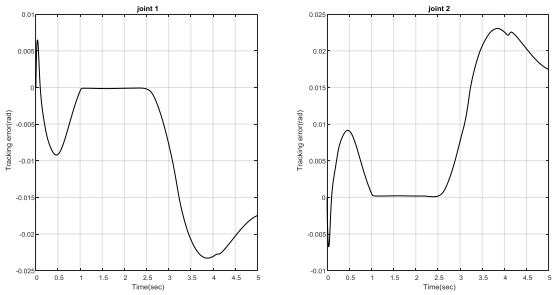

Figure 4.2 Tracking error for robust controller [3]

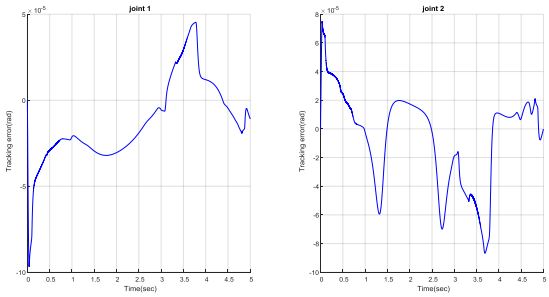

Figure 4.3 *Tracking errors for robust control with fuzzy based neural network*

As depicted in Figure 4.3, the proposed control law utilizing a neural network controller, was able to effectively reduce the tracking error of the two-linked manipulator system. The neural network controller, through the use of α and β, adapts the system's dynamics in real-time by updating the values of α and β as the simulation progresses. This results in the selection of the most appropriate values of α and β, leading to a reduction in the tracking error of the system.

As a result of the proposed control law, a very small tracking error was obtained for the two-linked manipulator system. The performance of the proposed controller was compared with a known robust controller, and the results are presented in Figure 4.4. As can be seen from the figure, the proposed controller provides superior performance when compared to the known robust controller. The results show that the proposed controller is able to achieve a much smaller tracking error compared to the known robust controller.

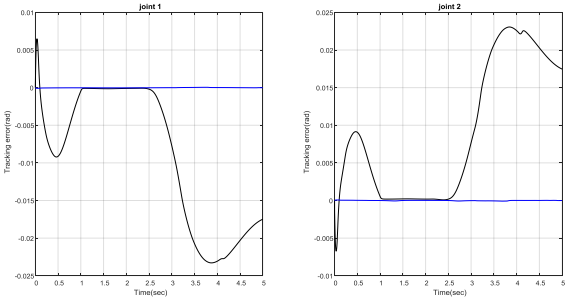

Figure 4.4 *Comparison of orbital tracking errors*

4. Conclusion

Computer simulations were conducted using the same model and trajectory. The effect of control parameters, α and β, on control performance were evaluated by keeping the values of K and constant while varying α and β. The results, depicted in figures 4.2 and 4.3, indicate that the tracking error of the robust control is substantial. In contrast, the proposed adaptive control algorithm effectively reduces the tracking error. It was observed that α and β values have a significant impact on tracking error, however, these values are fixed, making it difficult to select optimal values. Furthermore, the tracking error may not always be improved with these fixed values of α and β. Therefore, the proposed control algorithm was developed to enhance the control law. As depicted in the figures, the tracking error is significantly reduced through the implementation of the neural network controller.

5. References

1. SLOTINE, J.J., LI, W., 1987, On the adaptive control of robotic manipulator, The International Journal of Robotics Research, 6 (3), 49-59.

2. SCIAVICCO, L., SICILIANO, B., 1996, Modeling and Control of Robot Manipulators, The McGraw-Hill Companies, Great Britain,1-85233-221-2.

3. SPONG,M.W., 1992, On the robust control of robot manipulators, IEEE Transactions on Automatic Control, 37 (11), 1782-1786.

4. MUTLU A., BURKAN R., 2017, Fuzzy-Robust Control Of a Two-Link Robot Arm, International Journal for Science, Technics and Innovations for the Industry. 5, 214-217.

5. ZADEH, L.A., 1965, Fuzzy sets, Information and control, 8, 338-353.

6. MAMDANI, E.H., 1974, Application of fuzzy algorithms for control of simple dynamic plant, IEEE Proc., 121 (12), 1585-1588.

7. ZOR, C., ÇEBİ, F., 2018, Demand prediction in health sector using fuzzy grey forecasting, Journal of Enterprise in Information Management, 31 (6), 937-949.

8. ARIK, A.E., BİLGİÇ, B., 2023, Fuzzy control of a landing gear system with oleo-pneumatic shock absorber to reduce aircraft vibrations by landing impacts, Aircraft Engineering and Aerospace Technology, 95 (2), 284-291.

9. BURKAN, R., MUTLU, A., 2021, Robust control of robot manipulators with an adaptive fuzzy unmodelled parameter estimation law, Robotica, 40 (7), 2365-2380.

10. HUANG, S.J., HU, C.F., 1996, Neural Network Controller for Robotic Motion Control, Int J Adv Manuf Technol, 12, 450-454.

Comparison of Energy Savings Measures in Plant Fruit Storage Facility

Giorgio Mustafaraj[1] Irida Markja, Klodian Dhoska
[1]Politecnic University of Tirana, Tirana, Albania

Abstract: *This research will analyse the utilization of photovoltaic plant in a fruit storage facility to produce electricity for running the refrigerators to keep cool the fruit preservation in the Storage Facility. The building has two sets of refrigerators with a power of 18.2 kW each. Firstly, the work analysis deals with the convenience of installing a Photovoltaic Plant to produce electricity for supplying the refrigerators. Secondly, implementing energy efficiency measures such as adding a new layer of insulation to the walls has been analysed. Result analysis shows that the return of investment by the installation of Photovoltaic plant is less convenient compared to that of a thermal insulation layer on the interior sites. In conclusion, it has been decided to implement only thermal insulation as energy efficiency measures to this facility where the saving is about 15% of electricity consumption per year. Given that the saving in one year is 3069kWh and the cost of electricity is 0.09 EUR/kWh, the savings in monetary value is 276 EUR /year.*
Keywords: *PHOTOVOLTAIC PLANT, ENERGY SAVINGS MEASURES, REFRIGERATOR, THERMAL INSULATION*

1. Introduction

In Albania, final energy consumption in building sector is equal to 30% percent of national consumption and the sector was responsible for the use of 60% of electricity, as part of final energy consumption. The service quality of electricity equipment is much lower than the European Union average [1].

Albania is a part of the Energy Community Treaty, so it is obliged to adopt EU legislation on energy efficiency. In April 2015, the country transposed Directive 2006/32 / EC on Energy Efficiency in End Users and Energy Services and Directive (ESD) 2010/30 / EU on Energy Product Labels (Former Directive 92/75 / EEC). In line with ESD, in 2018, the country should achieve energy saving targets of up to 9% of the total amount of energy sold, compared to 2010. According to the ESD, Albania should save 1.5% of the amount of energy each year sold compared to the period of the last three years, using the mandatory scheme for enterprises, or other alternative routes. Achieving these goals requires more ambitious policy and investment efforts than ever before for energy efficiency [2-4].

The main objective of this research work is the comparison of energy savings measures in plant fruit storage facility in the city of Korca (Albania). The project deals with the analysis of different energy efficient measurements and ends with the selection of most suitable one such as the implementation of thermal insulation.

2. General Description of Fruit Storage Building and Electricity Consumption Analysis

2.1 Architecture and Cooling Plant

The Fruit Storage building is located in the city of Korca (see Fig. 2.1). The building has the total area of A = 150 m^2. Building is composed only with one floor with the height of about 6 meter. The facility is mainly used for conserving apples.

Figure 2.1 *Fruit Storage Building in Korce*

From the analysis made on the building, its architecture is composed with sheet metal cladding and a layer of thermal insulation in the middle. The building uses only electricity for running the cooling system and other electrical equipment such as lighting. Figure 2.2 presents the cooling system, and this plant is composed by two refrigerators with a power of 18.2kW each.

Figure 2.2 *Cooling Plant*

2.1 Electricity Consumption

The graphs in Figure 2.3 presents historical data on electricity consumption for each month for the years 2018 and 2019.

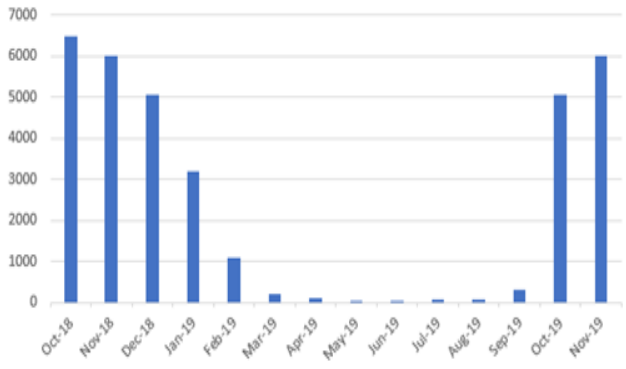

Months	Consumptions (kWh
Oct-18	6497
Nov-18	6013
Dec-18	5057
Jan-19	3185
Feb-19	1090
Mar-19	190
Apr-19	113
May-19	10
Jun-19	48
Jul-19	55
Aug-19	62
Sep-19	289
Oct-19	5057
Nov-19	6013

Figure 2.3 *Electricity Consumption [kWh /month]*

3. Implementation of Energy Efficiency Measures

3.1 Implementation of Photovoltaic Panels for Electricity Generation

The area that could be installed the photovoltaic panel is 300m^2. From the technical sheet is given an average electricity production of 3kW per 30m^2 panel surface. As a result for an area of 300m^2 it can be generated 30kW of electricity.

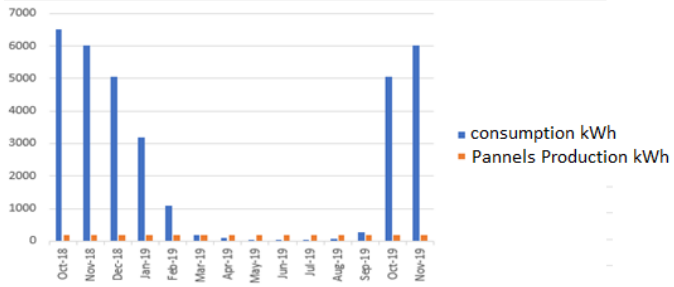

Figure 3.1 *Electricity produced versus that consumed on monthly based*

Figure 3.1 presents the electricity produced by the photovoltaic plant versus that consumed monthly for one year. From Fig 3.1 it can be shown that the photovoltaic panels can satisfy the electricity required by the facility from March to September. Throughout the remaining months, electricity produced by photovoltaic plants is about only 5% of the required energy consumed.

3.2 Calculation of Thermal Transmission Coefficient and Total Refrigeration Load

3.2.1 Existing Building

To analyze the thermal conductivities of the walls a software has been utilized called Design Builder [5]. Figure 3.2 presents external wall structure of the existing building. The wall is composed by three layers such as: sheet metal with 100mm layer, thermal insulation with 40mm thickness and 13mm aluminum layer. It has been calculated that, the value of the equivalent is transmission coefficient K = 0.760 [W/m^2 -K], while the total refrigeration load is Et = 52.39 kW. It has to be noted by the result analysis shows that the effect of the roof and floor on heat transfer is negligible compared to that of the roof and the floor.

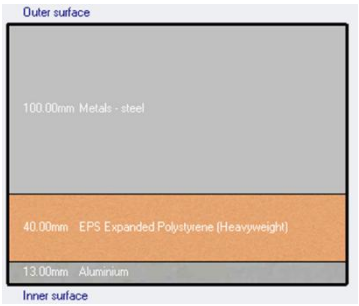

Figure 3.2 *Exterior wall structure layers [5]*

3.2.2 Improved Building

To further reduce the heat losses from the walls another insulation layer has been added such as improve the properties of the building in thermal with a thickness of 40mm. Figure 3.3 shows the improved wall composed by four layers. Results analysis from the software gives an equivalent heat transfer coefficient of 0.232 [kW/m^2 - K], which is smaller to that compared to the existing building. Finally, total cooling load is Etm = 48 kW.

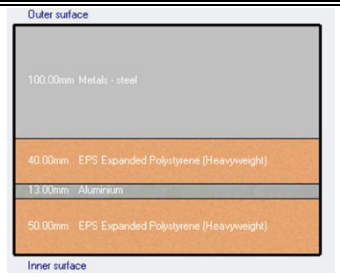

Figure 3.3 *Exterior wall structure - Improved building [5]*

3.2.3 Summary Results

Figure 3.4 presents a comparison between implementation of electricity generated by photovoltaic plant versus that by adding an insulation layer. Result analysis shows that implementation of Photovoltaic plant is less convenient compared to that by adding an insulation layer. Electricity savings is about 15% from 141.36 [kWh/m^2 year] to 122.58 [kWh/m^2 year]. Finally, the total electricity consumed: E = 18100 kWh/year. The saving in one year is 3069kWh/year. Given that the cost of electricity is 0.09 EUR/kWh, the savings in monetary value is: 3069kWh/year * 0.09EUR/kWh = 276EUR/year.

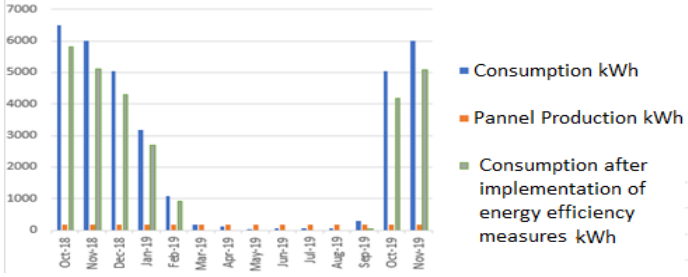

Figure 3.4 *Summary results*

4. Conclusions

In this work research the facility is analyzed to identify what is the most suitable energy efficiency measures to applied. The aim of this work research is the comparison of energy savings measures in plant fruit storage facility in the city of Korca (Albania).

The existing building has an electricity consumption of 141.36 [kWh / m^2 year]. Energy efficiency measures includes addition of a thermal insulation layer and photovoltaic plants. Results analysis is conducted by utilizing an energy software [5]. Results analysis shows that adding thermal insulation layer is much more suitable compared to that of photovoltaic plant. In conclusion, after implementing thermal insulation layer the saving of about 15% of electricity consumption per year. On yearly basis the saving 3069kWh and taking into account the cost of electricity 0.09 EUR/ kWh, the savings in monetary value is 276 EUR / year.

Finally, the methodology used in this research work can be used to analyze energy saving opportunities to other types of buildings.

References

[1] Energy data 2020 edition - European Commission.

[2] Cansino, J.M., Román-Collado, R. & Nassar, S. The clean development mechanism in Eastern Europe: an in-depth exploration. Environ Science and Pollution Research 29, 74797–74822 (2022). https://doi.org/10.1007/s11356-022-20988-3.

[3] EU (2018) Energy performance of buildings directive. Revised in 2018, the directive will help reach the building and renovation goals set out in the European Green Deal.

[4] EN 15232-1:2017. Energy Performance of Buildings - Energy performance of buildings - Part 1: Impact of Building Automation, Controls and Building Management.

[5] DesignBuilder version v7.0.2.006. Last accessed February 2023 www.designbuildersoftware.com

Analysis of Different Energy Efficiency Technologies Based on Cost and Return of Investment

Giorgio Mustafaraj[1] Irida Markja, Klodian Dhoska
[1]Politecnic University of Tirana, Tirana, Albania

Abstract: *Application of different retrofitting technologies can play a significant role in reducing energy consumption of existing buildings. This research work analyses a building in Cork (Ireland) where underfloor heating system, and natural ventilation are used to maintain comfort conditions. Underfloor heating system is the main electricity consumer of this building. Different energy efficient technologies were implemented and analyzed in terms of reducing electricity consumption through an energy software. These technologies include replacing illumination with high efficiency light; replacement of electric motos with high efficiency; introducing underfloor heating time scheduling turning on and off based on predicted weather condition; installation of presence sensors to switch ON/OFF lighting. Finally, it was decided to implement underfloor heating time scheduling as energy efficient technology to be analyzed because of limited budget available and high return on investments provided by applying this method. Result analysis shows that electricity saving on bills was about 20% on monthly basis compared to previous consumption.*
Keywords: *ENERGY EFFICIENCY, BUILDING RETROFITTING, UNDERFLOOR HEATING SYSTEM*

1. Introduction

To reduce the pollution, in recent years were developed advanced technologies to cut down energy consumption. In European Union (EU) building consume for around 38% of overall electricity. The EU built the Energy Efficiency Directive (EED) in year 2012 which then was further improved throughout the coming years. The aim of EED is to encourage the EU countries to reduce energy consumption of buildings by developing new advanced technologies [1].

The main objective of energy retrofit is to enhance energy efficiency of building by improving for example building properties such as envelope and/or heating ventilation and air conditioning (HVAC) systems. Retrofitting existing building is necessary because HVAC plants and other properties deteriorate with time, and an improvement of these properties reduces energy consumption.

Griffith et. al. [2] analysed different retrofitting technologies for energy savings opportunities. They consider both cost of investment of applying different retrofit technologies and the obtained energy savings. Results analysis showed around 40% energy savings. Chidiaca et al [3] used different retrofit methods on nine different office buildings. They analysed the result related to energy savings and return on investment for different weather condition. Mills et. al. [4], demonstrated that by retrofitting different buildings produced an reduction of energy consumption by 16%. Aste and Pero [5] performed a research analysis in developing a retrofit approach. The procedure is based on an iterative process that allows selecting the most suitable energy retrofit technology for a particular building. Result analysis, shown a reduction of energy consumption by 40%.

The aim of this research work is: firstly, analyzing different energy retrofit technologies through an energy software called Design Builder [7], and secondly selecting the most appropriate such as underfloor heating time scheduling in terms of limited available budget.

Finally, the outline of this research work includes: Section II presents an overview of the building architecture and heating ventilation and air conditioning (HVAC) plants, Section III describes results analysis on different energy retrofit technologies, and Section IV provides conclusions.

2. Overview of the Building Architecture and HVAC Plants

The building under examination is part of University College of Cork in Ireland. Is a three floor that contains offices and labs with a total area of 4500 m^2 . The floors are reinforced concrete structure which presents a high thermal mass. A general overview of the building is presented in Figure 1.

Fig. 1 *General overview of building model [6,7]*

Figure 2 gives the Heating Ventilation and Air Conditioning (HVAC) plant that is present in the building. The majorities of the areas in the building (around 80% of the entire building areas) are supplied by natural ventilation and underfloor heating. The remaining zones of the building that includes toilets, stores and clean rooms are supplied by five Air Handling Units (AHUs). Water to water heat pump system is used to heat up the water up to 35oC, while a further increment of the temperature up to 38oC is obtained by the heat exchanger that on the other side is flowing water coming from the boiler. The water is then passed through underfloor heating system. Finally, for more detail information about the architectural and system plants refer to Mustafaraj et. al. [6].

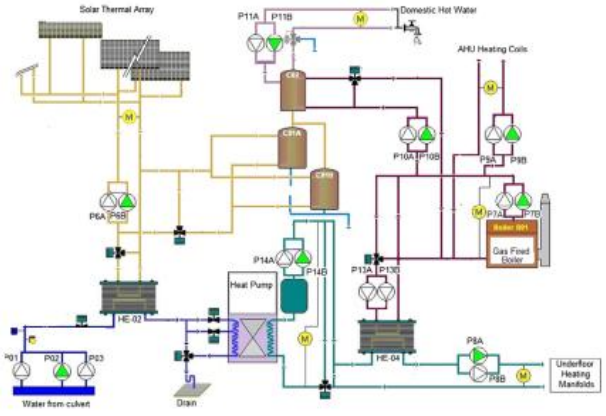

Fig. 2 *Overview of HVAC plant [6]*

3. Analysis of Results

Past researchers such as Mustafaraj et al. [6] completed model calibration. Present research work implemented a certain number of energy retrofit technologies. The energy retrofit technologies includes replacement with high efficiency lighting & occupancy sensors, substituting old motors with high efficiency motors, installation of variable speed drivers on water pump and high efficiency air conditioning systems. Three energy retrofit technologies were identified. The total cost savings were calculated based on the average cost electricity in Ireland that was fixed at 0.18 €/kWhr.

Table 1 summarizes the energy retrofit recommendation obtained. Replacement of lighting and motors with more efficient alternatives, could provide potential cost savings of €3881 but would include an implementation cost of €2736.

Table 4 *Energy Retrofit Technologies: Summary of Savings and Costs.*

Description of Energy Retrofit Technologies	Potential Savings (€/yr)	Implementation Cost (€)	Simple Payback Period (yrs)	Energy Savings (kWhr/yr)	Demand Reduction (kW)
Process Improvements					
1. Time schedule Heat Pump Modification	290	0	Immediate	5050	0
2. Replacement with High Efficiency Lighting	1858	1146	0.6	10327	0.241
3. Replacement with High Efficiency Motors	2023	1590	0.6	11240	1.757

Result analysis from Table 1 shows by applying ‘’Time schedule heat pump modification’’ the initial cost of investments is almost negligible, and the payback period is immediate. Because of limited budget available, this energy retrofit technology was chosen to be analyzed in more detail compared to the others through the present research. Before the heat pump was turned “ON” and “OFF” manually by a technician. Based on its experience and on weather forecast the time that the heat pump was kept “ON” varied between 6 and 12 hours. Present research work discovered that is required less time that varied between 4 to 8 hours to keep “ON” the heat pump. This was done automatically based on the real thermal behavior of the building. Figure 3 present a comparison between model simulation and manual real measurements for monthly electricity usage. Result analysis shows that electricity consumption was reduced between 20% and 27% monthly.

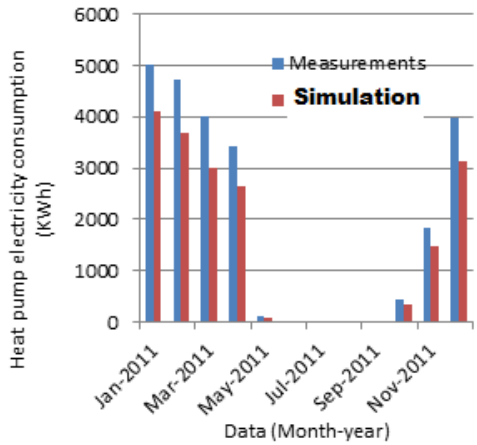

Fig. 3 *Monthly comparison of electricity consumption between manual (Measurement) and automatic control (Simulation by the software [7]) of the heat pump*

Finally, total electricity savings were calculated to be 5050 kWh/year (i.e. corresponding to a total savings of 290€/year). The payback period is immediate because there is no cost on investment for implementing this energy retrofit technology.

4. Conclusions

In this research work, three different types of energy retrofit technologies were investigated. Firstly, the time schedule of the heat pump was modified based on real thermal behavior of the building where the potential energy saving was calculated to be 5050 kWhr/yr with a potential cost savings of €290. Secondly, the proposed replacement of standard lighting with high efficiency lighting incorporating luminosity sensors would deliver a potential of €1858 which includes a simple payback period of 6 months. In this scenario, the cost of implementation was calculated to be €1146. Thirdly, the replace of standard motors with high efficiency motors was estimated to result in potential cost savings of €2023. In present work ‘’Time schedule heat pump modification’’ was chosen to be analyzed in more detail and implemented practically because limited badged and immediate payback. Finally, result analysis shows that electricity consumption by implementing ‘’Time scheduling heat pump’’ was reduced between 20% and 27% monthly.

References

[1] EU Energy Efficiency Directive (2012/27/EU).
[2] B. Griffith, N. Long, P. Torcellini, R. Judkoff. Assessment of the Technical Potential for Achieving Net Zero-Energy Buildings in the Commercial Sector[R].Technical Report NREL/TP-550–41957, 2007.
[3] S.E. Chidiaca, E.J.C. Catania, E. Morofskyb, S. Foob, A screening methodology for implementing cost effective energy retrofit measures in Canadian office buildings,Energy and Buildings 43 (2011) p614–620.
[4] E. Mills, Building commissioning: a golden opportunity for reducing energy costs and greenhouse gas emissions, Technical Report, Lawrence Berkeley National Laboratory, 2009.
[5] N. Aste, C. D. Pero. Energy retrofit Commercial Buildings: Case Study and Applied Methodology. Energy Efficiency 6, pp. 407-423, 2013.
[6] G. Mustafaraj, D. Marini, A. Costa and M. Keane, “Model Calibration for Building Energy Efficiency Simulation,” Applied Energy, vol. 130, pp. 72-85, 2014.
[7] DesignBuilder-www.designbuildersoftware.com.

Simulation of toolpaths and program verification of a CNC lathe machine tool

Violeta Krcheva[1], Marija Chekerovska[1], Sara Srebrenkoska[1]
[1]Faculty of Mechanical Engineering
'Goce Delcev' University - Stip, Republic of North Macedonia
violeta.krceva@ugd.edu.mk, marija.cekerovska@ugd.edu.mk, sara.srebrenkoska@ugd.edu.mk

Abstract: *This paper presents the simulation and verification of programs created for the CNC Hitachi Seiki Seicos LIII lathe machine tool. The main purpose of program simulation and verification is to ensure the quality and accuracy of the cutting process, which can significantly improve production efficiency. In addition to defining the toolpath, simulation can perform linear and circular interpolation according to specific programs based on G - codes. Therefore, all the motions of the moving parts of the real lathe machine tool can be clearly visualized. The use of simulation is a good solution not only to precise the toolpath, but also verify the program and detect any possible collision between cutting tools and mobile components, before loading the program into the lathe machine tool and starting cutting processes.*
Keywords*: MANUFACTURING, MACHINING, PROGRAMMING, CODES, SOFTWARE*

1. Introduction

Constant monitoring and control over the dimensions, dimensional tolerances, and surface finish of the designed parts during the manufacturing process provides increased process efficiency and product durability.

Therefore, Computer Numerical Controlled (CNC) machine tools have been widely implemented in the manufacturing industry in the last few years for the reason that their reliability is greater than that of conventional manufacturing machine tools. In order to machine the part in a drawing by using CNC machine tools, it is necessary to generate a series of instructions for activating those CNC machine tools. This task is called CNC programming [1].

CNC programming is a term that refers to the methods for generating the instructions that drive the CNC machine tool [2]. A series of instructions to be performed by the CNC machine tool compose a program of instructions. It consists of G – codes, also known as geometric codes, that control the motion of the machine tool. The standard format for a G – code command begins with "G" and is followed by a two – digit number. These common G – code instructions provide the geometric position of the moving parts of the machine tool, which is generally determined by a coordinate system, as an instrument for identifying the location of the moving parts, moving them in a particular direction, and indicating their precise position in 3D space. This programming language also includes M – codes that control the CNC machine tool or its functions (such as spindle rotation speed, cutting tool feed, cutting tool change, coolant, etc.). M – codes are also written in alphanumeric format, beginning with "M" and two digits following.

G – code, in the act of being a programming language, leads to particular programs of instructions generated by Computer – Aided Manufacturing (CAM) systems that use Computer – Aided Design (CAD) information. These innovative manufacturing systems are used to both design and manufacture products, and they significantly improve the design and productivity of manufacturing processes.

CAD refers to the implementation of computer technology for design and design documentation. On the other side, CAM software programs are used for generating tool paths and verifying program correctness.

The purpose of CAM software programs is to design products and arrange manufacturing processes, particularly CNC machining. Extremely complex parts in large quantities, requiring complex machining processes, are produced on CNC machine tools. Most frequently, final parts and prototypes are machined using CAD/CAM software programs. As a consequence, before being applied to an actual CNC machine tool, these complex manufacturing processes need to be thoroughly verified. For that reason, one of the most well-known, practical, and helpful CAM software programs is the Computer Numeric Control (CNC) Simulator.

The CNC Simulator is an application designed to predict the behavior, performance, and outcome of certain manufacturing processes based on simulation - driven design that has been defined by Sellgren [10] as: "a design process where decisions related to the behaviour and the performance of the design in all major phases of the process are significantly supported by computer – based product modelling and simulation".

Simulation in manufacturing refers to a broad collection of computer based applications to imitate the behavior of manufacturing systems [2]. Numerous simulation software programs have been developed to graphically verify the program of instructions prior to running the part on the machine tool with an actual workpiece. Because of the complexity of generating the program of instruction, simulation software was developed to identify programming errors prior to actual part production. Additionally, it is much easier to edit the program of instruction at this stage of development [3].

The information input to the program regarding the toolpath, tool, material, and parameters specific to each are linked to the geometry. This means that if any of the parameters for the parts mentioned above are changed, the other related data can be regenerated to take these changes into account without recreating the entire operation [4].

2. Research

This research illustrates a simulation of part of the clutch hub manufacturing process. It refers to a machining chip removal process that can be performed on a CNC Hitachi Seiki Seicos LIII lathe machine tool.

Machining is one of the most important manufacturing processes. Machining is a manufacturing process in which a sharp cutting tool is used to cut away material to leave the desired part shape. The predominant cutting action in machining involves shear deformation of the work material to form a chip; as the chip is removed, a new surface is exposed. Machining is most frequently applied to shape metals [8].

Machining with chip removal includes methods in which the design of workpieces is achieved by removing excess of materials [9].

Machining is not just one process; it is a group of processes. There are many kinds of machining operations, each of which is capable of generating a certain part geometry and surface texture The common feature is the use of a cutting tool to form a chip that is removed from the workpart. [8].

In this research, the required machining operations to machine the clutch hub on the mentioned CNC lathe machine tool are

discussed. These are: turning, boring, drilling, facing, and chamfering.

In the turning process, the cutting tool is set at a certain depth of cut (mm) and travels to the left with a certain velocity as the workpiece rotates. The feed, or feed rate, is the distance the tool travels horizontally per unit revolution of the workpiece (mm/rev). This movement of the tool produces a chip, which moves up the face of the tool [12].

Turning, boring and drilling generate cylindrical or more complex surfaces of rotation. Facing, also carried out on a lathe, generates a flat surface, normal to the axis of rotation, by feeding the tool from the surface towards the center or outward from the center. [11]

In order to analyze the cutting operations, accurate 2D drawings have been created using a CAD system, i.e., AutoCAD software, for the starting and final workpieces. The starting workpiece is a forged clutch hub (Fig. 1b), and the final part is the machined clutch hub (Fig. 1a).

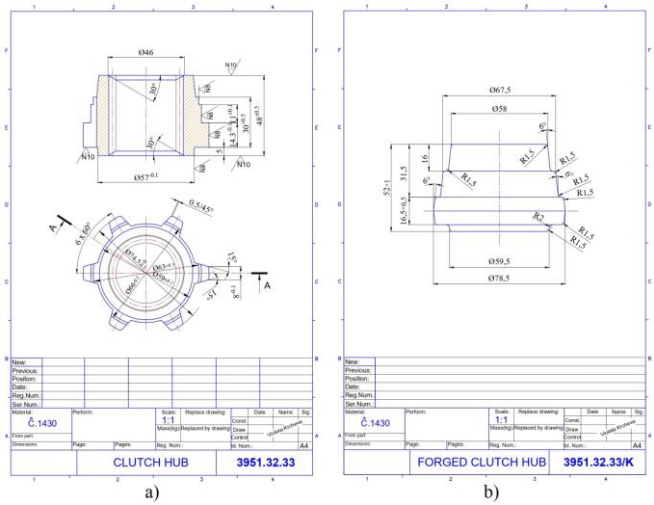

Fig. 1 *(a) Clutch hub, (b) Forged clutch hub*

To precisely define the metal cutting processes performed on this CNC lathe, these drawings are converted into simple 2D models. In that way, the kind of metal cutting operation and final geometry of the part in every phase of the manufacturing process can be clearly explained. Depending on which side of the clutch hub is machined, two phases are determined.

The first phase refers to the shorter side of the forged clutch hub and is defined by four passes.

The first pass (Fig. 2a) is drilling, and the chosen cutting tool is a straight - flute drill DS20 - D3400DM40 – 04 (Fig. 2b) that uses indexable inserts, produced by SANDVIK Coromant.

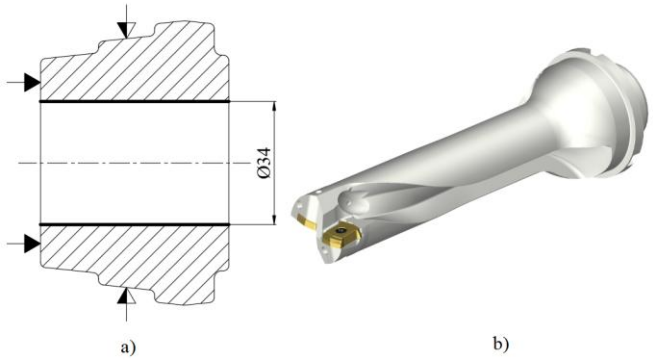

Fig. 2 *(a) First pass, (b) Straight - flute drill that uses indexable inserts*

The second pass (Fig. 3a) is defined by two cutting operations: turning and facing. The chosen cutting tool is a combination of the PCLNR 2525M 12 shank tool (Fig. 3b) and the CNMG 12 04 08-PM 4325 indexable insert (Fig. 3c), both produced by SANDVIK Coromant.

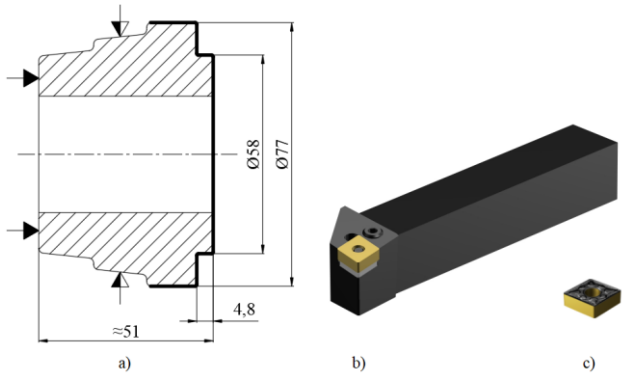

Fig. 3 *(a) Second pass, (b) Shank tool, and (c) Indexable insert*

The third pass (Fig. 4a) is defined by two cutting operations: turning and facing. The chosen cutting tool is a combination of the DDHNL 2525M 15 shank tool (Fig. 4c) and the DNMG 15 06 08-KF 3225 indexable insert (Fig. 4b), both produced by SANDVIK Coromant.

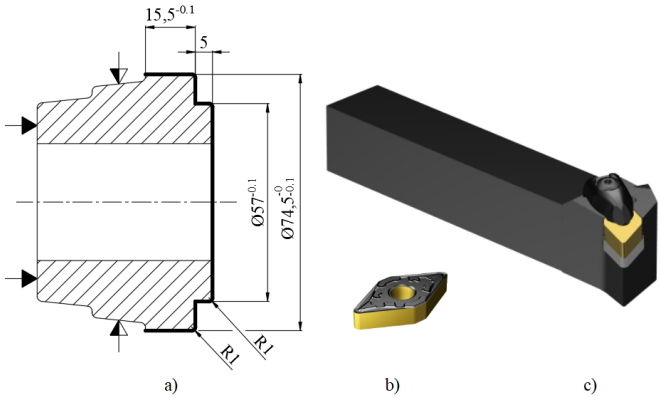

Fig. 4 *(a) Third pass, (b) Indexable insert, and (c) Shank tool*

And the fourth pass (Fig. 5a) is defined just by one cutting operation: chamfering. The chosen cutting tool is a combination of the S25T-PTFNR16 16-W shank tool (Fig. 5b) and the TNMX 16 04 08-WF 1515 indexable insert (Fig. 5c), both produced by SANDVIK Coromant.

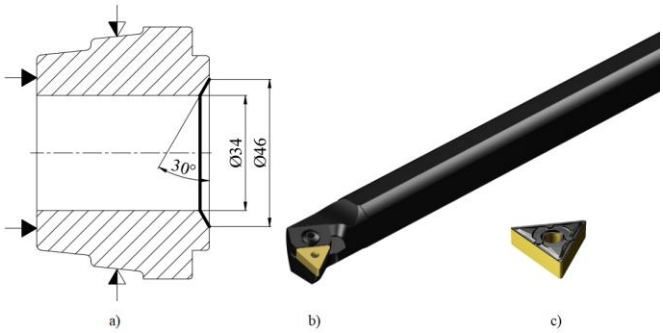

Fig. 5 *(a) Fourth pass, (b) Shank tool, and (c) Indexable insert*

The second phase refers to the longer side of the forged clutch hub and is defined by three passes.

The first pass (Fig. 6a) is defined by two cutting operations: turning and facing, and the chosen cutting tool is the same as in the second pass in the previous phase (Fig. 3b, Fig. 3c).

The second pass (Fig. 6b) is defined by two cutting operations: turning and facing, and the chosen cutting tool is the same as in the third pass in the previous phase (Fig. 4b, Fig. 4c).

And the third pass (Fig. 6c) is defined by two cutting operations: chamfering and boring, and the chosen cutting tool is the same as in the fourth pass in the previous phase (Fig. 5b, Fig. 5c).

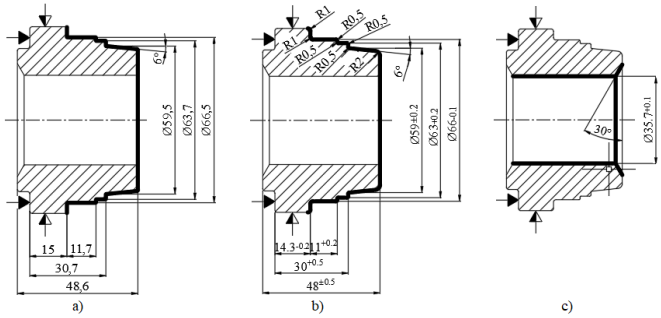

Fig. 6 *(a) First pass, (b) Second pass, and (c) Third pass*

Additionally, for each cutting operation, a program of instructions is created. In that way, two programs of instructions are created, and each one is simulated and verified by the CIMCO Edit v6.1 software program.

3. Results and discussion

Considering the created programs of instructions, in the CIMCO Edit v6.1 software program, the toolpath of the chosen cutting tool is visualized for each of the passes, for every cutting operation. Each block of the program of instructions is provided in a clear manner in accordance with a certain pass (or the complete phase).

The following pictures present a simulation of the toolpath corresponding to the program of instructions created for the mentioned passes and phases, testing and verifying it in the process of design and development.

A linear interpolation movement on the cutting tool using the Z-axis as the direction of movement completes the first pass in the first phase (Fig. 7).

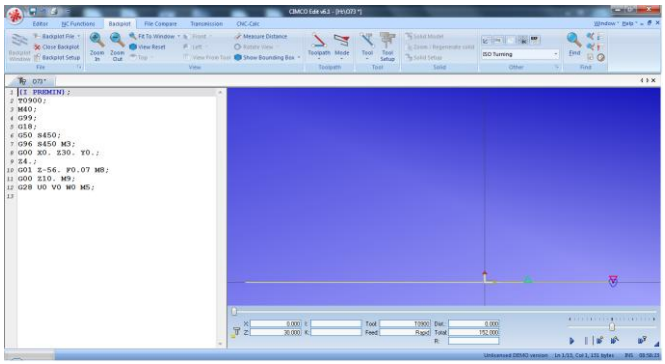

Fig. 7 *Simulation of the first pass*

The cutting tool is moved linearly and circularly interpolatively along the X and Z axes to finish the second pass in the first phase (Fig. 8).

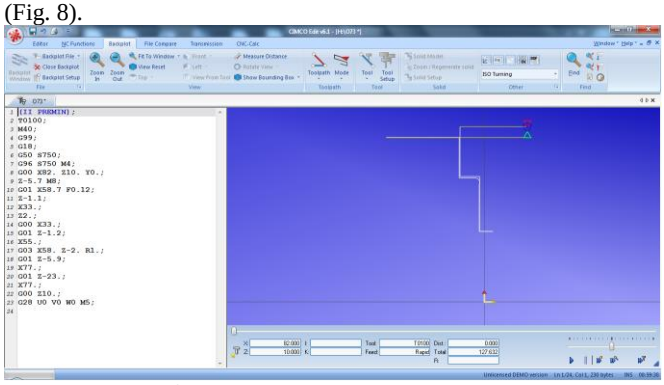

Fig. 8 *Simulation of the second pass*

Linear and circular interpolation motions on the cutting tool oriented on the X and Z axes complete the third pass in the first phase (Fig. 9).

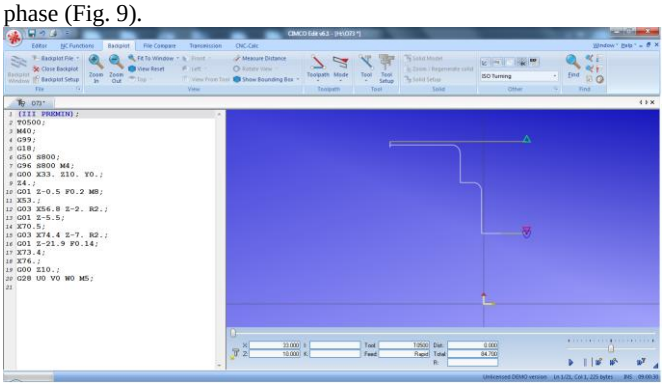

Fig. 9 *Simulation of the third pass*

The fourth pass in the first phase is finished with linear movements of the cutting tool pointed in the X and Z axes (Fig. 10).

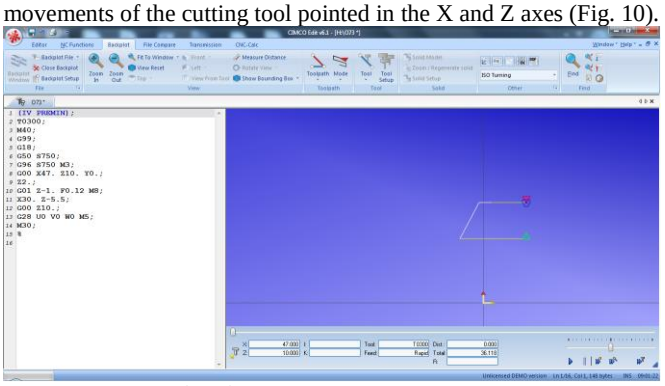

Fig. 10 *Simulation of the fourth pass*

Completing the four passes results in the realization of the first phase (Fig. 11).

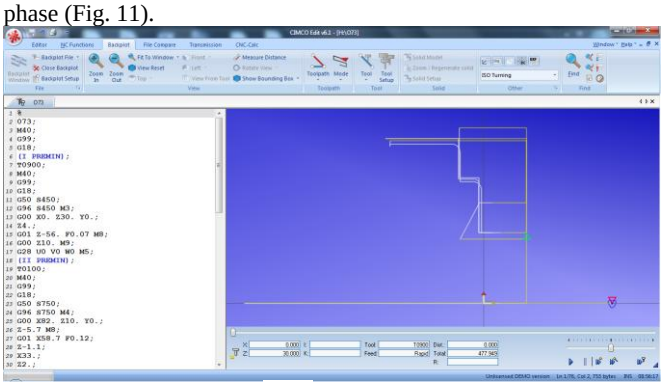

Fig. 11 *Simulation of the first phase*

To complete the first pass in the second phase, the cutting tool is moved along the X and Z axes in a linear and circular interpolative motion (Fig. 12).

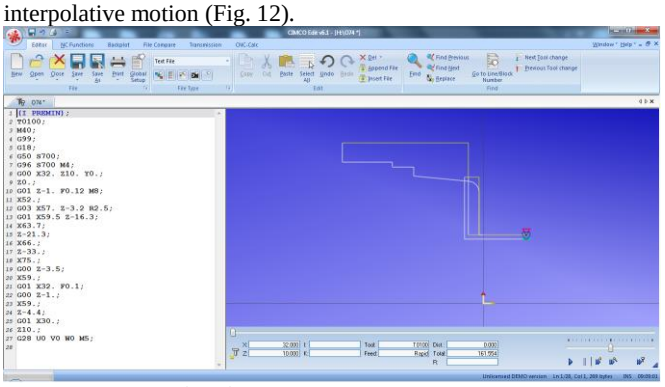

Fig. 12 *Simulation of the first pass*

The second pass in the second phase is finished with linear and circular interpolation motions on the cutting tool oriented on the X and Z axes (Fig. 13).

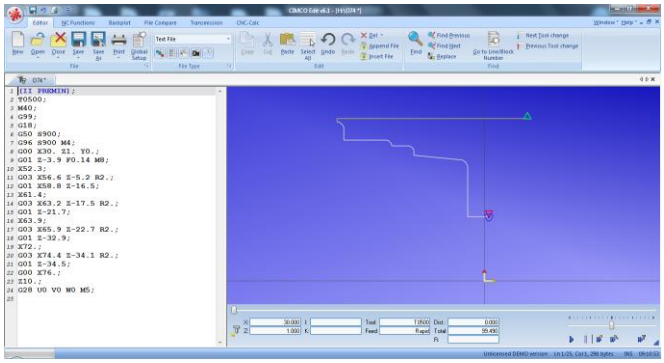

Fig. 13 *Simulation of the second pass*

The cutting tool is moved in a linear interpolative motion along the X and Z axes to finish the third pass in the second phase (Fig. 14).

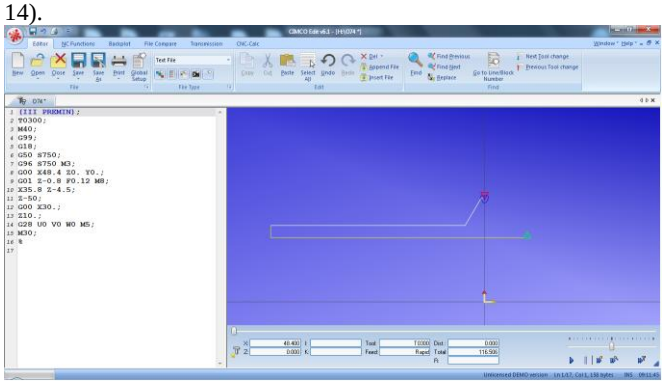

Fig. 14 *Simulation of the third pass*

The realization of the second phase follows the completion of the three passes (Fig. 15).

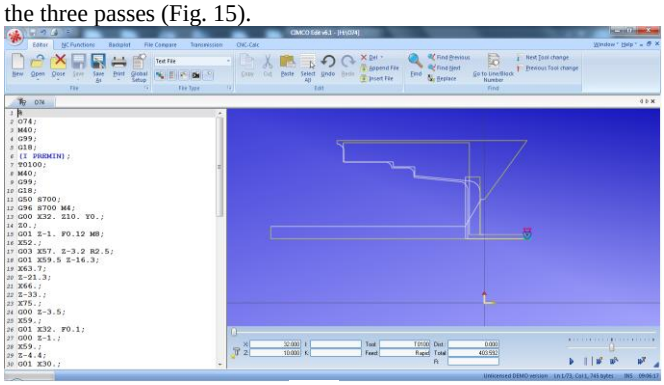

Fig. 15 *Simulation of the second phase*

4. Conclusion

In order to develop parts from design to end product with acceptable accuracy, compatibility, machinability, and processability on a CNC machine tool, certain steps must be followed. According to the reliable manufacturing method, the target workpiece is first constructed using particular design software. Then, a specific program of instructions based on G-code is created.

After receiving the program of instructions in the CIMCO Edit v6.1 software program, simulations of the toolpath are generated. Actually, the program of instructions is tested and visualized in the interest of its verification before being applied to the CNC lathe machine tool. Through simulation and verification of the program of instructions, every possible collision is predicted, detected, and eliminated.

The benefit of current and future usage and development of this type of software is that they can rapidly examine various manufacturing strategies without causing any disturbance, damage, or waste. In addition, they are convenient for continuous analysis of the manufacturing processes in order to optimize machining operations, reducing cost and time while raising quality and conserving materials.

5. References

[1] S. Suh, S. Kang, D. Chung, I. Stroud, *Theory and Design of CNC Systems* (Springer - Verlag, London, 2008), pp.278

[2] P. Radhakrishnan, S. Subramanyan, V. Raju, *CAD/CAM/CIM*, 3th ed., (New Age International Publishers, New Delhi, 2008), pp. 403

[3] D. E. Kandray, *Programmable Automation Technologies: An Introduction to CNC, Robotics ans PLCs* (Industrial Press, United States of America, 2010), pp.120

[4] K. Evans, *Programming of CNC Machines*, 4th ed., (Industrial Press, United States of America, 2016), pp. 311

[5] P.R.Nair, H. Khokhawat, R.G. Chittawadigi, Int. Con. Ro. S. Ma. 133, 823-830 (2018)

[6] S. Zivanovic, N. Slavkovic, Z. Dimic, G. Vasilic, R. Puzovic, D. Milutinovic, 6th ICMEN, 41-51 (2017)

[7] L. N. B. Misman, (2017). Application Of Cnc Simulator For CNC Machining Via CAD/CAM [dissertation], 35.

[8] M. P. Groover, *Fundamentals of Modern Manufacturing: Materials, Processes, and Systems*, 4th ed., (John Wiley & Sons, United States of America, 2010), pp.483-485

[9] G. Globocki Lakić, D. Kramar, J. Kopač, *Metal Cutting: Theory and Applications* (University of Ljubljana, Ljubljana, 2014), pp. 6

[10] U. Sellgren, *Simulation-driven design: motives, means, and opportunities*, [Doctoral thesis], 1999

[11] E. Trent, P. Wright, *Metal Cutting*, 4th ed., (Butterworth–Heinemann, United States of America, 2000), pp. 32

[12] S. Kalpakjian, S. R. Schmid, *Manufacturing Engineering and Technology*, 6th ed., (Prentice Hall, United States of America, 2009), pp.575

[13] D. M. Yip-Hoi, 120th ASSE Ann. Co. Expo. 6201, 23.1336-1 – 15 (2013)

[14] H. Yau, J. Chen, B. Yu, T. Yang, Int. Con. Sim. Mod. Methodol., 717-724 (2014)

[15] S. Zivanovic, N. Slavkovic, B. Kokotovic, D. Milutinovic, Int. J. Eng, 1854, 189 – 194 (2017).

Conceptual design and 3D modeling of a microfluidic device for liver cells investigation

Tihomir Tjankov[1], Dimitar Trifonov[1]
Institute of Mechanics, Bulgarian Academy of Sciences, Acad. G. Bonchev str., bl. 4, 1113, Sofia, Bulgaria[1]
tihomir@imbm.bas.bg

Abstract: *The cell engineering is one of the most developing fields during the last decade needing specially fabricated polymer microfluidic devices and systems. One of the main functionalities of the microfluidic devices is to mimic the in-vivo environment where the cells and tissue live. The various types in-vitro microfluidic devices and systems could replace the experiments with animals in the biomedical investigations. The aim of this publication is 3D modeling and simulation of a microfluidic device for liver cells investigation. Suitable materials could be used with main properties related with fully transparency and bio-compatibility of the selected polymers. A new technology for development of the microfluidic device will be proposed, incorporating a thin layer of liver cells for investigation of their behavior during treatment with different substances. The conceptual work principle of the developed bio-chip will be presented. The future investigations, related to the fabrication of a real physical prototype and research experiments will be mentioned briefly in conclusions.*
Keywords*: CELL ENGINEERING, POLYMER MICROFLUIDIC DEVICES, 3D CAD MODELING, LIVER CELL INVESTIGATIONS*

1. Introduction

The liver is one of the most complicated organs in the human body. The main "building blocks" of the liver are the lobules. Each liver lobule consists of several hexagonal microscopic structures where the liver cells are radially located around the central vein. In the periphery of each lobule, up to 6 portal triads are located at the apex of the hexagons. The triads consists from a portal vein, hepatic artery and bile duct. There are vascular sinusoids connecting the central vein of each lobule with the portal vein and hepatic artery. The sinusoids are surrounded by the main liver cells - hepatocytes (HPs). The liver sinusoid's wall is mainly composed by three cell types (liver sinusoidal endothelial cells (LSECs), Kupffer cells (KCs), and hepatic stellate cells (HSCs)). The LSECs are perforated by small fenestrae therefore the gap between the liver sinusoid and the HPs (Disse space) is easily filled up with blood. The direct exposure of HPs to the blood stream increases the surface for transportation between HPs and blood flow. This process facilitates various liver functions as resorption and release of nutrients, and detoxication [1, 2].

Microfluidics handles and analyzes fluids at the submillimeter scales. Microfluidic technology enables the implementation of advanced platforms (such as micro-total-analysis systems [3], lab-on-a-chip [4], lab-on-a-disc [5], organ-on-a-chip (OOC) [6], or body-on-a-chip (BOC) [7]) for research in life sciences. Some of the significant advantages of microfluidic devices, particularly for biological research, are direct screening, better control of the fluid flow, low consumption of reagents, mimicking the *in vivo* cellular microenvironment and low sample requirement [8].

In the last few years, the organ-on-a-chip became one of the most important and emerging technologies emulating human organs and especially the human liver. Organ-on-a-chip systems are microfluidic devices, used to culture live cells in microfluidic chambers with continuous flow conditions mimicking the physiological function of tissues and organs *in-vivo*. The microfluidic devices from the type organ-on-a-chip are used mainly for evaluating the safety and efficacy of different drugs *in-vitro*. Because of the size of the microfluidic devices they could be used for modeling and simulation of extremely fine and complex main components of the tissues (liver sinusoids), rather than creating a complete liver tissues. Liver chips have been used in different format for better cultivation of HPs [9]. Various geometries and dimensions of the cell and tissue culture chamber have been developed where oxygen and nutrition gradients were fine tuned. The creation of a successful liver microfluidic device is related with a lot of important parameters that could be taken into account. (medium flow, mass transfer of nutrients and metabolites, purification, sufficient supply of oxygen, mechanical forces as shear stress) [9].

A conceptual design and 3D modeling of a liver microfluidic device have been proposed in this publication. In fact, a microfluidic device with two microchannels have been modeled, mimicking the liver sinusoid and Disse space (the most important part of the liver which is in direct contact with the HPs). A 3D model of the liver chip has been created using a suitable CAD software. New geometry of the liver chip has been presented for better culturing and investigation of HPs. Appropriate pressures driving the laminar flow into the microchanels have been applied and as a result, the wall shear stress have been obtained. A suitable fabrication technology has been described regarding the concept design of the liver chip. The working principle of the new microfluidic device has been presented comparing the advantages and disadvantages with the developed already organ-on-a-chip liver devices.

2. Conceptual Design

The direct contact of the hepatocytes with the blood, circulating in the liver, is realized through a Disse space. A huge amount of blood penetrates via the fenestrea of the LSECs, in the liver sinusoids. The microfluidic device, presented in the current publication, represents an *in-vitro* 3D model of Disse space and the liver vascular sinusoid. The liver chip consists from one microfluidic channel, separated in two identical parallel microchannels with a polymer perforated membrane (the diameter size of the microholes is up to 400 nm). The dimensions of each one of the microchannels are 0.1 (height) / 1 (width) / 15 (length) mm. The thickness of the polymer membrane is 0.01 mm and the diameter size of the microholes is up to 0.4 μm. The HPCs under investigation could be cultured at the bottom side of the lower microchannel.

The KCs and LSECs (from liver sinusoids) could be cultured over the polymer perforated membrane. The HSCs will be cultured on the lower surface of the membrane. Various chemical substances and/or drugs could be injected into the microfluidic device - a laminar fluid flow. The region where the HPCs will be cultured is in the middle of the channel as a circular shape. On this way more liver cells could be investigated at once (fig. 1). The feeding of the microfluidic liver chip with four types of cells is realized by the protocol from [1].

3. 3D Modeling and Simulation of a liver sinusoid microfluidic device

Two main types (type 1 and type 2) [1, 10] of microfluidic devices for liver cells investigation are analysed. A standard organ-on-a-chip device consists from 2 microfluidic channels separated by a perforated membrane. The geometry of the microchannels and the membrane, as well as the fabrication materials are extremely important during the design of the liver microfluidic devices. Both commercially available liver on-a-chips from [1, 10] are modeled using Solid Works (fig. 1, fig. 2).

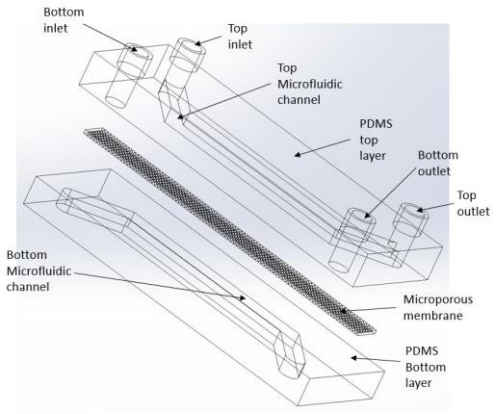

Fig. 1 *3D modeling of the liver-on-a-chip device (type 1). The device consists from 3 main parts – 2 parts with identical straight micro-channels and a polymer perforated (microporous) membrane.*

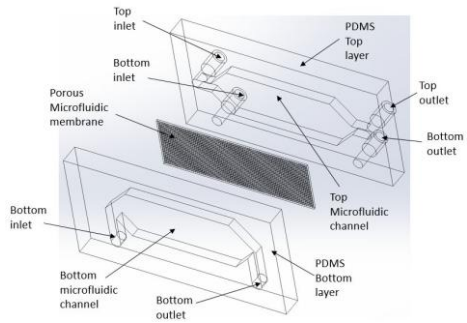

Fig. 2 *3D modeling of the liver-on-a-chip device (type2). The device consists from 3 main parts – 2 parts with micro-channels extended in the middle (complex shape) and a polymer perforated (microporous) membrane.*

Regarding models' features, it is proposed a new design of a microfluidic device for HPCs analysis. It consists from one channel separated in two identical parallel microchannels. The height, length and width of each one of the microchannels are 0.1 mm, 15 mm and 1 mm, respectively. In the middle, the shape of the microchannels is a circle with a diameter size equal to 5 mm. Both microchannels are separated from a perforated membrane with a thickness from 0.01 mm. The micro-holes of the membrane are 400 nm in diameter (fig. 3).

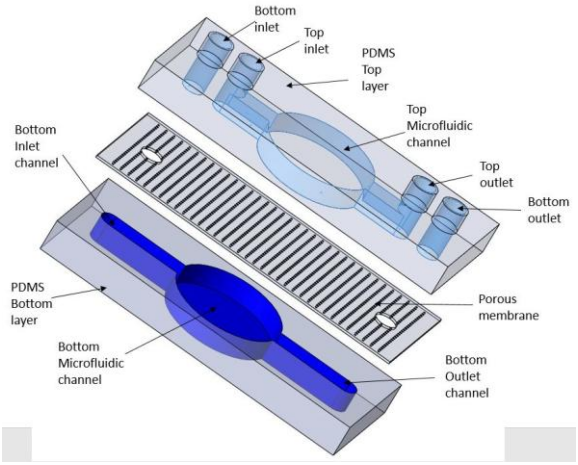

Fig. 3 *3D modeling of a liver-on-a-chip (new design). The device consists from 3 main parts – 2 parts with identical micro-channels (extended in the middle as a circle shape) and a polymer perforated membrane.*

All three microfluidic structures, before analyzed, are simulated with a computational fluid dynamics (CFD) software.

The STL files, created with SolidWorks have been imported in Flow 3D (CFD software). A suitable mesh has been created for simulation. The fluid used for CFD is water at 37ºC. A Newtonian fluid has been defined, calculating the Reynolds number using this equation:

$$Re = \frac{\rho u D_H}{\mu} \quad (1)$$

where

ρ - density fo the fluid (kg/m^3)

u - mean velocity of the fluid (m/s)

μ - dynamic viscosity of the fluid (Pa.s = N.s/m^2=kg/(m.s))

D_H - hydraulic diameter of the pipe (In our case the cross-section of the microchannel is a rectange. Therefore, $D_H = \frac{4A}{P}$, where - A - cross-sectional area of the microchannel (m^2); P - wetted perimeter of the microchannel (m)

For all simulated microfluidic devices, the velocity (input parameter) is equal to 0.24 mm/s. The main goal is to obtain the shear stress into the microchannel, simulating the liver sinusoid (upper channel).

The shearing is a deformation process that may impact the structure of the LSECs situated at the top surface of the perforated membrane. For a Newtonian fluid (laminar flow), the shear stress (τ) is directly proportional to the shear rate (γ) which in turn is proportional to the fluid velocity gradient (dv/dy) [11]. The LSECs which are located close to the lower plate (membrane) are exposed to the maximum shear stress (fig. 4).

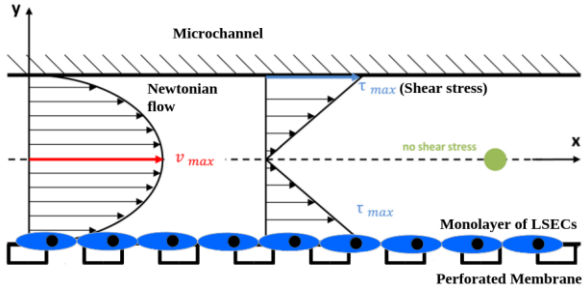

Fig. 4 *Illustration of velocity profile and shear stress for a Newtonian liquid in a channel between two plates (plate and a perforated membrane – simulated as a solid wall). The shear stress of all 3 types of microfluidic devices are identical.*

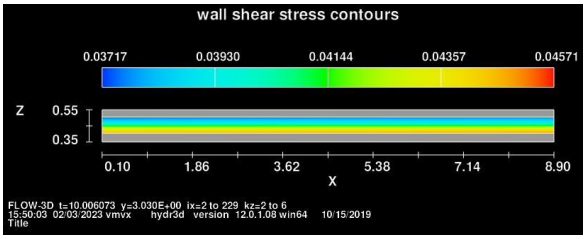

Fig. 5 *Simulation results the microfluidic device – type 1; The wall shear stress (straight microchannel) is up to 0.022 dyn. The pressure along the microchannel is approximately 1014 mbar.*

The shear stress of all 3 types of microfluidic devices are identical. The obtained results could be seen on figures 5, 6, 7, respectively. Therefore all of them could be used successfully for investigation of HPCs situated in the proximity of the liver sinusoid.

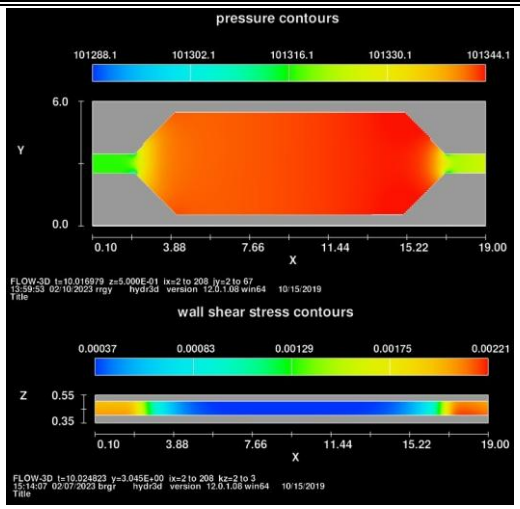

Fig. 6 *Simulation results of the microfluidic device – type 2; The wall shear stress is up to 0.028 dyn. The pressure along the microchannel is approximately 1013 mbar. The pressure in the wide part of the microfluidic device is 0.01 dyn.*

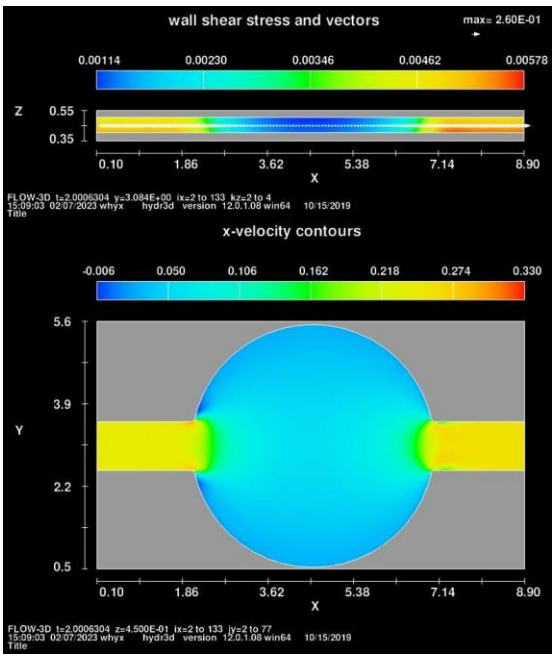

Fig. 7 *Simulation results of the new microfluidic structure – type 3; The pressure in the wide part (circle) of the microfluidic device is up to 0.01 dyn. The wall shear stress of the narrow part (straight channel) is up to 0.057 dyn. The pressure is approximately 1014 mbar.*

Regarding the simulation results, a micropump with a pressure range from 0 to 2000 mbar could be applied for control of the Newtonian fluid into the future prototype of the organ-on-a-chip liver sinusoid device. Companies as Elveflow have this type of micropumps available on the market. Our optical system BioFlux 200 also could be used for creation of such laminar flows with the same pressures.

4. Fabrication Technology of a Liver Sinusoid on a Chip Microfluidic Device

The proposed microfluidic device mimicking the liver sinusoidal structure will consist from 2 main blocks with identical microchannel geometry. The height of the microchannel will be 0.1 mm. The width of the straight part is 1 mm. The region in the shape of a circle will be with a diameter size from 5 mm. The length of the microchannel is 9 mm.

The geometry of the microfluidic device will be fabricated by a xurography technique [12], performed at low cost in a straightforward manner.

The microchannel will be drawn using a CAD software. The molds will be cut by a cutting plotter from a vinyl paper. The mold will be transferred to any polymer / glass substrate (petri dish) using an adhesive. The PDMS prepolymer will be prepared by mixing a commercial prepolymer and a curing agen (10:1 ratio) and poured onto master mold in the petri dish and cured in an oven at 80ºC for 20 minutes. Using a blade, the microchannels will be cut off and the inlet and outlet holes will be made using a suitable micro puncher. Both identical parts of the microfluidic device will be aligned with a mask aligner. The perforated (the diameter size of the holes is 400 nm) polymer membrane (commercially available) will be incorporated between both PDMS parts. The whole microfluidic structure will be sealed finally.

5. Conclusions

In this paper, a new design of a microfluidic device mimicking the liver sinusoidal structure has been proposed. 3D models of the proposed microfluidic device and two types of the most widely used liver on-a-chip devices have been prepared for CFD simulation. The results obtained, helped to estimate the wall shear stress generated over the polymer membrane where the LSECs are cultured. Regarding the used pressure, suitable micropumps could be selected for creation of an appropriate Newtonian flow. As a future activity, a fabrication technology based on a soft lithography has been proposed. Regarding the perforated polymer membrane, we have plans to develop innovative membrane using two photon polymerization technique and our high-technological equipment for 3D micro/nano-printing (Photonic Professional GT2 – Nanoscribe).

Acknowledgments

This work has been accomplished with the financial support by the Grant No. BG05M2OP001-1.002-0011-C02 financed by the Science and Education for Smart Growth Operational Program (2014-2020). Thanks also to Assoc. Prof. Elissaveta Zvetkova from the Bulgarian Society of Biorheology, for the useful discussion and valuable advices.

References

1. Y. Du, N. Li, H. Yang, Ch. Luo et al., Lab on a Chip, 17(5) (2017)
2. S. Soydemir, O. Comella, D. Abdelmottaleb, J. Pritchett, Front. Med., Sec. Gastroenterology, 6 (2020)
3. T.D. Luong, N.-T. Nguyen, Micro Nanosyst., 2 (3) (2010)
4. N. Nguyen, S.A.M. Shaegh, N. Kashaninejad, D. Phan, Adv. Drug Deliv. Rev., 65 (2013)
5. J.J. Kim, E. Sinkala, A.E. Herr, Lab Chip 17 (5) (2017)
6. N. Bhise, J. Ribas, V. Manoharan, Y. Zhang, A. Polini, S. Massa, M. Dokmeci et al., Control. Release 190 (2014)
7. A. Perestrelo, A. Aguas, A. Rainer, G. Forte, Sensors 15 (12) (2015)
8. Y. Zhang, P. Ozdemir, Anal. Chim. Acta 638 (2) (2009)
9. E. Moradi, S. Firoozinezhad, M. Hashjin, Acta Biomaterialia 116 (2020)
10. S. Lu, F. Cuzzucoli, J. Jiang, L. Liang, Y. Wang et al., Lab on a Chip, 22, (2018)
11. T. Ladner, S. Odenwald, K. Keris, G. Zieres, A. Boillon, J. Boeuf, Pharm Res., Springer-Verlag (2018)
12. E. Pinto, V. Faustino, R. Rodrigues, D. Pinho et al., Micromachines 2015, Vol. 6

Study of Vitamin C stability in thermal water for ecofriendly application in the pharmaceutical industry

Sabolč Bognar*, Nina Finčur, Daniela Šojić Merkulov
University of Novi Sad Faculty of Sciences, Department of Chemistry, Biochemistry and Environmental Protection,
Trg Dositeja Obradovića 3, 21000 Novi Sad, Serbia
sabolc.bognar@dh.uns.ac.rs

Abstract: *Free radicals and reactive species of oxygen are destructive for living organisms. Antioxidants are capable to reduce the effect of free radicals and to recover the organisms' health. On the other hand, during the fabrication process various chemicals are released into the water ecosystems from the factories, causing harmful effects on the aquatic organisms. The Autonomous Province of Vojvodina in Serbia is rich in thermal waters. Thankfully to the various minerals, they could have antioxidant effect and could be used as raw material for the production of different pharmaceutical products. In this study we examined the possible effect of different thermal water samples on the degradation rate of Vitamin C as an antioxidant with UV radiation. Furthermore, the influence of initial pH value was also investigated. Our results showed that the thermal water reduced the degradation rate of vitamin C. In addition, the lowest removal rate was observed at initial pH 7, which is close to the skin's natural pH. These findings showed that the thermal water could be used in preparations for skin.*
Keywords*: FREE RADICALS, ANTIOXIDANTS, ENVIRONMENTAL POLLUTION, ECO-FRIENDLY INDUSTRY, THERMAL WATER, STABILITY STUDY, FORCED PHOTODEGRADATION, SKIN PREPARATIONS.*

1. Introduction

Oxygen is an essential element for life. This element is necessary for the basic chemical and biological reactions and without oxygen there would be no energy for cells [1]. Consequently, it is amusing that oxygen can also destroy the living organism [2].Namely, during the ATP degradation by the mitochondria free radicals are produced, which can be both harmful and useful [1]. Reactive oxygen species can also be generated due to environmental factors, such as UV irradiation [3]. At low concentrations they have positive effect on the immune system, while at higher concentrations they can cause oxidative stress and damage living cells. These damages in the living cells result in the development of various serious disorders, such as cancer, arthritis, aging, autoimmune disorders, cardiovascular and neurodegenerative diseases [1].

Based on the mentioned, it is obvious that these substances have to be eliminated in order to keep organisms healthy. The compounds, which are capable to reduce the oxidation of proteins, carbohydrates, lipids and DNA, are known as antioxidants. Antioxidants can be synthetic and natural. The sources of natural antioxidants are most commonly fruits and vegetables. On the other hand, the synthetic sources are mostly drugs, made by various pharmacy companies [4].

Unfortunately, pharmaceutical factories during the production release high amount of wastewater to the natural ecosystem, which results in the appearance of different active pharmaceutical ingredients (API) in the environment. API can cause various, unexpected effects on the non-target organisms. Thus, the amount of released water should be reduced and the wastewater should be adequately treated prior to reaching the water ecosystems [5].

Nowadays, great attention is paid to the personal care products, which are present in aquatic environment at high concentrations. For instance, various UV filters has been found in different water samples, especially in summer, due to the outdoor activities when they are washed from the skin into the water [6].

Based on the mentioned, eco-friendly but effective antioxidants should be found or developed. Fortunately, Serbia and the Autonomous Province of Vojvodina, which belongs to the Pannonia Basin, are very rich in thermal mineral waters. Many of them are used mostly in balneology. Thermal waters in Vojvodina possess above-average geothermal qualities in comparison to the European hydro geological standards and can be successfully applied for medical purposes [7].

In this study, the possible antioxidant effect of thermal water from Kanjiža Spa was investigated, under simulated sunlight. Furthermore, the possible effect of initial pH and mineral concentration on the photodegradation rate was also examined.

2. Materials and methods

Thermal water was sampled from Kanjiža Spa (Kanjiža, Vojvodina, Serbia) and kept in refrigerator. Thermal water was used without further treatment, except the experiments with various mineral concentrations, when 30%, 50%, and 70% of the water samples was evaporated, in order to concentrate the present elements.

For the investigation of the possible antioxidant effect of thermal water, solution of vitamin C (0.05 mM) was freshly prepared prior to photodegradation experiments, dissolving appropriate amount of vitamin C () in ultrapure and thermal water.

The initial pH values were set using 0.1 M $HClO_4$ (70% (*w*/*w*), >99.99%, Sigma−Aldrich, St. Louis, MO, USA) and 0.1 M NaOH (*pro analysis*, MOSS &HeMOSS, Belgrade, Republic of Serbia).

In order to determine the antioxidant efficiency of thermal water, the samples taken after photodegradation were analysed using liquid chromatography with the following components of mobile phase: acetonitrile (99.9%, Sigma−Aldrich, St. Louis, MO, USA) and orthophosphoric acid (85%, pro analysis, Sigma–Aldrich, St. Louis, MO, USA).

3. Sample preparation and analytical procedures

The photodegradation experiments were performed in a photoreactor (TOPT-V, Toption, China). The samples were prepared and irradiated in a photochemical cell made of quartz glass (total volume of ca. 100 mL). The photochemical cells were placed in a circle around the Xe lamp, which was used as simulated solar irradiation (SSI). The cells were equally exposed to the irradiation source. Xenon lamp was in a quartz cold trap, which was equipped with water-circulating jackets and connected to a cooler in order to ensure a constant temperature inside the photoreactor (Fig. 1).

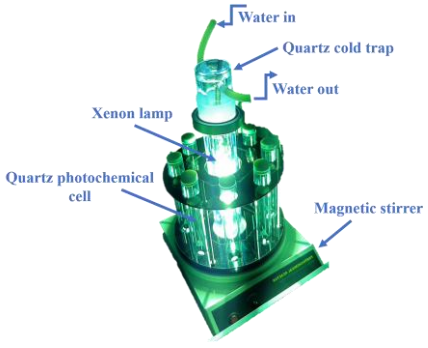

Fig. 1. *TOPT-V photoreactor*

The samples of vitamin C, taken after different times of irradiation (5, 10, 15 and 30 min) using SSI, were firstly filtered through Millipore (Millex-GV, Burlington, MA, USA, 0.22 µm) membrane filter to remove all possible impurities. After that, they were analyzed using a high-pressure liquid chromatograph with a diode array detector (UFLC-DAD, Shimadzu Nexera, Tokyo, Japan) (wavelength of vitamin C absorption maximum at 243 nm) equipped with Inertsil® ODS-4 column (2.1 mm × 50 mm i.d., particle size 2 µm, 30 °C). Prepared samples (20 µL) were injected and analyzed. The mobile phase (flow rate 1.0 mL/min) was a mixture of acetonitrile and water (50:50, *v*/*v*, pH 2.56), while the water was acidified with phosphoric acid so that the mass fraction of phosphoric acid was 0.1%.

4. Results and discussion

Firstly, the degradation of vitamin C was investigated in ultrapure water, under different initial pH values, at pH 10 and 7, using SSI. Based on the obtained results (Fig. 2) it can be seen, that the degradation rate was higher under basic conditions. This can be explained by the auto-oxidation process of vitamin C, which is accelerated under alkaline conditions [8].

Table 1. *Chemical characteristics of thermal water from Kanjiža Spa*

Parameter	Value
pH	7.9
Sodium (g/L)	1.298
Potassium (g/L)	0.0097
Lithium (g/L)	0.0001
Ammonium (g/L)	0.0002
Calcium (g/L)	0.0064
Magnesium (g/L)	0.0027
Strontium (g/L)	0.0004
Manganese (g/L)	0.00001
Iron (g/L)	0.00001
Aluminum (g/L)	0.00005
Hydrogen carbonate (g/L)	2.934
Chloride (g/L)	0.073
Bromide (g/L)	0.00013
Iodide (g/L)	0.0006
Fluoride (g/L)	0.0003
Nitrate (g/L)	0.0001
Hydrogen phosphate (g/L)	0.0002
Sulphate (g/L)	0.0009

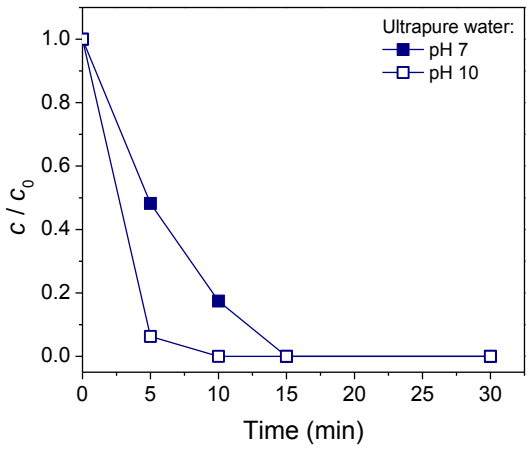

Fig. 2 *Degradation kinetics of vitamin C (0.05 mM) in ultrapure water, under SSI*

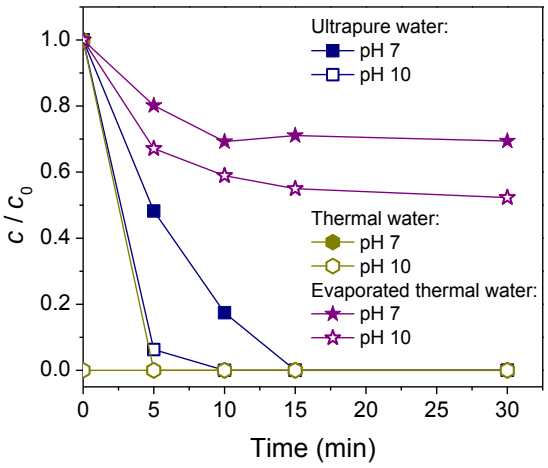

Fig. 3 *Degradation kinetics of vitamin C (0.05 mM) in ultrapure, thermal and evaporated thermal water, under SSI*

In the next step, we investigated the degradation efficiency of vitamin C in thermal water from Kanjiža Spa. There were two different water samples used. Namely, the degradation studies were conducted in pure thermal water (i.e without any treatment) and in samples where 50% of initial volume of water was evaporated in order to increase the concentration of present minerals (Table 1). The experiments were carried out under two different inital pH (10 an 7) and the obtained results are represented in Fig. 3. Based on our findings it can be seen that the degradation rate of vitamin C was higher in the non-treated thermal water compared to ultrapure water at both initial pH. The higher degradation in non-treated thermal water can be explained by the presence of different ions and by the higher natural pH value, which can accelerate the degradation. On the other hand, in the evaporated water samples the degradation of vitamin C under SSI was lower at both inital pH comperated to other samples (Fig. 3). The possible explanation for this behaviour lies in the fact, that the concentration of present cations and anions was higher and reduced the degradation, i.e vitamin C was protected from forced photodegradation under SSI. Furthermore, after 15 min of irradiation the degradation process stopped and no further amounts of vitamin C were degraded in the last 15 min of irradiation.

Finally, in order to determine the optimal conditions, further experiments were carried out with thermal water evaporated to 30% and 70% (Fig. 4) at initial pH 7 and 10, under SSI. Based on our findings it can be seen that in the samples with thermal water evaporated 30% higher degradation was observed compared to 50% and 70%, after 30 min of irradiation under SSI. It can be explained by the lower concentration of various ions which could not reduce the degradation of vitamin C. On the other hand, in the case of thermal water samples evaporated to 70% lower degradation was observed compared to 30%, but higher compared to 50%. This behavior is probably due to the very high concentration of present ions.

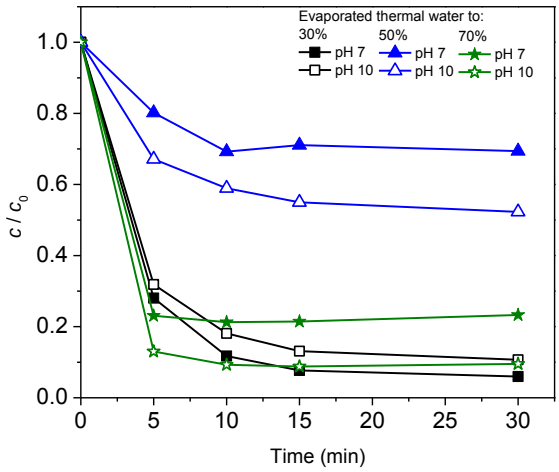

Fig. 4 *Degradation kinetics of vitamin C (0.05 mM) in ultrapure, thermal and evaporated thermal water, under SSI*

5. Conclusion and outlooks

In this study the possible antioxidant effect of thermal water from Kanjiža Spa was investigated. In order to prove this effect, the stability of vitamin C was followed during forced photodegradation under SSI and at initial pH 7 and 10. Firstly, our findings showed a different behaviour of vitamin C in ultrapure and thermal water. Based on the obtained data it also can be concluded, that in alkaline medium, both in ultrapure and thermal water, the degradation rate was higher, which can be the result of vitamin C auto-oxidation, which is more intense above pH 7. The influence of present ion concentration on the photodegradation efficiency was examined, as well. Namely, thermal water was evaporated to 30%, 50% and 70% in order to reach different concentration of the present natural cations and anions in the samples. According to the obtained data, the lowest vitamin C degradation was achieved when 50% of thermal water was evaporated. Whereas, in the case of 30% and 70% the degradation efficiency was higher. The reduced photodegradation rate of vitamin C in the case of 50% indicates a possible antioxidant effect of thermal water, since the irradiated compound was protected from the total degradation.

Our findings indicate that evaporated thermal water to 50% could be used as an antioxidant and has potential application in pharmaceutical industry. Namely, different preparations could be developed, for instance skin care products, using an eco-friendly, natural resource instead of chemicals. Furthermore, various experiments should be carried out in order to determine the possible use of thermal water as an active pharmaceutical ingredient, which would make pharmacy and medicine more sustainable.

6. Acknowledgement

The authors acknowledge the financial support of the Provincial Secretariat for Higher Education and Scientific Research (Grant Number 142-451-2367/2022-01/01) and the Science Fund of the Republic of Serbia (Grant No 7747845, *In situ* pollutants removal from waters by sustainable green nanotechnologies-CleanNanoCatalyze).

7. References

1. L. A. Pham-Huy, H. He, C. Pham-Huy, Int. J. Biomed. Sci. **4** (2009), 89−96.
2. V. Lobo, A. Phatak, N. Chandra, Pharmacogn. Rev. **4** (2010), 118−126.
3. J.-Y. Meng, C.-Y. Zhang, F. Zhu, X.-P. Wang, C.-L. Lei, J. Insect Physiol. **55** (2009), 588−592.
4. V. Sindhi, V. Gupta, K. Sharma, S. Bhatnagar, R. Kumari, N. Dhaka, J. Pharm. Res **7** (2013), 828−835.
5. J.L. Wilkinson, A.B.A. Boxall, D.W. Kolpin, (…) and C. Teta, PNAS **119** (2022), Art. No. e2113947119.
6. M. Picot Groz, M.J. Martinez Bueno, D. Rosain, H. Fenet, C. Casellas, C. Pereira, V. Maria, M.J. Bebianno, E. Gomez, Sci. Total Environ. **493** (2014), 162−169.
7. M. Bubalo-Živković, T. Lukić, B. Đerčan, R. Stojsavljević, D. Bjelajac, B. Ristanović, Zbornik radova – Geografski fakultet Univerziteta u Beogradu **66** (2018), 53−70.
8. X. Yin, K. Chen, H. Cheng, X. Chen, S. Feng, Y. Song, L. Liang, Antioxidants, **11** (2022), Art. No. 153.

Formation of the structure of polymeric products on the based of polyamide 6 produced by fdm-printing

Alexander Skaskevich[1], Valery Sarokin[1], A. Sudan[1], A.N. Gaiduk[1], Angel Velikov[2]
Yanka Kupala Grodno State University[1] – Grodno, Belarus, Bulgarian Academy of Sciences, Institute of Metal Science, Equipment and Technologies with Center for Hydro- and Aerodynamics "Acad. A. Balevski",, Bulgaria[2]
E-mail: askas@grsu.by, sorvg@grsu.by, anmabg@abv.bg

Abstract: *An analysis of the prospects for the development of FDM printing technology has been carried out. The paper studies the possibility of obtaining polymer products based on polyamide 6 and its compositions by layer-by-layer deposition. Tests of the strength indicators of the printed experimental products were carried out. The mechanism of the influence of the composition and modes of formation of printed products on their strength characteristics is proposed. The influence of the composition of the composite polymer material based on PA6 on the quality of printing products has been studied. Methods for controlling the shrinkage parameters of products obtained by layer-by-layer deposition are proposed. The obtained results of the study can be used in the development of composites for the production of polymer filament to ensure the process of FDM printing of polymer products, including for the needs of mechanical engineering.*
KEYWORDS: *FDM PRINTING, POLYAMIDE 6, TECHNOLOGICAL PARAMETERS, TENSILE STRENGTH, RELATIVE ELONGATION, POLYMER PRODUCTS*

1. Introduction

The production of polymer products using additive technologies has become available due to the intensive development of the production of FDM printers, as well as consumable polymer materials (filaments), which allows solving various production problems. At the same time, during the printing process, control over the main operational characteristics of products is ensured by choosing the composition of the polymer filament, as well as the technological settings of the FDM printer. In the Republic of Belarus, aliphatic polyamides and composites based on them are actively and effectively used for the production of structural products with high values of consumer characteristics of the widest range. At the same time, the effective processing of polyamides into products and the realization of the advantages and advantages of the indicated thermoplastic polymer when using various technologies are hampered by high values of hygroscopicity (up to 12 wt.% with an acceptable value during processing of 0.05-0.1 wt.%) and thermal shrinkage (up to 2.5% for unfilled materials) polyamide 6. For the active use of polyamide 6 in additive technologies, this is a significant drawback that affects the quality of the resulting products. And if polyamide processors effectively cope with a high tendency to moisture absorption by pre-drying the raw material and using heating of the material in the loading zone of the process equipment, then the thermal shrinkage of the binder requires more complex solutions. Most often, it is possible to reduce the thermal shrinkage of the polyamide matrix by modifying it with polymer components [1], as well as by introducing dispersed and (or) fibrous fillers [2]. At the same time, glass fibers in the composition of polyamide 6 can significantly increase the level of deformation and strength parameters of products, and carbon fibers increase impact strength and wear resistance. Polyamide 6 and composites based on it are mainly processed into products by injection molding due to the high values of the melt flow parameter. The use of PA6 for FDM printing in products seems difficult due to the high melt fluidity (MFR PA6 210/310 is more than 20 g/10 min), and therefore the use of composite compositions based on it for 3D printing is promising.

In modern conditions of limited availability of the raw material base, as well as increasing logistics costs for the supply of material resources and components of machine-building equipment, it is promising to study the possibility of using domestic polymer composite materials to obtain piece products in the conditions of enterprises operating and maintaining equipment that includes products based on polymer materials.

Thus, the purpose of the work is to substantiate the feasibility and effectiveness of using a polymer filament based on polyamide 6 and its composites for printing polymer products by the layer-by-layer deposition method.

2. Materials and Methods

To study the features of the formation of the structure of the material in products obtained by 3D printing, in this article, the authors used polyamide PA6-210/310 (Grodnamid) TU RB 500048054.009-2001 in granules produced by GrodnoAzot OJSC, carbon fiber UPA6-10 TU RB 00204056-086-94 in granules produced by OJSC SvetlogorskKhimvolokno, composite material PA6 + 10 wt.% HDPE, obtained by thermomechanical combination of components during extrusion. To study the parameters of polymer products, a filament with a diameter of 1.75 mm was obtained for these materials by extrusion on a Z-7M laboratory extruder (Russia) in modes that take into account the rheological characteristics of the starting materials. The parameters of the extrusion process when obtaining a filament are shown in Table 1.

Table 1: *MFR values for PA6-210/310 (Grodnamid)*

Options	Material		
	PA6-210/310	UPA6-10	ПА6+10 mas.% HDPE
Cylinder temperature by zones, °C (±10°C)	230	230	230
Head temperature, °C (±10°C)	240	240	240
Feed-screw speed, rpm	20	10	20
Retraction speed, m/min	0,9	0,5	0,8

Previously to printing product samples, the polymer filament was subjected to thermostating in an oven at a temperature of 95 ± 5 °C for 4 hours to reduce the moisture content by no more than 0.1 wt%. To assess the deformation-strength characteristics of materials under uniaxial tension and to study the features of the formation of the structure of materials during layer-by-layer deposition, a product was printed in the form of standard blades (type 1) GOST 11262-80 on an Ultimaker 3 3D printer. The FDM printing parameters of the blades were set in the CraftWare 1.19 slicer program. A series of 6 standard samples was printed in the given technological parameters of the print settings per cycle (table 2). Evaluation of the deformation-strength characteristics of the studied samples was carried out on a tensile testing machine RM-500 in the mode of uniaxial tension at a speed of 10 mm/min with fixation of the deformation and tensile force. It was of interest to investigate the mechanism of the formation of autohesive bonds within the slab space and between the layers of a polymer product during the manufacture by the method of layer-by-layer deposition. The resulting samples of polymer products in the form of blades with different orientations in the intralayer volume (± 45º and 0º/90º) were subjected to 5% deformation in uniaxial tension for further study of brittle cleavage of product images obtained in the

longitudinal direction of the tension axis. The structure of the materials was studied by scanning electron microscopy on blades that were brittle fractured after soaking in liquid nitrogen. At the same time, in order to manifest the effects of interlayer autohesion and study the effect of fillers on the structure of composites in the product, the blades were subjected to deformation within a 5% elongation under uniaxial tension. It was of interest to analyze the interaction of the polyamide-based filament melt in the interlayer and intralayer locations.

Table 2: *Parameters of print settings for test samples*

Basic print settings	PA 6	UPA 6-10	PA6+10 mas.% HDPE
The speed of movement of the nozzle of the extruder during printing, mm / sec	40	20	40
Print layer thickness, mm	0,2	0,2	0,2
Print width, mm	0,4	0,4	0,4
Number of layers of the perimeter of the product	2	2	2
Table temperature, ℃	100	70	100
Extrusion Temperature,℃	250	250	240
Unspecified print settings were the same for all samples			

3. Results and discussion

As a result of visualization of internal stresses arising in a polymer material obtained by layer-by-layer deposition of Nylon, a higher level of stresses arising in the peripheral part of the material, in comparison with the volume [3], was shown. In this case, the level of internal stresses decreases with a decrease in the degree of filling of the product volume with a polymer melt. It was shown in [4,5] that the degree of filling of the volume of the material affects the dimensional stability of products obtained by layer-by-layer deposition. At the same time, a number of research authors indicate [6,7,8] that the highest values of the deformation-strength characteristics of the material in the product are achieved at zero angles of orientation of the printing direction to the tension axis. However, to ensure the isotropy of strength indicators, layer-by-layer filling of the volume of the product was carried out in the "parallel lines" mode, changing the direction of printing in the next layer by 90 º, as recommended by many researchers [6,8].

The analysis of the morphology of the brittle fracture surface of blade samples based on UPA 6/10 carbon fiber, obtained by FDM printing with polymer orientation ±45º inside the layers when filling the volume of the product, was carried out on SEM images of the surface shown in Figure 1. A snapshot of the sample surface within the interlayer brittle The cleavage is shown in Figure 1a, which shows several adjacent layers of fibers with print orientation in the layer at angles of +45° and -45°. In Figure 1a, several important morphological features of the destruction of the polymer binder can be distinguished: interlayer voids resulting from the 3D printing process, layers with a rough fracture surface morphology, and layers with a smoother surface. For a detailed display of the nature of the contact of adjacent layers, an increase in the survey area is given (Figure 1b). The presented images indicate that between the threads between the layers, insufficient adhesion is characteristic along the tension axis, at which the formed crack grows. A rough fracture surface can also be noted in the interlayer region where fibrillation of the polymeric binder is noted with the formation of filamentous fragments.

This nature of the destruction of UPA 6/10 carbon fiber suggests that the binder layers oriented perpendicular to the tension axis hinder the growth of cracks. In this case, the participation of the remaining layers of the material in the mechanism of resistance to destruction of the matrix can be considered insignificant due to insufficient adhesion between them, due to the limited mobility of the binder polymer filled with carbon fibers.

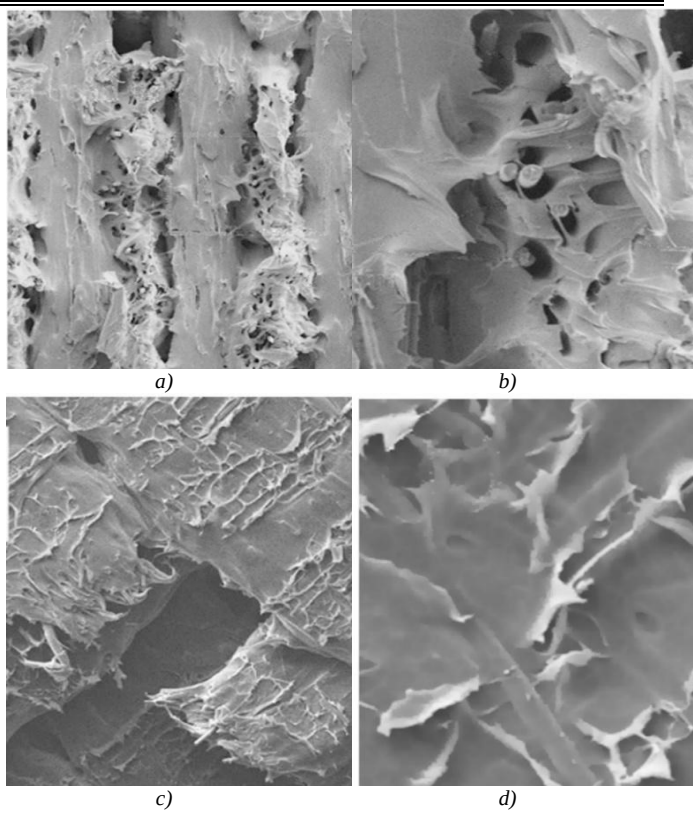

a) *b)* *c)* *d)*

a) general view of the fracture surface morphology of the sample in the interlayer location (magnification ×100); b) close-up of surface features in adjacent layers (×500 magnification); c) general view of the fracture surface morphology of the sample in the intralayer location (magnification ×100); d) close-up of surface features within the layer (×500 magnification)

Figure 1 *SEM images of brittle fracture surfaces of samples with a print orientation of ± 45°*

The role of short elements of carbon fiber contained in the PA6 matrix in the process of deformation destruction of the layered structure of a carbon fiber product is also noticeable. Fibrillation of the polymer matrix during uniaxial tension of the carbon-filled PA6 sample suggests the implementation of a local mechanism of strengthening the polymer matrix in the product formed by the FDM-printing method.

At the same time, within the imprinted layer, a sufficiently strong autohesive adhesion is observed in the intralayer location of the matrix, which is observed in the image of the brittle fracture morphology of the sample (Figure 1c). This is due to the good rheological characteristics of PA6, which contribute to the realization of the phenomenon of autohesion between the polymer threads within the printed layer. Figure 1d shows that the traces of fracture surface roughness are concentrated along short fibers. This fact confirms the assumption that short carbon fibers enhance autohesion during FDM printing of polymer products based on carbon fiber.

Figure 2 shows SEM images of the brittle cleavage surfaces of specimens based on UPA6-10 carbon fiber obtained with the printing direction oriented in the 0º/90º layer. The surface of a brittle fractured sample, representing the interlayer space of the matrix, is shown in Figure 2 a. The image shows layers located at an angle of 0º and at an angle of 90º. At the same time, layers at an angle of 0º under conditions of preliminary 5% deformation have a rough surface, and layers at an angle of 90º retain a smooth appearance. An enlarged view of the cleavage surface of this sample is shown in Figure 2b. It should be noted traces of stretching of the fibers in the layers located at an angle of 0º, which indicate the course of the processes of fibrillation of the polyamide binder during deformation.

The surface morphology of a brittle cleavage of a sample of the studied carbon fiber with a polymer orientation angle of 0º/90º demonstrates a similar morphological pattern, as in the case of

printing products with an orientation of ± 45º. The brittle fracture surface of CFRP contains traces of piles of polymer fibrils of destroyed threads. The presented images indicate some similarity of the fracture mechanism in the case of deformation of the sample obtained by printing with an orientation of ± 45º.

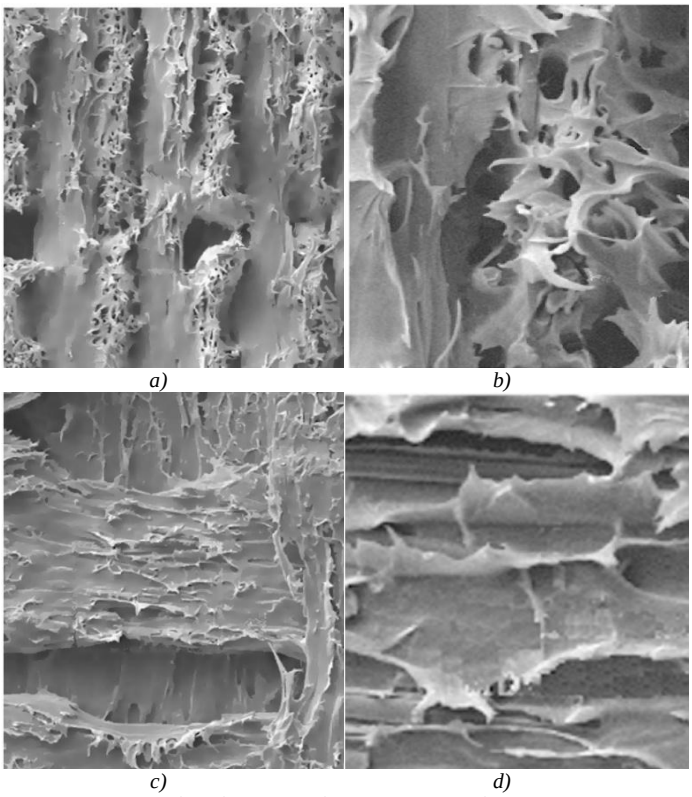

a) *b)* *c)* *d)*

a) general view of the fracture surface morphology of the sample in the interlayer location (magnification ×100); b) close-up of surface features in adjacent layers (×500 magnification); c) general view of the fracture surface morphology of the sample in the intralayer location (magnification ×100); d) close-up of surface features within the layer (×500 magnification)

Figure 2 *SEM images of brittle fracture surfaces of specimens with print orientation 0°/90°*

An analysis of the features of the operation of the specified product indicates the predominant destruction in the place of the most weakened section, located between the body of the pusher and the surfacing. An example of a destroyed product is shown in Figure 3.

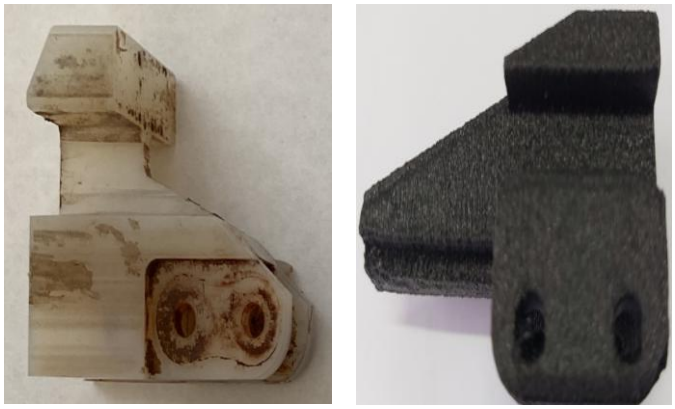

a) *b)*

Figure 3 *Appearance of the products "Pusher F08575326" (a) and "Pusher 406.42.0490" (b), obtained by injection molding (a) and FDM printing technology (b)*

3. Conclusion

Thus, the results of the study of the accuracy parameters of FDM printing of polymer products based on PA6-210/310 (Grodnamid), as well as the indicators of their deformation and strength characteristics, indicate the promise of using polyamide both in the initial state and in the state of the composite. The printing efficiency of PA6 in the product is achieved by ensuring a stable geometry of the polymer filament, as well as choosing the optimal printing temperature not exceeding 250℃. The obtained results of the work can be taken into account when determining the technological modes of production of filaments based on PA6, as well as when choosing the modes of FDM printing of thin-layer elements of polymer structures and elements of parts that are most loaded during operation. The data obtained indicate the prospects for conducting scientific research in the creation of materials based on aliphatic polyamides and their composites, as well as studying the influence of technological factors in the process of processing polyamide filaments into products by FDM printing.

4. References

1. Nanocomposite and nanostructured engineering materials and technologies for their production. Monograph / S.V. Avdeychik and [others], Ed. A.V. Kirichek. – M.: Spektr Publishing House, 2013. – 224 p.

2. Liopo, V. A. Physical bases of polymer modification with doping additives of layered minerals / V. A. Liopo, G. A. Kuznetsova, V. A. Struk, A. A. Skaskevich // Materials, technologies, tools. - 2002. - T. 7, No. 4. - S. 54-58.

3. Skaskevich, A. A. Influence of technological parameters of FDM-print on the strength characteristics of samples of polyamide / A. A. Skaskevich, A. Sudan, D. Dzhendov // Machines. Technologies. Materials. – 2020. – T. XIV. – № 5. – C. 210-212.

4. Skaskevich, A. A. Features of the formation of the structure of polymer products based on carbon fiber plastics obtained by the FFF-printing method / A. A. Skaskevich, A. S. Sudan // Petrochemistry-2021: materials of the IV Intern. sci.-tech. forum on chem. technologies and oil and gas processing, Minsk, November 22-23. 2021 - Minsk: BSTU, 2021. - S. 88-91.

5. Sudan, A. On the prospects for the production of filaments based on polyamide 6 for FDM printing / A. Sudan, A. N. Gaiduk, A. A. Skaskevich // Bulletin of Yanka Kupala Grodno State University. Ser. 6. Technique. - 2021. - T. 11. - No. 2. - S. 83-90.

6. Kondrashov, S.V. Influence of technological modes of FDM printing and the composition of the materials used on the physical and mechanical characteristics of FDM models (review) / S.V. Kondrashov [and others] // Proceedings of VIAM. - T.82, No. 10. - 2019. - S. 34-49.

7. Nefelov, I.S., Baurova, N.I. Ways to prevent technological defects in machine parts manufactured using additive technologies / I.S. Nefelov, N.I. Baurova // Bulletin of modern technologies. - No. 5. - 2017. - P.36-40.

8. Erofeev, V.T. Study of the physical and mechanical characteristics of polylactide samples in additive technology / V.T. Erofeev [et al.] // Building materials and products. - Number 3. - 2019. - P.92-101.

Results from the plastic pressing of experimental ceramic pavers of "yellow" paving stone type

Gergana Mutafchieva[1], Lyuben Lakov[1], Gabriel Peev[1], Dimo Mihaylov[1]
Bulgarian Academy of Sciences, Institute of Metal Science, Equipment and Technologies with Hydro- and Aerodynamics Centre "Acad. Angel Balevski"1, 67 "Shipchenski Prohod" Blvd, 1574 Sofia, Bulgaria
e-mail: cl.creativeline@gmail.com

Abstract: *The results of the plastic forming of ceramic pavers with a large volume and size are observed to produce better compaction of the raw material. The used ceramic mixture is based on a sedimentary rock with relatively high moisture content and firing shrinkage which gives the common yellow colour after a high-temperature liquid phase synthesis. The results of one-fold pressing revealed the occurrence of deformation processes in the drying stage and during the temperature regime. As a consequence, the pressing pressure should be increased and the residual water amount needs to be reduced to an optimal content.*
Keywords*: CERAMIC MOULDING, PRESSING TECHNOLOGY, PLASTIC PRESSING*

1. Introduction

The term plastic pressing could be conditionally divided into forming two kinds of ceramic products. The first group is connected to small-by-size holloware such as porcelain tableware, whereas the second is related to mini-series dense ceramic goods like a floor or wall tiles [1]. In terms of this, the technology is innovative not only in Bulgaria because of the used forming process to produce large by size and volume ceramic pavers "yellow" paving stone type.

An innovative die construction for plastic forming is contrived, which includes metal parts and composite inserts. The development is made up and mounted to the specific press facilities on the territory of the IMSETHC-BAS which possess an ability to press up to 185 000 kg/cm^2. The used mixture is based on a sedimentary rock from the quarry Aleksandra, the village of Lovets with the modifying agents to stabilize the high temperature and brighten the colour [2].

Part of the results are presented in front of the scientific area, however, the experimental work amplifies the technological process and the new research observes the structure of the experimental synthesized samples. A specimen for computed tomography analysis is given which reveals the presence of porosity and flaws in the structure due to approximately high moisture content and not enough densification of the material.

According to this, an additional implement should be applied in the forming process for more compaction of the ceramic mass [1,3-5].

2. Experiments

The technological regulation is contrived for plastic pressing of ceramic items that are associated with original by size and form products "yellow" paving stone type. The used ceramic batch is based on a sedimentary rock that gives the analogous yellow color after a high-temperature liquid phase synthesis [6]. The task development could be divided into the production of the metal construction and composite pressing die, and the research includes analysis of the structure of the synthesized end product.

Although good results and advantages of this technology, the process requires additional compaction of the raw mass before the major molding. It is necessary due to the relatively high moisture content in the used composition of 20 %, in contrast to the optimal water content of 15 % for better results. The higher quantity of water increases the volume drying and firing shrinkage as well as emerging unacceptable flaws such as a larger range of deformation and cracking of the products during the temperature synthesis.

The constituents of the die construction could be classified as metal frames (punch holders), holder, and guide posts; metal pressing die with embedded composite inserts, and two composite punches. Mounting of the construction over the press facility is achieved by the metal frame means, whereas stabilization is reached through the additional holder. The frames with mounted punches are fixed to each other by the guide posts and the distance bars are placed which determine the volume of the pressing form. The scheme of the die construction is given in fig. 1, whereas fig. 2 reveals the elements of the construction, and the mounted construction on the press facility is presented in fig. 3.

The composite material is a type of technical stone; the composition ingredients are polymer and filler. The proportions of the mixture are given in table 1, and the mechanical properties of the specific resin are presented in table 2 [7]. The ratio of the components is 70 % of resin and 30 % of filler, which is separated between 20 % of quartz glass in different fractions with hardness by Mohs 7 and 10 % of corundum with hardness by Mohs 9.

The characteristics of the added agents and their hardness reduce the percentages containing filler on account of the resin, in contrast to traditional products of technical stone which the filler content is approximately 90-95 %. The increases of the resin in the used composite leads to decreases in the viscosity and makes the composition liquidity enough which contributes to the whole form being filled and reproducing detailed and smooth imprint with no further treatment.

The specific aspect of the approach becomes from the production of the composite elements which are cast in silicone moulds. In terms of this, the models with the necessary expansion of the ceramic plastic mass, in this case of 17 %, are made in advance. Silicone moulds are cast for each model and the hardness of the used elastomer is 22 by Shore A with very high properties of tear strength and very detailed imprint. The characteristics of the silicone are given in table 2 [8].

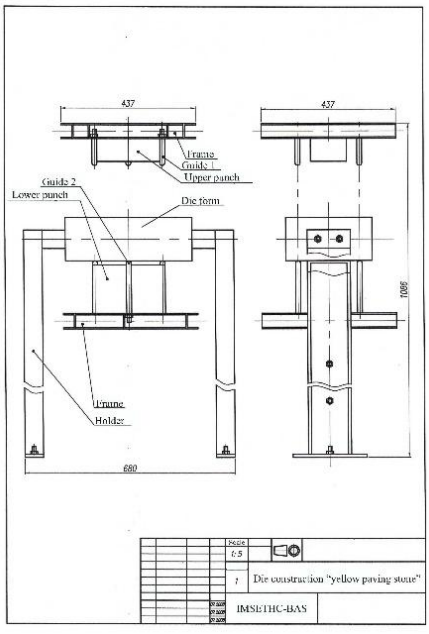

Fig. 1 *Technical drawing of the die construction for plastic pressing of ceramic pavers.*

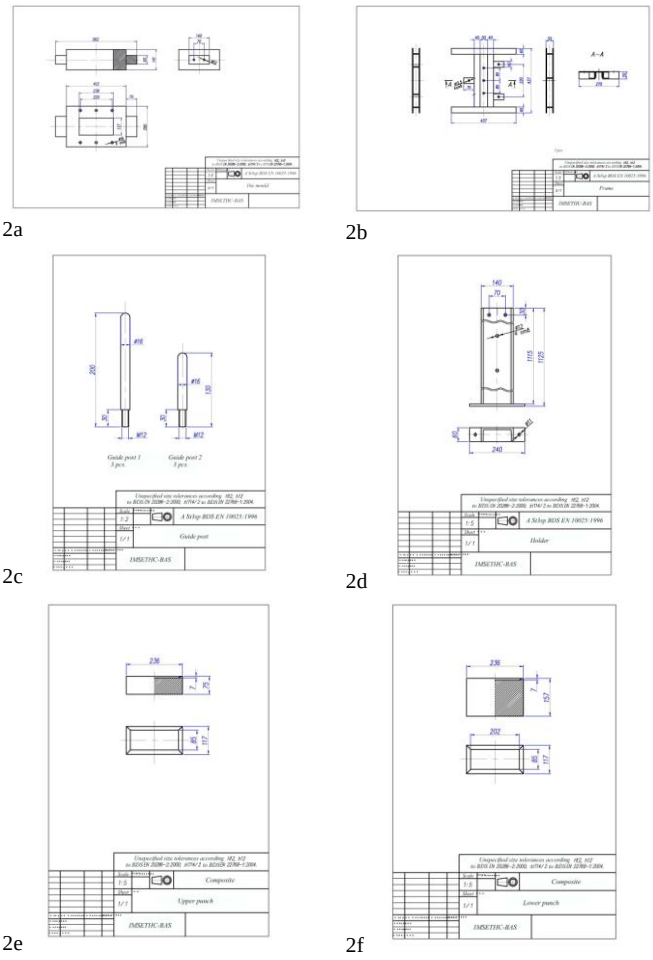

2a 2b 2c 2d 2e 2f

Fig. 2 *Technical drawing of the die construction constituents:* ***2a****. Pressing die: metal frame and composite insert;* ***2b****. Punch holder: metal frame and composite punch;* ***2c****. Guide posts: St3sp steel guides;* ***2d****. St3sp steel holder;* ***2e****. Upper punch: composite plunger;* ***2f****. Lower punch: composite plunger.*

Fig. 3. *View of the mounted die construction of the press facility for the main moulding.*

Table 1: *Proportion of the components in the used composite mixture.*

Composition	Amount %
Epoxy resin Biresin CR170	70
Quartz glass fraction of 30-50 μ	10
Quartz glass fraction of 50-100 μ	10
Corundum fraction of 120 μ	10

Table 3. *Properties of the polymer used for casting the composite inserts.*

Elastomer Zhermack ZA 22	Index
Hardness after 24 hours [ShA]	22
Viscosity [mPa.s]	4000
Elongation at break [%]	380
Tear strength [KN/m]	20
Reproduction of details [μ]	2
Dimensional variation after 24 hours [%]	0.05

The structure of the experimental ceramic paver is observed with the CT scanning means. The end products are synthesized with the tentative temperature regime, and the specimens are presented in fig. 4. The research reveals the presence of open pores and cracks as a consequence of the not enough densification of the ceramic material. The results of the computed tomography analysis are shown in fig. 5. The hypothesis of these flaws is the obtaining of the multi-layer in the ceramic mass still in the pressing process. It is probably due to not enough pressure during the press forming as well as the higher content of water.

Fig. 4 *Synthesized to 1127 °C end products ceramic pavers "yellow paving stone" type.*

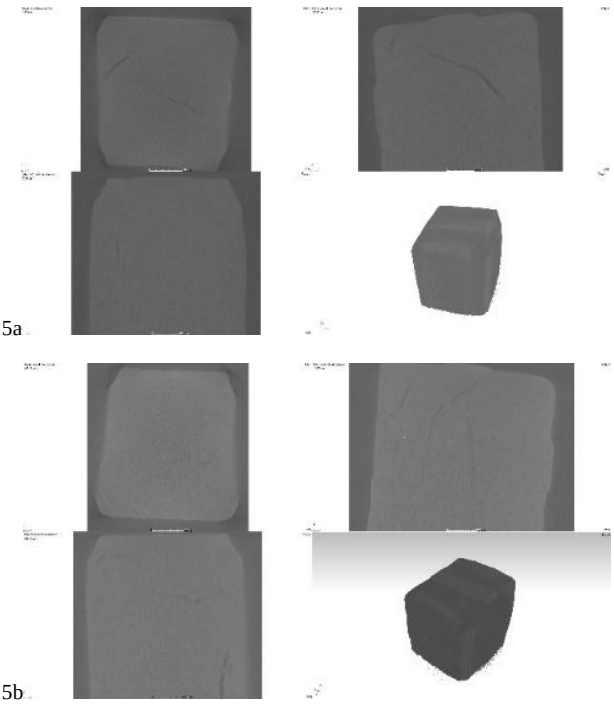

5a 5b

Fig. 5 *Research of the structure of the synthesized specimen reveals cracks and pores:* ***5a****. Up section;* ***5b****. Down section.*

The process of plastic pressing is given in fig. 6. The forming begins with placing 5100 grams of ceramic raw mixture slug on which pressure of 13000 kg/см^2 acts. The weight of the dry specimens declines to 4800 grams, as a consequence of higher moisture content and slightly more ceramic material which is expelled during the pressing process. Thus, make the green body is not dense enough in the raw condition and requires an additional implement for more compaction.

6a 6b

Fig. 6 *The Forming process of ceramic products "yellow" paving stone type:* ***6a****. Placing a slug into the pressing die;* ***6b****. Removing the expelled material.*

3. Conclusion

Experimental samples of ceramic plastic mass, based on sedimentary rocks with the addition of modifying agents to stabilize the firing process as well as brighten the clay color, are contrived.

The used mixture has approximately 20 % of moisture content which gives a relatively higher volume drying and firing shrinkage. The end products are made through the one-fold plastic pressing which displayed a vitreous body after high-temperature liquid phase synthesis. However, the held research reveals porous and multilayer structures of the ceramic material. The higher water content is due to not enough densification of the raw material. In terms of this, the process requires considering the possibilities for the preliminary extract of the moisture content and increasing the forming pressure through the additional two-fold moulding which should be led to the appropriate compaction of the ceramic mass.

Acknowledgment

The authors are grateful to the financial support of the Bulgarian National Science Fund at the Ministry of Education and Science, Contract No КП-06-ОПР 03/4 14.12.2018, for carrying out the necessary research.

4. References

1. Subota, I., Spasonova, L., Sholom, A. Influence of Forming Pressure on Frost Resistance of Ceramics. Technology audit and production reserves. № 2/1(58) (2021). p.p. 15-20
2. Mutafchieva, G., Lakov, L., Aleksandrova, M., Gacheva, M., Peev G., Mihaylov, D. Development and Production of Molding Equipment and Plastic Masses Using New Compounding Formulations, Plastic Pressing, Drying, High-temperature Liquid-phase Synthesis and Properties of a Prototype Batch of "yellow" Paving Stones. International Scientific Journal "INDUSTRY 4.0" YEAR VII, ISSUE 6, (2022) p.p. 228-231
3. Sikalidis, C., and all. Advances in Ceramics - Characterization, Raw Materials, Processing, Properties, Degradation and Healing. Edited by Costas Sikalidis (InTech, Croatia 2011)
4. Callister, Jr. W., Rethwisch, D. Materials Science and Engineering. (John Wiley & Sons, Inc. USA 2009)
5. Rozina, V., Shestakov, N. Hyperpressed Ceramic Products Based on Industrial Waste. IOP Conf. Series: Earth and Environmental Science 751 012121 (2021) p.p. 1-4
6. Jivov, B., Dimitriev, Y., Kashchieva, E., Petkov, C. Glasses and Glass Ceramics in the System P2O5-B2O3-Ag2O. Physics and Chemistry of Glasses. 41 (6) (2000)
7. Resins. Smoli-Bg. Retrieved February 8, 2023, from https://smoli-bg.com
8. Industrial silicone rubbers. Zhermack. Retrieved February 8, 2023, from https://www.zhermack.com/en/product_category/industrial/

Technology and technological scheme of a workshop for the production of beehives made of amorphous quartz ceramics

Lyuben Lakov, Todorka Lepkova, Gacheva M., Krasimira Toncheva, Gabriel Peev, Dimo Mihaylov

Bulgarian Academy of Sciences, Institute of Metal Science, Equipment and Technologies with Hydro- and Aerodynamics Centre „Acad. A. Balevski", 67 "Shipchenski Prohod" Blvd, 1574 Sofia, Bulgaria,
e-mail: mvgacheva@abv.bg; krasiton4@abv.bg

Abstract: *The development refers to an innovative technology and technological scheme of a workshop for the production of beehives made of amorphous quartz ceramics. The conditions for obtaining stable suspensions from quartz glass are emphasized and investigated. The time for the treatment of the glass in the grinding device, the amount of water, the influence of the modifiers in stabilizing the suspension by adjusting the pH level, as well as the most suitable sedimentary composition of the glass particles are established. The factors determining the speed and degree of sintering of the ceramics are investigated and established. They include the density of the raw products, the dispersion of the quartz glass particles and its purity, as well as the environment in the furnace and the sintering mode.*

Keywords: *BEEHIVE, AMORPHOUS CERAMICS, SUSPENSION, SEDIMENT COMPOSITION*

1. Introduction

Quartz ceramics is a sintered material made of ground quartz glass, which is molded using the known ceramic technologies. The resulting products are opaque and white in color. Quartz ceramic is the only ceramic material made not of crystals but of a vitreous phase. There is no material better suited for building beehives than quartz ceramics, as it is an extremely pure material which, as opposed to marl clays on their own or mixed with kaolin, does not contain any other mineral phases apart from amorphous silica.

Quartz ceramic is applied in many areas where ordinary quartz glass is also used. This is due to its high thermal stability, the stability of its thermophysical properties and its high thermal insulation properties. It is extremely suitable for the production of structural elements with a high level of cavities, such as those used for the construction of beehives, since it is not only thermally and acoustically insulating but is also atmospherically and chemically resistant to acid rain, etc. At the same time, quartz ceramic products are highly resistant against mites and rodents [1].

2. Choice of Forming method on structural parts with a high level of cavities designed for beehives

The most suitable method in this case is slip casting of aqueous suspensions. It is important to note that it is mandatory to ensure that the starting material maintains its high purity during all technological operations [2].

It is known that practically all impurities activate the crystallization of quartz glass. Therefore, the correct selection of both the material of the lining of the grinding unit and the grinding bodies is of great importance. The lining and the grinding bodies are best made of quartz glass, but due to its high wear (up to 10%), it is permissible to use high alumina ceramics with a density above 3.65-3.75 g/cm^2. This leads to a significant reduction of the grinding time (4-5 times), and the observed wear is below 1%, which is essential for the quality of the final product. The use of devices with metal working parts is undesirable.

The slip casting of quartz ceramic parts with cavities results in products with the highest density. This helps to reduce not only the time of the sintering but also its temperature.

An important stage in the technology is the preparation of a suspension of finely ground quartz glass. This is done by coarse and fine wet grinding of the glass in the same grinding unit. Thus, a slip with a minimum amount of water (16÷20%) is obtained [3]. The effectiveness of wet grinding is explained primarily by the fact that water is one of the best surfactants in relation to SiO_2. The adsorptive decrease of strength, the saturation of the unsaturated bonds of the material, the disaggregating action of water, the high specific impact energy of the milling bodies and the reduced soothing action of the suspension are also essential. The wet grinding process is exothermic and the total amount of bound water decreases sharply with the increasing of the temperature. As the temperature increases, the strength of the aqueous layers decreases due to the greater mobility of the ions. Thus the amount of bound water decreases and the free water in the suspension increases.

To create a suspension with low humidity, we use the method of maximum saturation. Its essence is that during wet grinding, the unit is stopped two or three times and ground glass with a sediment composition of 50÷100 microns is added to the suspension in a ratio of about 1/10 of the amount of glass in the suspension. Equilibrium viscosity is reached after 2-3 hours of additional grinding. In this way, the water content of the maximally saturated suspension is reduced by about 4 times. The suspension is quickly sintered, which reduces the shrinkage during drying of the obtained products. The suspension is quickly absorbed on the walls of the mold, as a result of which the shrinkage of the obtained product during drying is minimal. The thickness of the absorbed layer depends on the running time of the process.

The quartz glass particles in the suspension are considered chemical compounds of SiO_2 with ionized silicic acid, continuously dissociating according to equations:

$$[H_4SiO_3] \rightleftarrows SiO_4^{4-} + 4H^+ \quad (1)$$

$$[H_2SiO_3] \rightleftarrows SiO_3^{2-} + 2H^+ \quad (2)$$

It is assumed that the hydration of SiO_2 is limited by the specific surface area of the particles in the suspension as a result of the building of surface tetrahedra.

The particles of the unstabilized slips are whole aggregates (floccules) with water-filled voids which are preserved during molding. Therefore, a traditional method for stabilizing such slips is gravity stirring. The electric double layer formed by reactions (1) and (2) is insignificant due to the small amount of silicic acid (up to 0.01%) and its low degree of dissociation. The stability of the slip is achieved through a uniform distribution of water dipoles around the ionized solid SiO_2 particles, which is achieved by prolonged stirring (for about 70-80 hours).

The rate of absorption of the suspension on the walls of the mold and the casting density depend significantly on the pH of the suspension. Its optimal value lies in the range from 4.5 to 6. At a pH value of 5 ± 0.3, the silicic acid is most stable, while in a neutral environment it polymerizes intensively, releasing water and reducing the concentration of H^+ ion. HCl is used to lower the pH of the suspension, and NH_4OH to increase it [4].

3. Molding hollow structural details for beehives from amorphous ceramics

After preparing a stable suspension of amorphous quartz glass powder, the next stage in the technology involves casting test bodies, carrying out drying and high temperature sintering, and establishing the shrinkage coefficient of the samples. Following this is the making of models and mold outfits for each of the hollow structural details of the ceramic beehive. The residence time of the slip in the mold is determined experimentally and the uncollected slip is drained from the molds.

The time between the filling of the mold with slip and its draining is 12 minutes. The thickness of the cavity wall is 3 cm, and the width of the cavity is 18 mm.

A technological diagram of a workshop for the production of beehives is shown in Fig. 1.

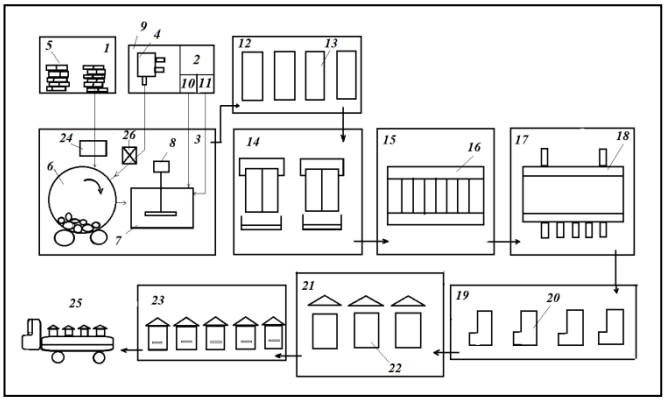

Fig. 1. *Technological diagram of a workshop for the production of beehives*

1. Quartz glass warehouse;
2. Modifier sector;
3. Sector for the preparation of quartz glass suspension with particle size below 100μm;
4. Distiller;
5. Quartz glass with particle size below 100μm;
6. Grinding device;
7. Container for ready-mixed suspension;
8. Stirrer;
9. Distilled water and modifiers sector;
10. Tank for HCl;
11. Tank for NH_4OH;
12. Molding equipment sector;
13. Mold outfits;
14. Molding sector;
15. Sector for drying structural ceramic parts with cavities;
16. Drying sector;
17. Furnace sector;
18. Furnace;
19. Warehouse for finished structural ceramic parts;
20. Sintered structural details for beehives;
21. Ceramic beehive assembly sector;
22. A beehive made of amorphous quartz ceramics
23. Warehouse for finished products;
24. Scales;
25. Dispatch vehicle;
26. Container measuring the volume of the drained fluid (distilled water).

4. Sintering of amorphous quartz ceramics

The main factors determining the sintering mode include: the purity of the quartz glass, the density of the cast details, the sedimentary composition of the ground quartz glass and the crystallization tendency.

The quality of the final product is significantly dependent on the heating rate in the temperature range from 1000 ^{0}C to a final temperature of 1200-1300 ^{0}C (in this case 1250 ^{0}C). At slow increase in the temperature (50 - 100 K/h), the crystallization ability also rises, leading to phase formation of high temperature cristobalite, which is a contributing factor to the reduction of the strength of the products. The established optimal heating rate, at which the formation of crystallization centres is avoided, is 400 K/h [5].

The chosen method of obtaining articles from slip ensures a sufficiently high density of the final product. Nevertheless, sintering should not necessarily aim for high density, which is achieved with longer heating and higher temperature, as this leads to an increase in crystallization and sharply reduced strength.

In our case, since the products are not used at high temperatures, a sintering intensifier – 1.2% $B2O_3$ – was added to prevent crystallization.

Fig. 2 shows ceramic structural details with cavities - an intermediate stage of assembling the ceramic beehive, and a completely finished, ready-to-use hive.

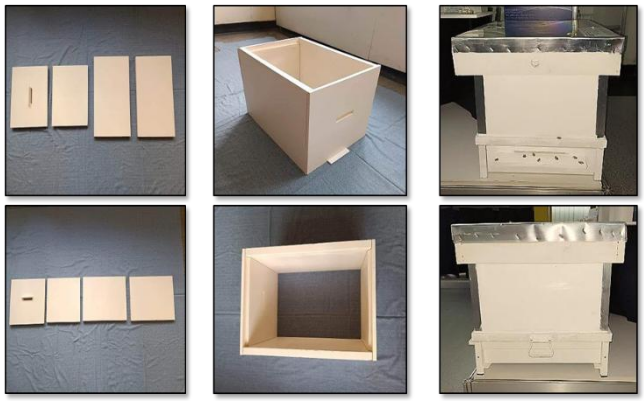

a) ***b)*** ***c)***

Fig. 2. a) *hollow ceramic structural details;* ***b)*** *intermediate stage of assembling a ceramic beehive;* ***c)*** *ceramic hive ready for the settlement of a bee family*

5. Properties useful for the amorphous quartz ceramics and supporting its use, such as ceramic structural details with high level of cavities designed for beehives

The mechanical properties are determined by the grain structure and porosity of the suspension absorbed on the walls of the mold. Amorphous quartz ceramic samples with a porosity of 3% had a hardness of about 5.5 Mohs. As the porosity increases to 20%, the hardness drops sharply to about 2 Mohs.

The flexural strength ranges from 3 to 80 MPa. It should be noted that the relationship between porosity and strength typical of other ceramics is not observed in quartz ceramics.

The compressive strength ranges from 50 to 600 MPa depending on the technological parameters, the porosity and the environment in the furnace. It reaches 500 MPa in an air environment and 600 MPa in a vacuum.

It is interesting to note that the value of tensile strength is 75% - 85% of that of flexural strength. This is a very high value, unusual for a ceramic material.

An important indicator for beehives is thermal conductivity. In the case under consideration, it depends both on the structure and the porosity of the material and on the presence of impurities. For opaque materials and for materials with an amorphous structure, such as quartz ceramics, the heat transfer process is determined by the so-called phonon conductive thermal conductivity.

6. Conclusions:

1. A technology and a scheme of a workshop for the production of structural details from amorphous quartz ceramics and their assembly into whole beehives have been developed.
2. The factors for obtaining stabilized suspensions of amorphous quartz particles, as well as the conditions for proper high temperature sintering, have been established.

3. A prototype of a beehive has been created, built from structural ceramic details made of amorphous quartz ceramics with a high level of cavities.

7. References

[1] Luben Lakov, Bojidar Jivov, Todorka Lepkova, Krasimira Toncheva, Stancho Yordanov, "Comparison of innovative collapsible ceramic hive and traditional non-separable hives made on the basis of natural plastic raw materials", Machines. Technologies. Materials. Vol. 16, (2022), Issue 10, pg(s) 340-343.
[2] E. Gerasimov and others. under the editorship of Prof. Dr. Eng. S. Bachvarov, "Technology of ceramic products and materials", IC "Sarasfati", Sofia, (2003)
[3] Yu. E. Pivinsky, F. T. Gorobets, "Ogneopory", No. 8, (1968)
[4] G. Solovushkova, Yu. Polonsky, etc., "Ognepory", No. 7, 5÷6, (1980)
[5] Yu. E. Pivinsky, A. G. Romashkin, "Quartz ceramics", Moscow, ed. Literate. in construction, (1972)

Analyze of welding arc parameters in shielded metal arc welding

Yordan Denev[1]
Technical University of Varna[1]
e-mail: y.denev@tu-varna.bg

Abstract: *Shielded metal arc welding is widely used in heavy industries in partly shipbuilding and ship repair. This method didn't required special personal skills and equipment. Different scientists are analyzed welding parameters, mechanical characteristics and chemical composition in welding seam but interesting is to be investigated welding arc characteristics in different electrodes. The paper deal with analyze of welding arc parameters in shielded metal arc welding. For this purpose on mild steel plates are welded seams with different diameters of electrodes and different welding current. In welding process are measured welding arc burning time, length of electrodes melted part, welding machine voltage and weight of melted electrodes part. For analyze welding arc parameters are used response surface methodology method (RSM). Used RSM in the paper is 2^k factorial design where k=2 factors. The influence of each to other factors of welding arc is presented by meta models.*
KEYWORDS*: SHIELDED WELDING, ARC LENGHT, MODELS, EXPERIMENT PLANING*

1. Introduction.

Welding arc is main component of welding seams. Its role is to transfer melted metal in weld seam. Transfer of melted metal from electrodes to weld pool depends from electrodynamics forces, gravity, welding arc pressure and gases in welding arc. The type of melted metal transfer is large dropped, middle dropped or like a stream.

Welding arc analyzation is widely area of scientists. Characterization of welding arc and weld pool formation in vacuum gas hollow tungsten arc welding is analyzed in [1]. In this paper authors obtain the effective arc radii for various welding conditions in vacuum gas hollow tungsten arc welding. They used Abel inversion algorithm to CCD arc image and determine the distribution of arc heat flux, arc pressure and current density from the physical relations of arc irradiance, temperature and current density in gas tungsten arc welding.

Physical characteristics of arc ignition process are analyzed in[4]. In their publication they focused attention on stable combustion state and the research on the mechanism of welding arc ignition process is quite lack. They used tungsten arc welding process for their analysis and physically characteristic of welding arc are investigated by camera with height resolution. The welding arc electron density during the period of the arc ignition is calculated by the Stark-broadened lines of Hα.

In[3] is studied effect of arc length on oxygen content and mechanical properties of weld metal in pulsed gas metal arc welding. For the analyze the authors used Q 690 high strength steel and ER69-G wire with diameter 1,2mm. Shielded gas used for experimental procedure is 82%Ar and 18% CO_2. Conclusion is that arc length raised, oxidation in drop transfer and oxygen content in weld metal increased significantly.

Determination of welding parameters is important stage from welding process. Proper parameters selection resulting to minimization of deformation. This process is widely described in[5]. They describe step by step stages in parameters determine. This information is useful for production of welded construction in heavy industry, shipbuilding and ship repair sector.

There aren't enough information, data and analyses about welding arc in shielded metal arc welding process and mainly about its parameters. The main parameters of welding arc are burning time, burning stability and weight melted metal. Burning stability of welding arc method is developed by akad. Hrenov. It is consist of burned of arc of rigid electrode. The arc burn while length of electrode is enough to touch the steel plates.

2. Description of shielded metal arc welding process.

Shielded metal arc welding is most applicable method in industry. It is characterized with simplicity in equipment and not so special skills of operator. The main method equipment is shown on fig.1.

Welding arc is the distance form electrodes to surface where arc is formed. Based on this welding arc can be divided into three types:

- Medium or normal;
- Long;
- Short;

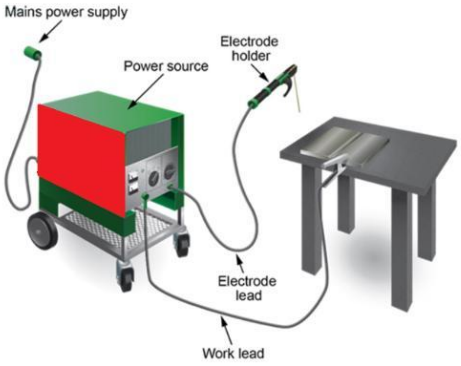

Fig.1. *Shielded metal arc welding scheme[8]*

Power source is direct or alternative current. This power sources has static dropping V-A characteristic. Welding arc temperature in this power sources is about 6000-9000°C.

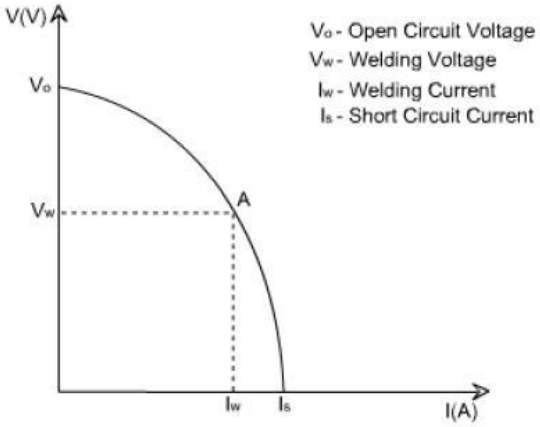

Fig.2.*V-A characteristic of power source[9]*

Welding arc can be divided into three regions: anode, cathode and arc column. On fig.3. is shown welding arc structure and voltage distribution.

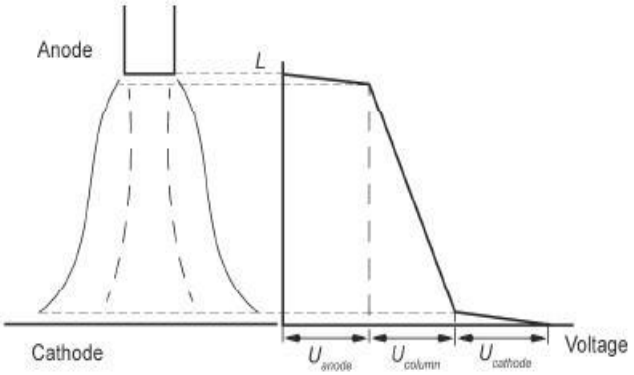

Fig.3. *Voltage arc distribution[6]*

At the anode region, as the temperature falls higher voltage is required to maintain ionization in the arc. The heat loss is compensated by electrons in the plasma. In cathode area is the same situation with the difference that more heat is generated in anode area than in cathode. In the arc column, high temperature concentrations are accumulated. This process together with ionized metals kept welding arc burning at temperatures of about 6000K.

Electrodes for shielded metal arc welding are covered electrodes. The role of a cover is to protect welding seams from atmospheric . The cover contains stabilizing, shielding, fluxing, deoxidizing and other elements supporting the welding process. Depending on the type of electrode being used, the electrode covering provides the welding seam in air[7].In proper selection of cored electrodes is important to be considered followed rules:

- R_m electrodes≈R_m base metal
- Chemical composition electrodes≈ Chemical composition base metal

If these rules are considered working characteristic of welding construction is absolutely reliable.

According[2] shielded metal arc welding cored electrodes are with diameter range 2.00, 2.5, 3.0,3.25,4.0,5.0,6.0mm and length from 350mm and 450mm.

The value of welding current depends form electrodes diameter. It is calculated by following formulae:

$$Iweld = de * k \quad (1)$$

where: de- diameter of electrode, k- coefficient depended from steel grade, k=40 for low carbon, low alloyed steels, k=30 for other carbon steels.

Shielded metal arc welding method is used in different welding positions. This gave it widely application in industry, shipbuilding and ship repairing.

3. Experimental procedure.

The experimental procedure is consisting of welding seams on the mild steels plate St 235. Welding is done by rutile electrodes with different diameter and different values of welding current.

Table 1. *Welding current for different electrodes diameters*

№	De, mm	I weld, A
1	3.25	80
2	2.5	100
3	3.25	120
4	4.00	150

For purpose achieving in the paper is used welding machine for shielded metal arc welding shown of fig.4.

In selection of electrodes rules for equal or approximate chemical composition and mechanical characteristic of electrodes and base metal are kept. Chemical composition of steel plates are shown on table 2 and chemical composition of electrodes are shown on table 3.

Table 2. *Chemical composition of steel plates base metal*

C	Si	Mn	Ni	S	P	Cr	N	Cu
≤0.22	≤0.05	≤0.6	≤0.3	≤0.040	≤0.040	≤0.3	≤0.012	≤0.3

Table 3. Chemical composition of electrodes

C, %	Si, %	Mn, %
0.08	0.3	0.4

Fig.4. *Overview of welding machine*

Mechanical characteristic of steel plates and electrodes are shown on table 4 and table 5.

Table 4. *Mechanical characteristic of base metal*

Rm, MPa	Rpl, MPa	A, %
470	340	26

Table 5. *Mechanical characteristic of electrodes*

Rm, MPa	Rpl, MPa	A,%
510	400	28

In welding process are measured parameters of welding arc: welding arc burning time, length of electrodes, melted part, welding machine voltage.

To analyze influence of parameters on each other are used response surface methodology. The commonly used response surface methodology is the simplest 2k factor design. In this 2k factor design, every factor has two levels(+1, -1) and each run at two levels. The levels of the factors can be called,, low" and,, high". The two levels can be quantitative and qualitative. In engineering analysis, for example, quantitative factors are forces, pressure, speed and etc. and qualitative factors can be number of machines, ships and other. To convert factorial design into regression models, we used some of the following models:

- First model

$$y = \beta_0 + \beta_1 x_1 + \beta_2 x_2 + ...\beta_k x_k \quad (2)$$

- Iteraction model

$$y = \beta_0 + \sum_{i=1}^{k} \beta_i x_i + \sum\sum_{i<j}^{k} \beta_{ij} x_i x_j \quad (3)$$

- Second model

$$y = \beta_0 + \sum_{i=1}^{k} \beta_i x_i + \sum\sum_{i<j}^{k} \beta_{ij} x_i x_j + \sum_{i=1}^{k} \beta_{i\,j} x_i^{\,2} \quad (4)$$

where: x_1 is the coded variable that represent the reactant concentration, x_2 is the coded variable that represent the feed rate, β-s are correlation coefficients.

Design matrix of 2^2 factor planning is shown on table 6.

Table 6. *Design matrix*

№	X1	X2
1	-1	-1
2	+1	-1
3	-1	+1
4	+1	+1

4. Results

Experimental results are processed by software STATISTICA and Excel worksheet. To analyzed impact of welding arc parameters is used first regression model of RSM. Widely matrix of experimental plan matrix is shown in table and the actual matrix of plan matrix is shown in table 7.

Table 7. *Full design matrix*

№	X1	X2	X3	X4
1	1	-1	-1	1
2	1	1	-1	-1
3	1	-1	1	-1
4	1	1	1	1

Time for welding arc burning time and length of welding arc are objects of analysis. These two parameters describe and characterize the welding arc. Based on the model are done graph dependence of:

Length of welding arc against diameter of electrode and welding current fig. 5.

Welding arc burning time against voltage of welding machine and welding current, fig.6.

Table 8. *Experimental data*

№	Voltage, V	L weld arc, mm	de, mm	I weld, A	T weld arc, sec
1	14	24	2.0	80	30.3
2	17	27	2.5	100	44.45
3	21	30	3.25	120	67.7
4	26	34	4.0	150	79.5

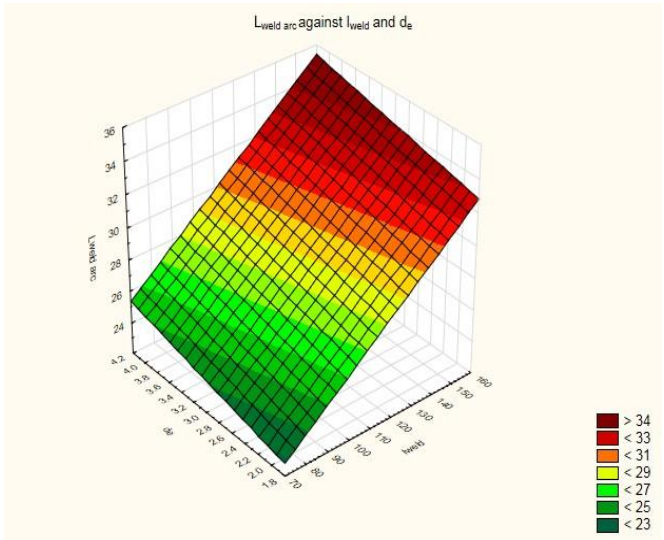

Fig.5. *Length of welding arc against diameter of electrodes and welding current*

1. Conclusion

In the paper are analyzed welding arc parameters in manual shielded metal arc welding. For experimental procedure are used retile electrodes with diameters of 2.00; 2.5; 3.25 and 4.00mm and steel plates grade ST235.

To analyze the results are used response surface methodology. Two-level factorial design of experiments is used. Based on methodology regression models, regression equations for analyzed welding arc parameters were developed.

Length of welding arc closely depends form welding current. With higher welding current values, the length of the welding arc is higher. Type and diameter of electrodes haven't a so important impact on length of welding arc. This is confirmed by the developed regression equation.

Time for welding arc burning closely depends on voltage of welding machine. Impact degree of welding current in burning time is not so clearly expressed. In higher values of welding machine voltages burning

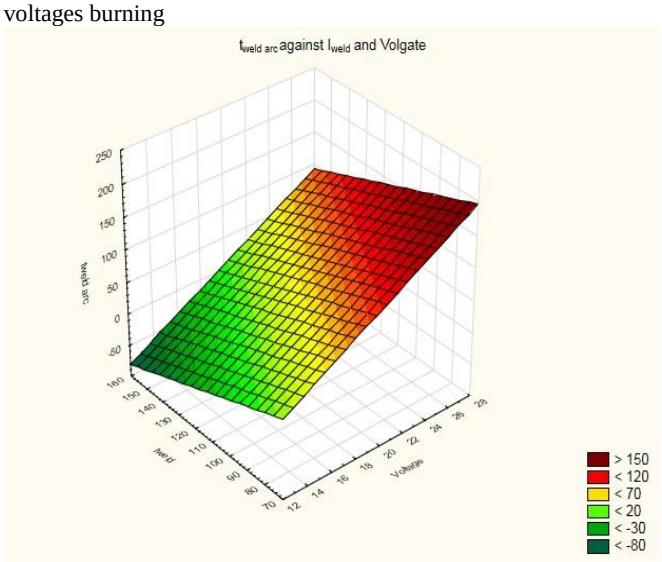

Fig.6. *Welding arc burning time against voltage and welding current*

$$t_{weldarc} = -25.5333 + 10.8306V - 1.1567I_{weld} \quad (5)$$

$$L_{weldarc} = 13.0385 + 0.1115V + 1.0769I_{weld} \quad (6)$$

time is bigger. This is in close relation to welding current.

2. Declarations

Conflict of interests: The author has no conflicts of interest to declare that are relevant to the content of this article.

3. Bibliography

[1] Cho, D.W., Lee, S.H., Na, S.J., 2013, Characterization of welding arc and weld pool formation in vacuum gas hollow tungsten arc welding, Journal of Materials Processing Technology, ELSIVIER, pp. 143-152;

[2] ESAB, catalogue;

[3] Jiache, Xu, Xiaoxiao Zhou, Dawei Zhu, 2022, Effect of Arc Length on Oxygen Content and Mechanical Properties of Weld Metal during Pulsed GMAW, 12,176, Basel, Switzerland;

[4] Shi, L., Song, Y., Xiao, T., Ran, G., 2012, Physical Characteristics of Welding Arc Ignition Process, CHINESE JOURNAL OF MECHANICAL ENGINEERING Vol. 25, No. 4, pp. 786-791;

[5] Ugur Soy, Osman Lyibilgin, Fehim Findak, Cemiz Oz, Yasar Kiyan, 2011, Determination of welding parameters for shielded metal arc welding, Scientific Research and Essays Vol. 6(15), pp. 3153-3160, DOI: 10.5897/SRE10.1073;

[6] Weman, K., 2012, Welding process handbook, second edition, Woodhead Publishing Limited, Cambridge, UK

[7] https://www.fabtechexpo.com/blog/2018/01/04/shielded-metal-arc-welding-basics;

[8] https://www.materialwelding.com/what-is-shielded-metal-arc-welding-smaw/;

[9] https://weldknowledge.com/2016/02/06/characteristics-of-arc-welding-power-sources/;

Measures to overcome the pandemic consequences: insights from entrepreneurs

Mina Angelova, Daniela Pastarmadzhieva
University of Plovdiv Paisii Hilendarski, Faculty of Economic and Social Sciences
mina.angelova@uni-plovdiv.bg, daniela.pastarmadzhieva@uni-plovdiv.bg

Abstract: *The COVID-19 pandemic remains the most reported risk, cited by scientists and business representatives, to growth in their home economies as well as the coronavirus effect on global economic sentiment. The research presents the results of in-depth interviews obtained in the period April - June 2022 with entrepreneurs who are managers and/or owners of enterprises whose headquarters are registered in the territory of the city of Plovdiv, Bulgaria. This paper aims to study their attitudes toward the measures taken to overcome the pandemic consequences and strikes to recommend to the government reasonable measures for overcoming the negative effect of the pandemic. The findings of this study can help managers in national institutions and business organizations recognize the strengths and weaknesses of various dimensions of entrepreneurship revival measures that influence innovation and competitiveness.*

Keywords: Measures, Pandemic, Entrepreneurship, Bulgaria

1. Introduction

COVID-19 has had a devastating effect on entrepreneurship and other economic issues. Many businesses have failed as a result of the significant drop in demand caused by confinement and other restrictions on travel imposed by countries to stop the spread of the disease. At the EU and national levels, numerous procedures have been developed for creating and developing new enterprises in priority sectors of the National Strategy for the promotion of small and medium-sized enterprises and specific areas related to overcoming European and regional challenges forced by the pandemic. During this critical period, it should be emphasized that SMEs must maintain an intensely positive and focused attitude in the face of the economic slowdown and the resulting environmental constraints.

The research object is entrepreneurs who are managers and/or owners of enterprises whose headquarters are registered in the territory of the city of Plovdiv. **The focus** is their suggestions for adequate measures that can support the development of their business in the crisis caused by the pandemic of COVID-19. **This paper aims** to study the entrepreneurs' attitudes toward the measures taken to overcome the pandemic consequences and strikes to recommend to the national authorities reasonable measures for overcoming the negative effect of the pandemic.

A wide range of **research methods** was used giving us the opportunity to test the ideas, build knowledge, and gain insightful context and nuance to the recommendations. As part of a research project titled "*Economic Dimensions of the COVID-19 Pandemic: The Impact of Psychological, Legal and Socio-political Factors and Approaches for Overcoming their Negative Effects*" funded by the Bulgarian National Science Fund, a content validity evaluation exercise was conducted by PhD students as the initial step in the data collection process. In the second phase of data collection, two representative studies were conducted - with persons, residents of the city of Plovdiv, and enterprises registered on the territory of the city of Plovdiv [1]. The paper presents the results of the third phase, i.e. in-person verbal interviews with 14 entrepreneurs. The data were obtained in the period April - June 2022. The findings of this research can assist managers in the national institution and business organizations to recognize the strengths and weaknesses of different dimensions of measures toward entrepreneurship revival which influence innovation and competitiveness. **The authors' standpoint** is that the degree of success of the measures is an indicator of the strength of the state policy in the context of promoting entrepreneurship and entrepreneurial initiative.

The paper structure follows the main purpose and aims of the research, i.e., after the introduction, the second part presents a literature review based on current research in the field of entrepreneurship. The third section focuses on the research methodology. The latter serves as the study's framework and as the foundation for the fourth section, which presents the empirical findings. The paper concludes with conclusions and recommendations for future research in the field of entrepreneurship and the implementation of adequate state measures to mitigate the negative consequences of the pandemic.

2. Literature Review

Successful entrepreneurship, described as an ability and willingness for development, organization and management of a business taking all the risks for gathering profits, is an essential part of the ability of a nation to succeed in the eternal changing and strongly competitive market. An entrepreneur is a person who perceives an opportunity and creates an organization to pursue it. And the entrepreneurial process includes all the functions, activities, and actions associated with perceiving opportunities and creating organizations to pursue them [2].

A large piece of evidence from the literature shows that in a situation of crisis adopting efforts by the state in the development of strong entrepreneurial culture and competencies in entrepreneurs in developing economies contributes to increased entrepreneurial initiatives [3]. In the 2021-2027 program period, the European Commission approved the "Competitiveness and Innovations in Enterprises" Program, which provides for the continuation of support for micro, small, and medium-sized enterprises in the country through scientific research and the implementation of innovative solutions for their production [4]. In the event of a pandemic, providing relief and assistance to businesses is critical, but it is also important to determine how much the state's efforts are appreciated and approved by the organizations.

Entrepreneurs exploit new opportunities and often revolutionize industries overturning long-established technologies, business models, and dominant companies [5]. To do so, they innovate and take risks. Improving and increasing innovation and the ability to develop innovation is the most important factor for growth and serves as a prerequisite for ensuring a higher level of economic development. The scientific literature provides evidence that innovativeness has a significant direct effect on behavioral intention to acquire new opportunities during crisis conditions [1]. Entrepreneurs act on what they believe is an opportunity in high uncertainty, they use their judgment about whether to act [6]. According to Bosma and Schutjens [7], an evident gap exists in entrepreneurial activity studies encompassing regions and countries. Therefore, investigating determinants of entrepreneurship over a region enables disentangling regional demography attributes, institutional components, and specific regional attributes [5].

An entrepreneurial revolution has transformed the economy since the mid-1970s and in the conditions of Industry 4.0 the successful entrepreneurship practice is an exciting phenomenon with broad implications on strategy, innovation, and the workplace environment. No issue gets the attention of politicians more than job creation. Furthermore, the declared state of emergency and the strict measures that followed had a significant impact on the country's economic life. The pandemic has increased the need for Bulgarian businesses to seek out innovative business models and niches in order to combat the consequences of the country's deteriorating economic conditions. This set of goals could not be possible without the state support and the approbation of adequate

measures toward business stakeholders to fight the crisis consequences. And this process has a positive relation to both the state and the business.

3. Methodology of the Research

The applied methodology has been tested in previous research conducted by the authors [8]. The Research Design method is thought to use direct interviews to investigate the research problem. These interviews are based on open-question sessions lasting one hour. Data is gathered through interview responses and statements. Analytical information was synthesized and produced for the purposes of the research based on data collection. In fact, data collection as a technique in the research was formalized through our direct interaction in a discussion format with the Top Executives and CEOs. All the entrepreneurs are seasoned leaders and managers who have aided in the development and growth of businesses. Because of their leadership and long tenure at their firms, these individuals are regarded as experts on entrepreneurship and organizational culture. The entrepreneurs were selected for their expertise and knowledge to explore the business threats and application of the state's measures in-depth.

We used a semi-structured own questionnaire focused on gathering the entrepreneurs' evaluation related to the Bulgarian government's reaction to the pandemic. On a scale of 0 to 10 (where 0 means "I do not agree at all" and 10 means "I strongly agree"), we asked them how much they agreed with the following statements: political communication, unified EU support, government communication strategy, and so on. We asked them to evaluate the business support measures in the event of a pandemic. First, we wanted to know if the entrepreneurs had benefited from any of the state's programs. Furthermore, we wanted to hear from respondents about what else could be done to support them. We asked them an open-ended question about suggestions in the context of government actions and what politicians could do better. The respondents evaluated the truthfulness of statements that best captured their perspectives on how to assist their businesses and improve the entrepreneurial climate in Bulgaria.

In addition to the interview sessions, desk research was carried out to check the information for inconsistencies and to construct a correct and up-to-date logical model of reasoning.

4. Discussion and Results

The objective of this phase of data collection was to ask the managers and experts about the evaluation related to the Bulgarian government's reaction and proposed measures to business during the pandemic While the interviews sought confirmation of the proposed ideas, they also sought modifications and emergent concepts that could influence the construct's development. This phase of the research was primarily intended to contrast the largely theoretical and literature-based conceptualization of economic and social strategies with the practical experience and knowledge of managers and experts.

The study consisted of interviewing 14 entrepreneurs who were picked from a convenience sample of SMEs whose headquarters are registered in the territory of the city of Plovdiv, Bulgaria. As no such research was conducted in the companies before, it took some months to make the Top Management willing to cooperate and finish the research. We selected a potential pool of 20 enterprises to contact for interviews based on our strongest personal relations. All the respondents were contacted from April 2022 to June 2022, of which 14 agreed to be interviewed. Nine of the interviews were conducted at the manager's place of business while five were conducted via Internet video conference. 64 % of the respondents are men and the others are women. All the respondents have master's degree of education.

4.1. Government's Commitment to Entrepreneurs' Problems

More than 80 % of the entrepreneurs think that the politicians in Bulgaria do not seem to have a clear vision of how to deal with the pandemic. The respondents give suggestions that the state must follow the good practices abroad from countries that manage the pandemic well. The results show that most of entrepreneurs do not believe in the government's ability to create a proper vision for dealing with the crises and implement it.

They evaluate the communication strategy of the Bulgarian government as weak (93% of the respondents). The messages from the politicians are contradictory and confusing, and together with a lack of unity, they create mistrust and thwart the entrepreneurial initiative. The communication strategy must be elaborated and applied by experts in communication and political management, but the reality in Bulgaria does not confirm this statement. In managing the pandemic, politicians are focusing more on public health and less on business issues that create the feeling that their problems are underestimated.

4.2. Assessment of Measures Introduced by the State to Fight the Pandemic

During the discussion, we introduced to managers an exhausted list of all measures the government has implemented to encourage entrepreneurship. All the respondents had benefited from some of the introduced measures. Most of them (86%) used the "60/40 Measure" hoping to keep their employees. The "Support for medium-sized enterprises to overcome the economic consequences of the COVID-19 pandemic under the Operational Program "Innovation and Competitiveness" was the second most valued measure. Moreover, they mark many opportunities created by the approved program "Competitiveness and Innovations in Enterprises", which provides for the continuation of support for micro, small, and medium-sized enterprises in the country through scientific research and the implementation of innovative solutions for their production. This is a good perspective in obtaining communication between business and scientific institutions and participating in common projects and research.

All entrepreneurs used the opportunity of "Preferential crediting measures" aiming to minimize the loss during the pandemic. They believe that the cyclical nature of business and economic processes will lead to more opportunities and development, particularly for those who have survived such severe crises.

In an open-ended question, respondents were asked to make their own recommendations for government policies. The most frequently proposed measure is direct financial assistance to businesses. This is followed by a change in relevant legislation and a prohibition on interfering with business decisions.

4.3. Recommendations for Future "Action Plan" of the Government

Entrepreneurs anticipate that a well-chosen measure will have several positive effects, including encouraging entrepreneurial initiative, motivating entrepreneurs, and increasing trust in institutions. The level of trust is affected by how entrepreneurs perceive the national government's commitment to dealing with the pandemic and business problems. All respondents are adamant about the introduction of new machinery, equipment, and technology, and are participating in various funding programs. All the participants state that the regulatory mechanisms of the institutions are not well developed and "*Bulgarian institutions are an obstacle not a supporter for the development of business initiatives*".

Many surveys assess the impact of entrepreneurial skills to launch managerial initiatives in the sphere of innovation activities. At the most valuable level is the communication skills, the initiative, the ability to work in a team, and managerial skills and abilities of the manager. The dominant qualities of interviewed entrepreneurs are communication skills, activity, and initiative, ability to work in a team, pro-activeness, leadership, and strategic planning capabilities. However, more procedures for promoting entrepreneurship must be applied including targeted training.

However, the findings of the interviews, which included concepts such as strategic planning, shared struggle, and motivated employees, appeared to describe concepts other than work expectations and job responsibilities. Instead, the desired emphasis was on teamwork and mutual support. Accessing cohesion through work expectations and job responsibilities may be too indirect in comparison to more direct questions such as relying on others in the organization and the state for assistance.

Several questions centered on broad risk-taking and innovation rather than shifting to pursue or develop new opportunities during a pandemic. These risk-taking and innovation items appeared too abstract and disconnected from the intended concept of opportunity-driven innovation and change. While these may be related to innovation and change, they may represent conceptually different ideas.

Developing entrepreneurship in the conditions of Industry 4.0 is defined as part of the application of new digital technologies in the production sector and includes a wide range of technological solutions and business models that contribute to qualitatively new forms of economic activity. Cooperation between individual research institutions and universities, on the one hand, and entrepreneurs, on the other, will become an inseparable part of enterprise staffing. Summarized results of the suggested measures by the entrepreneurs can be observed in scheme 1.

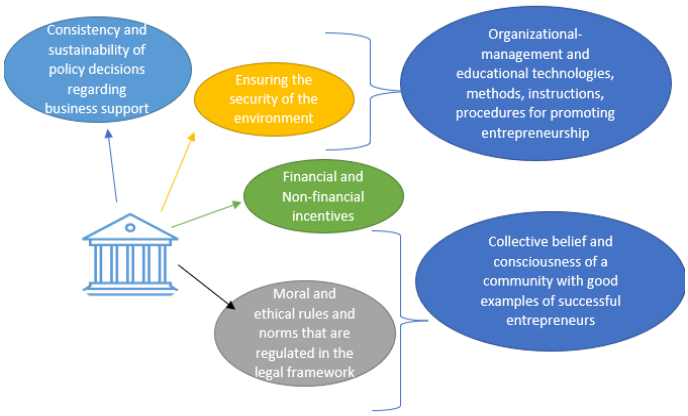

Scheme 1: ***Suggested measures by entrepreneurs***

Source: Own interpretation

5. Conclusion

This paper described the objective, procedure, sample selection, analysis, and results of the third phase of data collection for the research project, which was based on interviews with entrepreneurs. The goal of this phase was to investigate the state's response to the pandemic and to shed light on proposed additional measures based on entrepreneurs' experiences, expertise, and insights.

The 14 interviews with entrepreneurs yielded a wealth of data that largely supported the conceptual thinking forced in developing a model for mitigating pandemic consequences while also providing important context, nuance, and explanation of respondents' perspectives on applied measures and state-supported procedures.

In terms of the role of institutions in mitigating the negative effects of the crisis, it appears that they are more of an impediment than support for such activity. This rich qualitative data helped to ground the conceptual model for overcoming the pandemic consequences and provided evidence for the veracity of the proposed dimensions. This data also provided critical foundational evidence for future research that may investigate the formation of national strategy in a pandemic context and how it changes in organizations. The dynamically changing economic and political environment necessitates greater flexibility in businesses and a willingness to adapt to new conditions. The role of the state in mitigating the effects of the crisis and encouraging entrepreneurial initiatives is critical. Developing and/or starting a new business is a prerequisite for increasing the economy's overall competitiveness. This study's findings have responded to several academic requests for more current research on entrepreneurship during a pandemic. Such findings are significant because they show policymakers where entrepreneurship and innovation have the greatest potential. As a result, state assistance can be directed specifically at these groups.

The study and proposed measures would be useful for implementation in the new adapted National Plan to deal with the SARS-CoV-2 [9] pandemic, ensuring preparedness for a maximally adequate response to the another wave of the COVID-19 pandemic, and introducing an inter-agency and comprehensive approach to the management of such unusual situations to counter the adverse health and public consequences associated with the mass spread of an infectious disease.

ACKNOWLEDGEMENTS

This paper is part of a project № KP-06-DK2/7/30.03.21, financed by the National Science Fund, Ministry of Education and Science, Bulgaria.

REFERENCES

1. Angelova, M.N.; Pastarmadzhieva, D.D.; Naydenov, A.T. Determinants of the Entrepreneurial Initiative during a Pandemic: The Case of Plovdiv. *Sustainability 2022*, 14, 13753. https://doi.org/10.3390/su142113753.

2. Bygrave, W. and Zacharakis, A. (2011) *Entrepreneurship*, 2nd ed., John Wiley & Sons, Inc., ISBN 978-0-470-45037-6 (pbk.)

3. Ramadani V. and Schneider, R. C., Eds. (2013) *Entrepreneurship in the Balkans: Diversity, Support and Prospects*, 1st ed. Springer Berlin Heidelberg: Imprint: Springer, 2013. doi: 10.1007/978-3-642-36577-5.

4. European Regional Development Fund, Program "Competitiveness and Innovations in Enterprises", available online https://opic.bg/opik/nov-programen-period-2021-2027-g [19.01.23]

5. Širec,K. and Močnik, D. (2017) The competitiveness of established entrepreneurs in Balkan countries. *World Review of Entrepreneurship, Management and Sust. Development*, Inderscience Enterprises Ltd. Vol. 13 (2/3): 141-158.

6. Hisrich, R., Peters, P., Shepherd, D.A. (2017) *Entrepreneurship*, 10th ed., Irwin McGraw-Hill, New York. ISBN 978-0-07-811284-3.

7. Bosma, N. S. and Schutjens, V. A. J. M. (2007) Outlook on Europe: patterns of promising entrepreneurial activity in European regions, *Tijdschrift voor Economische en Sociale Geografie*, Vol. 98 (5): 675–686.

8. Angelova, M. & Pastarmadzhieva, D. (2020) Attitudes Towards Innovations: Evidence from Wine Industry Enterprises. *Trakia Journal of Sciences*, 18 (1): 582-590, ISSN 1313-3551 (online), doi:10.15547/tjs.2020.s.01.093.

9. National operational plan to deal with the COVID-19 pandemic approved by the Council of Ministers, Ministry of Health, Bulgaria, available online https://www.mh.government.bg/bg/novini/aktualno/nacionalen-operativen-plan-za-spravyane-s-pandemiy/ [19.01.2023]

Development of automation in Bulgaria in the 20th century

Boyan Asparuhov
University of library studies and information technology, Sofia, Bulgaria[1]

b.asparuhov@unibit.bg

Abstract: *In the 8th decade of the 20th century, a state program was implemented to automate the entire production in the spirit of scientific and technical progress. More than 160 types of systems for the automation of technological processes have been developed, including individual high-performance machines, industrial robots and manipulators, managed with the most advanced microprocessor technology for its time, subsequently implemented in pilot complex automated workshops and production areas in various economic sites of the country. Prioritizing the production of means of automation of technological processes intensifies machine-building, intellectualizes labor and increases its productivity. Gradually, with our forces and means, experience and a base for further design and implementation of flexible automated production systems in all branches of industry are created. The achieved technical and organizational experience guarantees the membership of Bulgaria in the Permanent Commission on Mechanical Engineering at the SIV and its coordinating role in agreements for multilateral specialization and scientific and technical cooperation in the field of industrial manipulators and robots.*

Keywords*: HISTORY, AUTOMATION, ROBOTS, MACHINE-BUILDING*

1. Introduction

The proposed report aims to present part of the documentation of the executive power in Bulgaria in the second half of the 20th century, concerning the development of production automation. The object of research are annual reports on the activities of the Ministry of Mechanical Engineering, reports on achieved results in scientific developments and their implementation in production, concluded trade agreements and future intentions for investments and development. The chronological frame spans 20-25 years, beginning in the early 1960s and ending in the mid-1980s. The research does not pretend to present a complete history of the development of automation in Bulgaria, but to show archival documents testifying to a successful policy, thanks to which Bulgarian society is technologically on par with developed Western countries and becomes a leader among socialist countries in the successful transition to an automated economy.

Automation is a qualitatively new, higher stage in the development of technology. Automation of production is a process of developing and implementing automatic means and systems with the aim of freeing man from physical and mental labor and expanding his capabilities to manage machines and processes. On the one hand, the level of assurance of production by automatic means determines the degree of improvement of working conditions and reduction of physical and mental efforts of management. On the other hand, automation affects the technological processes in the direction of their improvement as a result of the possibilities for quick reporting of violations in them and the impact of their removal, to maintain the most economically advantageous mode of operation of the machines and equipment. The economic benefit for society from the introduction of automatic means and systems in production is expressed in the economy of public labor.

2. Solutions

In the 1960s, the General perspective for the development of the Bulgarian economy predicted a 6-7 times increase in industrial production by 1980, which required extensive mechanization and automation of production processes.[1] The new technology, offering more precise management of the production process, leads to great savings in raw materials and to optimal utilization of capacities.[ibid]

The beginning of the organization of the work on automation was set with Order No. 245 of the Council of Ministers of 1.03.1961, which created the Central Development Base for Automation (CRBA). By Decree No. 163 of 27.09.1962. The base grew into the Scientific - Research and Design - Construction Institute of Applied Automation (NIPKIPA).[2]

In 1964 the first automated control system for the four sections of the concrete unit of ZSK Kremikovtsi was put into operation. In the same year, NIPKIPA completes the topics: Automation of the pulping process at the plant in Krichim; Automation of an unloading trolley in the OCZ, Kardzhali; System for automatic regulation of air during cotton processing in DIP "Thracian Cotton" - St. Zagora; Automation of the ore grinding cycle for DPM "Panagyur mines"; Automation of the heating furnaces at the rolling mills of the "Lenin" MZ; Automation of nitric acid production for the Chemical plant in Dimitrovgrad; Automation of soda production at the plant in Devnya, etc.[3]

In 1965 NIPKIPA presents a study on the efficiency of mechanical engineering for the period 1966-1970, according to which the optimal flow of processes in various productions and the achievement of the best indicators are possible only on the basis of complex automation, the implementation of controlling analog and digital machines and the mass use of measuring, control and regulating instruments and devices. [4]

In 1966 the "Automation of Ferrous Metallurgy" section at the Institute (now NIPIA) works on 8 topics with MH "Lenin" and 1 with MK Kremikovtsi; section "Automation of construction materials production" works on 3 topics; section "Automation of non-ferrous metallurgy" works on 4 topics; section "Automation of the food industry" works on 6 topics; section "Computing equipment" works on the topics: program and address management of electric hoists; program management of electric cars; mathematical description of technological processes in the chemical, metallurgical and construction industries; device for demonstrating program and address control of electric hoists. [5]

In 1966 The institute begins active international cooperation. Six engineers specialized in the USSR, another three - in Denmark and France. A delegation visited the fair in Leipzig, the International Congress in Belgium on Automation of the Pulp and Paper Industry and the International Congress on Automatic Control in England. NIPIA enters into direct cooperation with the Institute of Automation in Kyiv, with CNIIKA in Moscow, and with Hungary a permanent working group on automation is established. (ibid)

In 1969 automation has been identified as a major factor in technical progress.[6] There are a total of 241 contracts concluded by section, and the total conditional economic effect of the implemented systems is worth BGN 834,000 (ibid.)

In a report to Prime Minister Todor Zhivkov, presented in 1970. by the Minister of Mechanical Engineering Mariy Ivanov and the Chairman of the State Committee for Science and Technical Progress (SCSP) Prof. Ivan Popov, a concept was laid out, providing for the automation of technological processes in small and medium-scale serial engineering production during the period 1971-1980, which foresees the implementation of systems of metalworking units with digital - program control (CPU), controlled by digital electronic - computing machines (CM – CEIM) [7]

The authors emphasize that due to the significant complexity of CM-CEIM, it is necessary to import it and implement it in production, as well as mastering the production of digitally controlled feeding manipulator and transport devices, necessary to connect the individual machines in complex automation. (ibid).

One of the heads of state of Bulgaria and directly responsible for the development of mechanical engineering, Ognyan Doinov saw in 1968 the first robots implemented in production in Japan by Fujitsu-Fanuk. The Japanese scoff at the desire expressed by the Bulgarian side for possible cooperation, considering the absolute unpreparedness of Europe to move into this new stage of organization and development of production. In front of Doinov, the Japanese shared about the difficulties they had when introducing robots into the production of a Mercedes-Benz plant. [8]

Despite the mistrust, in 1968 Bulgaria signs an agreement with the Japanese company Fujitsu for the acquisition and production of the first electronic computing machines (EIM) "Facom", which began to be produced in our country by 1970. under the name ZIT 151. [9]

High technologies soon fell into the list of prohibited goods for socialist economies, but Bulgaria's ties with the Japanese company were not permanently severed, since in 1980 in cooperation with Fujitsu - Fanuk in our country begins serial production of robots for various purposes. [8]

Since 1974 the transformation of the Bulgarian economy towards subject-technological specialization of enterprises, known as the Multiplication effect, began. According to the Deputy Chairman of the Council of Ministers responsible for mechanical engineering, Ognyan Doinov, the copying of the Soviet model,in which each enterprise tried to produce only everything it needed, in our country led to the overspending of raw materials and the commitment of a lot of manpower and machine time. The result was an increase in production costs and an unsatisfactory quality. [8]

In order to avoid this, it moves to an optimal concentration of the capacities producing basic elements, specialization of individual parts, units and aggregates with a wide range of application with the subsequent possibility to produce a variety of final products in many machine-building plants. (ibid)

On 28.01.1978 The Council of Ministers adopts Decision No. 4 on the creation of a scientific-production association Automation of Production as an organization for the implementation of the processes of research and implementation in production of production automation systems. [10]

With the 39th Resolution of the Court of Justice of August 1, 1978. the association has been assigned the functions of a leading executive organization for the automation of production in the country, of a leading development and implementation organization for complex automation of production in the mechanical engineering industry. (ibid)

At the 84th meeting of the Standing Committee of the SIV on Mechanical Engineering, held in Brno, Czechoslovakia in 1980. issues related to the further development and deepening of the multilateral specialization and cooperation of production, the conduct of joint research and design and construction works on the creation of new types of machines and equipment were discussed. The main place is occupied by questions about the specialization of Bulgaria in the production of robots – manipulators. [11]

The Minister of Mechanical Engineering, Toncho Chakarov, insisted on signing a contract in 1981. for the specialized production of 65 types of robots - manipulators, intended for servicing 8 main groups of machines and technological processes.In addition, specialization was adopted in 4 new positions of manipulators and robots for transport and warehouse work. With this, the Bulgarian production specializes in a total of 50 positions or over 75% of the specialized nomenclature. We are followed by Poland with 40 positions, Czechoslovakia with 30 and Romania with 22 positions. NRB emerged as the main exporter of working manipulators for the period 1981-1985. (ibid)

At the beginning of the 8th decade of the 20th century, two documents trace the ongoing development of automation in our country: Development for the development of metal-cutting machines and robotics by applying the multiplication approach in the period 1981-1985. and Automation VIII Program.

The two documents define the main nomenclatures in the production direction, the directions of their technical development, the principles of the international division of labor, as well as the activities of the reproduction process in the industry, aimed at increasing the social productivity of labor to obtain a multiplier effect in the country's economy.

Program "Automation VIII" envisages unification, specialization and supplies of components and building elements, which are of decisive importance for the creation of high-performance and precise machines on the one hand, and supplies of finished products and complexes based on industrial manipulators and robots, on the other.With building elements of this type, as well as with the newly created high-performance and precise machines and industrial manipulators - robots, Bulgaria began in 1980. its participation in the international specialization and cooperation within the SIV.

It is established, at the highest state level, that we already have the necessary technical and organizational experience in building automatic technological lines and modules. Created before 1980 lines are based on Bulgarian transport and supply systems - conveyors and manipulators.In the field of industrial manipulators and robots, Bulgaria has also declared its readiness to fully participate in the international division of labor, which is also confirmed by its coordinating role in agreements for multilateral specialization and scientific and technical cooperation in the field of industrial robots and manipulators. [12]

The years 1981-1985 were devoted to automation in production. In connection with this, the National Program Automation VIII was developed. The main directions in it are 3: 1. creation of the necessary conditions and accumulation of experience for the design and implementation of complex automated workshops and plants for discrete production; 2. creation of technical means and systems for automation of production and management in other branches of the national economy;

3. increasing the level of automation and electronicization of individual machines and equipment, of complete equipment and lines produced by our engineering for the food industry, heavy engineering, construction equipment, etc., intended for newly built sites and for the modernization of existing factories. [13]

The extremely ambitious task for its time was set to put into operation over 2,000 CNC machines, 500 aggregate machines, over 3,000 industrial robots and manipulators, about 100 automated enterprise management systems (AEMS) and 20 automated dispatching systems and 10 automated production the section and workshops in OZZU - St. Zagora, NPKR "Beroe" - St. Zagora, "Dinamo" - Sliven, ZMM - Nova Zagora, KPM "Georgi Kostov" - Sofia, KHI "Hydravlika" - Kazanlak, etc. It is estimated that the total economic effect of the program amounts to BGN 320 million (ibid.)

The implementation was particularly successful in Stara Zagora, where a number of basic means of automation such as hydraulics, industrial robots and manipulators, metal cutting machines, control devices for robots and manipulators, disk drives, technological lines, etc. are produced.The main efforts to implement pilot complex-automated workshops and sections and systems for automation of engineering work are directed there.At the end of 1982, the Minister of Mechanical Engineering, Toncho Chakarov, presented a report to the senior state leaders on the development of NPKR "Beroe" - St. Zagora. [14]

By means of BGN 29 million of basic funds, facilities were built and operating in the plant, ensuring an annual production of 1,000 units of robots. The production is on the basis purchased in 1980.

license from the Japanese company Fanuk, with which Bulgaria has traditional ties. Two types of robots are mastered, with hydraulic and pneumatic drive. In order for our country to maintain its lead in the framework of international specialization, it is necessary to build additional capacities to reach an annual production of 5,000 units of robots. Since mechanical processing constitutes 60% of the labor intensity, it is necessary to search for solutions for complex automation. Currently, socialist countries lack the experience and

equipment to create automated production systems at a high technical level,and cooperation with Western companies is being sought. The highest indicators for the complex construction of an automated workshop for the mechanical processing of the main details for the robots were offered by the FANUC company, thanks to which the processing of 60% of the details for the electromechanical robots was achieved with the service of 24 workers. 9 units were delivered from Japan. lathe machines and 21 pcs. machine centers served by robots and automated transport carts, 2 automated warehouses – for blanks and finished parts, as well as a computer system for managing the complex.The automated workshop also includes 6 lathes and 4 machine centers, manufactured by NRB, and Mashproekt is included in the engineering project. (ibid)

With the project for the expansion of NPKR Beroe, the total production funds increase to BGN 70 million, and conditions are created for the production of commodity products for over BGN 150 million. On March 25, 1982, a joint meeting of the collegiums of the MME and the Ministry of Instrumentation, Automation and Control Systems in the USSR was held in Moscow. Issues regarding the expansion of scientific and technical cooperation, the expansion of cooperation in production, the development of joint activity in the field of automated control systems, the expansion of contacts and the establishment of direct scientific and technical ties were discussed.

An Industry Program for the development of specialization and cooperation in the field of instrument making, automated control systems and computer technology for them until 1990 was signed.

Possibilities for expanding cooperation in the automation of design activities, the creation of distributed systems for the automated management of discrete and continuous technological processes and the development of an automated section using robots and manipulators were discussed.[15]

In 1982, accelerated implementation of advanced technologies and technological complexes of machines and systems in agriculture began. For this purpose, a program for accelerating the complex mechanization and automation in the agricultural sector was developed and adopted by the Council on Agriculture under the Council of Ministers with a period of 1986-1990. [16]

The execution of the tasks is largely related to the staffing of the automation activity. 3500 are the specialists who are concentrated in the engineering and design organizations under the umbrella of the Ministry of Electronics and Energy alone. To increase the qualification of management and executive staff on automation issues, a departmental training center was organized at the National Institute of Civil Engineering, and a regional robotics training center was established in Stara Zagora. Together with the Scientific and Technical Union (NTS), educational centers with automation and electronicization laboratories have been established in eleven district cities. Together with the Ministry of Education, a comprehensive program for the training of personnel in microelectronics was developed and adopted, which also foresees the creation of a center for postgraduate qualification in microelectronics in Botevgrad. [13]

The production of means for the automation of technological processes led to the intensification of production and the intellectualization of labor in Bulgaria in the 60s, 70s and especially in the 80s of the XX century.During this period, statistics report a sharp increase in the social productivity of labor in the economy. The production of means of production automation is characterized by features that create completely new working conditions.

Such are the low seriality of the products with a large nomenclature in terms of modifications; the continuous increase in the complexity of the technique and increase in the concentration of the operations performed by one machine;the use to the greatest extent of the latest achievements of pneumatics, hydraulics, electronics and electric drives; the constant increase in requirements for higher operational reliability and accuracy of machines.

The new working conditions also increase the requirements for personnel service: a high degree of literacy and technical intelligence in order to be able to respond to the frequent change of nomenclature and modifications;ability for high internal mobilization and concentration, ensuring in a short time the study and understanding of constantly changing and complicating relationships in the production of new products; high mental and physical endurance; high erudition and wide specialization as a result of the use of the latest achievements of pneumatics, hydraulics, electronics; ability for quick thinking activity and analysis of the influence of imposed changes and programs on the final manifestations of the behavior of the machine organs and processing processes; an opportunity to effectively exercise professional knowledge and skills in a foreign place, in an unfamiliar work environment. [17]

Conclusion

At the end of the 80s, Bulgaria was among the 30 most developed countries in the world and took third place in the export of industrial robots for welding, painting, assembly and palletization. In conditions of tightening of the COCOM regime to limit the access of new technologies for Eastern European countries, Bulgaria offers production that is vital for the development of socialist economies.The economic policy led by the state leadership does not pursue spectacular display actions and demonstrations, but higher efficiency in the utilization of resources and greater labor productivity, which results directly from the automation of the means of production. As a result, a rapid increase in the national income and an increase in the standard of living of the population were achieved.

References

1. ASA, f.20, des.2K, a.u. 22, p. 19
2. ASA, f.20, des 3, a.u. 8, p.1
3. ASA, f.20, des. 3, a.u. 6,
4. ASA, f. 20, des. 2, a.u. 44
5. ASA, f.20, des. 3, a.u. 7
6. ASA, f. 20, des. 3, a.u. 7, p. 39
7. ASA, f. 531, des. 4, a.u. 67, p. 268
8. Doinov, O., Memories, 2002, p. 92, p.71
9. Asparuhov, B. Development of EIT in Bulgaria, 2021
10. ASA, f.531, des. 5, a.u. 105, p. 3
11. ASA, f.531, des.5, a.u. 103, p. 70
12. ASA, f. 531, des.6, a.u. 57, p. 3
13. ASA, f. 531, des.6, a.u. 57, p.77
14. ASA, f. 531, des. 6, a.u. 57, p. 204
15. ASA, f. 531, des. 6, a.u. 57, p.93
16. ASA, f. .531, des. 6, a.u. 61 p. 41
17. ASA, f. .531, des. 6, a.u. 57, p.98